Conductivity reconstruction on Riemannian manifolds from power densities

Schlüter, Hjørdis Amanda

Publication date:
2022

Document Version
Publisher's PDF, also known as Version of record

Ph.D. Thesis
Doctor of Philosophy

DTU Compute
Department of Applied Mathematics and Computer Science

Conductivity reconstruction on Riemannian manifolds from power densities

Hjørdis Amanda Schlüter

Kongens Lyngby, Denmark 2022

DTU Compute
Department of Applied Mathematics and Computer Science
Technical University of Denmark

Matematiktorvet
Building 303B
2800 Kongens Lyngby, Denmark
Phone +45 4525 3031
compute@compute.dtu.dk
www.compute.dtu.dk

Summary (English)

Weakly electric fish such as the *elephantnose fish* have for millions of years used electric signals for navigation. Elephantnose fish create an electric field around their body to detect, localise, and analyse objects within this field. This allows them to access the conducting properties of unknown objects.

Knowing the conducting properties of objects is not only useful for elephantnose fish, but is also useful for human society. In medical imaging for instance, information about the conducting properties inside the body can indicate the presence of a tumor. However, it is not an easy task to access the conducting properties of organs from outside the body. The elephantnose fish is a showcase that can do all at once: Taking exterior measurements while perturbing its surroundings with the electric field and afterwards interpreting these measurements to understand the electric properties of objects in its surroundings. In order for scientists to accomplish similar results they need a thorough understanding of the physics involved: How the conductivity inside an object connects to currents and potentials on the outside of the object. Furthermore, they need an idea what measurements on the outside give suitable information of the interior, so that they can recover the conductivity.

There are certain imaging modalities that have accomplished and build on these insights such as acousto-electric tomography, magnetic resonance electrical impedance tomography or current density imaging. What these methods have in common is that they combine measurements of the electric current at the boundary of the object with either ultrasound-induced deformations or measurements of the magnetic field to obtain internal information linked to the conductivity of the object. From this internal information, power or current densities, it is then possible to recover the conductivity in the interior.

We address the problem of recovering the conductivity from the internal information obtained through exterior measurements. We investigate under which mathematical circumstances one is successful with recovering the conductivity. Here we consider different settings: A limited view setting, where one can only access the

object from a part of the boundary or recovering the conductivity in a region on a surface. The former setting is inspired by applications such as breast cancer screening, where one cannot access the boundary of the breast from all angles. The latter setting is inspired by scenarios such as a pipe through a wall that can only be accessed from each side of the wall. The conducting properties of the inaccessible region on the pipe in the wall could give information about possible cracks.

We build the theoretical foundation for problems that are difficult to address in medical imaging or for crack detection. This is only a small step in the complex reconstruction problem and requires modifications in order to be used in practical applications. It is impressive that evolution has helped to create a species of fish that can solve the whole problem, while it requires a tremendous effort to understand and solve the problem from a mathematical perspective.

Summary (Danish)

Svagt elektriske fisk som *elefantfisken* har igennem millioner af år brugt elektriske signaler til at navigere. De genererer et elektrisk felt omkring deres krop, som de kan bruge til at opspore, lokalisere og analysere objekter inden for dette felt. På denne måde har de adgang til de ledende egenskaber af objektet.

Det er ikke kun en fordel for elefantfisken at kende objekters ledende egenskaber, men også for verdens befolkning. For eksempel i medicinsk billedannelse kan information om ledningsevnen i kroppen indikere om personen har en tumor. Det er ikke en nem opgave at tilgå ledningsevnen i organer fra det ydre af kroppen. Elefantfisken er et udmærket eksempel, der kan det hele: Tage målinger fra det ydre af objekter ved at påvirke dens omgivelser med det elektriske felt og efterfølgende tolke disse målinger for at forstå de ledende egenskaber af disse objekter. Det kræver en god forståelse af fysikken involveret for at videnskabsmænd har en chance for at opnå lignende resultater: Hvordan er sammenhængen mellem ledningsevnen i et objekt og strøm eller spændsforskel på det ydre objektet? Derudover kræver det, at videnskabsmændene har et overblik over hvilke målinger fra det ydre vil give den passende information fra det indre, sådan at det er muligt at rekonstruere ledningsevnen.

Der findes eksempler på billedgivende metoder, der har opnået og bygget på netop denne indsigt såsom akustik-elektrisk tomografi, magnetisk resonans elektrisk impedans tomografi eller strømtæthedstomografi. Disse metoder har tilfælles at de kombinerer målinger af den elektriske strøm på ydersiden af objektet med enten ultralyd eller målinger af magnetfeltet for at få information i det indre af objektet. Fra denne information er det så muligt at rekonstruere ledningsevnen i det indre af objektet.

Vi angriber den del af problemet der svarer til at rekonstruere ledningsevnen fra information i det indre af objektet, som er opnået igennem målinger på det ydre. Vi undersøger under hvilke matematiske omstændigheder det lykkedes at rekonstruere ledningsevnen. Her undersøger vi to forskellige scenarier: Et scenarie, hvor vi kun har en begrænset adgang til det ydre af objektet og et andet scenarie, hvor vi vil

rekonstruere ledningsevnen i et areal på en flade. Det første scenarie er motiveret fra anvendelser, hvor man vil undersøge om en kvinde har brystkræft; i dette tilfælde er det ikke muligt at tilgå overfladen af brystet fra alle vinkler. Det andet scenarie er inspireret af anvendelser som et rør i en betonvæg, der kun kan tilgås fra hver side af væggen. De ledende egenskaber fra den utilgængelige del af røret kan give informationer om der er sprækker i røret.

Vi danner det teoretiske grundlag for komplekse problemer i medicinsk billeddannelse eller anvendelsesområder, hvor man skal lokalisere sprækker. Det er kun en lille del i den overordnede problemstilling og kræver modifikationer for at kunne blive brugt i praktiske anvendelsesområder. Det er imponerende, at evolutionen har frembragt en fiskeart der kan løse det hele komplekse problem, mens det kræver en enorm indsats for at forstå og løse problemet fra et matematisk perspektiv.

Preface

This PhD thesis was prepared at the department of Applied Mathematics and Computer Science at the Technical University of Denmark in fulfillment of the requirements for acquiring a PhD degree. The research covered in this thesis was performed between August 1st 2019 and July 31st 2022 in the Section for Scientific Computing under principal supervisor Professor Kim Knudsen and co-supervisor Professor Steen Markvorsen. The period at the Section for Scientific Computing was interrupted by an external research stay between September 25th 2021 and December 31st 2021 at the Department of Mathematics and Statistics at the University of Jyväskylä under supervision of Professor Mikko Salo.

This thesis covers the research on reconstructing electrical conductivities from power densities performed during my PhD studies. The aim is to summarize and present the work and results detailed in the following submitted journal papers and unpublished manuscripts:

(A) Mikko Salo, Hjørdis Schlüter. Jacobian of solutions to the conductivity equation in limited view.
Submitted. Preprint available on arXiv: `http://arxiv.org/abs/2207.03849`.

(B) Bjørn Jensen, Kim Knudsen, Hjørdis Schlüter. Conductivity reconstruction from power density data in limited view.
Submitted. Preprint available on arXiv: `https://arxiv.org/abs/2202.12370`.

(C) Kim Knudsen, Steen Markvorsen, Hjørdis Schlüter. Reconstructing anisotropic conductivities on two-dimensional Riemannian manifolds from power densities.
Manuscript under development. We aim at including results on Riemannian manifolds with higher genus as discussed in section 4.4.2. Preprint available on arXiv: `https://arxiv.org/abs/2202.12056`.

Chapter 1 introduces the different settings studied in this thesis and chapter 2 gives the necessary preliminaries for the geometric setting. Chapters 3-4 are the main chapters that cover the different settings, possible future work and summarizes the papers A-C attached in Appendix A-C. Chapter 5 provides concluding remarks.

Kongens Lyngby, Denmark, July 31, 2022

Hjørdis Amanda Schlüter

Acknowledgements

First, I would like to thank my supervisors Kim Knudsen and Steen Markvorsen. Despite being very busy as the head of PhD school, I know that you, Kim, allocated as much time possible to this project. I would like to thank you for giving me the necessary freedom on the project, for your support and for always believing in me. I would like to thank you, Steen, for always keeping your door open and cheer me up, when things did not go as planned. I enjoyed how you both never lost your enthusiasm for the project and I look forward to continue our collaboration.

I would like to thank my host on the external stay, Mikko Salo. You made me feel very welcome and included me in the research group. This made my experience very rewarding both from a social and scientific perspective. It was a pleasure to collaborate with you and I hope that we can continue the collaboration in the future.

I would like to thank my colleagues for great company and entertaining Friday bars. Especially, I want to thank my office mate and friend, Katrine Ottesen Bangsgaard, for her support and for being there on all the good and bad days. I don't think the PhD experience would have been as pleasant without you.

I would like to thank my boyfriend, Mathias Zambach. You handled all my frustrations and provided me with infinite support. Most importantly, you forced me to take weekends off, when I really needed it. Thank you for always helping me to pursue my dreams.

I would like to thank my family. I particularly want to thank my mother for always believing in me and supporting me.

Contents

CHAPTER 1

Introduction

In this thesis, we address the problem of reconstructing the electrical conductivity γ in a domain Ω from internal power density data. The power density data is assumed to be obtained from exterior measurements. We address the problem in different settings: In the Euclidean plane with either full or limited access to the boundary of Ω and on a Riemannian manifold (M, g) with full access to the boundary.

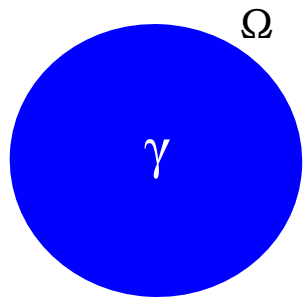

Figure 1.1: Two-dimensional domain in the plane

The electrical conductivity is a materials ability to conduct electric current. Certain materials such as muscle tissue are more conducting in one direction than the other. This motivates to distinguish between isotropic and anisotropic conductivities. In the former case one models the conductivity as a scalar valued function, while in the latter case it is modeled as a matrix valued function to incorporate directional dependencies. In this thesis, we focus on anisotropic conductivities.

Reconstructing the electrical conductivity has received increasing interest over the past 40 years since electrical impedance tomography (EIT) was developed for use in medical imaging. EIT is based on the Calderón problem of determining the conductivity of a medium from voltage and current measurements at the boundary. The interest in conductivity imaging for medical applications is due to the fact that an abnormal conductivity distribution, for instance, can be used for detection and classification of strokes [18, 24, 27]. Furthermore, it can indicate the presence of a

tumor [19, 28], as tumors are more conducting than organs and tissue.

1.1 Applications

Since the 1980s, several hybrid methods has evolved to improve the resolution of EIT. Examples of such hybrid methods are acousto-electric tomography (AET) [4, 30], magnetic resonance electrical impedance tomography (MREIT) [25, 26] and current density imaging (CDI) [5, 16, 29]. These hybrid methods couple two imaging modalities: EIT to provide high contrast with another imaging modality providing high resolution. In AET one thus combines EIT with ultrasound-induced deformations to obtain internal power density data. The ultrasound-induced deformations are realised by acoustic waves that are generated by sources located at the exterior. The acoustic waves perturb the conductivity in the interior of the object. In MREIT and CDI one combines EIT with magnetic resonance imaging (MRI) to obtain current density data. In these modalities on uses the MRI scanner to measure the magnetic field generated by an input current. For MREIT one component of the magnetic field is measured, while for CDI all components are measured. The following two steps summarise the reconstruction approach for all three methods:

1. Combine EIT measurements with ultrasound/MRI measurements to obtain internal power/current density data
2. Reconstruct the conductivity from the internal data

This thesis focuses on the second step under the assumption that internal data is available. Here we mainly address the AET approach of reconstructing the conductivity from power density data.

1.2 Reconstruction in the Euclidean plane

Let us now formulate the problem in Euclidean space in mathematical terms. The conductivity γ is linked to the electric potential u via the conductivity equation:

$$\begin{cases} \operatorname{div}(\gamma \nabla u) = 0 & \text{in } \Omega, \\ u = f & \text{on } \partial\Omega. \end{cases} \tag{1.1}$$

Here $\Omega \subset \mathbb{R}^d$ and f corresponds to a Dirichlet boundary condition imposed on the boundary of Ω, denoted $\partial\Omega$. The imposed potential f gives rise to the current flux $\Lambda_\gamma f = \gamma \nabla u \cdot n|_{\partial\Omega}$ at the boundary, with n denoting the unit outward normal. The

aim of EIT and Calderóns problem is to reconstruct γ from the map $f \mapsto \Lambda_\gamma f$, which is known as the Dirichlet-to-Neumann map (DN map). In AET, one combines measurements of the current flux and ultrasound-induced deformations. This allows one to recover internal power density measurements $H_{ij} = \gamma \nabla u_i \cdot \nabla u_j$ for $1 \leq i, j \leq m$. Here u_i solves (1.1) for the corresponding potential f_i imposed on the boundary. A naive illustration of this procedure is shown in figure 1.2. The reconstruction problem of recovering γ from power densities H_{ij} was addressed for $d = 2$ in [6, 8, 21] and for dimensions $d \geq 3$ in [9, 20, 22]. In this thesis, we will consider the reconstruction approach in [21].

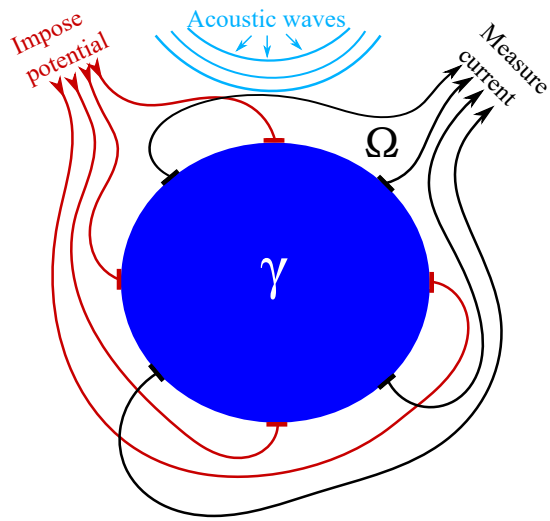

Figure 1.2: A naive illustration of the AET procedure.

1.3 Limited view settings

In certain applications, it is not possible to access the full boundary of the object to take measurements. For instance, for breast cancer detection, one cannot access the breast from all angles and for patients recovering from early-stage breast cancer one is mainly interested in the area of the original tumor bed [13, 17]. This motivates to study reconstruction problems in limited view. Formally, this corresponds to one part of the boundary, $\Gamma \subset \partial\Omega$, that can be controlled by a Dirichlet condition, while on the remaining boundary there is either a zero Dirichlet or a zero Neumann condition. In these cases, the boundary value problems for the potential u take the following

form:

$$\begin{cases} \operatorname{div}(\gamma \nabla u) = 0 & \text{in } \Omega, \\ u = f & \text{on } \Gamma, \\ u = 0 \,/\, \gamma \nabla u \cdot n = 0 & \text{on } \partial\Omega \backslash \Gamma. \end{cases} \tag{1.2}$$

The AET procedure for these settings is illustrated in figure 1.3. In the following, we refer to the boundary value problem (1.1) as the full view setting and the boundary value problems (1.2) as limited view settings.

For the imaging applications AET, MREIT and CDI, it is essential that the Jacobian of a pair of solutions to the boundary value problem (1.2) is non-vanishing:

$$\det[\nabla u_1 \, \nabla u_2] \neq 0, \quad \text{in } \Omega.$$

This poses the question:

Q 1 *Can one find a set of boundary functions $(f_1, \ldots, f_n)$ so that for any γ the corresponding solutions have a non-vanishing Jacobian?*

For the full view setting in dimension $d = 2$ this question has a positive answer and gives constructive conditions on the boundary functions so that the corresponding Jacobian is non-vanishing. In the most simple case of a constant conductivity $\gamma = \mathbb{I}_2$ an answer to this question is formulated in the Radó-Kneser-Choqet theorem [11, 12, 23] and this answer has been generalised to non-constant and anisotropic coefficients in [2, 3, 10]. These results do not generalise to three dimensions; in fact, it is impossible to find explicit choices of a triplet of boundary conditions that work for any γ [1, sec. 6.5]. However, for the n-dimensional case there are results that guarantee existence of a finite number of boundary functions so that locally the Jacobian constraint is satisfied [1, sec. 7.3], [7].

For the limited view setting in (1.2) with a zero Dirichlet condition on $\partial\Omega\backslash\Gamma$ we address question 1 in two dimensions. We cannot apply the Radó-Kneser-Choquet type results mentioned above directly, as these require that the mapping $(x_1, x_2) \mapsto (u_1|_{\partial\Omega}, u_2|_{\partial\Omega})$ is injective, which is not the case in limited view. Therefore, we adapt these results to limited view and propose sufficient conditions under which the corresponding Jacobian is non-vanishing.

For the limited view setting in (1.2) with a zero Neumann condition on $\partial\Omega\backslash\Gamma$ we address question 1 in two and three dimensions. Here, we generalise the results in [1, sec. 7.3] from full view to limited view. This yields existence of a finite number of boundary conditions, so that locally the Jacobian constraint is satisfied.

1.4 Reconstruction on a manifold (M, g)

We consider the problem of reconstructing an electrical conductivity from power density measurements on a Riemannian manifold. This has not been studied in the literature before. However, our work is inspired by the geometric Calderón problem [14,

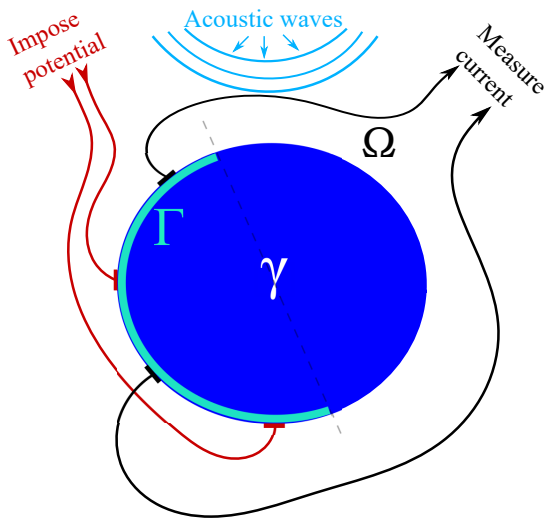

Figure 1.3: A naive illustration of the AET procedure in limited view.

15]. In the following, we therefore present the approach for the geometric Calderón problem and address how this relates to settings that we consider throughout this thesis.

For the Calderón problem one considers a smooth, d-dimensional, compact manifold (M, g) with boundary and solutions u to the conductivity equation

$$\begin{cases} \operatorname{div}_M \left(\operatorname{grad}_M (u)\right) = 0 & \text{in } M, \\ u = f & \text{on } \partial M. \end{cases} \tag{1.3}$$

One is then interested in recovering g from the DN map:

$$\Lambda_g f = g(\operatorname{grad}_M (u), n),$$

where n denotes the outward unit normal of M. It has been shown that in dimensions $d \geq 3$ the problem of recovering the Riemannian metric g from Λ_g is equivalent to recovering γ from Λ_γ in Euclidean space when

$$G = (\det \gamma)^{\frac{1}{d-2}} \gamma^{-1},$$

as they in this case produce the same DN map: $\Lambda_\gamma = \Lambda_g$. Further research on the geometrical Calderón problem concerns which Riemannian metrics $g, \tilde{g}$ produce the same DN map. This is the case for any $g = \psi^* \tilde{g}$, where $\psi : \overline{M} \to \overline{M}$ is a diffeomorphism that is the identity on ∂M. For $d = 2$ this result holds true when g is a conformal multiple of $\psi^* \tilde{g}$ [15].

For our setting one does not have the same equivalence between the problems of recovering an anisotropic conductivity γ from power density data $H_{ij} = \gamma \nabla u_i \cdot \nabla u_j$

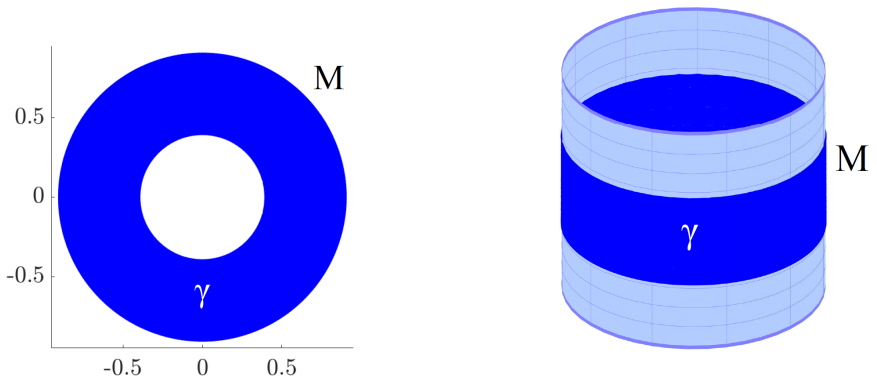

Figure 1.4: Example of a two-dimensional Riemannian manifold with its parameter domain to the left.

in the plane and recovering a Riemannian metric g from power density data $H_{ij} = g(\operatorname{grad}_M(u_i), \operatorname{grad}_M(u_j))$. While for Calderóns problem $G^{-1}\sqrt{\det G}$ enters the PDE and the DN map the same way as the conductivity γ, for our setting the metric g does not appear the same way in the PDE in (1.3) and the power density data. In our setting we have data available over the whole manifold M and not only the boundary, therefore questions addressing which conductivities or metrics give rise to the same data do not make sense.

This motivates that we treat the metric g and the conductivity γ separately: We consider an electrically conductive, compact, two-dimensional Riemannian manifold (M, g) with a smooth boundary ∂M. Here we model the electrical conductivity on M by a $(1,1)$ tensor field γ. We consider the unique solution u to the boundary value problem:

$$\begin{cases} \operatorname{div}_M(\gamma \operatorname{grad}_M(u)) = 0 \text{ in } M, \\ u = f \text{ on } \partial M. \end{cases} \tag{1.4}$$

Figure 1.4 illustrates an example of such a manifold, with M being a strip on a cylinder. The interior current field is $\gamma \operatorname{grad}_M(u)$, i.e. γ is the tensor turning the electric field $\operatorname{grad}_M(u)$ into the current field. By considering m different boundary functions $f = f_i$, $1 \leq i \leq m$, the corresponding solutions to equation (1.4) are denoted by u_i. They define the so-called power density $(m \times m)$-matrix H with elements:

$$H_{ij} = H_{ji} = g(\gamma \operatorname{grad}_M(u_i), \operatorname{grad}_M(u_j)) \quad \text{for} \quad 1 \leq i, j \leq m.$$

There is no literature available on the feasibility of obtaining internal power density measurements following the AET approach on manifolds. This has only been investigated for Euclidean domains. Throughout this thesis we will assume that the data

is available and generalise the constructive reconstruction formula in [21] for 2D Euclidean domains to 2D Riemannian manifolds with a conformal or diagonal metric g. We will discuss why the formula to our knowledge cannot be generalised to general 2D Riemannian manifolds. Furthermore, we show that the PDE in (1.4) and (1.1) are preserved, when g is conformal. As by the Poincaré-Koebe uniformisation theorem every general 2D Riemannian manifold has a conformal representation, this implies that one can use the Euclidean approach to reconstruct γ.

Figure 1.5 shows an illustration of the reconstruction procedure on a 2D Riemannian manifold (M, g), represented by the strip on a cylinder. Here the left hand side represents five power densities, which is the minimal amount necessary in practice (corresponding to $m = 3$ measurements at the boundaries of the strip) to be able to reconstruct γ determined by the three scalar functions γ_{11}, γ_{12} and γ_{22}:

$$\underbrace{\begin{bmatrix} H^{11} & H^{12} & \\ & H^{22} & H^{23} \\ & & H^{33} \end{bmatrix}}_{H} \quad \Longrightarrow \quad \underbrace{\begin{bmatrix} \gamma_{11} & \gamma_{12} \\ & \gamma_{22} \end{bmatrix}}_{\gamma}. \tag{1.5}$$

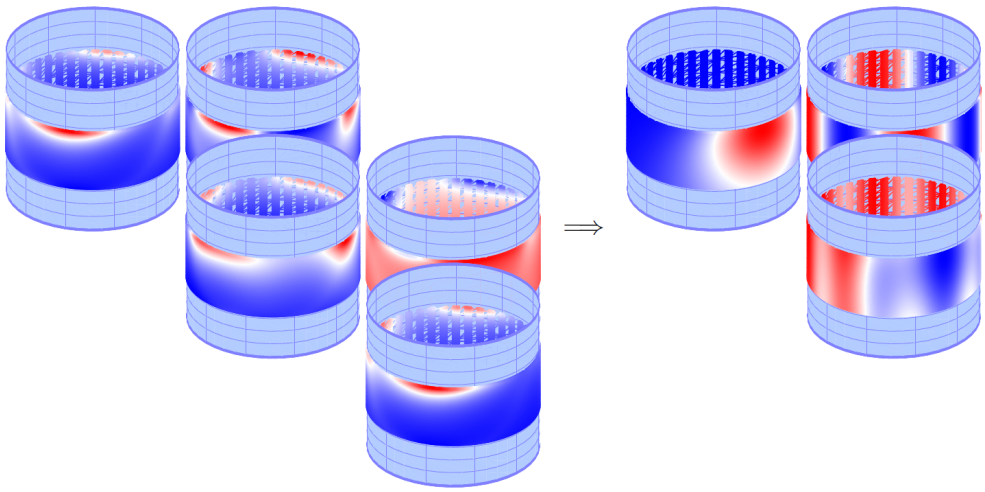

Figure 1.5: Reconstruction procedure on a cylinder: Illustration of the power density measurements needed for reconstructing γ.

1.5 Structure of this thesis

We use the following structure throughout this thesis: Chapter 1 is the introduction that gives an overview over the different settings, puts them into context and presents relevant applications. Chapter 2 contains the geometric preliminaries needed

for our analysis on Riemannian manifolds. Chapter 3 addresses the full and limited view setting in the Euclidean plane. Here we give an overview over the constructive reconstruction procedure from power densities in the plane based on [21] and summarise the results in paper A and B obtained for the different limited view settings. Possible future work for paper A is also discussed. Chapter 4 addresses the reconstruction problem on a 2D Riemannian manifold. It shows a generalisation of the reconstruction procedure in the plane to manifolds with conformal or diagonal metric. It summarises the result in paper C on the preservation of the conductivity equations between a conformal manifold and the Euclidean plane. Furthermore, it addresses possible future work on these topics. Chapter 5 holds concluding remarks and the appendices A-C contains the papers A-C produced during this project. In order to keep page turning to a minimum, each chapter is followed by a bibliography.

Bibliography

[1] Giovanni Alberti and Yves Capdeboscq. *Lectures on elliptic methods for hybrid inverse problems*. Societe Mathematique De France, 2018. ISBN: 978-2-85629-872-5.

[2] G. Alessandrini and V. Nesi. "Quantitative estimates on jacobians for hybrid inverse problems." eng. In: *Bulletin of the South Ural State University, Series: Mathematical Modelling, Programming and Computer Software* 8.3 (2015), pages 25–41. ISSN: 23080256, 20710216. DOI: 10.14529/mmp150302.

[3] Giovanni Alessandrini. "An identification problem for an elliptic equation in two variables." In: *Ann. Mat. Pura Appl. (4)* 145 (1986), pages 265–295. ISSN: 0003-4622. DOI: 10.1007/BF01790543. URL: https://doi-org.proxy.findit.cvt.dk/10.1007/BF01790543.

[4] H. Ammari et al. "Electrical impedance tomography by elastic deformation." In: *Siam Journal on Applied Mathematics* 68.6 (2008), pages 1557–1573.

[5] Guillaume Bal. "Hybrid inverse problems and internal functionals." In: *Inverse problems and applications: inside out. II.* Volume 60. Math. Sci. Res. Inst. Publ. Cambridge Univ. Press, Cambridge, 2013, pages 325–368.

[6] Guillaume Bal, Chenxi Guo, and Francçois Monard. "Linearized internal functionals for anisotropic conductivities." In: *Inverse Problems and Imaging* 8.1 (March 2014), pages 1–22.

[7] Guillaume Bal, Chenxi Guo, and François Monard. "Inverse anisotropic conductivity from internal current densities." In: *Inverse Problems* 30.2 (2014), pages 025001, 21. ISSN: 0266-5611. DOI: 10.1088/0266-5611/30/2/025001.

[8] Guillaume Bal and Gunther Uhlmann. "Reconstruction of Coefficients in Scalar Second-Order Elliptic Equations from Knowledge of Their Solutions." In: *Communications on Pure and Applied Mathematics* 66.10 (April 2013), pages 1629–1652.

[9] Guillaume Bal et al. "Inverse diffusion from knowledge of power densities." In: *Inverse Problems & Imaging* 7.2 (2013), pages 353–375.

[10] Patricia Bauman, Antonella Marini, and Vincenzo Nesi. "Univalent solutions of an elliptic system of partial differential equations arising in homogenization." In: *Indiana Univ. Math. J.* 50.2 (2001), pages 747–757. ISSN: 0022-2518. DOI: 10.1512/iumj.2001.50.1832. URL: https://doi-org.proxy.findit.cvt.dk/10.1512/iumj.2001.50.1832.

[11] Gustave Choquet. "Sur un type de transformation analytique généralisant la représentation conforme et définie au moyen de fonctions harmoniques." In: *Bull. Sci. Math.* 69 (1945), pages 156–165.

[12] Hellmuth Kneser. "Lösung der Aufgabe 41." In: *Jahresbericht der Deutschen Mathematiker-Vereinigung* 35 (1926), pages 123–124.

[13] Cherie M. Kuzmiak et al. “Mammographic Findings of Partial Breast Irradiation.” eng. In: *Academic Radiology* 16.7 (2009), pages 819–825. ISSN: 18784046, 10766332. DOI: 10.1016/j.acra.2009.01.021.

[14] Matti Lassas and Gunther Uhlmann. “On determining a Riemannian manifold from the Dirichlet-to-Neumann map.” eng. In: *Annales Scientifiques De L'ecole Normale Superieure* 34.5 (2001), pages 771–787. ISSN: 18732151, 00129593. DOI: 10.1016/S0012-9593(01)01076-X.

[15] John M. Lee and Gunther Uhlmann. “Determining anisotropic real-analytic conductivities by boundary measurements.” In: *Comm. Pure Appl. Math.* 42.8 (1989), pages 1097–1112. ISSN: 0010-3640. DOI: 10.1002/cpa.3160420804. URL: https://doi-org.proxy.findit.cvt.dk/10.1002/cpa.3160420804.

[16] Wei Li et al. “An acousto-electric inverse source problem.” In: *SIAM J. Imaging Sci.* 14.4 (2021), pages 1601–1616. DOI: 10.1137/21M1406568. URL: https://doi.org/10.1137/21M1406568.

[17] Lingxia Liao et al. “Primary experience of conventional fractionated three-dimensional conformal partial breast irradiation for early-stage breast cancer.” eng. In: *Experimental and Therapeutic Medicine* 2.3 (2011), pages 551–555. ISSN: 17921015, 17920981. DOI: 10.3892/etm.2011.223.

[18] A. McEwan et al. “Design and calibration of a compact multi-frequency EIT system for acute stroke imaging.” eng. In: *Physiological Measurement* 27.5 (2006), S17. ISSN: 13616579, 09673334. DOI: 10.1088/0967-3334/27/5/S17.

[19] Zi Jun Meng et al. “Numerical simulations of MREIT conductivity imaging for brain tumor detection.” In: *Comput. Math. Methods Med.* (2013), Art. ID 704829, 10. ISSN: 1748-670X. DOI: 10.1155/2013/704829. URL: https://doi-org.proxy.findit.cvt.dk/10.1155/2013/704829.

[20] François Monard and Guillaume Bal. “Inverse Anisotropic Conductivity from Power Densities in Dimensionn ≥ 3.” In: *Communications in Partial Differential Equations* 38.7 (July 2013), pages 1183–1207.

[21] François Monard and Guillaume Bal. “Inverse anisotropic diffusion from power density measurements in two dimensions.” eng. In: *Inverse Problems* 28.8 (2012), page 084001. ISSN: 13616420, 02665611. DOI: 10.1088/0266-5611/28/8/084001.

[22] François Monard and Donsub Rim. “Imaging of isotropic and anisotropic conductivities from power densities in three dimensions.” In: *Inverse Problems* 34.7 (May 2018), page 075005.

[23] Tibor Radó. “Aufgabe 41.” In: *Jahresbericht der Deutschen Mathematiker-Vereinigung* 35 (1926), page 49.

[24] A. Romsauerova et al. “Multi-frequency electrical impedance tomography (EIT) of the adult human head: Initial findings in brain tumours, arteriovenous malformations and chronic stroke, development of an analysis method and calibration.” eng. In: *Physiological Measurement* 27.5 (2006), S13. ISSN: 13616579, 09673334. DOI: 10.1088/0967-3334/27/5/S13.

[25] Jin Keun Seo, Ohin Kwon, and Eung Je Woo. “Magnetic resonance electrical impedance tomography (MREIT): conductivity and current density imaging.” In: *Journal of Physics: Conference Series* 12 (January 2005), pages 140–155. DOI: 10.1088/1742-6596/12/1/014. URL: https://doi.org/10.1088/1742-6596/12/1/014.

[26] Jin Keun Seo and Eung Je Woo. “Magnetic resonance electrical impedance tomography (MREIT).” In: *SIAM Rev.* 53.1 (2011), pages 40–68. ISSN: 0036-1445. DOI: 10.1137/080742932. URL: https://doi-org.proxy.findit.cvt.dk/10.1137/080742932.

[27] Xuetao Shi et al. “Experimental study on early detection of acute cerebral ischemic stroke using electrical impedance tomography method.” eng. In: *Ifmbe Proceedings* 25.2 (2009), pages 510–513. ISSN: 14339277, 16800737. DOI: 10.1007/978-3-642-03879-2_143.

[28] Jaewook Shin et al. “Initial study on in vivo conductivity mapping of breast cancer using MRI.” eng. In: *Journal of Magnetic Resonance Imaging* 42.2 (2015), pages 371–378. ISSN: 10531807, 15222586. DOI: 10.1002/jmri.24803.

[29] Thomas Widlak and Otmar Scherzer. “Hybrid tomography for conductivity imaging.” In: *Inverse Problems* 28.8 (2012), pages 084008, 28. ISSN: 0266-5611. DOI: 10.1088/0266-5611/28/8/084008. URL: https://doi.org/10.1088/0266-5611/28/8/084008.

[30] Hao Zhang and Lihong V. Wang. “Acousto-electric tomography.” In: *Proc. SPIE 5320, Photons Plus Ultrasound: Imaging and Sensing* (2004).

CHAPTER 2

Geometric preliminaries

As this thesis was written from the viewpoint of an author with a background in Analysis and PDEs, we include some preliminaries on two-dimensional Riemannian manifolds that we need for our investigations in chapter 4. This chapter is inspired by [1].

2.1 Tangent spaces & cotangent spaces

Consider a two-dimensional Riemannian manifold (M, g) that is defined by the manifold M and metric g. We start by introducing the concept of *tangent spaces* and *cotangent spaces* for (M, g). To every point $x = (x^1, x^2)$ on the manifold one can attach a *tangent space* T_xM which is a vector space formed by the derivations, i.e. the tangent vectors of smooth curves on (M, g) through that point. When we consider standard coordinates x^1 and x^2 and the corresponding standard basis $\{\frac{\partial}{\partial x^1} = e_1\,,\ \frac{\partial}{\partial x^2} = e_2\}$ in $\mathbb{R}^2$, each tangent vector $V \in T_xM$ has unique coordinates (v^1, v^2) so that:

$$V = v^1\, e_1(x) + v^2\, e_2(x).$$

The Riemannian metric g, which is symmetric and positive definite, allows us to measure lengths of vectors in each tangent space. To g we associate the metric matrix function $G(x^1, x^2)$ with the following coordinate expression:

$$G(x^1, x^2) = \begin{bmatrix} G_{11}(x^1, x^2) & G_{12}(x^1, x^2) \\ G_{12}(x^1, x^2) & G_{22}(x^1, x^2) \end{bmatrix}.$$

Similar to the tangent space, at every point x there exists a *cotangent space* T_x^*M, defined as the dual space of T_xM consisting of linear functionals on T_xM. Collecting the tangent spaces and cotangent spaces for all points x on the manifold yields the *tangent bundle* TM and *cotangent bundle* T^*M respectively.

2.2 Derivatives, gradient and divergence

Next, we introduce the concept of the *directional derivative*. Let $V = v^1 e_1 + v^2 e_2$ be a vector field and f be a function on (M, g). Then the *V-directional derivative* of f at each point x is:

$$V_x(f) = v^1(x)\frac{\partial f}{\partial x^1} + v^2(x)\frac{\partial f}{\partial x^2}.$$

From this, we can define the *gradient vector field* of f as the unique vector field $\operatorname{grad}_M(f)$ which satisfies

$$g(\operatorname{grad}_M(f), V) = V(f),$$

for all vector fields V. This yields the following expression in local coordinates of the gradient at the point x:

$$\operatorname{grad}_M(f)(x) = \sum_{k,\ell=1}^{2} G^{k\ell}(x)\frac{\partial f}{\partial x^\ell} e_k.$$

Furthermore, we can define the *divergence* of a vector field. For that purpose we introduce the *Christoffel symbols* Γ_{ij}^m:

$$\Gamma_{ij}^m = \Gamma_{ji}^m = \frac{1}{2}\sum_{\ell=1}^{2}\left(\frac{\partial g_{j\ell}}{\partial x^i} + \frac{\partial g_{\ell i}}{\partial x^j} - \frac{\partial g_{ij}}{\partial x^\ell}\right) g^{\ell m}.$$

Using the Christoffel symbols, we have the following equivalent coordinate expressions for the divergence of a vector field V:

$$\begin{aligned}\operatorname{div}_M(V) &= \frac{1}{\sqrt{\det(G)}}\sum_{i=1}^{2}\frac{\partial}{\partial x^i}\left(v^i\sqrt{\det(G)}\right)\\ &= \sum_{i,j=1}^{2}\left(\frac{\partial v^i}{\partial x^i} + \Gamma_{ij}^i v^j\right).\end{aligned}$$

2.3 Integrals

We define the *volume form*, which is a unique 2-form on M. As M is oriented, at each point x on the manifold (M, g) there is a local orthonormal frame $\{E_1, E_2\}$ which gives a positive orthonormal basis of $T_y M$ for y near x. The volume form is denoted by $\mathrm{d}V$ such that $\mathrm{d}V(E_1, E_2) = 1$ for any positive local orthonormal frame. It is given by the following expression in local coordinates:

$$\mathrm{d}V = \sqrt{\det G}\,\mathrm{d}x^1 \wedge \mathrm{d}x^2.$$

For the function f on (M, g) we can use the volume form to obtain $f\,\mathrm{d}V$, which is a 2-form. We can then integrate f over M, by integrating the 2-form $f\,\mathrm{d}V$. The

L^2-inner product between real valued functions $u, v \in C^\infty(M)$ is given by

$$(u, v)_{L^2(M)} = \int_M uv \, \mathrm{d}V.$$

Similarly to Euclidean space the L^2 norm is defined by

$$\|u\|_{L^2(M)} = (u, u)^{\frac{1}{2}}_{L^2(M)}.$$

Furthermore, we can define the L^2 inner product for vector valued functions $u, v \in C^\infty(M, T^2M)$:

$$(u, v)_{L^2(M)} = \int_M g(u, v) \, \mathrm{d}V.$$

From this we can define the $H^1(M)$ inner product for functions $u, v \in H^1(M)$:

$$\begin{aligned}(u, v)_{H^1(M)} &= (u, v)_{L^2(M)} + (\mathrm{grad}_M(u), \mathrm{grad}_M(v))_{L^2(M)} \\ &= \int_M uv \, \mathrm{d}V + \int_M g(\mathrm{grad}_M(u), \mathrm{grad}_M(v)) \, \mathrm{d}V.\end{aligned}$$

Bibliography

[1] Mikko Salo. “The Calderón problem on Riemannian manifolds.” In: *Inverse problems and applications: inside out. II.* Volume 60. Math. Sci. Res. Inst. Publ. Cambridge Univ. Press, Cambridge, 2013, pages 167–247.

CHAPTER 3

Reconstructing conductivities from power densities in the Euclidean plane

In section one of this chapter we go through the reconstruction approach for anisotropic conductivities from power densities in the Euclidean setting. The approach is implemented and used for numerical examples in section two of this chapter and builds the basis for the reconstruction approach on 2D Riemannian manifolds in chapter 4. In section two we address two limited view settings, where only a part of the boundary of the domain can be controlled by a Dirichlet condition. These two settings were the basis for two papers: Paper A, *Jacobian of solutions to the conductivity equation in limited view* and Paper B, *Conductivity reconstruction from power density data in limited view*. Section two is based on and summarises these two papers.

3.1 Constructive reconstruction approach for anisotropic conductivities

This section lists the reconstruction procedure for an anisotropic conductivity from power densities based on [5]. To distinguish between the quantities in Euclidean space and on the Riemannian manifold in the next chapter, we denote the quantities in this section with upper index "E", while in the next chapter they are denoted by upper index "M".

Throughout this section, we consider the following setting:

We consider solutions u_i to the conductivity equation

$$\begin{cases} -\operatorname{div}(\gamma \nabla u_i) = 0 & \text{in } \Omega, \\ u_i = f_i & \text{on } \partial\Omega, \end{cases} \tag{3.1}$$

where u_i corresponds to the electric potential that solves the boundary value problem above for the corresponding electric potential f_i imposed on the boundary of Ω. Existence and uniqueness of solutions $u_i \in H^1(\Omega)$ to the above boundary value problem is classical, see e.g. [6, Corollary 8.22]. We let $\Omega \subset \mathbb{R}^2$ be an open, connected, bounded domain and $\gamma \in L^\infty(\Omega)$ be a real 2×2 symmetric matrix that satisfies the uniform ellipticity condition

$$\lambda |\xi|^2 \leq \gamma \xi \cdot \xi \leq \Lambda |\xi|^2 \quad \text{for every } \xi = (\xi^1, \xi^2) \in \mathbb{R}^2,$$

for some $\lambda, \Lambda > 0$. The reconstruction procedure is characterised by reconstructing the anisotropic conductivity γ from internal power density measurements on the form

$$H_{ij}^E = \gamma \nabla u_i \cdot \nabla u_j, \quad 1 \leq i, j \leq m.$$

These measurements are stored in a $m \times m$ matrix H^E. For the reconstruction procedure to be well-defined we assume throughout the following that the boundary functions f_i were chosen such that the corresponding solutions u_i satisfy the following Jacobian constraint and gradient condition:

$$\min\left(\det([\nabla u_1 \, \nabla u_2]), \det([\nabla u_3 \, \nabla u_4])\right) \geq c_0 > 0, \tag{3.2}$$

$$\nabla \log\left(\frac{\det([\nabla u_1 \, \nabla u_2])}{\det([\nabla u_3 \, \nabla u_4])}\right) \neq 0, \tag{3.3}$$

for every $x \in \Omega$. The first condition corresponds to positive Jacobians for the pairs of solutions (u_1, u_2) and (u_3, u_4). Non-vanishing of the Jacobians ensures invertibility of the submatrices of H^E corresponding to each pair of solutions. We restrict ourselves to positive Jacobians to avoid complex values in the reconstruction procedure, when calculating $\sqrt{\det([\nabla u_1 \, \nabla u_2])}$ or $\sqrt{\det([\nabla u_3 \, \nabla u_4])}$. The latter condition (3.3) is directly motivated by the reconstruction procedure and guarantees that the right hand side in a linear system of equations is non-vanishing.

Based on γ another 2×2 symmetric matrix function $A \in L^\infty(\Omega)$ is introduced that satisfies the pointwise relation $A^2(x) = \gamma(x)$ with $x = (x_1, x_2)$. Also, the vector fields $S_i^E = A \nabla u_i$ are introduced for $1 \leq i \leq m$ so that the power density data formulates to

$$H_{ij}^E = S_i^E \cdot S_j^E.$$

Now the conductivity equation in (3.1) can be expressed in terms of the vector fields S_i^E as

$$\operatorname{div}(A S_i^E) = 0.$$

The focus of the reconstruction procedure is then to reconstruct A, as this will give γ immediately. The procedure consists of two steps and for that purpose, A is decomposed into two parts. In that regard the normalised anisotropy $\tilde{A}$ is defined as

$$\widetilde{A} = \det(A)^{-\frac{1}{2}} A, \quad \text{such that} \quad \det\Big(\widetilde{A}\Big) = 1,$$

so that A can be decomposed into $A = \det(A)^{\frac{1}{2}} \widetilde{A}$.

The procedure is based on two important equations to be presented in the next subsection. For that purpose $S^E = [S_1^E, S_2^E]$ is orthonormalised into a $SO(2)$-valued frame $R^E = [R_1^E\, R_2^E]$. This is obtained by finding a matrix T such that $R^E = S^E (T^E)^T$. This matrix T^E gives rise to the vector fields V_{ij}^E:

$$V_{ij}^E = \sum_{k=1}^{2} \nabla(T_{ik}^E) T^{E,kj}, \quad 1 \le i,j \le 2, \quad V_{ij}^{E,a} = \frac{1}{2}(V_{ij}^E - V_{ji}^E).$$

The frame R^E is then parameterised as the following rotational operator

$$R^E = \begin{bmatrix} \cos\theta^E & -\sin\theta^E \\ \sin\theta^E & \cos\theta^E \end{bmatrix}, \tag{3.4}$$

rotating any vector by θ^E degrees in positive direction. As S_1^E and S_2^E are assumed to satisfy the following by the Jacobian constraint (3.2)

$$\det\big(H^E\big)^{\frac{1}{2}} = \det\left(\big[S_1^E\, S_2^E\big]\right) \ge c_1 > 0, \tag{3.5}$$

one can derive the first important equation. This is based on the fact that

$$0 = \operatorname{div}\left(\begin{bmatrix} -\partial_2 u_i \\ \partial_1 u_i \end{bmatrix}\right) = \operatorname{div}(J^E A^{-1} S_i^E) \quad \text{with} \quad J^E = \begin{bmatrix} 0 & -1 \\ 1 & 0 \end{bmatrix}.$$

The first important equation corresponding to [5, eq.(8)] then reads

$$\nabla \log(\det A) = \frac{1}{2} \nabla \log\big(\det H^E\big) + \sum_{j,\ell=1}^{2} \Big(\nabla \big(H^E\big)^{j\ell} \cdot \widetilde{A} S_\ell^E\Big)\, \widetilde{A}^{-1} S_j^E. \tag{3.6}$$

The second important equation corresponding to [5, eq.(10)] is on the form

$$\widetilde{A}^2 \nabla\theta + [\widetilde{A}_2, \widetilde{A}_1] = \widetilde{A}^2 V_{12}^{E,a} - \frac{1}{2} J^E N^E, \tag{3.7}$$

with $N^E = \frac{1}{2}\nabla \log\big(\det\big(H^E\big)\big)$. It is derived by writing the Lie bracket $[\tilde{A}R_2, \tilde{A}R_1]$ in two different ways. The main challenge in the reconstruction procedure is to reconstruct $\tilde{A}$ from equation (3.7), as (3.7) both depends on $\tilde{A}$ and the unknown

function θ^E. For this purpose one needs two pairs of boundary conditions that both give rise to solutions that satisfy equation (3.7):

$$\widetilde{A}^2\nabla\theta_i^E + [\widetilde{A}_2, \widetilde{A}_1] = \widetilde{A}^2 V_{12}^{E,a(i)} - \frac{1}{2}J^E N^{E,(i)}. \tag{3.8}$$

Here (i) in θ_i^E, $V_{12}^{E,a(i)}$ and $N^{E,(i)}$ indicates the respective pair of solutions that gives rise to these functions and vector fields for $i = 1, 2$. Subtracting equation (3.8) with $i = 1$ from the same equation with $i = 2$ yields

$$\tilde{A}^2\left(\nabla(\theta_2^E - \theta_1^E) - V_{12}^{E,a(2)} + V_{12}^{E,a(1)}\right) = -\frac{1}{2}J^E(N^{E,(2)} - N^{E,(1)}). \tag{3.9}$$

From (3.9) it is then possible to express the functions $\cos\big(\theta_2^E - \theta_1^E\big)$ and $\sin\big(\theta_2^E - \theta_1^E\big)$, and hence also $\nabla(\theta_2^E - \theta_1^E)$ by the data, when taking inner products between columns of the two R-matrices $R^{E,(1)}$ and $R^{E,(2)}$:

$$\begin{aligned}\cos\big(\theta_2^E - \theta_1^E\big) &= R_1^{E,(1)} \cdot R_1^{E,(2)} = \sum_{i,j=1}^{2} T_{1i}^{E,(1)} T_{1j}^{E,(2)} H_{i(2+j)}^E \\ \sin\big(\theta_2^E - \theta_1^E\big) &= R_2^{E,(1)} \cdot R_1^{E,(2)} = \sum_{i,j=1}^{2} T_{2i}^{E,(1)} T_{1j}^{E,(2)} H_{i(2+j)}^E.\end{aligned} \tag{3.10}$$

By the chain rule it follows that

$$\nabla(\theta_2^E - \theta_1^E) = \cos\big(\theta_2^E - \theta_1^E\big)\nabla\sin\big(\theta_2^E - \theta_1^E\big) - \sin\big(\theta_2^E - \theta_1^E\big)\nabla\cos\big(\theta_2^E - \theta_1^E\big)$$

so the gradient $\nabla(\theta_2^E - \theta_1^E)$ is solely determined by entries of the $T^{E,(i)}$-matrices and the 4×4 matrix H^E that contains all possible combinations of power density data.

3.1.1 Equations for the reconstruction procedure

Parts of this section are taken from Appendix A section 4.
For the first step in the reconstruction procedure one reconstructs $\widetilde{A}$ from equation (3.9) and therefore needs data corresponding to $m = 4$ boundary conditions. By the above analysis all quantities apart from $\widetilde{A}$ depend solely on the data. Therefore, solving this equation for $\widetilde{A}$ boils down to solving a linear system of equations.

For the second step in the reconstruction procedure one reconstructs the angle θ^E to be able to determine the vector fields $S_i^E = A\nabla u_i$ from the entries of $H_{ij}^E = \gamma\nabla u_i \cdot \nabla u_j$. For this one needs data corresponding to $m = 2$ measurements. θ^E is reconstructed by solving the following gradient equation which is deduced from equation (3.7):

$$\nabla\theta^E = F^E, \tag{3.11}$$

with

$$F^E = V_{12}^{E,a} - \widetilde{A}^{-2}\left(\frac{1}{2}J^E N^E + [\widetilde{A}_2, \widetilde{A}_1]\right).$$

Once θ^E is known at at least one point on the boundary one can integrate F^E along curves originating from that point to obtain θ^E throughout the whole domain. Alternatively, when assuming that θ^E is known along the whole boundary one can apply the divergence operator to (3.11) and solve the following Poisson equation with Dirichlet boundary condition:

$$\begin{cases} \Delta\theta^E = \nabla \cdot F^E & \text{in } \Omega, \\ \theta^E = \theta^E_{\text{true}} & \text{on } \partial\Omega. \end{cases} \tag{3.12}$$

For the third step in the reconstruction procedure one reconstructs the determinant $(\det A)$ from equation (3.6) requiring data from $m = 2$ measurements. Equation (3.6) can be simplified further to be on the following form:

$$\nabla \log(\det A) = G^E,$$

with

$$\begin{aligned} G^E &= \cos\big(2\theta^E\big)K^E + \sin\big(2\theta^E\big)J^E K^E, \\ K^E &= U^E \tilde{A}(V^E_{11} - V^E_{22}) + J^E U^E \tilde{A}(V^E_{12} + V^E_{21}), \quad \text{and} \quad U^E = \begin{bmatrix} 1 & 0 \\ 0 & -1 \end{bmatrix}. \end{aligned}$$

Similarly as for θ^E, one needs to solve a gradient equation to obtain $(\det A)$ and has the possibility of either integrating along curves or solving a Poisson equation, assuming knowledge of γ in one point or along the whole boundary respectively. We assume knowledge of γ along the whole boundary and solve the following Poisson problem with Dirichlet condition:

$$\begin{cases} \Delta \log(\det A) = \nabla \cdot G^E & \text{in } \Omega, \\ \log(\det A) = \log(\det A_{\text{true}}) & \text{on } \partial\Omega. \end{cases} \tag{3.13}$$

These steps yield the reconstruction procedure outlined in algorithm 1.

Algorithm 1 Euclidean anisotropic reconstruction procedure

Choose a set of boundary conditions (f_1, f_2, f_3, f_4) so that the corresponding solutions satisfy condition (3.2) and (3.3)

1. Reconstruct $\tilde{A}$ by solving equation (3.9) and using data from all four boundary conditions above
2. Reconstruct θ^E by solving the boundary value problem (3.12) and using data from the pair (f_1, f_2) of boundary conditions above
3. Reconstruct $(\det A)$ by solving the boundary value problem (3.13) and using data from the pair (f_1, f_2) of boundary conditions above

3.1.1.1 Simplification of the equations when the conductivity is isotropic

When the conductivity is isotropic we will denote it by σ instead of γ. In this case $\widetilde{A}$ equals the identity which makes the first step in the reconstruction procedure redundant. Therefore, the assumption (3.3) is redundant as well, the only requirement on the power density data is the Jacobian constraint (3.2). We note, that for the second step in algorithm 1 F^E simplifies to:

$$F^E = V_{12}^{E,a} - \frac{1}{2} J^E N^E, \tag{3.14}$$

while K^E in the third step simplifies to:

$$K^E = U^E(V_{11}^E - V_{22}^E) + J^E U^E(V_{12}^E + V_{21}^E). \tag{3.15}$$

Note also that in this case $(\det A) = \sigma$ so that the Poisson problem for σ reads:

$$\begin{cases} \Delta \log(\sigma) = \nabla \cdot G^E & \text{in } \Omega, \\ \log(\sigma) = \log(\sigma_{\text{true}}) & \text{on } \partial\Omega. \end{cases} \tag{3.16}$$

The simplified reconstruction procedure for an isotropic conductivity is outlined in algorithm 2.

Algorithm 2 Euclidean isotropic reconstruction procedure

Choose a pair of boundary conditions (f_1, f_2) so that the corresponding solutions satisfy condition (3.2)

1. Reconstruct θ^E by solving the boundary value problem (3.12) with F^E defined in (3.14)
2. Reconstruct $(\det A)$ by solving the boundary value problem (3.16) with K^E defined in (3.15)

3.1.2 Well-posedness of the reconstruction procedure

The question is, whether one can be sure that there exists a set of boundary conditions for which the conditions (3.2) and (3.3) are satisfied. Using a construction with Complex Geometrical Optics (CGO) solutions it is shown in the proof of [5, Lemma 2.1] that these conditions are satisfied under the assumption that $(\det \gamma)^{\frac{1}{2}} \in H^{5+\varepsilon}(\Omega)$ for some $\varepsilon > 0$ and that the function ν is locally of class C^4 over Ω. With ν defined as

$$\nu(x) = \frac{\gamma_{22} - \gamma_{11} - 2i\gamma_{12}}{\gamma_{11} + \gamma_{22} + 2\det(\gamma)^{\frac{1}{2}}}(x).$$

Furthermore, by [5, Theorem 2.2 & Theorem 2.4] $\tilde{A}$ and $(\det A)$ are determined uniquely by the power density measurements H and they can be reconstructed stably according to the following stability estimates:

$$\left\|\tilde{A}-\tilde{A}'\right\|_{L^\infty(X)} \leq C\|H-H'\|_{W^{1,\infty}} \tag{3.17a}$$

$$\|\log(\det A)-\log(\det A')\|_{W^{1,\infty}(X)} \leq C\|H-H'\|_{W^{1,\infty}}, \tag{3.17b}$$

Where H and H' correspond to power densities that are determined by γ and γ' respectively, using the same boundary measurements (f_1, f_2, f_3, f_4).

3.1.3 Choice of the transfer matrix T^E used for numerical experiments

This is taken from Appendix B section 4.3.

The transfer matrix T^E with corresponding rotation matrix R^E is uniquely defined up to a rotation. In theory, the choice of T^E will not influence the reconstruction procedure, as every choice of T^E with corresponding θ^E will work to extract the vector fields $S_i^E = A\nabla u_i$ from the entries of $H_{ij} = \gamma\nabla u_i \cdot \nabla u_j$. However, numerically a simple choice of T^E can be an advantage. For this reason, we choose Gram-Schmidt orthonormalisation to obtain the following T^E, as in this case the vector fields V_{ij}^E have the simplified form as in (3.20):

$$T^E = \begin{bmatrix} (H_{11}^E)^{-\frac{1}{2}} & 0 \\ -H_{12}^E(H_{11}^E)^{-\frac{1}{2}}(D^E)^{-1} & (H_{11}^E)^{\frac{1}{2}}(D^E)^{-1} \end{bmatrix}, \tag{3.18}$$

with $D^E = (H_{11}^E H_{22}^E - H_{12}^2)^{\frac{1}{2}}$. By the Jacobian condition (3.22), $H_{11}^E > 0$ and thus T^E is well-defined. For this choice of T^E the function θ^E is given by the angle between $A\nabla u_1$ and the x_1-axis, as in this case the first column of R^E simplifies to

$$R_1^E = T_{11}^E S_1^E + T_{12}^E S_2^E = \frac{A\nabla u_1}{|A\nabla u_1|},$$

so that

$$\theta^E = \arg(A\nabla u_1). \tag{3.19}$$

In addition, the vector fields V_{ij}^E can be written explicitly in terms of H^E:

$$\begin{aligned} V_{11}^E &= \nabla \log\left(H_{11}^E\right)^{-\frac{1}{2}}, \qquad V_{12}^E = 0, \\ V_{21}^E &= -\frac{H_{11}^E}{D^E}\nabla\left(\frac{H_{12}^E}{H_{11}^E}\right), \quad V_{22}^E = \nabla \log\left(\frac{(H_{11}^E)^{\frac{1}{2}}}{D^E}\right). \end{aligned} \tag{3.20}$$

3.1.4 Knowledge of θ^E at the boundary

From equation (3.19) we know that θ^E is the angle between $A\nabla u_1$ and the x_1-axis (for an isotropic conductivity this is the angle between ∇u_1 and the x_1-axis). As it is assumed that the conductivity γ can be measured along the boundary, this corresponds to knowledge of the current $\gamma\nabla u_1$. We can decompose the current into two parts with contribution from the unit normal n and the tangent vector $t = J^E n$:

$$\gamma\nabla u_1 = (\gamma\nabla u_1 \cdot n)n + (\gamma\nabla u_1 \cdot t)t.$$

In the case of pure Dirichlet boundary conditions, the tangential component of $\gamma\nabla u_1$ is known. In order to have full information of $\gamma\nabla u_1$ along the boundary one also needs information about the normal component corresponding to the Neumann data $\gamma\nabla u_1 \cdot n$.

3.2 Different limited view settings

3.2.1 Paper A: *Jacobian of solutions to the conductivity equation in limited view*

In paper A we aim at generalising theoretical results for the Jacobian of solutions to the conductivity equation from a full view to a limited view setting. We consider solutions u_1 and u_2 to the boundary value problem

$$\begin{cases} -\mathrm{div}(\gamma\nabla u_i) = 0 & \text{in } \Omega, \\ u_i = f_i & \text{on } \Gamma, \\ u_i = 0 & \text{on } \partial\Omega\backslash\Gamma. \end{cases} \tag{3.21}$$

Here $\Omega \subset \mathbb{R}^2$ is a bounded Lipschitz domain, $\gamma \in L^\infty(\Omega, \mathbb{R}^{2\times 2})$ is an anisotropic conductivity and $\Gamma \subset \partial\Omega$ a non-empty closed part of the boundary that we can control. We propose sufficient conditions on the boundary functions f_1 and f_2 so that the corresponding solutions satisfy

$$\det[\nabla u_1\, \nabla u_2] \neq 0. \tag{3.22}$$

Existing results for the full view setting (e.g. [3]) cannot be applied directly, as the mapping defined by the boundary functions $(x_1, x_2) \mapsto (u_1|_{\partial\Omega}, u_2|_{\partial\Omega})$ is not injective. However, we can adapt these results to limited view. In this context it is natural to allow for discontinuous boundary functions. Therefore, we consider the problem (3.21) in weighted Sobolev spaces. To obtain similar results as in [3] we then prove a weak maximum principle for solutions to (3.21) in these weighted spaces.

As pointed out in section 3.1 the non-vanishing Jacobian is an essential assumption for the reconstruction procedure of the conductivity from power densities. For that

purpose we supplement the theoretical result with numerical examples on a choice of boundary functions (f_1, f_2) that yield power density data from which an isotropic conductivity σ is reconstructed.

3.2.1.1 Theoretical results

Throughout the paper we assume that the conductivity matrix γ is symmetric and satisfies for some $\lambda, \Lambda > 0$ the ellipticity condition

$$\lambda|\xi|^2 \leq \gamma\xi \cdot \xi \leq \Lambda|\xi|^2 \quad \text{for a.e. } x \in \Omega \text{ and all } \xi \in \mathbb{R}^2. \tag{3.23}$$

We want to prescribe discontinuous boundary functions $u_i|_{\partial\Omega}$ that are piecewise C^1 and hence they are also in $H^s(\partial\Omega)$ when $s < \frac{1}{2}$. The corresponding solutions u_i to the boundary value problem (3.21) are then in the weighted space $H^1(\Omega, d^{1-2s})$ (see Thm. 2.5 in Appendix A). Therefore, we limit ourselves to work with these weighted spaces, where $H^1(\Omega, d^{1-2s})$ is the space of all $u_i \in L^2_{\text{loc}}(\Omega)$ with $\|u_i\|_{H^1(\Omega,d^{1-2s})} < \infty$, where the norm is defined as:

$$\begin{aligned}
\|u_i\|_{L^2(\Omega,d^{1-2s})} &= \left\| u_i d^{\frac{1-2s}{2}} \right\|_{L^2(\Omega)}, \\
\|u_i\|_{H^1(\Omega,d^{1-2s})} &= \|u_i\|_{L^2(\Omega,d^{1-2s})} + \|\nabla u_i\|_{L^2(\Omega,d^{1-2s})}.
\end{aligned}$$

For these solutions we prove a weak maximum principle when $\left|s - \frac{1}{2}\right| < \varepsilon$ so that we can use a similar approach as in [3] to relate the number of critical points of u_i to the oscillations of u_i at the boundary. This result can be used to obtain the non-vanishing Jacobian condition (3.22).

Main result

In order to proscribe any zeros of the Jacobian, we use an existing result in the literature. This gives a lower bound for the number of oscillations of u at the boundary induced by a single critical point in the interior. For this result γ is required to be $C^{0,\alpha}(\overline{\Omega})$. To arrive at the lower bound we use that the solution u oscillates locally around a critical point x_0. In fact, there are at least two regions around x_0 for which u is larger than $u(x_0)$ and at least two regions for which u is smaller than $u(x_0)$ in alternating order around x_0 (see Prop. 2.1 Appendix A). By the weak maximum principle this local behavior translates to the boundary. One can then prevent existence of an interior critical point by prescribing a boundary function that has at most one nonincreasing part and at most one nondecreasing part along the boundary.

The same approach can be used to prevent existence of a point for which the Jacobian is zero. If such a point $x_{(1)}$ exists, this implies that there is a linear combination between ∇u_1 and ∇u_2 at $x_{(1)}$ so that

$$\alpha_1 \nabla u_1(x_{(1)}) + \alpha_2 \nabla u_2(x_{(1)}) = 0,$$

for some $\alpha_1, \alpha_2 \in \mathbb{R}^2\backslash\{0\}$. This corresponds to a critical point of the following function u:

$$u = \alpha_1 u_1 + \alpha_2 u_2.$$

By the above observation this function has no interior critical points and hence the Jacobian is non-vanishing, when it has at most one nonincreasing and at most one nondecreasing part at the boundary for arbitrary $\alpha_1, \alpha_2 \in \mathbb{R}^2\backslash\{0\}$.

In order to satisfy the above condition on nonincreasing and nondecreasing parts on the boundary, one needs to pick suitable boundary functions f_1 and f_2. For that purpose we parameterise Γ as the closed arc $\Gamma = \beta([0, \ell])$ in $\partial\Omega$. We then consider the regular curve $\eta : [0, \ell] \to \mathbb{R}^2, \eta(t) = (f_1(\beta(t)), f_2(\beta(t)))$, and consider the winding number of $\dot{\eta}$ (when the curve is closed). However, as the winding number is only defined for closed curves, we consider a generalised definition for non-closed curves:

$$\mathrm{Ind}(\dot{\eta}) = \frac{\arg(\dot{\eta}(\ell)) - \arg(\dot{\eta}(0))}{2\pi}.$$

We then use the following parameterisation of u on Γ:

$$g(t) = u(\beta(t)) = \alpha \cdot \eta(t), \tag{3.24}$$

with $\alpha = (\alpha_1, \alpha_2) \in \mathbb{R}^2\backslash\{0\}$. We extend g by zero to $[0, 2\pi)$. Following this definition its derivative satisfies

$$g(t) = \alpha \cdot \dot{\eta}(t). \tag{3.25}$$

This yields the main result (corresponding Theorem 2.2 in Appendix A) with the following two sufficient conditions on f_1 and f_2 for which (a) is related to continuous boundary conditions, while (b) concerns discontinuous boundary conditions:

Theorem 3.1 *Let $\Omega \subset \mathbb{R}^2$ be a bounded simply connected domain with C^1 boundary curve $\beta : [0, 2\pi] \to \partial\Omega$, and let $\gamma \in C^{0,\alpha}(\overline{\Omega}; \mathbb{R}^{2\times 2})$ satisfy (3.23). Let $\Gamma = \beta([0, \ell])$ be a closed arc in $\partial\Omega$. Let $f_1, f_2 \in C^1(\Gamma)$ be linearly independent, and assume that u_i is the unique solution of*

$$\begin{cases} -\mathrm{div}(\gamma \nabla u_i) = 0 & \text{in } \Omega, \\ u_i = f_i & \text{on } \Gamma \\ u_i = 0 & \text{on } \partial\Omega\backslash\Gamma. \end{cases} \tag{3.26}$$

Assume that the curve $\eta : [0, \ell] \to \mathbb{R}^2$, $\eta(t) = (f_1(\beta(t)), f_2(\beta(t)))$ is regular, $\arg(\dot{\eta}(t))$ is monotone, and that one of the following holds:

(a) $u_i|_{\partial\Omega}$ are continuous, and $|\mathrm{Ind}(\dot{\eta})| \leq 1$; or

(b) $u_i|_{\partial\Omega}$ are continuous at $\eta(0)$, and $|\mathrm{Ind}(\dot{\eta})| \leq 1/2$.

Then $\det[\nabla u_1(x)\, \nabla u_2(x)] \neq 0$ for all $x \in \Omega$.

(a) Idea of the proof: As $|\mathrm{Ind}(\dot{\eta})|$ is at most 1, the vectors α and $\dot{\eta}(t)$ in the expression for g' in (3.25) can be orthogonal at most twice (or three times, when they are orthogonal at the endpoints of Γ). Therefore g as defined in (3.24) has at most two local extremum points in the interior of Γ.

(b) Idea of the proof: As $|\mathrm{Ind}(\dot{\eta})|$ is at most $\frac{1}{2}$, the vectors α and $\dot{\eta}(t)$ can be orthogonal at most once (or two times, when they are orthogonal at the endpoints of Γ). Therefore g has at most one local extremum point in the interior of Γ, while an additional extremum point can appear at the discontinuity $t = \ell$.

In all cases g and thus $u|_{\partial\Omega}$ has at most one nonincreasing and one nondecreasing part so that the Jacobian in the interior of Ω is non-vanishing. Examples of pairs of functions (f_1, f_2) that yield $(u_1|_{\partial\Omega}, u_2|_{\partial\Omega})$ which satisfy condition (a) and (b) respectively in the main result for Ω being the unit disk are illustrated in figure 3.1. The explicit expressions are given by:

$$\left(f_1^{(a)}(t), f_2^{(a)}(t)\right) = \left(\cos(2t) - 1, \sin(2t)\right), \tag{3.27a}$$

$$\left(f_1^{(b)}(t), f_2^{(b)}(t)\right) = \left(\cos(t) - 1, \sin\left(\frac{5}{4}t\right)\right), \tag{3.27b}$$

The assumptions on $\mathrm{Ind}(\dot{\eta}(t))$ and $\arg(\dot{\eta}(t))$ for these functions are investigated in figure 3.2. The index is given by:

$$\mathrm{Ind}(\dot{\eta}_{(a)}(t)) = 1, \quad \mathrm{Ind}(\dot{\eta}_{(b)}(t)) = \frac{1}{2},$$

and from figure 3.2(b) we see that in both cases the argument of $\dot{\eta}$ is monotonic increasing. Hence, each of the pair of functions satisfies the respective assumptions in condition (a) and (b), so that both pairs of boundary functions yield a non-vanishing Jacobian in the interior of Ω.

Weak maximum principle

We did not find a weak maximum principle for weighted Sobolev spaces in the literature, as the classical weak maximum principles only apply for H^1-solutions to (3.21) (see e.g. [6, Thm. 8.20] or [4, Thm. 8.1]). For that purpose, we include a proof in paper A. For the proof we need the following ingredients:

- The fact that the set $C^\infty(\overline{\Omega})$ is dense in $H^1(\Omega, d^{1-2s})$
- A definition of the trace space of $H^1(\Omega, d^{1-2s})$ in terms of a Sobolev space on $\partial\Omega$ (see Thm. 3.2 in Appendix A)
- The Hardy inequality that gives an estimate of $\left\| d^{\frac{1-2s}{2}-1} u \right\|_{L^2(\Omega)}$ with respect to $\left\| d^{\frac{1-2s}{2}} \nabla u \right\|_{L^2(\Omega)}$ (see Lemma 3.3 in Appendix A)

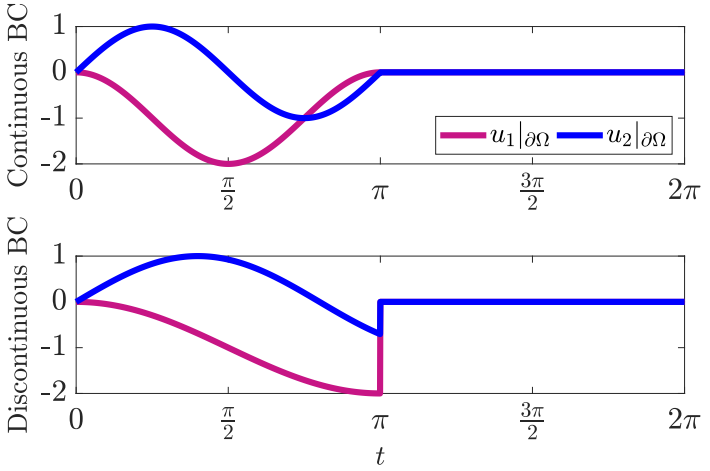

Figure 3.1: Two pairs of functions (f_1, f_2) that yield $(u_1|_{\partial\Omega}, u_2|_{\partial\Omega})$ which are examples of functions that satisfy condition (a) and (b) respectively in the main result. In this case $\ell = \pi$

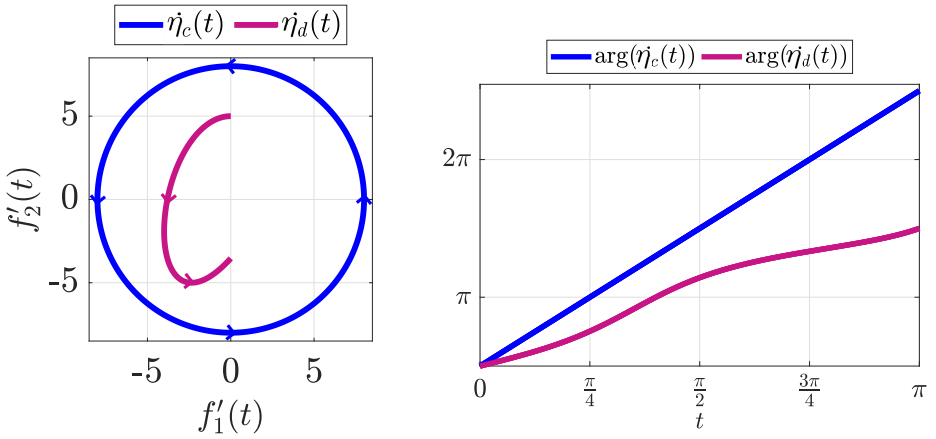

(a) Illustration of $\mathrm{Ind}(\dot{\eta}(t))$ (b) Illustration of $\arg(\dot{\eta}(t))$

Figure 3.2: Illustration of how the functions in figure 3.1 satisfy the assumptions on $\mathrm{Ind}(\dot{\eta}(t))$ and $\arg(\dot{\eta}(t))$ in the main result

- The facts that $u \in H^1(\Omega, d^{1-2s})$ implies $u_\pm = \max\{\pm u, 0\} \in H^1(\Omega, d^{1-2s})$, the weak derivatives satisfy $\nabla u_\pm = \nabla u\, \chi_{u_\pm > 0}$ and $T(u_\pm) = (Tu)_\pm$ (see Lemma 3.7 in Appendix A)

The proof of the weak maximum principle then follows the standard approach that if $Tu \leq 0$ a.e. on $\partial\Omega$ then $\nabla u_+ = 0$, which implies that $u_+ = 0$, and therefore $u = u_-$ a.e. in Ω. The main difficulty for weighted Sobolev spaces compared to classical Sobolev spaces is that for the bilinear form more terms appear due to the weighting by d^{1-2s}. To prove the desired result we in particular need the Hardy inequality to deduce from the bilinear form that $\nabla u_+ = 0$. This only works when s satisfies $\left|s - \frac{1}{2}\right| < \varepsilon$ and ε is small enough.

3.2.1.2 Numerical examples

The PYTHON code to generate the numerical examples in paper A can be found on GITLAB: `https://lab.compute.dtu.dk/hjsc/jacobian-of-solutions-to-the-conductivity-equation-in-limited-view.git`.

We want to illustrate numerically how two boundary conditions can be selected so that the non-vanishing Jacobian condition (3.22) for corresponding solutions is satisfied in accordance with the main result. We then choose the order of the corresponding solutions so that $\det[\nabla u_1 \, \nabla u_2] > 0$. As we restrict ourselves to reconstruction of an isotropic conductivity this is the only relevant assumption on the power density data in the reconstruction approach in section 3.1, since the condition (3.3) only applies for anisotropic conductivities. We implemented the reconstruction approach as outlined in algorithm 2 in PYTHON and use FENICS to solve the PDEs.

We use a fine mesh $N_{\text{data}} = 79281$ nodes to generate our power density data and a coarser mesh $N_{\text{recon}} = 50845$ nodes to address the reconstruction problem. We consider the domain Ω to be the unit disk: $\Omega = B(0,1)$ and the conductivity σ to have the following coordinate expression:

$$\sigma(x_1, x_2) = \begin{cases} 2 & \left(x_1 + \frac{1}{2}\right)^2 + (x_2)^2 \leq 0.3^2, \\ 2 & (x_1)^2 + \left(x_2 + \frac{1}{2}\right)^2 \leq 0.1^2, \\ 2 & \left(x_1 - \frac{1}{2}\right)^2 + \left(x_2 - \frac{1}{2}\right)^2 \leq 0.1^2, \\ 1 & \text{otherwise}, \end{cases} \tag{3.28}$$

for $(x_1, x_2) \in \Omega$. Figure 3.4(a) illustrates the conductivity and figure 3.4(b) illustrates different sizes of the boundary of control, Γ, used for reconstruction. As Γ_{medium} corresponds to the support of the boundary functions defined in (3.27) we can use these functions as boundary conditions for this size of Γ, as we know they satisfy condition (a) and (b) in the main result respectively. As we obtain similar reconstruction performance for both pairs of boundary functions when there is no noise in the data, we restrict ourselves to use the discontinuous functions here. For the other sizes of Γ we extend and shrink these boundary functions, while maintaining their shape and number of oscillations. This yields the following different pairs of discontinuous boundary

functions:

$$(f_1(t), f_2(t)) = \begin{cases} (\cos(4t) - 1, \sin(5t)) & \text{for } \Gamma_{\text{small}} = \{t \in [0, \frac{\pi}{4}]\} \\ (\cos(t) - 1, \sin(\frac{5t}{4})) & \text{for } \Gamma_{\text{medium}} = \{t \in [0, \pi]\} \\ (\cos(\frac{4t}{7}) - 1, \sin(\frac{5t}{7})) & \text{for } \Gamma_{\text{large}} = \{t \in [0, \frac{7\pi}{4}]\}. \end{cases} \tag{3.29}$$

The corresponding functions $u_i|_{\partial\Omega}$ extended by zero along the whole boundary are illustrated in figure 3.3.

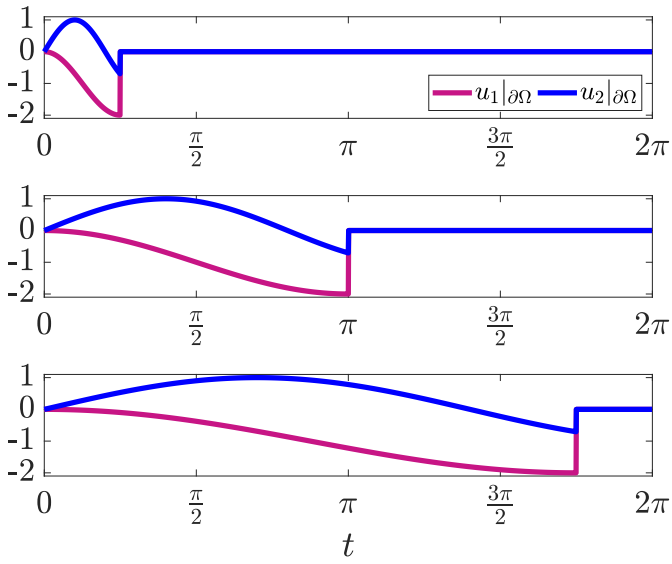

Figure 3.3: The discontinuous boundary functions $u_1|_{\partial\Omega}$ and $u_2|_{\partial\Omega}$ used for the reconstruction procedure for Γ_{small}, Γ_{medium} and Γ_{large} (top to bottom)

The reconstructions of σ for these choices of Γ are shown in figure 3.5 with corresponding relative errors in table 3.1. We see that in regions close to the boundary of control the reconstructed values of σ are close to the true values. This is especially evident from the three red circular features; for Γ_{large} all features are reconstructed well, as they are located closer to Γ than $\partial\Omega\backslash\Gamma$. For Γ_{medium} this is only the case for half of the features; in fact half of the large circular feature close to Γ is captured well, while for the other half the reconstructed values are too small, as this half is located closer to the boundary $\partial\Omega\backslash\Gamma$. In the case of Γ_{small} most of the features are located further towards $\partial\Omega\backslash\Gamma$ than Γ, so that all reconstructed values are way smaller than the true values. In general, we therefore see that the quality of the reconstruction decreases with decreasing size of Γ. Note that the decrease in quality of the reconstruction towards $\partial\Omega\backslash\Gamma$ might be explained by the fact that the Jacobian constraint is violated on this part of the boundary. Here the gradients ∇u_1 and ∇u_2 are parallel

to the unit normal following from the zero Dirichlet condition on this part of the boundary. Therefore, close to this part of the boundary the values of the Jacobian will be small and less reliable.

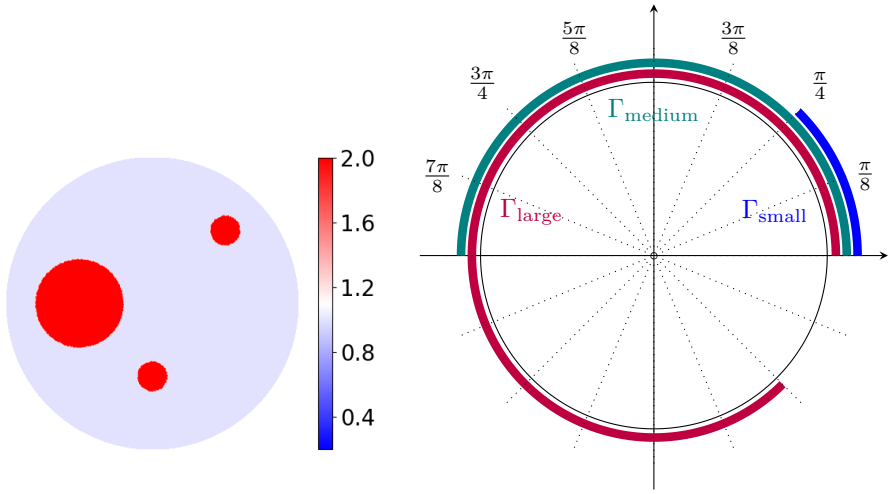

(a) True σ (b) Different Γ

Figure 3.4: Conductivity and different sizes of Γ used for the reconstruction procedure.

Table 3.1: Relative L^2 errors on the reconstructions of σ

	Γ_{large}	Γ_{medium}	Γ_{small}
Relative L^2 error σ	15.0%	39.9%	56.4%

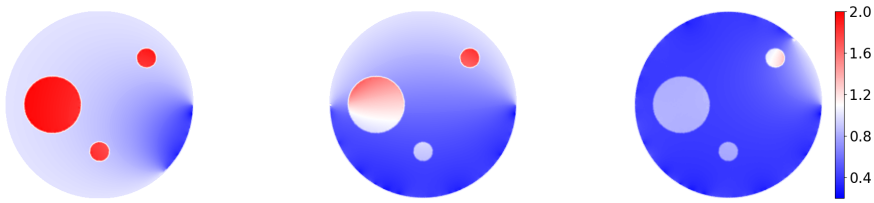

Γ_{large} Γ_{medium} Γ_{small}

Figure 3.5: Reconstructions of σ for varying sizes of Γ as in Figure 3.4(b).

3.2.1.3 Conclusion

We presented sufficient conditions on two boundary functions so that the corresponding solutions to the conductivity equation satisfy a non-vanishing Jacobian constraint in limited view. This approach allows for boundary functions that have discontinuities. This is relevant both in limited view and in full view settings, as these conditions and the use of discontinuous boundary functions apply for both settings.

Numerical examples showed that this approach can be used to select boundary conditions for reconstruction of the conductivity from power densities. Here the quality of the reconstruction is good close to the boundary of control. However, towards the boundary with zero Dirichlet condition the reconstructed values were too small.

3.2.2 Paper B: *Conductivity reconstruction from power density data in limited view*

In paper B we address existence of boundary conditions so that the corresponding Jacobian is positive. This is a generalisation from a full view to a limited view setting. We consider solutions $u_1, \dots, u_d$ to the boundary value problem

$$\begin{cases} Lu_i = -\mathrm{div}(\sigma \nabla u_i) = 0 & \text{in } \Omega, \\ u_i = f_i & \text{on } \Gamma, \\ L_\nu u_i = \sigma \partial_\nu u_i = 0 & \text{on } \partial\Omega \backslash \Gamma, \end{cases} \tag{3.30}$$

where ν denotes the unit outward normal to $\partial\Omega$. Here $\Omega \subset \mathbb{R}^d$, $d = 2, 3$ is a bounded Lipschitz domain and $\Gamma \subset \partial\Omega$ a non-empty open part of the boundary that we can control. σ is an isotropic conductivity that satisfies $\sigma \in L^\infty_+(\Omega)$, i.e. there exists $\lambda \in (0, 1)$ such that $\lambda \leq \sigma \leq \lambda^{-1}$. If $d = 3$ we further assume that σ is Lipschitz on Ω. We prove a result on existence of a finite number of boundary conditions $f_1, \dots, f_d$ so that locally the corresponding solutions satisfy the Jacobian constraint

$$\det[\nabla u_1 \cdots \nabla u_d] \geq \delta > 0, \tag{3.31}$$

for some $\delta > 0$. For the proof, we use the Runge approximation approach; this is a generalisation of the proof in [1, section 7.3].

The theoretical findings are supplemented with numerical examples for the case $d = 2$. Instead of repeating the numerical examples for the same numerical set up as in Appendix B, we use the set up as in paper A. This allows to compare how the two different limited view settings affect the Jacobian and reconstruction performance in section 3.2.3.

3.2.2.1 Theoretical results

We aim at proving existence of a finite number of boundary conditions so that the Jacobian constraint (3.31) is satisfied locally. In order to address this problem in higher

dimensions than two, we use the Runge approximation property. For our main result we prove that the operator L in (3.30) satisfies the Runge approximation property. Using this property, we can construct solutions to the boundary value problem (3.30) which approximate x_i in a given ball inside the domain. We then cover the domain Ω with a finite number of these balls and enforce the Jacobian constraint globally.

Runge approximation property
We say that L satisfies the *Runge approximation property* if for any simply connected Lipschitz domain $\Omega' \Subset \Omega$ and any $u \in H^1(\Omega')$ such that $Lu = 0$ in Ω' there exists a sequence $u_n \in H^1(\Omega)$ such that

(a) $Lu_n = 0$ in Ω,

(b) $u_n|_{\Omega'} \to u$ in $L^2(\Omega')$.

We prove our first important result (see Theorem 2.2 in Appendix B): L satisfies the Runge Approximation property with the sequences (u_n) satisfying the boundary restriction $L_\nu u_n = 0$ on $\partial\Omega\backslash\Gamma$ for all $n \in \mathbb{N}$.
Outline of the proof:

- If this was not true, by the Hahn-Banach theorem there would exist a u and a functional $g \in L^2(\Omega')$ such that $(g, u)_{L^2(\Omega')} \neq 0$ and $(g, v)_{L^2(\Omega')} = 0$ for all v
- It is well known that L and L_ν have the unique continuation property
- This property implies that the solution to the BVP

$$\begin{cases} Lw = g & \text{in } \Omega, \\ w = 0 & \text{on } \Gamma, \\ L_\nu w = 0 & \text{on } \partial\Omega\backslash\Gamma, \end{cases}$$

  satisfies $w = 0$ and $L_\nu w = 0$ on $\partial\Omega'$
- This implies $(g, u)_{L^2(\Omega')} = 0$; a contradiction

Solutions to (3.30) that approximate x_j in balls inside Ω
We want to construct solutions to (3.30) that approximate x_j and their gradients respectively in given balls inside Ω. This is motivated by the fact that for the coordinate functions it is known that the Jacobian constraint is satisfied: $\det[\nabla x_1 \cdots \nabla x_d] = 1$.

The first result follows by using Schauder estimates, the Sobolev embedding theorem, standard elliptic theory, and the Runge approximation property (see Lemma 2.3 in Appendix B). Here we assume that σ is Lipschitz, $\Omega' \Subset \Omega$, $x_0 \in \overline{\Omega'}$ and $s \in (0, \operatorname{dist}(\Omega', \partial\Omega))$. We then consider $u_0 \in C^{1,\alpha}$ with $\alpha \in (0, 1)$ that solves

$$-\Delta u_0 = 0, \quad \text{in } B(x_0, s).$$

The result reads:

- For any $\delta > 0$ we can find a radius $r \in (0, s)$ and a solution $u_{x_0,\delta} \in H^1(\Omega)$ to $Lu_{x_0,\delta} = 0$ in Ω and $L_\nu u_{x_0,\delta} = 0$ on $\partial\Omega\backslash\Gamma$ such that $u_{x_0,\delta}$ approximates u_0:

$$\|u_{x_0,\delta} - u_0\|_{C^1(\overline{B(x_0,r)})} \leq \delta.$$

The second result follows immediately (see Corollary 2.4 in Appendix B):

- For any $\delta > 0$ and $\mathbf{v} \in \mathbb{R}^d$ we can find a radius $r \in (0, 1)$ with $B(x_0, r) \subset \Omega'$ and a solution $u_{x_0,\delta} \in H^1(\Omega)$ to $Lu_{x_0,\delta} = 0$ in Ω and $L_\nu u_{x_0,\delta} = 0$ on $\partial\Omega\backslash\Gamma$ such that $\nabla u_{x_0,\delta}$ approximates $\mathbf{v}$:

$$\|\nabla u_{x_0,\delta} - \mathbf{v}\|_{C^0(B(x_0,r))} \leq \delta. \tag{3.32}$$

Covering Ω with a finite number of balls in which the Jacobian constraint is satisfied

We want to show that it follows by the previous result that Ω can be covered by a finite number of balls in which there is a positive lower bound for the Jacobian.

For the result we assume that σ is Lipschitz in $\overline{\Omega}$ and consider any compactly embedded domain $\Omega' \Subset \Omega$. Our result reads (see Theorem 3.1 in Appendix B):

- There exists a finite set of boundary conditions $\{\phi_j\}_{j=1}^{Md}$ with corresponding solutions $\{u_j\}_{j=1}^{Md}$ to (3.30), such that at any point $x_0 \in \Omega'$ there is an open neighborhood V_{x_0} of x_0 and a subset $\{u_{n_1}, \ldots, u_{n_d}\}$ satisfying

$$\det\left[\nabla u_{n_1}(x) \cdots u_{n_d}(x)\right] \geq \frac{1}{2}, \quad \text{for all } x \in V_{x_0}.$$

Idea of the proof:

- Using the previous result in (3.32) for each $x_0 \in \Omega'$ we can find approximating solutions $\tilde{u}_j$ to x_j and by fixing δ sufficiently small we can guarantee that

$$|\det[\nabla\tilde{u}_1 \cdots \nabla\tilde{u}_d] - \det[\mathbf{e}_1 \cdots \mathbf{e}_d]| < \frac{1}{2}$$

- By the reverse triangle inequality it follows: $|\det[\nabla\tilde{u}_1 \cdots \nabla\tilde{u}_d]| > \frac{1}{2}$
- By the compact embedding $\Omega' \Subset \Omega$ there exists a finite subcover $\{B(x_m, r_m)\}_{m=1}^{M}$ of Ω' yielding the Md boundary conditions

3.2.2.2 Numerical examples

The Python code to generate the numerical examples in paper B can be found on GitLab: `https://lab.compute.dtu.dk/hjsc/conductivity-reconstruction-from-power-density-data-in-limited-view.git`.

We illustrate numerically how an isotropic conductivity can be reconstructed from power density data in dimension $d = 2$. Here we restrict ourselves to two boundary conditions. We use the same implementation in PYTHON of the reconstruction approach as in paper A. This is based on a simplified version of the reconstruction procedure in section 3.1 as outlined in algorithm 2.

We use the same numerical set up as in paper A: A fine mesh with $N_{\text{data}} = 79281$ nodes to generate our power density data and a coarser mesh with $N_{\text{recon}} = 50845$ nodes to address the reconstruction problem. We consider the domain Ω to be the unit disk: $\Omega = B(0, 1)$. For the conductivity σ we also consider the coordinate expression (3.28) as in paper A. Figure 3.6(a) illustrates the conductivity and figure 3.6(b) illustrates different sizes of the boundary of control, Γ, used for reconstruction. Motivated by the theoretical analysis for Dirichlet boundary conditions in a limited view setting in paper A, we use the boundary functions defined in (3.29).

The reconstructions of σ for these choices of Γ are shown in figure 3.7 with corresponding relative errors in table 3.2. Similar to the analysis in section 3.2.1.2 we see that in regions close to the boundary of control the reconstructed values of σ are close to the true values. Reconstructed values closer to $\partial\Omega\backslash\Gamma$ are too large. Especially for Γ_{small} the reconstructed values in the circular features towards $\partial\Omega\backslash\Gamma$ are way too large: 5.0 instead of 2.0. Note that the decrease in quality of the reconstruction towards $\partial\Omega\backslash\Gamma$ similar to paper A can be explained by the fact that the Jacobian constraint is violated on this part of the boundary. Here the gradients ∇u_1 and ∇u_2 are parallel to the tangent vector along the boundary following from the no-flux condition on this part of the boundary. Therefore, close to this part of the boundary the values of the Jacobian will be small and less reliable.

We notice that there are small artifacts along the part of the boundary $\partial\Omega\backslash\Gamma$ for all sizes of Γ. This phenomenon was already observed for the numerical examples in Appendix B in figure 6. However, in contrast to the reconstructions in the Appendix B, the artifacts in figure 3.7 are way smaller. This is due the mesh refinement, as for this experiment we use the same meshes as used for paper A. It was already mentioned and observed (see figure 9, Appendix B) that the mesh size had large influence on the magnitude of the artifacts.

Table 3.2: Relative L^2 errors on the reconstructions of σ

	Γ_{large}	Γ_{medium}	Γ_{small}
Relative L^2 error σ	22.4%	72.9%	120%

3.2.2.3 Conclusion

We presented a result on existence of a finite number of boundary conditions so that the corresponding Jacobian is locally positive. This holds for a limited view setting in two or three dimensions. In two dimensions we included numerical examples for reconstruction of the conductivity from power densities from two fixed boundary

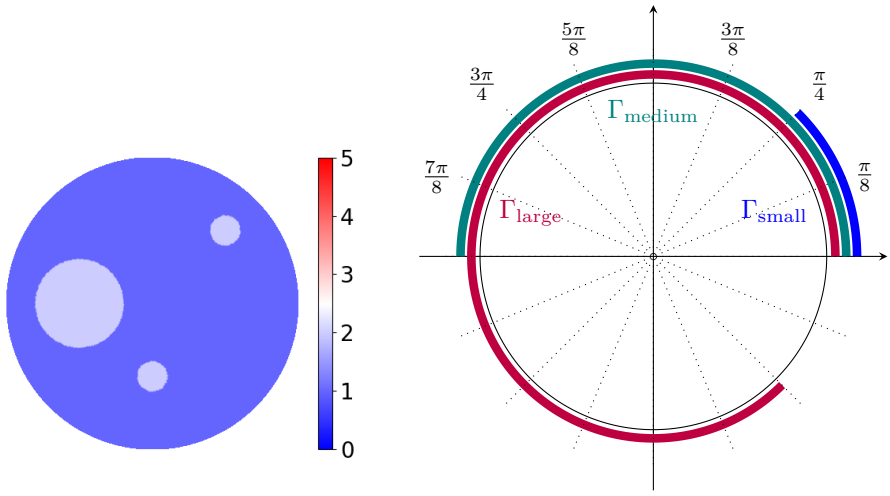

(a) True σ (b) Different Γ

Figure 3.6: Conductivity and different sizes of Γ used for the reconstruction procedure.

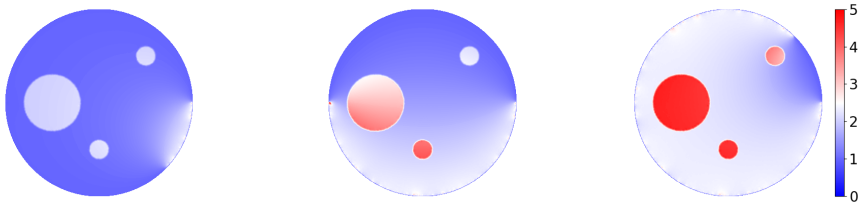

Γ_{large} Γ_{medium} Γ_{small}

Figure 3.7: Reconstructions of σ for varying sizes of Γ as in Figure 3.6(b).

conditions. Here the quality of the reconstruction is good towards the boundary of control. However, towards the boundary with the no-flux condition the reconstructed values are too large.

3.2.3 Comments on numerical performance of the different limited view settings in paper A and paper B

As we conducted numerical experiments on two different limited view settings, it seems natural to address how the different settings affected the quality of the reconstructions. We want to emphasize that we cannot compare performance directly, as

the solutions to the PDEs are different and yield different power density data. Furthermore, for the experiments in paper A we have theoretical foundation for the choice of boundary functions and it is not clear whether this translates to mixed boundary conditions. However, numerical investigations with different boundary conditions gave very similar results in paper B. For instance, the choice of boundary functions defined in (3.29) and the coordinate functions (x_1, x_2) yielded very similar reconstructions.

For both settings it is clear that the quality of the reconstruction is worse towards the part of the boundary that cannot be controlled. In case of pure Dirichlet conditions the reconstructed values here are too small, while in case of mixed Dirichlet and Neumann conditions the reconstructed values are too large. The deviation from the true values is even larger for the mixed conditions which results in way higher relative errors than the Dirichlet conditions as can be seen from table 3.1 and 3.2. A physical explanation to this phenomenon might be that the no-flux condition prevents energy to exit on this part of the boundary and thus has a damming effect yielding higher values towards this part of the boundary. On the contrary, by the zero Dirichlet condition values are forced to be small towards this part of the boundary.

3.2.4 Thoughts on a limited view setting with pure Neumann boundary conditions

An interesting question is, whether the approach of posing sufficient conditions on a pair of boundary functions yields a non-vanishing Jacobian in a limited view setting with Neumann boundary conditions. Consider the following limited view setting: There is a part of the boundary Γ that can be controlled by a non-zero Neumann condition, while on the remaining boundary there is a no-flux condition:

$$\begin{cases} -\operatorname{div}(\gamma \nabla u_i) = 0 & \text{in } \Omega, \\ \gamma \nabla u_i \cdot n = f_i & \text{on } \Gamma, \\ \gamma \nabla u_i \cdot n = 0 & \text{on } \partial\Omega \backslash \Gamma. \end{cases} \tag{3.33}$$

Here $\Omega \subset \mathbb{R}^2$ is a bounded Lipschitz domain, $\gamma \in L^\infty(\Omega, \mathbb{R}^{2\times 2})$ is an anisotropic conductivity, $\Gamma \subset \partial\Omega$ a non-empty closed part of the boundary that we can control and n is the unit outward normal. For $H^{-\frac{1}{2}}(\partial\Omega)$ boundary functions it is known that the boundary functions should have at most one nonpositive and one nonnegative part along the boundary in order to prevent existence of a critical point [2, Thm. 2.8]. Similar to the Dirichlet case one can then prevent existence of a point x_0 for which the Jacobian vanishes:

$$\det[\nabla u_1(x_0)\, \nabla u_2(x_0)] = 0.$$

This is accomplished by ensuring that any linear combination of a pair of boundary functions $(u_1|_{\partial\Omega}, u_2|_{\partial\Omega})$ satisfies that there is at most one nonpositive and at most one nonnegative part along the boundary. Assuming that $f_i \in C^1(\Gamma)$ yields that $u_i|_{\partial\Omega}$

are piecewise smooth functions and hence in $L^2(\partial\Omega)$ and $H^{-\frac{1}{2}}(\partial\Omega)$. By the zero Dirichlet condition on $\partial\Omega\backslash\Gamma$ in the limited view setting for paper A, the boundary functions in this paper are aligned with respect to the function value zero. Therefore, the number of nonincreasing and nondecreasing parts and the number of nonpositive and nonnegative parts coincide. This indicates that one can use the same sufficient conditions on the boundary conditions for the Neumann case as for the Dirichlet case. To repeat the proof in the Neumann case one then needs to replace Proposition 2.1 Appendix A with [2, Thm. 2.8] in the Neumann case to obtain a contradiction.

Bibliography

[1] Giovanni Alberti and Yves Capdeboscq. *Lectures on elliptic methods for hybrid inverse problems*. Societe Mathematique De France, 2018. ISBN: 978-2-85629-872-5.

[2] Giovanni Alessandrini and Rolando Magnanini. "Elliptic Equations in Divergence Form, Geometric Critical Points of Solutions, and Stekloff Eigenfunctions." In: *Siam Journal on Mathematical Analysis - SIAM J MATH ANAL* 25 (September 1994). DOI: 10.1137/S0036141093249080.

[3] Patricia Bauman, Antonella Marini, and Vincenzo Nesi. "Univalent solutions of an elliptic system of partial differential equations arising in homogenization." In: *Indiana Univ. Math. J.* 50.2 (2001), pages 747–757. ISSN: 0022-2518. DOI: 10.1512/iumj.2001.50.1832. URL: https://doi-org.proxy.findit.cvt.dk/10.1512/iumj.2001.50.1832.

[4] David Gilbarg and Neil S. Trudinger. *Elliptic Partial Differential Equations of Second Order*. Classics in Mathematics. U.S. Government Printing Office, 2001. ISBN: 9783540411604. URL: https://books.google.dk/books?id=eoiGTf4cmhwC.

[5] François Monard and Guillaume Bal. "Inverse anisotropic diffusion from power density measurements in two dimensions." eng. In: *Inverse Problems* 28.8 (2012), page 084001. ISSN: 13616420, 02665611. DOI: 10.1088/0266-5611/28/8/084001.

[6] Sandro Salsa. *Partial Differential Equations in Action*. Springer, 2016.

CHAPTER 4

Reconstructing conductivities from power densities on 2D Riemannian manifolds

In this chapter we aim at reconstructing an anisotropic conductivity from power densities on a two-dimensional Riemannian manifold. The natural setting here is an electrically conductive compact Riemannian manifold with a smooth boundary. In the reconstruction procedure the solutions to the conductivity equation play a central role. For that purpose we show existence and uniqueness of the solutions in the first section. In the second section we generalise the reconstruction formula in section 3.1 from Euclidean space to certain types of geometries. In the third section we find a shortcut between Euclidean space and general 2D Riemannian manifolds that allows us to use the Euclidean reconstruction procedure. This setting was the basis for paper C, *Reconstructing anisotropic conductivities on two-dimensional Riemannian manifolds from power densities*. Therefore, section three is based on and summarises this paper. Finally, in section four we discuss further research ideas related to this work.

Throughout this chapter we consider the following setting, which is taken from section 1 in Appendix C:

Let (M, g) denote the mentioned compact Riemannian manifold with smooth boundary ∂M and genus zero. An electrical conductivity on M is modelled by a – generally anisotropic – $(1,1)$ tensor field γ, which is self-adjoint and uniformly elliptic with respect to g, i.e. for some $\kappa > 1$ and for all tangent vectors v and w:

$$g(\gamma(v), w) = g(v, \gamma(w)) \quad \text{and} \quad \kappa^{-1} |v|_M^2 \leq g(\gamma(v), v) \leq \kappa |v|_M^2. \tag{4.1}$$

On the boundary ∂M we prescribe an electrostatic potential f that generates an interior voltage potential u. In the absence of interior sinks and sources, $u \in H^1(M)$

is characterised as the unique solution to the boundary value problem

$$\begin{cases} \operatorname{div}_M(\gamma \operatorname{grad}_M(u)) = 0 \text{ in } M, \\ u = f \text{ on } \partial M. \end{cases} \tag{4.2}$$

The interior current field is $\gamma \operatorname{grad}_M(u)$, i.e. γ is the tensor turning the electric field $\operatorname{grad}_M(u)$ into the current field. By considering m different boundary functions $f = f_i,\ 1 \leq i \leq m$, the corresponding solutions to equation (4.2) are denoted by u_i. They define the so-called power density $(m \times m)$-matrix H with elements:

$$H_{ij}^M = H_{ji}^M = g(\gamma \operatorname{grad}_M(u_i), \operatorname{grad}_M(u_j)) \quad \text{for} \quad 1 \leq i, j \leq m. \tag{4.3}$$

For the reconstruction procedure to work, we need the following two conditions on the power density matrix H^M:

$$\min(\det(\operatorname{grad}_M u_1, \operatorname{grad}_M u_2), \det(\operatorname{grad}_M u_3, \operatorname{grad}_M u_4)) \geq c_0 > 0 \text{ for every } x \in M, \tag{4.4}$$

$$\operatorname{grad}_M \left(\log \left(\frac{\det(\operatorname{grad}_M u_1, \operatorname{grad}_M u_2)}{\det(\operatorname{grad}_M u_3, \operatorname{grad}_M u_4)} \right) \right) \neq 0 \text{ for every } x \in M. \tag{4.5}$$

4.1 Existence and uniqueness of solutions to the conductivity equation

Let $u \in H_0^1(M)$ be a weak solution that solves the following Dirichlet problem

$$\begin{cases} -\operatorname{div}_M(\gamma \operatorname{grad}_M(u)) = h & \text{in } M, \\ u = 0 & \text{on } \partial M, \end{cases} \tag{4.6}$$

with $h \in H^{-1}(M)$. As γ is positive definite, we can in each tangent space define A as $A^2(x) = \gamma(x)$. By definition the weak solution u satisfies the variational equation

$$-\int_M \operatorname{div}(\gamma \operatorname{grad}_M(u)) v \, \mathrm{d}V = \int_M hv \, \mathrm{d}V$$

for any test function $v \in H_0^1(M)$. It follows from integration by parts (see e.g. [12, Eq. (2.20)]) that this equation can be rewritten as:

$$\int_M g(\gamma \operatorname{grad}_M(u), \operatorname{grad}_M(v)) \, \mathrm{d}V = \int_M hv \, \mathrm{d}V$$

From the equation above we introduce the bilinear form $B[u, v]$:

$$B[u, v] = \int_M g(\gamma \operatorname{grad}_M(u), \operatorname{grad}_M(v)) \, \mathrm{d}V,$$

and the linear functional H:

$$Hv = \int_M hv \, \mathrm{d}V,$$

with $H \in H^{-1}(M)$, so that H is a bounded linear functional on $H_0^1(M)$. The bilinear form is symmetric, as it satisfies $B[u,v] = B[v,u]$. In the following we want to show that it is continuous. We use the Schwarz inequality (see e.g. [7, p. 141]) and the upper bound for the uniform ellipticity condition:

$$\begin{aligned}
|B[u,v]| &= \left| \int_M g(\gamma \operatorname{grad}_M(u), \operatorname{grad}_M(v)) \, \mathrm{d}V \right| \\
&= \left| \int_M g(A \operatorname{grad}_M(u), A \operatorname{grad}_M(v)) \, \mathrm{d}V \right| \\
&\leq \left(\int_M |A \operatorname{grad}_M(u)|_g^2 \, \mathrm{d}V \right)^{\frac{1}{2}} \left(\int_M |A \operatorname{grad}_M(v)|_g^2 \, \mathrm{d}V \right)^{\frac{1}{2}} \\
&= \left(\int_M g(\gamma \operatorname{grad}_M(u), \operatorname{grad}_M(u)) \, \mathrm{d}V \right)^{\frac{1}{2}} \left(\int_M g(\gamma \operatorname{grad}_M(v), \operatorname{grad}_M(v)) \, \mathrm{d}V \right)^{\frac{1}{2}} \\
&\leq \kappa \|\operatorname{grad}_M(u)\|_{L^2(M)} \|\operatorname{grad}_M(v)\|_{L^2(M)} \\
&\leq \kappa \|u\|_{H_0^1(M)} \|v\|_{H_0^1(M)}.
\end{aligned}$$

By the Poincaré inequality (see e.g. [8, Theorem p.28]) there exists a constant $C_p > 0$ so that

$$\|u\|_{L^2(M)} \leq C_p \|\operatorname{grad}_M(u)\|_{L^2(M)},$$

for $u \in H_0^1(M)$. It then follows that

$$\|u\|_{H_0^1(M)}^2 = \|u\|_{L^2(M)}^2 + \|\operatorname{grad}_M(u)\|_{L^2(M)}^2 \leq (C_p^2 + 1) \|\operatorname{grad}_M(u)\|_{L^2(M)}^2.$$

Using this inequality and the lower bound from the uniform ellipticity condition, we can prove that B is coercive:

$$B[u,u] = \int_M g(\gamma \operatorname{grad}_M(u), \operatorname{grad}_M(u)) \, \mathrm{d}V \geq \frac{1}{\kappa} \|\operatorname{grad}_M(u)\|_{L^2(M)}^2 \geq \frac{1}{\kappa(C_p^2+1)} \|u\|_{H_0^1(M)}^2.$$

By the Lax-Milgram Theorem (see e.g. [9, Theorem 6.39]) it now follows that there exists a unique solution $u \in H_0^1(M)$ to the variational problem

$$B[u,v] = Hv,$$

for all $v \in H_0^1(M)$. Furthermore, the following stability estimate holds:

$$\|u\|_{H_0^1(M)} \leq \kappa(C_p^2+1) \|H\|_{H^{-1}(M)}.$$

Following the existence, uniqueness and stability of the solution $u \in H_0^1(M)$ to (4.6), we can prove the same for $u \in H^1(M)$ that solves (4.2). Consider $w = u - \tilde{f}$, where

$\tilde{f} \in H^1(M)$ is the extension of f from ∂M to M. Now w solves the boundary value problem

$$\begin{cases} -\operatorname{div}_M(\gamma \operatorname{grad}_M(w)) = h_w & \text{in } M, \\ w = 0 & \text{on } \partial M, \end{cases}$$

with $h_w = \operatorname{div}(\gamma \operatorname{grad}_M(\tilde{f})) \in H^{-1}(M)$. This expression plays the same role as $h \in H^{-1}(M)$ in the boundary value problem (4.6), so by the previous derivations it follows that $w \in H_0^1(M)$ solves the problem above uniquely with the stability estimate $\|w\|_{H_0^1(M)} \leq \kappa(C_p^2+1)\|H_w\|_{H^{-1}(M)}$. This implies that $u = w + \tilde{f} \in H^1(M)$ is a unique solution to (4.2). Furthermore, by using the same tricks as for showing continuity of the bilinear form above, we can obtain an estimate for $\|H_w\|_{H^{-1}(M)}$ in terms of $\tilde{f}$:

$$\begin{aligned} |H_w v| &= \left| \int_M \operatorname{div}(\gamma \operatorname{grad}_M(\tilde{f}))v \, \mathrm{d}V \right| \\ &= \left| -\int_M g(\gamma \operatorname{grad}_M(u), \operatorname{grad}_M(v)) \, \mathrm{d}V \right| \\ &\leq \kappa \|\tilde{f}\|_{H^1(M)} \|v\|_{H_0^1(M)}, \end{aligned}$$

for all $v \in H_0^1(M)$. Hence, we have the estimate for $\|w\|_{H_0^1(M)}$:

$$\|w\|_{H_0^1(M)} \leq \kappa(C_p^2+1)\|H_w\|_{H^{-1}(M)} \leq \kappa^2(C_p^2+1)\|\tilde{f}\|_{H^1(M)}.$$

Yielding the following estimate for $\|u\|_{H^1(M)}$:

$$\|u\|_{H^1(M)} = \|w+\tilde{f}\|_{H^1(M)} \leq \|w\|_{H^1(M)} + \|\tilde{f}\|_{H^1(M)} \leq (\kappa^2(C_p^2+1)+1)\|\tilde{f}\|_{H^1(M)}.$$

4.2 Generalising the reconstruction approach in Euclidean space to (M, g)

4.2.1 Generalising the important equations to the manifold

In the Euclidean case equation (3.6) and (3.7) are the basis for the reconstruction procedure. In the following we transfer these formulas to the manifold.

Equation (3.6) is derived based on the fact that $\nabla \cdot (JA^{-1}S_i) = 0$. A similar version of this equation holds on M:

$$\operatorname{div}_M\left(J^M A^{-1} S_i^M\right) = 0,$$

with the rotational operator J^M defined as

$$J^M = \frac{1}{\sqrt{\det G}} \begin{bmatrix} -G_{12} & -G_{22} \\ G_{11} & G_{12} \end{bmatrix}. \tag{4.7}$$

The Jacobian constraint (4.4) yields:

$$\min\left(\det\, H^M\right)^{\frac{1}{2}} = \min\left(\sqrt{\det G}\det\left(S_1^M, S_2^M\right)\right) \geq c_0 > 0, \tag{4.8}$$

which guarantees invertibility of H^M. Based on the fact that $\operatorname{div}_M\left(J^M A^{-1} S_i^M\right)$ vanishes on M we can then derive a similar version of equation (3.6):

$$\operatorname{grad}_M\left(\log(\det A)\right) = N^M + \sum_{p,q=1}^{2} g(\operatorname{grad}_M\left(H^{M,qp}\right), \widetilde{A}\, S_p^M)\widetilde{A}^{-1}\, S_q^M, \tag{4.9}$$

with $N^M = \frac{1}{2}\operatorname{grad}_M\left(\log\left(\det H^M\right)\right)$. For the second equation in the reconstruction procedure we orthonormalise $S^M = (S_1^M, S_2^M)$ into a $SO(2)$-valued frame $R^M = (R_1^M, R_2^M)$ by finding T^M, such that $R^M = S^M(T^M)^T$. We parameterise the rotational operator R^M by an angle function θ^M:

$$R^M = \frac{1}{\sqrt{\det G}}\begin{bmatrix}\cos\left(\theta^M\right)\sqrt{\det G} - \sin\left(\theta^M\right)G_{12} & -\sin\left(\theta^M\right)G_{22} \\ \sin\left(\theta^M\right)G_{11} & \cos\left(\theta^M\right)\sqrt{\det G} + \sin\left(\theta^M\right)G_{12}\end{bmatrix}, \tag{4.10}$$

which rotates a vector by θ^M degrees in positive direction and maintains its length with respect to g. We note that R^M satisfies the requirements for a rotation matrix

$$\det R^M = 1 \quad \text{and} \quad g\left(R^M v, R^M w\right) = g(v, w) \quad \text{for all } v, w \in T_p M.$$

The transfer matrix T^M gives rise to the four vector fields V_{ij}^M and hence $V_{ij}^{M,a}$:

$$V_{ij}^M = \sum_{k=1}^{2} \operatorname{grad}_M\left(T_{ik}^M\right) T^{M,kj}, \quad 1 \leq i, j \leq 2, \quad V_{ij}^{M,a} = \frac{1}{2}(V_{ij}^M - V_{ji}^M). \tag{4.11}$$

By using the same approach as in the Euclidean case and writing the Lie bracket $[\widetilde{A}R_2^M, \widetilde{A}R_1^M]$ in two different ways, we obtain the following equation corresponding to a generalised version of equation (3.7):

$$U + \left[\widetilde{A}_2, \widetilde{A}_1\right] = P_C + \frac{1}{2}P_V + \frac{1}{2}P_g - \frac{1}{2}\sqrt{\det G}\, J^M N^M, \tag{4.12}$$

with

$$\begin{aligned}
U &= \sum_{i,j,k,\ell=1}^{2} \widetilde{A}_{ij}\widetilde{A}_{k\ell}\left(\left(R^M\right)_2^j \partial_i\left(R^M\right)_1^\ell - \left(R^M\right)_1^j \partial_i\left(R^M\right)_2^\ell\right) e_k, \\
P_C &= (\Gamma_{21}^1 + \Gamma_{22}^2)e_1 - (\Gamma_{11}^1 + \Gamma_{12}^2)e_2, \\
P_V &= \sum_{p,m,q=1}^{2} \Big[-g\left(V_{2p}^M, \widetilde{A}R_p^M\right)\widetilde{A}R_1^M + g\left(V_{1p}^M, \widetilde{A}R_p^M\right)\widetilde{A}R_2^M \\
&\qquad + g\left(V_{mq}^M G^{mp} G_{q2}, \widetilde{A}R_p^M\right)\widetilde{A}R_1^M - g\left(V_{mq}^M G^{mp} G_{q1}, \widetilde{A}R_p^M\right)\widetilde{A}R_2^M\Big], \\
P_g &= \sum_{q,p=1}^{2} \left[g\left(\operatorname{grad}_M\left(G^{qp}\right) G_{q2}, \widetilde{A}R_p^M\right)\widetilde{A}R_1^M - g\left(\operatorname{grad}_M\left(G^{qp}\right) G_{q1}, \widetilde{A}R_p^M\right)\widetilde{A}R_2^M\right].
\end{aligned}$$

4.2.2 Feasibility of reconstruction approaches on (M, g)

The challenge for the reconstruction approach is to reconstruct $\widetilde{A}$ from equation (4.12), as this formula both depends on the unknown normalised anisotropy $\widetilde{A}$ and the unknown function θ^M. In comparison to the Euclidean case there are now several occurrences of θ^M instead of one term that only depends on $\nabla\theta^M$. To simplify the problem, we consider three different types of manifolds:

- A conformal manifold (referred to as *the conformal case*), where
$$G(x) = \rho^2(x) \begin{bmatrix} 1 & 0 \\ 0 & 1 \end{bmatrix}.$$
- A manifold, where the metric is diagonal (referred to as *the diagonal case*):
$$G(x) = \begin{bmatrix} G_{11}(x) & 0 \\ 0 & G_{22}(x) \end{bmatrix},$$
where $G_{11}(x) \neq G_{22}(x)$.
- A general manifold, where the metric takes its general form (referred to as *the general case*):
$$G(x) = \begin{bmatrix} G_{11}(x) & G_{12}(x) \\ G_{12}(x) & G_{22}(x) \end{bmatrix},$$
where $G_{ij}(x)$ does not vanish on M for $1 \leq i, j \leq 2$ and the three functions are differing from each other: $G_{11}(x) \neq G_{22}(x)$ and $G_{11}(x) \neq G_{12}(x)$.

In the following we address feasibility of an reconstruction approach for $\widetilde{A}$. For that purpose we parameterise it by functions λ and μ and take into account that $\widetilde{A}$ is self-adjoint and has determinant 1:

$$\widetilde{A}(\lambda, \mu) = \begin{bmatrix} \lambda & \mu \\ \frac{-\lambda^2 G_{12} + \mu\lambda G_{11} + G_{12}}{\lambda G_{22} - \mu G_{12}} & \frac{\mu^2 G_{11} - \lambda\mu G_{12} + G_{22}}{\lambda G_{22} - \mu G_{12}} \end{bmatrix}.$$

4.2.2.1 The conformal case

In this case reconstructing $\widetilde{A}$ using equation (4.12) with $m = 4$ measurements boils down to solving the following system of equations for $\widetilde{A}$:

$$\widetilde{A}^2 \left(\operatorname{grad}_M \left(\theta_2^M - \theta_1^M \right) - V_{12}^{M,a(2)} + V_{12}^{M,a(1)} \right) = -\frac{1}{2} J^E \left(N^{M,(2)} - N^{M,(1)} \right), \quad (4.13)$$

with the operator J^E defined in Euclidean space: $J^E = \begin{bmatrix} 0 & -1 \\ 1 & 0 \end{bmatrix}$. Similarly to the Euclidean case, $\operatorname{grad}_M \left(\theta_2^M - \theta_1^M \right)$ can be expressed by the data, so a direct reconstruction procedure from this formula is feasible.

This gives rise to the conformal reconstruction procedure in algorithm 3.

Algorithm 3 Conformal reconstruction procedure

- Solve equation (4.13) for $\widetilde{A}$
- Solve the following equation for θ^M

$$\rho^2 \widetilde{A}^2 \mathrm{grad}_M\left(\theta^M\right) + [\widetilde{A}_2, \widetilde{A}_1] = -J^E \,\mathrm{grad}_M\left(\rho^2\right) + \rho^2 \widetilde{A}^2 V_{12}^{M,a} - \rho^2 \frac{1}{2} J^E N^M,$$

- Solve equation (4.9) for $(\det A)$

4.2.2.2 The diagonal case

In this case the quantities U, P_C, P_V, and P_g in (4.12) simplify to:

$$\begin{aligned} U - \frac{1}{2}P_g = {} & (G_{11}\, G_{22})^{\frac{1}{2}} \widetilde{A}^2 \mathrm{grad}_M\left(\theta^M\right) \\ & - \frac{1}{2}\left(\hat{A}_1 \,\mathrm{grad}_M\left(G_{11}\right) - \hat{A}_2 \,\mathrm{grad}_M\left(G_{22}\right)\right), \end{aligned} \tag{4.14a}$$

$$P_C = -\frac{1}{2} J^M \left[\left(\frac{G_{22}}{G_{11}}\right)^{\frac{1}{2}} \mathrm{grad}_M\left(G_{11}\right) + \left(\frac{G_{11}}{G_{22}}\right)^{\frac{1}{2}} \mathrm{grad}_M\left(G_{22}\right)\right], \tag{4.14b}$$

$$P_V = \tilde{A}^2 (G_{22} V_{12}^M - G_{11} V_{21}^M), \tag{4.14c}$$

with

$$\hat{A}_1 = \begin{bmatrix} \widetilde{A}_{11}\widetilde{A}_{12} & \widetilde{A}_{12}^2 \\ \widetilde{A}_{11}\widetilde{A}_{22} & \widetilde{A}_{12}\widetilde{A}_{22} \end{bmatrix} \quad \text{and} \quad \hat{A}_2 = \begin{bmatrix} \widetilde{A}_{11}\widetilde{A}_{21} & \widetilde{A}_{11}\widetilde{A}_{22} \\ \widetilde{A}_{21}^2 & \widetilde{A}_{21}\widetilde{A}_{22} \end{bmatrix}.$$

Therefore, reconstructing $\widetilde{A}$ using equation (4.12) with $m = 4$ measurements boils down to solving the following system of equations for $\widetilde{A}$:

$$\begin{aligned} & (G_{11}\, G_{22})^{\frac{1}{2}} \widetilde{A}^2 \,\mathrm{grad}_M\left(\theta_2^M - \theta_1^M\right) \\ & + \frac{G_{11}}{2} \widetilde{A}^2 \left(V_{21}^{M,(2)} - V_{21}^{M,(1)}\right) \\ & - \frac{G_{22}}{2} \widetilde{A}^2 \left(V_{12}^{M,(2)} - V_{12}^{M,(1)}\right) = -\frac{1}{2}(G_{11}\, G_{22})^{\frac{1}{2}} J^M (N^{M,(2)} - N^{M,(1)}), \end{aligned} \tag{4.15}$$

Similarly to the Euclidean case, $\mathrm{grad}_M\left(\theta_2^M - \theta_1^M\right)$ can be expressed by the data, so a direct reconstruction procedure from this formula is feasible. The reconstruction procedure is outlined in algorithm 4.

Algorithm 4 Diagonal reconstruction procedure

- Solve equation (4.15) for $\widetilde{A}$
- Solve equation (4.12) for θ^M with the quantities defined in (4.14)
- Solve equation (4.9) for $(\det A)$

4.2.2.3 The general case

In this case reconstructing $\widetilde{A}$ using equation (4.12) with $m = 4$ measurements boils down to solving the following system of third and fourth order polynomials for λ and μ:

$$\begin{aligned}(c_1 - c_2 y_f^1)\lambda + (c_3 - c_4 y_f^1)\mu + c_5\lambda^2\mu + c_6\lambda\mu^2 + c_7\lambda^3 + c_8\mu^3 = 0\\ k_1 + (k_2 + k_3 y_f^2)\lambda\mu + (k_4 - k_5 y_f^2)\lambda^2 + (k_6 - k_7 y_f^2)\mu^2\\ +k_8\lambda^2\mu^2 + k_9\lambda^3\mu + k_{10}\lambda\mu^3 + k_{11}\lambda^4 + k_{12}\mu^4 = 0,\end{aligned} \tag{4.16}$$

with $Y_f = (y_f^1, y_f^2) = -\frac{1}{2}\sqrt{\det G} J^M (N^{M,(2)} - N^{M,(1)})$, and where the functions c_j and k_j depend on $G, T^{M,(1)}, T^{M,(2)}, \theta_1^M$, and θ_2^M. We have the following issue with this formula: The functions c_j and k_j include terms on the form $\cos\big(\theta_i^M\big)^2$___ and $\cos\big(\theta_i^M\big)\sin\big(\theta_i^M\big)$___, which cannot be expressed by the data. So it seems currently not feasible to reconstruct $\widetilde{A}$ directly using this formula.

4.2.3 Proof of equation (4.9) and (4.12)

4.2.3.1 Geometrical setting and preliminaries

Since γ, and thus $A^r = \gamma^{\frac{r}{2}}$, is uniformly elliptic in the tangent spaces of M for any $r \in \mathbb{R}$, it follows that the vector fields $(A^r S_1^M, A^r S_2^M)$ form an oriented frame in each tangent space. By self-adjointness of γ and thus A^r, the power density measurements can be expressed as

$$H_{ij}^M = g(A^r S_i^M, A^{-r} S_j^M), \quad 1 \le i, j \le 2, \quad r \in \mathbb{R}.$$

We claim that the following formula holds for any vector field $V \in T_pM$:

$$V = \sum_{i,j=1}^{2} H^{M,ij} g(V, A^r S_i^M) A^{-r} S_j^M, \quad r \in \mathbb{R}. \tag{4.17}$$

In order to prove the formula above, it is sufficient to show that for all V and both S_1^M and S_2^M it holds that

$$g(V, A^r S_k^M) = \sum_{i,j=1}^{2} g\left(H^{M,ij} g(V, A^r S_i^M) A^{-r} S_j^M, A^r S_k^M\right).$$

We rewrite the right hand side and use the fact that H^M is symmetric:

$$\sum_{i,j=1}^{2} g\left(H^{M,ij} g(V, A^r S_i^M) A^{-r} S_j^M, A^r S_k^M\right) = \sum_{i,j=1}^{2} g(V, A^r S_i^M) H^{M,ij} H_{jk}^M = g(V, A^r S_k^M),$$

so that the formula (4.17) is satisfied. This formula holds for $\widetilde{A}$ as well.

Furthermore, we claim, that for any self-adjoint 2×2 matrix K in the tangent space of M, the following important relation holds

$$K J^M K = (\det K) J^M, \tag{4.18}$$

for the operator J^M having the properties of rotating any vector in the tangent space counterclockwise by 90 degrees, while maintaining its length with respect to g. This operator can be parameterised as follows:

$$J^M = \frac{1}{\sqrt{\det G}} \begin{bmatrix} -G_{12} & -G_{22} \\ G_{11} & G_{12} \end{bmatrix}. \tag{4.19}$$

Note, that this general representation of J^M is related to the Euclidean version J^E by the relationship $J^M = (\det G)^{-\frac{1}{2}} J^E G$. The selfadjointness assumption on K implies, that it has the following parameterisation in the standard basis

$$K = \begin{bmatrix} K_{11} & K_{12} \\ \frac{K_{12}G_{11} - K_{11}G_{12} + K_{22}G_{12}}{G_{22}} & K_{22} \end{bmatrix}.$$

Using these parametrisations, the relation (4.18) follows immediately.

4.2.3.2 Proof of equation (4.9)

The derivations for equation (4.9) rely on the fact that for the previously defined operator J^M the divergence of the vector field $J^M A^{-1} S_i^M$ vanishes in each tangent space. For that purpose we investigate the following inner products. First, since J^M rotates any vector to be g-orthonormal to itself implies that

$$g\left(J^M A^{-1} S_i^M, A^{-1} S_i^M\right) = 0, \quad i = 1, 2.$$

We want to simplify the expression for $g\left(J^M A^{-1} S_i^M, A^{-1} S_j^M\right)$ when $i \neq j$. For that purpose we now use relation (4.18), self-adjointness of A^{-1} and the fact that $g(J^M S_1^M, S_2^M) = \sqrt{\det G}\, \det\left(S_1^M, S_2^M\right) = \sqrt{\det H^M}$:

$$\begin{aligned} g\left(J^M A^{-1} S_1^M, A^{-1} S_2^M\right) = -g\left(J^M A^{-1} S_2^M, A^{-1} S_1^M\right) &= g\left(A^{-1} J^M A^{-1} S_1^M, S_2^M\right) \\ &= g\left((\det A)^{-1} J^M S_1^M, S_2^M\right) \\ &= (\det A)^{-1} \sqrt{\det H^M}. \end{aligned}$$

Using these expressions and the property (4.17) with $r = -1$, we can now express the vector fields $J^M A^{-1} S_i^M$:

$$\begin{aligned} J^M A^{-1} S_1^M &= \sum_{i,j=1}^{2} H^{M,ij} g\left(J^M A^{-1} S_1^M, A^{-1} S_i^M\right) A S_j^M \\ &= \sum_{j=1}^{2} H^{M,2j} (\det A)^{-1} \sqrt{\det H^M} A S_j^M, \end{aligned}$$

and

$$\begin{aligned} J^M A^{-1} S_2^M &= \sum_{i,j=1}^{2} H^{M,ij} g\left(J^M A^{-1} S_2^M, A^{-1} S_i^M\right) A S_j^M \\ &= -\sum_{j=1}^{2} H^{M,1j} (\det A)^{-1} \sqrt{\det H^M} A S_j^M. \end{aligned}$$

We now use the fact that $\operatorname{div}_M\left(J^M A^{-1} S_i^M\right) = 0$. Applying the divergence operator to the vector fields above yields:

$$\sum_{j=1}^{2} \operatorname{div}_M\left(H^{M,ij} (\det A)^{-1} \sqrt{\det H^M} A S_j^M\right) = 0, \quad i = 1, 2.$$

We use the identity $\operatorname{div}_M(fV) = f \operatorname{div}_M(V) + g(\operatorname{grad}_M(f), V)$ on $f = (\det A)^{-1}$ and $V = H^{M,ij} \sqrt{\det H^M} A S_j^M$, so the above equations formulate to the following for each $i = 1, 2$:

$$\begin{aligned} \sum_{j=1}^{2} \Big[& g\left(\operatorname{grad}_M\left((\det A)^{-1}\right), H^{M,ij} (\det H^M)^{\frac{1}{2}} A S_j^M\right) \\ & + (\det A)^{-1} \operatorname{div}_M\left(H^{M,ij} \sqrt{\det H^M} A S_j^M\right)\Big] = 0. \end{aligned}$$

Applying the identity again on the second term with $f = H^{M,ij} \sqrt{\det H^M}$ and $V = A S_j^M$ and using the PDE (4.2) yields for each $i = 1, 2$:

$$\begin{aligned} \sum_{j=1}^{2} \Big[& g\left(\operatorname{grad}_M\left((\det A)^{-1}\right), H^{M,ij} \sqrt{\det H^M} A S_j^M\right) \\ & + (\det A)^{-1} g\left(\operatorname{grad}_M\left(H^{M,ij} \sqrt{\det H^M}\right), A S_j^M\right)\Big] = 0. \end{aligned}$$

As this equation is zero for both i, we can add the equations, multiply by $A^{-1}S_i^M$, and divide by $(\det A)^{-1}\sqrt{\det H^M}$ to obtain

$$\sum_{i,j=1}^{2} \Big[-H^{M,ij} g\left(\operatorname{grad}_M\left(\log(\det A)\right), AS_j^M\right) A^{-1}S_i^M \\ +\sqrt{\det H^M}\, g\left(\operatorname{grad}_M\left(H^{M,ij}\sqrt{\det H^M}\right), AS_j^M\right) A^{-1}S_i^M\Big] = 0.$$

Using the formula (4.17) and the fact that

$$g(V, \widetilde{A}S_j^M)\widetilde{A}^{-1}S_i^M = g(V, \cancel{(\det A)^{-\frac{1}{2}}} AS_j^M)\cancel{(\det A)^{\frac{1}{2}}} A^{-1}S_i^M,$$

gives

$$\operatorname{grad}_M\left(\log(\det A)\right) = \sum_{i,j=1}^{2} \frac{1}{\sqrt{\det H^M}} g\left(\operatorname{grad}_M\left(H^{M,ij}(\det H^M)^{\frac{1}{2}}\right), \widetilde{A}S_j^M\right)\widetilde{A}^{-1}S_i^M.$$

Expanding the term $\operatorname{grad}_M\left(H^{M,ij}\sqrt{\det H^M}\right)$ yields

$$\operatorname{grad}_M\left(\log(\det A)\right) = N^M + \sum_{i,j=1}^{2} g\left(\operatorname{grad}_M\left(H^{M,ij}\right), \widetilde{A}S_j^M\right)\widetilde{A}^{-1}S_i^M, \tag{4.20}$$

where the term N^M solely depends on the data: $N^M = \frac{1}{2}\operatorname{grad}_M\left(\log\big(\det H^M\big)\right)$.

4.2.3.3 Proof of equation (4.12)

We orthonormalise S^M into a $SO(2)$-valued frame $R^M = (R_1^M, R_2^M)$, so that

$$R_i^M = \sum_{j=1}^{2} T_{ij}^M S_j^M, \qquad S_i^M = \sum_{j=1}^{2} T^{M,ij} R_j^M, \quad 1 \le i \le 2.$$

As R^M is $SO(2)$-valued, it is orthogonal $g(R^M(v), R^M(w)) = g(v, w)$ for all $v, w \in T_pM$ and $(\det R^M) = 1$. By orthogonality and the property $H^M = (S^M)^T G S^M$ it follows that the matrix T^M can be expressed by the data through the relation $(T^M)^T G^{-1} T^M = (H^M)^{-1}$, so that

$$\sum_{m,n=1}^{2} T_{mj}^M G^{mn} T_{n\ell}^M = H^{M,j\ell},$$

for $1 \le j, \ell \le 2$. We can construct T^M by the Gram-Schmidt procedure or by setting $T^M = G^{\frac{1}{2}}(H^M)^{-\frac{1}{2}}$. With the vector fields V_{ij}^M defined in (4.11) we have the following

relationship

$$\begin{aligned}\sum_{j,\ell=1}^{2} \operatorname{grad}_M\left(H^{M,j\ell}\right) T^{M,\ell p} T^{M,jq} &= \sum_{j,\ell,m,n=1}^{2} \operatorname{grad}_M\left(T^M_{mj} G^{mn} T^M_{n\ell}\right) T^{M,\ell p} T^{M,jq} \\ &= \sum_{j,\ell,m,n=1}^{2} \big[\operatorname{grad}_M\left(T^M_{mj}\right) T^{M,jq} \delta^p_n G^{mn} \\ &\quad + \operatorname{grad}_M\left(T_{n\ell}\right) T^{\ell p} \delta^q_m G^{mn} \\ &\quad + \operatorname{grad}_M\left(G^{mn}\right) \delta^p_n \delta^q_m\big] \\ &= \sum_{m,n=1}^{2} \left[V^M_{mq} G^{mp} + V^M_{np} G^{qn} + \operatorname{grad}_M\left(G^{qp}\right)\right],\end{aligned}$$

for $1 \le p, q \le 2$. We now rewrite equation (4.20) in terms of the vector fields R^M_1 and R^M_2 and use the relationship above:

$$\begin{aligned}\operatorname{grad}_M\left(\log(\det A)\right) &= N^M + \sum_{j,\ell=1}^{2} g\left(\operatorname{grad}_M\left(H^{M,j\ell}\right), \widetilde{A} S^M_\ell\right) \widetilde{A}^{-1} S^M_j \\ &= N^M + \sum_{j,\ell,p,q=1}^{2} g\left(\operatorname{grad}_M\left(H^{M,j\ell}\right) T^{M,\ell p} T^{M,jq}, \widetilde{A} R^M_p\right) \widetilde{A}^{-1} R^M_q \\ &= \sum_{m,n,p,q=1}^{2} g\left(V^M_{mq} G^{mp} + V^M_{np} G^{qn}\right. \\ &\qquad \left. + \operatorname{grad}_M\left(G^{qp}\right), \widetilde{A} R^M_p\right) \widetilde{A}^{-1} R^M_q + N^M. \qquad (4.21)\end{aligned}$$

In order to derive equation (4.12) we express the Lie Bracket $[\widetilde{A}R^M_2, \widetilde{A}R^M_1]$ in two different ways: First we use the classical definition from differential topology and secondly we use a 2d vector calculus identity. By the classical definition in the canonical basis (e_1, e_2) we have that

$$\begin{aligned}\left[\widetilde{A}R^M_2, \widetilde{A}R^M_1\right] &= \sum_{i,j,k,\ell=1}^{2} \left[\widetilde{A}_{ij}\left(R^M\right)^j_2 e_i, \widetilde{A}_{k\ell}\left(R^M\right)^\ell_1 e_k\right] \\ &= \sum_{i,j,k,\ell=1}^{2} \Big(\widetilde{A}_{ij}\widetilde{A}_{k\ell}\Big(\left(R^M\right)^j_2 \partial_i \left(R^M\right)^\ell_1 - \left(R^M\right)^j_1 \partial_i \left(R^M\right)^\ell_2\Big) \\ &\quad + \widetilde{A}_{ij}\partial_i\widetilde{A}_{k\ell}\Big(\left(R^M\right)^j_2 \left(R^M\right)^\ell_1 - \left(R^M\right)^j_1 \left(R^M\right)^\ell_2\Big)\Big) e_k.\end{aligned}$$

This definition is equivalent to the definition in Euclidean space. The first term cannot be simplified further due to the complicated parameterisation of R^M in (4.10).

However, for the second term we obtain:

$$\left(R^M\right)_2^j \left(R^M\right)_1^\ell - \left(R^M\right)_1^j \left(R^M\right)_2^\ell = \begin{cases} 0 & \text{if } j = \ell \\ 1 & \text{if } (j,\ell) = (2,1) \\ -1 & \text{if } (j,\ell) = (1,2) \end{cases}.$$

Now the expression for $[\widetilde{A}R_2^M, \widetilde{A}R_1^M]$ above can be reduced to

$$\begin{aligned}[\widetilde{A}R_2^M, \widetilde{A}R_1^M] &= \sum_{i,j,k,\ell=1}^{2} \Big(\widetilde{A}_{ij}\widetilde{A}_{k\ell}\left(\left(R^M\right)_2^j \partial_i \left(R^M\right)_1^\ell - \left(R^M\right)_1^j \partial_i \left(R^M\right)_2^\ell\right) \\ &\qquad + \widetilde{A}_{i2}\partial_i\widetilde{A}_{k1} - \widetilde{A}_{i1}\partial_i\widetilde{A}_{k2}\Big) e_k \\ &= U + [\widetilde{A}_2, \widetilde{A}_1],\end{aligned}$$

where we define

$$U = \sum_{i,j,k,\ell=1}^{2} \widetilde{A}_{ij}\widetilde{A}_{k\ell}\left(\left(R^M\right)_2^j \partial_i \left(R^M\right)_1^\ell - \left(R^M\right)_1^j \partial_i \left(R^M\right)_2^\ell\right) e_k.$$

Before we use the 2d vector calculus identity to write $[\widetilde{A}R_2^M, \widetilde{A}R_1^M]$ in a different way, we express the divergence equation for $\widetilde{A}R_1^M$ and $\widetilde{A}R_2^M$ in terms of known quantities, $\widetilde{A}$ and columns of R^M. This gives the following for each $i = 1, 2$:

$$\begin{aligned}\operatorname{div}_M\left(\widetilde{A}R_i^M\right) &= \sum_{j=1}^{2} \operatorname{div}_M\left(\widetilde{A}\,T_{ij}^M S_j^M\right) \\ &= \sum_{j=1}^{2} g\left(\left(\operatorname{grad}_M\left(T_{ij}^M\right), \widetilde{A}S_j^M\right) + T_{ij}^M \operatorname{div}_M\left(\widetilde{A}S_j^M\right)\right).\end{aligned}$$

We write the first part in terms of the columns of R^M and for the second part we rewrite $\operatorname{div}_M\left(\widetilde{A}S_j^M\right)$ as $\operatorname{div}_M\left((\det A)^{-\frac{1}{2}} AS_j^M\right)$ and use the identity $\operatorname{div}_M(fV) = f\operatorname{div}_M(V) + g(\operatorname{grad}_M(f), V)$. Note that $\operatorname{div}_M\left(AS_j^M\right)$ vanishes by the PDE. We then obtain for each $i = 1, 2$:

$$\begin{aligned}\operatorname{div}_M\left(\widetilde{A}R_i^M\right) &= \sum_{j,k=1}^{2} g\left(\operatorname{grad}_M\left(T_{ij}^M\right), \widetilde{A}\,T^{M,jk}\,R_k^M\right) \\ &\qquad + \sum_{j=1}^{2} T_{ij}^M\, g\left(\operatorname{grad}_M\left((\det A)^{-\frac{1}{2}}\right), AS_j^M\right) \\ &= \sum_{k=1}^{2} g\left(V_{ik}^M, \widetilde{A}R_k^M\right) - \frac{1}{2} g\left(\operatorname{grad}_M\left(\log(\det A)\right), \widetilde{A}R_i^M\right).\end{aligned}$$

Inserting the expression for $\operatorname{grad}_M(\log(\det A))$ from equation (4.21) then yields for each $i = 1, 2$:

$$\begin{aligned}
\operatorname{div}_M\left(\widetilde{A}R_i^M\right) &= \sum_{k=1}^{2} g\left(V_{ik}^M, \widetilde{A}R_k^M\right) - \frac{1}{2} g\left(N^M, \widetilde{A}R_i^M\right) \\
&\quad - \frac{1}{2} \sum_{m,n,p,q=1}^{2} g\Big(g\left(V_{mq}^M G^{mp} + V_{np}^M G^{qn}\right. \\
&\qquad \left. + \operatorname{grad}_M\left(G^{qp}\right), \widetilde{A}R_p^M\right)\widetilde{A}^{-1}R_q^M, \widetilde{A}R_i^M\Big) \\
&= \sum_{k=1}^{2} g\left(V_{ik}^M, \widetilde{A}R_k^M\right) - \frac{1}{2} g\left(N^M, \widetilde{A}R_i^M\right) \\
&\quad - \frac{1}{2} \sum_{m,n,p,q=1}^{2} g\left(V_{mq}^M G^{mp} + V_{np}^M G^{qn} + \operatorname{grad}_M\left(G^{qp}\right), \widetilde{A}R_p^M\right) G_{qi} \\
&= \sum_{k=1}^{2} g\left(V_{ik}^M, \widetilde{A}R_k^M\right) - \frac{1}{2} \sum_{n,p=1}^{2} g\left(V_{np}^M \delta_i^n, \widetilde{A}R_p^M\right) \\
&\quad - \frac{1}{2} \sum_{j=1}^{2} g\left(N^M, \widetilde{A}R_j^M\right) - \frac{1}{2} \sum_{m,p,q=1}^{2} g\left(V_{mq}^M G^{mp} G_{qi}, \widetilde{A}R_p^M\right) \\
&\quad - \frac{1}{2} \sum_{q,p=1}^{2} g\left(\operatorname{grad}_M\left(G^{qp}\right) G_{qi}, \widetilde{A}R_p^M\right) \\
&= \frac{1}{2} \sum_{p=1}^{2} g\left(V_{ip}^M, \widetilde{A}R_p^M\right) - \frac{1}{2} g\left(N^M, \widetilde{A}R_i^M\right) && \text{(4.22a)} \\
&\quad - \frac{1}{2} \sum_{m,p,q=1}^{2} g\left(V_{mq}^M G^{mp} G_{qi}, \widetilde{A}R_p^M\right) && \text{(4.22b)} \\
&\quad - \frac{1}{2} \sum_{p,q=1}^{2} g\left(\operatorname{grad}_M\left(G^{qp}\right) G_{qi}, \widetilde{A}R_p^M\right). && \text{(4.22c)}
\end{aligned}$$

It can be shown that the 2d vector calculus identity $[V, W] = \nabla \cdot (W \otimes V - V \otimes W) - (\nabla \cdot V)W + (\nabla \cdot W)V$ in Euclidean space also holds in a similar version on a manifold:

$$[V, W] = \operatorname{div}_M(W \otimes V - V \otimes W) - \operatorname{div}_M(V) W + \operatorname{div}_M(W) V. \tag{4.23}$$

We want to apply this identity to the vector fields $V = \widetilde{A}R_2^M$ and $W = \widetilde{A}R_1^M$. For that purpose we first investigate the first term on the right hand side. We simplify

the expression $W \otimes V - V \otimes W$ by using the relation (4.18):

$$\begin{aligned}\widetilde{A}R_1^M \otimes \widetilde{A}R_2^M - \widetilde{A}R_2^M \otimes \widetilde{A}R_1^M &= \widetilde{A}(R_1^M \otimes R_2^M - R_2^M \otimes R_1^M)\widetilde{A} \\ &= -\widetilde{A}J^E\widetilde{A} = -(\det\,\widetilde{A})J^E = -J^E.\end{aligned}$$

Taking the divergence of this constant coefficient matrix thus only gives a few contributions from the Christoffel symbols:

$$\mathrm{div}_M\left(\widetilde{A}R_1^M \otimes \widetilde{A}R_2^M - \widetilde{A}R_2^M \otimes \widetilde{A}R_1^M\right) = (\Gamma^1_{21} + \Gamma^2_{22})e_1 - (\Gamma^1_{11} + \Gamma^2_{12})e_2.$$

For the second part of right hand side in (4.23) we use the expression for the divergence equations in (4.22) and obtain the following for the Lie bracket:

$$\begin{aligned}[\widetilde{A}R_2^M, \widetilde{A}R_1^M] &= \mathrm{div}_M\left(\widetilde{A}R_1^M \otimes \widetilde{A}R_2^M - \widetilde{A}R_2^M \otimes \widetilde{A}R_1^M\right) \\ &\quad - \mathrm{div}_M\left(\widetilde{A}R_2^M\right)\widetilde{A}R_1^M + \mathrm{div}_M\left(\widetilde{A}R_1^M\right)\widetilde{A}R_2^M \\ &= (\Gamma^1_{21} + \Gamma^2_{22})e_1 - (\Gamma^1_{11} + \Gamma^2_{12})e_2 && \text{(4.24a)} \\ &\quad + \frac{1}{2}\sum_{m,p,q=1}^{2}\Big[-g\left(V^M_{2p}, \widetilde{A}R_p^M\right)\widetilde{A}R_1^M && \text{(4.24b)} \\ &\quad + g\left(V^M_{1p}, \widetilde{A}R_p^M\right)\widetilde{A}R_2^M && \text{(4.24c)} \\ &\quad + g\left(V^M_{mq}G^{mp}G_{q2}, \widetilde{A}R_p^M\right)\widetilde{A}R_1^M && \text{(4.24d)} \\ &\quad - g\left(V^M_{mq}G^{mp}G_{q1}, \widetilde{A}R_p^M\right)\widetilde{A}R_2^M && \text{(4.24e)} \\ &\quad + g\left(\mathrm{grad}_M\left(G^{qp}\right)G_{q2}, \widetilde{A}R_p^M\right)\widetilde{A}R_1^M && \text{(4.24f)} \\ &\quad - g\left(\mathrm{grad}_M\left(G^{qp}\right)G_{q1}, \widetilde{A}R_p^M\right)\widetilde{A}R_2^M && \text{(4.24g)} \\ &\quad + g\left(N^M, \widetilde{A}R_2^M\right)\widetilde{A}R_1^M - g\left(N^M, \widetilde{A}R_1^M\right)\widetilde{A}R_2^M\Big], && \text{(4.24h)}\end{aligned}$$

where the part in (4.24h) can be reduced to

$$\frac{1}{2}g\left(N^M, \widetilde{A}R_2^M\right)\widetilde{A}R_1^M - \frac{1}{2}g\left(N^M, \widetilde{A}R_1^M\right)\widetilde{A}R_2^M = -\frac{1}{2}J^E G N^M.$$

By the relationship $J^M = (\det G)^{-\frac{1}{2}}J^E G$ the above can be reposed as $-\frac{1}{2}(\det G)^{\frac{1}{2}}J^M N^M$. Denoting the part in (4.24a) by P_C, the following part in (4.24b)-(4.24e) by $\frac{1}{2}P_V$ and the next part in (4.24f)-(4.24g) by $\frac{1}{2}P_g$ yields the following for the Lie bracket:

$$[\widetilde{A}R_2^M, \widetilde{A}R_1^M] = P_C + \frac{1}{2}P_V + \frac{1}{2}P_g - \frac{1}{2}(\det G)^{\frac{1}{2}}J^M N^M,$$

with

$$
\begin{aligned}
P_C &= (\Gamma^1_{21} + \Gamma^2_{22})e_1 - (\Gamma^1_{11} + \Gamma^2_{12})e_2,\\
P_V &= \sum_{m,p,q=1}^{2} \Big[-g\left(V^M_{2p}, \widetilde{A}R^M_p\right)\widetilde{A}R^M_1 + g\left(V^M_{1p}, \widetilde{A}R^M_p\right)\widetilde{A}R^M_2\\
&\quad + g\left(V^M_{mq}G^{mp}G_{q2}, \widetilde{A}R^M_p\right)\widetilde{A}R^M_1 - g\left(V^M_{mq}G^{mp}G_{q1}, \widetilde{A}R^M_p\right)\widetilde{A}R^M_2\Big],\\
P_g &= \sum_{p,q=1}^{2} \Big[g\left(\operatorname{grad}_M\left(G^{qp}\right)G_{q2}, \widetilde{A}R^M_p\right)\widetilde{A}R^M_1 - g\left(\operatorname{grad}_M\left(G^{qp}\right)G_{q1}, \widetilde{A}R^M_p\right)\widetilde{A}R^M_2\Big].
\end{aligned}
$$

Combining the two ways to express the Lie bracket $[\widetilde{A}R^M_2, \widetilde{A}R^M_1]$, yields equation (4.12):

$$U + [\widetilde{A}_2, \widetilde{A}_1] = P_C + \frac{1}{2}P_V + \frac{1}{2}P_g - \frac{1}{2}(\det G)^{\frac{1}{2}} J^M N^M.$$

Here the vector fields U, P_V and P_g depend on the unknowns $\widetilde{A}$ and θ^M. Therefore, the composition of these vector fields determine if a direct reconstruction approach for $\widetilde{A}$ is feasible.

4.2.3.4 Simplification of equation (4.12) when g is diagonal or conformal

The diagonal case The main issue with equation (4.12) in the general case is the complicated parameterisation for R^M. For a diagonal metric R^M simplifies to

$$R^M = (\det G)^{-\frac{1}{2}} \begin{bmatrix} \cos\left(\theta^M\right)(\det G)^{\frac{1}{2}} & -\sin\left(\theta^M\right)G_{22} \\ \sin\left(\theta^M\right)G_{11} & \cos\left(\theta^M\right)(\det G)^{\frac{1}{2}} \end{bmatrix}$$

Due to this expression for R^M the vector fields U, P_C, P_V and P_g can be simplified, so that feasibility of a reconstruction approach for $\widetilde{A}$ can be assessed. We first investigate this part in the expression for U:

$$\left(R^M\right)^j_2 \partial_i \left(R^M\right)^\ell_1 - \left(R^M\right)^j_1 \partial_i \left(R^M\right)^\ell_2$$

For $j = \ell = 1$ this simplifies to:

$$(G_{11}\, G_{22})^{\frac{1}{2}}(G^{-1}_{11}\, \partial_i \theta^M) - (G^{-1}_{11}\, G_{22})^{\frac{1}{2}} \left(G^{-1}_{11}\, \partial_i G_{11} - G^{-1}_{22}\, \partial_i G_{22}\right) \sin\left(\theta^M\right)\cos\left(\theta^M\right).$$

For $(j, \ell) = (2, 1) = (1, 2)$ this simplifies to:

$$-\frac{1}{2}\left(G^{-1}_{11}\, \partial_i G_{11} - G^{-1}_{22}\, \partial_i G_{22}\right)\sin^2(\theta^M).$$

For $j = \ell = 2$ this simplifies to:

$$(G_{11}\, G_{22})^{\frac{1}{2}}(G^{-1}_{22}\, \partial_i \theta^M) - (G_{11}\, G^{-1}_{22})^{\frac{1}{2}} \left(G^{-1}_{11}\, \partial_i G_{11} - G^{-1}_{22}\, \partial_i G_{22}\right) \sin\left(\theta^M\right)\cos\left(\theta^M\right).$$

Now U can be expressed as:

$$\begin{aligned} U = \sum_{i,k=1}^{2} \Big[& (G_{11}\, G_{22})^{\frac{1}{2}} \left(\widetilde{A}_{i1}\widetilde{A}_{k1} G_{11}^{-1} \partial_i \theta^M + \widetilde{A}_{i2}\widetilde{A}_{k2} G_{22}^{-1} \partial_i \theta^M \right) e_k \\ & - \frac{1}{2} \left(\widetilde{A}_{i1}\widetilde{A}_{k1} (G_{11}^{-1} f)^{\frac{1}{2}} + \widetilde{A}_{i2}\widetilde{A}_{k2} (G_{11}\, G_{22}^{-1})^{\frac{1}{2}} \right) \big(G_{11}^{-1} \partial_i G_{11} \\ & \qquad - G_{22}^{-1} \partial_i G_{22} \big) \sin\big(\theta^M\big) \cos\big(\theta^M\big) e_k \\ & - \frac{1}{2} \left(\widetilde{A}_{i1}\widetilde{A}_{k2} G_{11}^{-1} + \widetilde{A}_{i2}\widetilde{A}_{k1} \right) \big(G_{11}^{-1}\, \partial_i G_{11} - G_{22}^{-1}\, \partial_i G_{22} \big) \sin^2(\theta^M) e_k \Big]. \end{aligned}$$

We note that in the canonical basis (e_1, e_2) the anistropy can be parameterised as a non-symmetric matrix by

$$\widetilde{A} = \begin{bmatrix} \widetilde{A}_{11} & \widetilde{A}_{12} \\ \widetilde{A}_{12} \frac{G_{11}}{G_{22}} & \frac{\widetilde{A}_{12}^2 G_{11} + G_{22}}{\widetilde{A}_{11} G_{22}} \end{bmatrix},$$

where the entries $\widetilde{A}_{21} = \widetilde{A}_{12} \frac{G_{11}}{G_{22}}$ and $\widetilde{A}_{22} = \frac{\widetilde{A}_{12}^2 G_{11} + G_{22}}{\widetilde{A}_{11} G_{22}}$ ensure self-adjointness and that $\widetilde{A}$ has determinant 1. In the following we will use this parameterisation to express the quantities in equation (4.12). To keep notation simple we still refer to the elements in the second row as $\widetilde{A}_{21}$ and $\widetilde{A}_{22}$. The first line in the expression for U then simplifies to

$$(G_{11}\, G_{22})^{\frac{1}{2}} \left(\widetilde{A}_{i1}\widetilde{A}_{k1} G_{11}^{-1} \partial_i \theta^M + \widetilde{A}_{i2}\widetilde{A}_{k2} G_{22}^{-1} \partial_i \theta^M \right) e_k = (G_{11}\, G_{22})^{\frac{1}{2}} \widetilde{A}^2 \mathrm{grad}_M \left(\theta^M \right),$$

where $\mathrm{grad}_M \left(\theta^M \right) = \begin{bmatrix} G_{11}^{-1} \partial_1 \theta^M \\ G_{22}^{-1} \partial_2 \theta^M \end{bmatrix}$. Next, we show that some of terms in the expression for U appear in the expression for P_g as well:

$$\begin{aligned} P_g &= \sum_{p,q=1}^{2} \left[g \left(\mathrm{grad}_M \left(G^{qp} \right) G_{q2}, \widetilde{A} R_p^M \right) \widetilde{A} R_1^M - g \left(\mathrm{grad}_M \left(G^{qp} \right) G_{q1}, \widetilde{A} R_p^M \right) \widetilde{A} R_2^M \right] \\ &= \sum_{p,q=1}^{2} \Big[g \left(\mathrm{grad}_M \left(G_{pp}^{-1} \delta_q^p \right) G_{22} \delta_q^2, \widetilde{A} R_p^M \right) \widetilde{A} R_1^M \\ &\qquad - g \left(\mathrm{grad}_M \left(G_{pp}^{-1} \delta_q^p \right) G_{11} \delta_q^1, \widetilde{A} R_p^M \right) \widetilde{A} R_2^M \Big] \\ &= -g \left(G_{22}^{-1} \mathrm{grad}_M \left(G_{22} \right), \widetilde{A} R_2^M \right) \widetilde{A} R_1^M + g \left(G_{11}^{-1} \mathrm{grad}_M \left(G_{11} \right), \widetilde{A} R_1^M \right) \widetilde{A} R_2^M \end{aligned}$$

When we insert the parameterisaton for $\tilde{A}$ and R^M, and write out the expressions for $\mathrm{grad}_M(G_{22})$ and $\mathrm{grad}_M(G_{11})$ explicitly, this yields:

$$\begin{aligned}
P_g = \sum_{i,k=1}^{2} \Big[&- \Big(\widetilde{A}_{i1}\widetilde{A}_{k1}G_{11}^{-\frac{1}{2}}G_{22}^{\frac{1}{2}} + \widetilde{A}_{i2}\widetilde{A}_{k2}G_{11}^{\frac{1}{2}}G_{22}^{-\frac{1}{2}}\Big)\big(G_{11}^{-1}\partial_i G_{11} \\
&\qquad -G_{22}^{-1}\partial_i G_{22}\big)\sin\big(\theta^M\big)\cos\big(\theta^M\big)e_k \\
&- \Big(\widetilde{A}_{i1}\widetilde{A}_{k2}G_{11}^{-1} + \widetilde{A}_{i2}\widetilde{A}_{k1}\Big)\big(G_{11}^{-1}\partial_i G_{11} - G_{22}^{-1}\partial_i G_{22}\big)\sin^2(\theta^M)e_k\Big] \\
&+ \Big(\widetilde{A}_{11}\widetilde{A}_{12}G_{11}^{-1}\partial_1 G_{11} - \widetilde{A}_{11}\widetilde{A}_{21}G_{11}^{-1}\partial_1 G_{22} \\
&+\widetilde{A}_{12}^2 G_{22}^{-1}\partial_2 G_{11} - \widetilde{A}_{11}\widetilde{A}_{22}G_{22}^{-1}\partial_2 G_{22}\Big)e_1 \\
&+ \Big(\widetilde{A}_{11}\widetilde{A}_{22}G_{22}^{-1}\partial_1 G_{11} - \widetilde{A}_{21}^2 G_{11}^{-1}\partial_1 G_{22} \\
&+\widetilde{A}_{12}\widetilde{A}_{22}G_{22}^{-1}\partial_2 G_{11} - \widetilde{A}_{21}\widetilde{A}_{22}G_{22}^{-1}\partial_2 G_{22}\Big)e_2.
\end{aligned}$$

We see, that the first two lines in the expression only differ by a factor of $\frac{1}{2}$ from the last two lines in the expression for U. To simplify the last two lines above, we introduce the matrices $\hat{A}_1$ and $\hat{A}_2$:

$$\hat{A}_1 = \begin{bmatrix} \widetilde{A}_{11}\widetilde{A}_{12} & \widetilde{A}_{12}^2 \\ \widetilde{A}_{11}\widetilde{A}_{22} & \widetilde{A}_{12}\widetilde{A}_{22} \end{bmatrix} \quad \text{and} \quad \hat{A}_2 = \begin{bmatrix} \widetilde{A}_{11}\widetilde{A}_{21} & \widetilde{A}_{11}\widetilde{A}_{22} \\ \widetilde{A}_{21}^2 & \widetilde{A}_{21}\widetilde{A}_{22} \end{bmatrix}.$$

Using these, we can express the last four lines in the expression for P_g by

$$\begin{aligned}
&\Big(\widetilde{A}_{11}\widetilde{A}_{12}G_{11}^{-1}\partial_1 G_{11} - \widetilde{A}_{11}\widetilde{A}_{21}G_{11}^{-1}\partial_1 G_{22} + \widetilde{A}_{12}^2 G_{22}^{-1}\partial_2 G_{11} - \widetilde{A}_{11}\widetilde{A}_{22}G_{22}^{-1}\partial_2 G_{22}\Big)e_1 \\
&\quad + \Big(\widetilde{A}_{11}\widetilde{A}_{22}G_{22}^{-1}\partial_1 G_{11} - \widetilde{A}_{21}^2 G_{11}^{-1}\partial_1 G_{22} + \widetilde{A}_{12}\widetilde{A}_{22}G_{22}^{-1}\partial_2 G_{11} - \widetilde{A}_{21}\widetilde{A}_{22}G_{22}^{-1}\partial_2 G_{22}\Big)e_2 \\
&= \hat{A}_1 \mathrm{grad}_M(G_{11}) - \hat{A}_2 \mathrm{grad}_M(G_{22}),
\end{aligned}$$

with $\mathrm{grad}_M(G_{11}) = \begin{bmatrix} G_{11}^{-1}\partial_1 G_{11} \\ G_{22}^{-1}\partial_2 G_{11} \end{bmatrix}$ and $\mathrm{grad}_M(G_{22}) = \begin{bmatrix} G_{11}^{-1}\partial_1 G_{22} \\ G_{22}^{-1}\partial_2 G_{22} \end{bmatrix}$. We take the difference between U and $\frac{1}{2}P_g$ and obtain

$$U - \frac{1}{2}P_g = (G_{11}\,G_{22})^{\frac{1}{2}}\widetilde{A}^2 \mathrm{grad}_M\left(\theta^M\right) - \frac{1}{2}\hat{A}_1 \mathrm{grad}_M(G_{11}) + \frac{1}{2}\hat{A}_1 \mathrm{grad}_M(G_{22}).$$

The Christoffel symbols appearing in the vector field P_C simplify to

$$\begin{aligned}
P_C &= (\Gamma_{21}^1 + \Gamma_{22}^2)e_1 - (\Gamma_{11}^1 + \Gamma_{12}^2)e_2 \\
&= \frac{1}{2}\begin{bmatrix} 0 & G_{11}^{-1}G_{22} \\ -1 & 0 \end{bmatrix}\mathrm{grad}_M(G_{11}) + \frac{1}{2}\begin{bmatrix} 0 & 1 \\ -G_{11}G_{22}^{-1} & 0 \end{bmatrix}\mathrm{grad}_M(G_{22}).
\end{aligned}$$

As the operator J^M in (4.4.1.2) takes the form

$$J^M = (G_{11}\, G_{22})^{-\frac{1}{2}} \begin{bmatrix} 0 & -G_{22} \\ G_{11} & 0 \end{bmatrix},$$

the previous expression can be written in terms of J^M as

$$P_C = -\frac{1}{2}(G_{11}^{-1}\, G_{22})^{\frac{1}{2}}\, J^M \mathrm{grad}_M\,(G_{11}) - \frac{1}{2}(G_{11}\, G_{22}^{-1})^{\frac{1}{2}}\, J^M \mathrm{grad}_M\,(G_{22})\,.$$

Finally, we can simplify the expression for P_V:

$$\begin{aligned}
P_V = & \sum_{m,p,q=1}^{2} \Big[-g\left(V_{2p}^M, \widetilde{A}R_p^M\right) \widetilde{A}R_1^M + g\left(V_{1p}^M, \widetilde{A}R_p^M\right) \widetilde{A}R_2^M \\
& + g\left(V_{mq}^M G^{mp} G_{q2}, \widetilde{A}R_p^M\right) \widetilde{A}R_1^M - g\left(V_{mq}^M G^{mp} G_{q1}, \widetilde{A}R_p^M\right) \widetilde{A}R_2^M \Big] \\
= & \sum_{m,p,q=1}^{2} \Big[-g\left(V_{2p}^M, \widetilde{A}R_p^M\right) \widetilde{A}R_1^M + g\left(V_{1p}^M, \widetilde{A}R_p^M\right) \widetilde{A}R_2^M \\
& + g\left(V_{mq}^M G_{pp}^{-1} \delta_m^p G_{22} \delta_q^2, \widetilde{A}R_p^M\right) \widetilde{A}R_1^M - g\left(V_{mq}^M G_{pp}^{-1} \delta_m^p G_{11} \delta_q^1, \widetilde{A}R_p^M\right) \widetilde{A}R_2^M \Big] \\
= & -g\left(V_{21}^M, \widetilde{A}R_1^M\right) \widetilde{A}R_1^M - g\left(G_{11}^{-1} G_{22} V_{21}^M, \widetilde{A}R_2^M\right) \widetilde{A}R_2^M \\
& + g\left(V_{12}^M, \widetilde{A}R_2^M\right) \widetilde{A}R_2^M + g\left(G_{11} G_{22}^{-1} V_{12}^M, \widetilde{A}R_1^M\right) \widetilde{A}R_1^M \\
= & -\widetilde{A}\left(R_1^M \otimes R_1^M + G_{11}^{-1} G_{22} R_2^M \otimes R_2^M\right) \widetilde{A}^T G V_{21}^M \\
& + \widetilde{A}\left(R_2^M \otimes R_2^M + G_{11} G_{22}^{-1} R_1^M \otimes R_1^M\right) \widetilde{A}^T G V_{12}^M \\
= & -\widetilde{A} \begin{bmatrix} 1 & 0 \\ 0 & G_{11} G_{22}^{-1} \end{bmatrix} \widetilde{A}^T G V_{21}^M + \widetilde{A} \begin{bmatrix} G_{11}^{-1} G_{22} & 0 \\ 0 & 1 \end{bmatrix} \widetilde{A}^T G V_{12}^M \\
= & -G_{11} \widetilde{A}^2 V_{21}^M + G_{22} \widetilde{A}^2 V_{12}^M . \qquad (4.25)
\end{aligned}$$

Combining these expressions yields the formula (4.12):

$$U + [\widetilde{A}_2, \widetilde{A}_1] = P_C + \frac{1}{2} P_V + \frac{1}{2} P_g - \frac{1}{2}(\det G)^{\frac{1}{2}}\, J^M N^M,$$

with the modified expressions

$$U - \frac{1}{2} P_g = (G_{11}\, G_{22})^{\frac{1}{2}}\, \widetilde{A}^2 \mathrm{grad}_M\left(\theta^M\right) \qquad (4.26a)$$

$$- \frac{1}{2}\left(\hat{A}_1 \mathrm{grad}_M\,(G_{11}) - \hat{A}_2 \mathrm{grad}_M\,(G_{22})\right), \qquad (4.26b)$$

$$P_C = -\frac{1}{2} J^M \left[\left(\frac{G_{22}}{G_{11}}\right)^{\frac{1}{2}} \mathrm{grad}_M\,(G_{11}) + \left(\frac{G_{11}}{G_{22}}\right)^{\frac{1}{2}} \mathrm{grad}_M\,(G_{22}) \right], \qquad (4.26c)$$

$$P_V = \widetilde{A}^2 \left(G_{22} V_{12}^M - G_{11} V_{21}^M\right). \qquad (4.26d)$$

Here we highlight that the mixed terms with $\sin^2(\theta^M)$ and $\sin(\theta^M)\cos(\theta^M)$ cancel out by taking the difference between U and $\frac{1}{2}P_g$.

The conformal case For a conformal metric, R^M simplifies to

$$R^M = \begin{bmatrix} \cos(\theta^M) & -\sin(\theta^M) \\ \sin(\theta^M) & \cos(\theta^M) \end{bmatrix}.$$

Such that in the conformal case, the expression for R^M is equivalent to the Euclidean version R^E and $\theta^M = \theta^E$. This implies that J^M is equivalent to J^E, as J^M is a special case of the rotational operator R^M for the angle $\theta = \frac{\pi}{2}$. Furthermore, a conformal metric is a special case of a diagonal metric so that the formula (4.12) holds for this case as well with the modified quantities in (4.26) when substituting G_{11} and G_{22} with ρ^2. This formula then simplifies to

$$\rho^2 \widetilde{A}^2 \operatorname{grad}_M\left(\theta^M\right) + [\widetilde{A}_2, \widetilde{A}_1] = -\frac{1}{2} J^E \operatorname{grad}_M\left(\rho^2\right) + \rho^2 \widetilde{A}^2 V_{12}^{M,a} - \frac{1}{2}\rho^2 J^E N^M, \quad (4.27)$$

where we highlight that in the conformal case self-adjointness implies that $\widetilde{A}$ is symmetric, so that $\hat{A}_1 - \hat{A}_2 = J^E$.

4.2.4 Derivation of the reconstruction procedures

4.2.4.1 Reconstruction of the normalised anisotropy $\widetilde{A}$ with $m = 3$ or 4

Comments on the general case Consider a quadruple of boundary conditions (f_1, f_2, f_3, f_4) with possibly $f_2 = f_3$. Let $S^{M,(1)} = [S_1^{M,(1)}|S_2^{M,(1)}] = [S_1^M|S_2^M]$ and $S^{M,(2)} = [S_1^{M,(2)}|S_2^{M,(2)}] = [S_3^M|S_4^M]$ be matrices that satisfy the positivity condition (4.8). Let us denote $R^{M,(i)} = S^{M,(i)}T^{M,(i)T}$ the $SO(2,\mathbb{R})$-valued matrix obtained after Gram-Schmidt orthonormalisation such that $g(R^{M,(i)}V, R^{M,(i)}W) = g(V,W)$ and $\det(R^{M,(i)}) = 1$. Here $T^{M,(i)}$ is such that $T^{M,(i)}H^M T^{M,(i)T} = G$ and we parameterise $R^{M,(i)}$ by an angle function θ_i^M for each i. We denote

$$H^{M,(i)} = S^{M,(i)T} G S^{M,(i)}, \quad N^{M,(i)} = \frac{1}{2}\operatorname{grad}_M\left(\log\left(\det H^{M,(i)}\right)\right),$$
$$V_{k\ell}^{M,(i)} = \sum_{j=1}^{2} \operatorname{grad}_M\left(T_{kj}^{M,(i)}\right)\left(T^{M,(i)}\right)^{j\ell}.$$

For each pair of solutions, we have the equation

$$U^{(i)} + [\widetilde{A}_2, \widetilde{A}_1] = P_C + \frac{1}{2}P_V^{(i)} + \frac{1}{2}P_g^{(i)} - \frac{1}{2}(\det G)^{\frac{1}{2}} J^M N^{M,(i)}, \quad (4.28)$$

where

$$
\begin{aligned}
U^{(i)} &= \sum_{i,j,k,\ell=1}^{2} \widetilde{A}_{ij}\widetilde{A}_{k\ell}\left(\left(R^{M,(i)}\right)_2^j \partial_i \left(R^{M,(i)}\right)_1^\ell - \left(R^{M,(i)}\right)_1^j \partial_i \left(R^{M,(i)}\right)_2^\ell\right) e_k,\\
P_C &= (\Gamma^1_{21} + \Gamma^2_{22})e_1 - (\Gamma^1_{11} + \Gamma^2_{12})e_2,\\
P_V^{(i)} &= \sum_{p,m,q=1}^{2} \Big[-g\left(V_{2p}^{M,(i)}, \widetilde{A}R_p^{M,(i)}\right)\widetilde{A}R_1^{M,(i)} + g\left(V_{1p}^{M,(i)}, \widetilde{A}R_p^{M,(i)}\right)\widetilde{A}R_2^{M,(i)}\\
&\quad + g\left(V_{mq}^{M,(i)} G^{mp} G_{q2}, \widetilde{A}R_p^{M,(i)}\right)\widetilde{A}R_1^{M,(i)}\\
&\quad - g\left(V_{mq}^{M,(i)} G^{mp} G_{q1}, \widetilde{A}R_p^{M,(i)}\right)\widetilde{A}R_2^{M,(i)}\Big],\\
P_g^{(i)} &= \sum_{q,p=1}^{2} \Big[g\left(\mathrm{grad}_M\left(G^{qp}\right) G_{q2}, \widetilde{A}R_p^{M}\right)\widetilde{A}R_1^{M,(i)}\\
&\qquad - g\left(\mathrm{grad}_M\left(G^{qp}\right) G_{q1}, \widetilde{A}R_p^{M,(i)}\right)\widetilde{A}R_2^{M,(i)}\Big].
\end{aligned}
$$

Subtracting equation (4.28) with $i = 1$ from the same equation with $i = 2$ cancels the Lie Bracket $[\widetilde{A}_2, \widetilde{A}_1]$ and the term P_C, and leaves the following expression:

$$
U^{(2)} - U^{(1)} + \frac{1}{2}\left(-P_V^{(2)} + P_V^{(1)} - P_g^{(2)} + P_g^{(1)}\right) = -\frac{1}{2} Jg(N^{M,(2)} - N^{M,(1)}). \quad (4.29)
$$

When we parameterise $\widetilde{A}$ by

$$
\widetilde{A}(\lambda, \mu) = \begin{bmatrix} \lambda & \mu \\ \frac{-\lambda^2 G_{12} + \mu\lambda G_{11} + G_{12}}{\lambda G_{22} - \mu G_{12}} & \frac{\mu^2 G_{11} - \lambda\mu G_{12} + G_{22}}{\lambda G_{22} - \mu G_{12}} \end{bmatrix},
$$

we can write the left hand side in (4.29) as a function of λ and μ. Doing so and denoting the right hand side in (4.29) by Y_f we obtain the following system of equations:

$$
\begin{aligned}
&(c_1 - c_2 y_f^1)\lambda + (c_3 - c_4 y_f^1)\mu + c_5\lambda^2\mu + c_6\lambda\mu^2 + c_7\lambda^3 + c_8\mu^3 = 0,\\
&k_1 + (k_2 + k_3 y_f^2)\lambda\mu + (k_4 - k_5 y_f^2)\lambda^2 + (k_6 - k_7 y_f^2)\mu^2\\
&\qquad + k_8\lambda^2\mu^2 + k_9\lambda^3\mu + k_{10}\lambda\mu^3 + k_{11}\lambda^4 + k_{12}\mu^4 = 0.
\end{aligned} \quad (4.30)
$$

Where c_i and k_i depend on $G, T^{M,(1)}, T^{M,(2)}, \theta_1^M$, and θ_2^M. In the Euclidean case the trick in equation (3.10) is used to express $\cos\left(\theta_2^E - \theta_1^E\right)$ and $\sin\left(\theta_2^E - \theta_1^E\right)$ with

respect to inner products of columns of R^E. We can obtain similar results:

$$G_{11}\cos\left(\theta_2^M-\theta_1^M\right) = R_1^{M,(1)} G R_1^{M,(2)} = \sum_{i,j=1}^{2} T_{1i}^{M,(1)} T_{1j}^{M,(2)} g(S_i^{M,(1)}, S_j^{M,(2)}), \tag{4.31a}$$

$$(\det G)^{\frac{1}{2}}\sin\left(\theta_2^M-\theta_1^M\right) + G_{12}\cos\left(\theta_2^M-\theta_1^M\right) = R_2^{M,(1)} G R_1^{M,(2)} = \sum_{i,j=1}^{2} T_{2i}^{M,(1)} T_{1j}^{M,(2)} g(S_i^{M,(1)}, S_j^{M,(2)}). \tag{4.31b}$$

Hence, $\cos\left(\theta_2^M-\theta_1^M\right)$, $\sin\left(\theta_2^M-\theta_1^M\right)$ and $\mathrm{grad}_M\left(\theta_2^M-\theta_1^M\right)$ can be expressed by the data:

$$\mathrm{grad}_M\left(\theta_2^M-\theta_1^M\right) = \cos\left(\theta_2^M-\theta_1^M\right)\mathrm{grad}_M\left(\sin\left(\theta_2^M-\theta_1\right)^M\right) - \sin\left(\theta_2^M-\theta_1^M\right)\mathrm{grad}_M\left(\cos\left(\theta_2^M-\theta_1^M\right)\right).$$

However, in the system of equations (4.30) there appear mixed terms on the form $\cos\left(\theta_i^M\right)^2\_\_\_$ and $\cos\left(\theta_i^M\right)\sin\left(\theta_i^M\right)\_\_\_$ for both $i=1$ and $i=2$ which cannot be substituted by any of the formulas above. Therefore a general reconstruction approach is currently not feasible.

The diagonal case In this case for each pair of solutions equation (4.28) simplifies with the following modified quantities:

$$U^{(i)} - \frac{1}{2}P_g^{(i)} = (G_{11}\,G_{22})^{\frac{1}{2}}\widetilde{A}^2\mathrm{grad}_M\left(\theta_i^M\right) \tag{4.32a}$$

$$-\frac{1}{2}\left(\hat{A}_1\mathrm{grad}_M\left(G_{11}\right) - \hat{A}_2\mathrm{grad}_M\left(G_{22}\right)\right), \tag{4.32b}$$

$$P_C = -J^M\left[\frac{1}{2}\left(\frac{G_{22}}{G_{11}}\right)^{\frac{1}{2}}\mathrm{grad}_M\left(G_{11}\right) + \left(\frac{G_{11}}{G_{22}}\right)^{\frac{1}{2}}\mathrm{grad}_M\left(G_{22}\right)\right], \tag{4.32c}$$

$$P_V^{(i)} = \widetilde{A}^2\left(G_{22}V_{12}^{M,(i)} - G_{11}V_{21}^{M,(i)}\right). \tag{4.32d}$$

Subtracting equation (4.28) with $i=1$ from the same equation with $i=2$ cancels the Lie Bracket $[\widetilde{A}_2,\widetilde{A}_1]$, the term P_C, and the term in (4.32b) so we obtain the system of equations

$$\widetilde{A}^2 X_f = Y_f, \tag{4.33}$$

with

$$\begin{aligned} X_f &= (G_{11}\, G_{22})^{\frac{1}{2}} \operatorname{grad}_M \left(\theta_2^M - \theta_1^M\right) - \frac{1}{2} G_{22} \left(V_{12}^{M,(2)} - V_{12}^{M,(1)}\right) \\ &\quad + \frac{1}{2} G_{11} \left(V_{21}^{M,(2)} - V_{21}^{M,(1)}\right), \\ Y_f &= -\frac{1}{2} (G_{11}\, G_{22})^{\frac{1}{2}} J^M \left(N^{M,(2)} - N^{M,(1)}\right). \end{aligned}$$

Here $\operatorname{grad}_M \left(\theta_2^M - \theta_1^M\right)$ can be expressed by the data using the relationships in (4.31):

$$\begin{aligned} G_{11} \cos\left(\theta_2^M - \theta_1^M\right) &= \sum_{i,j=1}^{2} T_{1i}^{M,(1)} T_{1j}^{M,(2)} g(S_i^{M,(1)}, S_j^{M,(2)}), \\ (G_{11}\, G_{22})^{\frac{1}{2}} \sin\left(\theta_2^M - \theta_1^M\right) &= \sum_{i,j=1}^{2} T_{2i}^{M,(1)} T_{1j}^{M,(2)} \underbrace{g(S_i^{M,(1)}, S_j^{M,(2)})}_{=H^M_{i(2+j)}}. \end{aligned}$$

We now parameterise $\widetilde{A}^2$ by two functions ξ and ζ:

$$\widetilde{A}^2(\xi, \zeta) = \begin{bmatrix} \xi & \zeta \\ \zeta \frac{G_{11}}{G_{22}} & \frac{\zeta^2 G_{11} + G_{22}}{\xi G_{22}} \end{bmatrix}.$$

Denoting $X_f = (x_f^1, x_f^2)^T$ and $Y_f = (y_f^1, y_f^1)^T$, the system (4.33) can be rewritten as

$$\xi x_f^1 + \zeta x_f^2 = y_f^1 \quad \text{and} \quad \xi\zeta G_{11} x_f^1 + (\zeta^2 G_{11} + G_{22}) x_f^2 = \xi G_{22} y_f^2.$$

On matrix form we can formulate this system of equations as

$$\begin{bmatrix} x_f^1 & x_f^2 \\ y_f^2 G_{22} & -y_f^1 G_{11} \end{bmatrix} \begin{bmatrix} \xi \\ \zeta \end{bmatrix} = \begin{bmatrix} y_f^1 \\ x_f^2 G_{22} \end{bmatrix}.$$

Inverting the matrix on the left hand side gives

$$\xi = g(X_f, Y_f)^{-1} \left(\left(x_f^2\right)^2 G_{22} + \left(y_f^1\right)^2 G_{11} \right) \tag{4.34a}$$

and

$$\zeta = g(X_f, Y_f)^{-1} \left(y_f^1 y_f^2 G_{22} - x_f^1 x_f^2 G_{22} \right). \tag{4.34b}$$

The formulas for ξ and ζ are well-defined, as condition (4.5) guarantees that Y_f never vanishes over M. This is sufficient as by uniform ellipticity for $\widetilde{A}$ and thus $\widetilde{A}^{-2}$ it follows that the inner product $g(X_f, Y_f)$ is bounded from below by the norm of Y_f:

$$g(X_f, Y_f) = g(\widetilde{A}^{-2} Y_f, Y_f) \geq \kappa^{-2} |Y_f|_M > 0.$$

The conformal case In the conformal case the vector fields X_f and Y_f appearing in the system of equations (4.33) are on the form:

$$X_f = \rho^2 \mathrm{grad}_M\left(\theta_2^M - \theta_1^M\right) - \rho^2\left(V_{12}^{M,a(2)} - V_{12}^{M,a(1)}\right),$$
$$Y_f = -\frac{1}{2}\rho^2 J^E\left(N^{M,(2)} - N^{M,(1)}\right).$$

Where $\mathrm{grad}_M\left(\theta_2^M - \theta_1^M\right)$ can be expressed by

$$\rho^2\cos\left(\theta_2^M - \theta_1^M\right) = \sum_{i,j=1}^{2} T_{1i}^{M,(1)} T_{1j}^{M,(2)} g(S_i^{M,(1)}, S_j^{M,(2)}),$$
$$\rho^2\sin\left(\theta_2^M - \theta_1^M\right) = \sum_{i,j=1}^{2} T_{2i}^{M,(1)} T_{1j}^{M,(2)} g(S_i^{M,(1)}, S_j^{M,(2)}).$$

Furthermore, the parameterisation of $\widetilde{A}^2$ simplifies to

$$\widetilde{A}^2(\xi,\zeta) = \begin{bmatrix} \xi & \zeta \\ \zeta & \frac{\zeta^2+1}{\xi} \end{bmatrix},$$

which is equivalent to the Euclidean parameterisation. It now follows from (4.34) that ξ and ζ can be obtained by

$$\xi = \rho^2 g(X_f, Y_f)^{-1}\left(\left(x_f^2\right)^2 + \left(y_f^1\right)^2\right) \quad \text{and} \quad \zeta = \rho^2 g(X_f, Y_f)^{-1}\left(y_f^1 y_f^2 - x_f^1 x_f^2\right).$$

4.2.4.2 Reconstruction of θ^M and $(\det A) = (\det \gamma)^{\frac{1}{2}}$

As the reconstruction approach is only feasible for manifolds with a diagonal or conformal metric, this section solely addresses these two cases.

The diagonal case Reconstruction of θ^M is based on equation (4.12) with the modified quantities in (4.26). Isolating $\mathrm{grad}_M\left(\theta^M\right)$ yields:

$$\begin{aligned}\mathrm{grad}_M\left(\theta^M\right) &= (\det G)^{-\frac{1}{2}}\left(G_{22}V_{12}^M - G_{11}V_{21}^M\right) \\ &+ \frac{1}{2}(\det G)^{-\frac{1}{2}}\tilde{A}^{-2}\left(\hat{A}_1\mathrm{grad}_M\left(G_{11}\right) - \hat{A}_2\mathrm{grad}_M\left(G_{22}\right)\right) \\ &- \frac{1}{2}(\det G)^{-\frac{1}{2}}\tilde{A}^{-2}J^M\left[\left(\frac{G_{22}}{G_{11}}\right)^{\frac{1}{2}}\mathrm{grad}_M\left(G_{11}\right) + \left(\frac{G_{11}}{G_{22}}\right)^{\frac{1}{2}}\mathrm{grad}_M\left(G_{22}\right)\right] \\ &- \frac{1}{2}\tilde{A}^{-2}J^M N^M - (\det G)^{-\frac{1}{2}}\tilde{A}^{-2}[\tilde{A}_2, \tilde{A}_1].\end{aligned} \tag{4.35}$$

Here the expressions for $\hat{A}_1$ and $\hat{A}_2$ are on the following form:

$$\hat{A}_1 = \begin{bmatrix} \widetilde{A}_{11}\widetilde{A}_{12} & \widetilde{A}_{12}^2 \\ \widetilde{A}_{11}\widetilde{A}_{22} & \widetilde{A}_{12}\widetilde{A}_{22} \end{bmatrix} \quad \text{and} \quad \hat{A}_2 = \begin{bmatrix} \widetilde{A}_{11}\widetilde{A}_{21} & \widetilde{A}_{11}\widetilde{A}_{22} \\ \widetilde{A}_{21}^2 & \widetilde{A}_{21}\widetilde{A}_{22} \end{bmatrix}.$$

In order to reconstruct θ^M, we thus need to express $\hat{A}_1, \hat{A}_2$ and $[\tilde{A}_2, \tilde{A}_1]$ with respect to the known functions ξ and ζ that are used to parameterise $\widetilde{A}^2$. We note that $\tilde{A}$ can be parameterised in a similar way as $\widetilde{A}^2$:

$$\widetilde{A}(\lambda, \mu) = \begin{bmatrix} \lambda & \mu \\ \mu\frac{G_{11}}{G_{22}} & \frac{\mu^2 G_{11} + G_{22}}{\lambda G_{22}} \end{bmatrix}.$$

From the first row of $(\tilde{A}(\lambda, \mu))^2$ and $\widetilde{A}^2(\xi, \zeta)$ we have the equalities:

$$\lambda^2 + \mu^2 \frac{G_{11}}{G_{22}} = \xi, \quad \lambda\mu + \mu\frac{\mu^2 G_{11} + G_{22}}{\lambda G_{22}} = \zeta.$$

This yields the following for λ and μ:

$$\lambda = (\xi + 1)\left(\frac{\xi G_{22}}{\zeta^2 G_{11} + (\xi+1)^2 G_{22}}\right)^{\frac{1}{2}}, \quad \mu = \zeta\left(\frac{\xi G_{22}}{\zeta^2 G_{11} + (\xi+1)^2 G_{22}}\right)^{\frac{1}{2}}. \tag{4.36}$$

When we write $[\tilde{A}_2, \tilde{A}_1]$ in terms of λ and μ we obtain:

$$\begin{aligned} [\tilde{A}_2, \tilde{A}_1] = &\begin{bmatrix} \mu G_{11} & \frac{\mu^2 G_{11} + G_{22}}{\lambda} \\ \frac{(\mu^2 G_{11} + G_{22}) G_{11}}{\lambda G_{22}} & \mu\frac{G_{11}(\mu^2 G_{11} + G_{22})}{\lambda^2 G_{22}} \end{bmatrix} \operatorname{grad}_M(\lambda) \\ &+ \begin{bmatrix} -\lambda G_{11} & -\mu G_{11} \\ -\mu\frac{G_{11}^2}{G_{22}} & \frac{(-\mu^2 G_{11} + G_{22}) G_{11}}{\lambda G_{22}} \end{bmatrix} \operatorname{grad}_M(\mu) \\ &+ \begin{bmatrix} 0 \\ \frac{\mu}{\lambda}(\operatorname{grad}_M(G_{11}))^2 - \frac{\mu G_{11}}{\lambda G_{22}}(\operatorname{grad}_M(G_{22}))^2 \end{bmatrix}. \end{aligned} \tag{4.37}$$

Here $(\operatorname{grad}_M(G_{11}))^2$ and $(\operatorname{grad}_M(G_{22}))^2$ denote the second element in $\operatorname{grad}_M(G_{11})$ and $\operatorname{grad}_M(G_{22})$ respectively. Now θ^M can be reconstructed from equation (4.35). When θ^M is known at one point on the boundary one can integrate the right hand side in the expression along curves originating from that point. Alternatively, when assuming that θ^M is known along the whole boundary one can apply the divergence operator to both sides of the equation and solve a Poisson equation with Dirichlet boundary.

Once $\tilde{A}$ and θ^M are known, the vector fields S_i^M are known as well such that we can reconstruct $\log(\det A)$ from equation (4.12), following a similar procedure as for θ^M:

$$\operatorname{grad}_M(\log(\det A)) = N^M + \sum_{p,q=1}^{2} g(\operatorname{grad}_M\left(H^{M,qp}\right), \widetilde{A}\, S_p^M)\widetilde{A}^{-1}\, S_q^M. \tag{4.38}$$

The conformal case In this case θ^M is obtained from the simplified equation:

$$\operatorname{grad}_M\left(\theta^M\right) = V_{12}^{M,a} - \widetilde{A}^{-2}\left(\rho^{-2}[\widetilde{A}_2, \widetilde{A}_1] + \frac{1}{2}\rho^{-2}J^E \operatorname{grad}_M\left(\rho^2\right) + \frac{1}{2}J^E N^M\right). \tag{4.39}$$

As the term with contribution from the matrices $\hat{A}_1$ and $\hat{A}_2$ vanishes there is only a need to express the Lie bracket $[\tilde{A}_2, \tilde{A}_1]$ in terms of the known functions ξ and ζ. The parameterisation for $\tilde{A}$ simplifies to:

$$\tilde{A}(\lambda, \mu) = \begin{bmatrix} \lambda & \mu \\ \mu & \frac{\mu^2+1}{\lambda} \end{bmatrix}.$$

From the formula in (4.36) it follows that λ and μ can be expressed as:

$$\lambda = (\xi+1)\left(\frac{\xi}{\zeta^2+(\xi+1)^2}\right)^{\frac{1}{2}}, \quad \mu = \zeta\left(\frac{\xi}{\zeta^2+(\xi+1)^2}\right)^{\frac{1}{2}}.$$

Now the Lie bracket can be written as:

$$[\tilde{A}_2, \tilde{A}_1] = \rho^2 \begin{bmatrix} \mu & \frac{\mu^2+1}{\lambda} \\ \frac{(\mu^2+1)}{\lambda} & \mu\frac{(\mu^2+1)}{\lambda^2} \end{bmatrix} \operatorname{grad}_M(\lambda) + \rho^2 \begin{bmatrix} -\lambda & -\mu \\ -\mu & \frac{(-\mu^2+1)}{\lambda} \end{bmatrix} \operatorname{grad}_M(\mu).$$

Note, that the last term in (4.37) vanishes for a conformal metric. Now θ^M can be reconstructed from equation (4.39) following the same procedure as for the diagonal case. Similarly $\log(\det A)$ can be reconstructed from equation (4.38) above.

4.3 A shortcut between Euclidean space and Riemannian manifolds

The following section is based on paper C and some parts are taken directly from Appendix C.

4.3.1 Paper C: *Reconstructing anisotropic conductivities on two-dimensional Riemannian manifolds from power densities*

In paper C we aim at reconstructing an anisotropic conductivity from power densities on a two-dimensional Riemannian manifold. Instead of generalising the reconstruction formula from Euclidean space to the manifold as in section 4.2, we consider a 'shortcut' that allows us to use the Euclidean approach independent of the type of the geometry.

We let (M, g) denote a compact Riemannian manifold with smooth boundary ∂M and genus zero. Consider solutions $u_1, \ldots, u_4$ to the boundary value problem

$$\begin{cases} \operatorname{div}_M (\gamma \operatorname{grad}_M (u_i)) = 0 \text{ in } M, \\ u_i = f_i \text{ on } \partial M. \end{cases} \tag{4.40}$$

By the Poincaré-Koebe uniformisation theorem for compact Riemann surfaces (with boundary) (M, g) admits a conformal isometric representation onto a fundamental domain N in $\mathbb{R}^2$. We make the observation that the PDE in (4.40) for a conformal manifold and the PDE in Euclidean space

$$\operatorname{div}_E(\gamma \operatorname{grad}_E(u)) = 0,$$

are preserved. Therefore, after finding a conformal isometric representation of (M, g) one can use the Euclidean approach to reconstruct γ. For general and constructive approaches to the uniformisation procedure we refer to work of [4, 5, 10]. We illustrate our approach numerically by an example of a conductivity on a non-simply connected surface in three-space.

4.3.1.1 Theoretical results

We assume that γ is a $(1, 1)$ tensor field, which is selfadjoint and uniformly elliptic with respect to g, i.e. for some $\kappa > 1$ and for all tangent vectors v and w there holds:

$$g(\gamma(v), w) = g(v, \gamma(w)) \quad \text{and} \quad \kappa^{-1} \|v\|_g^2 \leq g(\gamma(v), v) \leq \kappa \|v\|_g^2. \tag{4.41}$$

From the four different potentials f_i, imposed on the boundary, we consider the four corresponding solutions that gives rise to a (4×4)-power density matrix H with elements:

$$H_{ij}^M = H_{ji}^M = g(\gamma \operatorname{grad}_M (u_i), \operatorname{grad}_M (u_j)) \quad \text{for} \quad 1 \leq i, j \leq m.$$

For the reconstruction procedure to work, we need the following two conditions on the power density matrix H^M:

$$\min(\det(\operatorname{grad}_M u_1, \operatorname{grad}_M u_2), \det(\operatorname{grad}_M u_3, \operatorname{grad}_M u_4)) \geq c_0 > 0 \text{ for every } x \in M, \tag{4.42}$$

$$\operatorname{grad}_M \left(\log \left(\frac{\det(\operatorname{grad}_M u_1, \operatorname{grad}_M u_2)}{\det(\operatorname{grad}_M u_3, \operatorname{grad}_M u_4)} \right) \right) \neq 0 \text{ for every } x \in M. \tag{4.43}$$

Preservation of the conductivity equations Consider a conformal isometric representation of (M, g) given by a compact domain N in $\mathbb{R}^2$, equipped with the metric $g_N = \rho^2 g_E$. Here g_E denotes the Euclidean metric in $\mathbb{R}^2$ and ρ denotes the

conformal factor. We show that the divergence equation on N only differs by the conformal factor from the divergence equation in Euclidean space, so that the PDEs are preserved.

Note that the gradient on (N, g_N) can be expressed with respect to the Euclidean gradient as

$$\operatorname{grad}_N(u) = \sum_{i,j=1}^{2} \frac{\partial u}{\partial x^i} G^{ij} e_j = \frac{1}{\rho^2} \sum_i \frac{\partial u}{\partial x^i} e_i = \frac{1}{\rho^2} \operatorname{grad}_E(u),$$

and the g_N-divergence of a vector field $V = \sum_{i=1}^{2} v^i \, e_i$ is in 2D:

$$\operatorname{div}_N(V) = \frac{1}{\sqrt{\det(G)}} \sum_{i=1}^{2} \frac{\partial}{\partial x^i} \left(v^i \sqrt{\det(G)} \right) = \frac{1}{\rho^2} \sum_{i=1}^{2} \frac{\partial}{\partial x^i} \left(v^i \, \rho^2 \right).$$

Insertion of $V = \gamma \operatorname{grad}_N(u) = \frac{1}{\rho^2} \gamma \operatorname{grad}_E(u)$ now gives directly:

$$\operatorname{div}_N(\gamma \operatorname{grad}_N(u)) = \frac{1}{\rho^2} \operatorname{div}_E(\gamma \operatorname{grad}_E(u)).$$

Equivalence between the equations We want to show that since the conductivity equations are preserved, there is a direct relationship between the equations arising in the conformal and the Euclidean reconstruction procedure.

In section 4.2 the following two equations corresponding to (4.9) and (4.27) were derived for a constructive reconstruction procedure on a conformal manifold (N, g_N):

$$\operatorname{grad}_N(\log(\det A)) = N^N + \sum_{p,q=1}^{2} g(\operatorname{grad}_N(H^{N,qp}), \widetilde{A} \, S_p^N) \widetilde{A}^{-1} \, S_q^N, \tag{4.44}$$

and

$$\rho^2 \widetilde{A}^2 \operatorname{grad}_N(\theta^N) + [\widetilde{A}_2, \widetilde{A}_1] = -\frac{1}{2} J^E \operatorname{grad}_N(\rho^2) + \frac{1}{2} \rho^2 \widetilde{A}^2 V_{12}^{N,a} - \frac{1}{2} \rho^2 J^E N^N, \tag{4.45}$$

with $N^N = \frac{1}{2} \operatorname{grad}_N\big(\log\big(\det H^N\big)\big)$. In the Euclidean case these equations are on the following form, corresponding to equation (4.9) and (3.7):

$$\nabla \log(\det A) = \frac{1}{2} \nabla \log\big(\det H^E\big) + \sum_{j,\ell=1}^{2} \left(\nabla \left(H^E \right)^{j\ell} \cdot \widetilde{A} S_\ell^E \right) \widetilde{A}^{-1} S_j^E, \tag{4.46}$$

and

$$\widetilde{A}^2 \nabla \theta + [\widetilde{A}_2, \widetilde{A}_1] = \widetilde{A}^2 V_{12}^{E,a} - \frac{1}{2} J^E N^E, \tag{4.47}$$

with $N^E = \frac{1}{2} \nabla \log\big(\det H^E\big)$. One key observation between the conformal manifold and Euclidean space is, that the rotation operators R^M and R^E and J^M and J^E

respectively are equivalent. On the manifold we can express the quantities with respect to their Euclidean versions, and when we insert them in equation (4.45) it will reduce to equation (4.47). We note that since $\mathrm{grad}_N(V) = \rho^{-2}\nabla V$ the matrix S^M can be expressed in terms of its Euclidean version as $\rho^{-2}S^E$. For the power density data H^N we obtain

$$H^N = (S^N)^T G S^N = \rho^{-2}(S^E)^T S^E = \rho^{-2} H^E.$$

Furthermore, we want to express the matrix T^N in terms of its Euclidean version T^E. By the relationship $\left(R^N\right)^T G R^N = G$ it follows that T^N satisfies

$$T^N H^N (T^N)^T = G \quad \Leftrightarrow \quad \rho^{-2} T^N H^E (T^N)^T = \rho^2 I.$$

As its Euclidean version T^E is determined by the relationship $T^E H^E (T^E)^T = I$, it follows that $T^N = \rho^2 T^E$. The vector field V_{12}^N can now be expressed with respect to V_{12}^E by

$$\begin{aligned} V_{12}^N &= \frac{1}{2}\sum_{k=1}^{2} \mathrm{grad}_N(T_{1k}^N) T^{N,k2} \\ &= \rho^{-2} \sum_{k=1}^{2} \nabla(\rho^2 T_{1k}^E) \rho^{-2} T^{E,k2} \\ &= \rho^{-2} \sum_{k=1}^{2} \nabla(T_{1k}^E) T^{E,k2} + \rho^{-4}\nabla(\rho^2) \underbrace{\sum_{k=1}^{2} T_{1k}^E T^{E,k2}}_{=0} \\ &= \rho^{-2} V_{12}^E. \end{aligned}$$

As the same holds for the vector field V_{21}^N it follows that $V_{12}^{N,a} = \rho^{-2} V_{12}^{E,a}$. Finally, we can express N^N in terms of N^E by

$$\begin{aligned} N^N &= \frac{1}{2}\mathrm{grad}_N(\log\left(\det H^N\right)) \\ &= \frac{1}{2}\rho^{-2}\nabla(\log\left(\rho^{-4}\det H^E\right)) \\ &= -\rho^{-4}\nabla(\rho^2) + \rho^{-2} \underbrace{\frac{1}{2}\nabla(\log(\det H))}_{=N^E}. \end{aligned}$$

Insertion of these quantities in equation (4.45) yields exactly equation (4.47), as claimed. Similarly, we can substitute the expression for N^N and $(H^N)^{-1}$ into equation (4.44) which yields equation (4.46) in Euclidean space.

Reconstruction procedure The reconstruction procedure is outlined in algorithm 5.

Algorithm 5 Reconstruction procedure

Choose a set of boundary conditions (f_1, f_2, f_3, f_4) so that H^M satisfies (4.42) and (4.43).

1. Use [4, 5, 10] to determine a conformal diffeomorphism that gives the conformal isometric representation $(N, \rho^2\, g_E)$ of (M, g)
2. Express the power density data in the conformal coordinates and transform the power density data by the known conformal factor ρ: $H^E = \rho^2\, H^N$
3. Use the Euclidean reconstruction approach in algorithm 1 to reconstruct γ from H^E

4.3.1.2 A numerical example

The MATLAB and PYTHON code to generate the numerical example can be found on GITLAB: `https://lab.compute.dtu.dk/hjsc/reconstructing-anisotropic-conductivities-on-two-dimensional-riemannian-manifolds-from-power-densities.git`.

To illustrate the reconstruction procedure we consider a manifold $(N, g_N = \rho^2 \cdot g_E)$ represented by a catenoid. The fundamental domain N is seen in the left part of figure 4.1, and the catenoid is already 'uniformized' via the following two different analytic conformal representations r_1 and r_2, and corresponding conformal factors ρ_1 and ρ_2:

$$
\begin{aligned}
r_1(x^1, x^2) &= \begin{pmatrix} \cosh\left(x^1\right)\cos\left(x^2\right) \\ \cosh\left(x^1\right)\sin\left(x^2\right) \\ x^1 \end{pmatrix}, \\
r_2(x^1, x^2) &= \begin{pmatrix} \cosh\left(\log\left(\sqrt{(x^1)^2 + (x^2)^2}\right)\right)\cos\left(\arg(x^1 + ix^2)\right) \\ \cosh\left(\log\left(\sqrt{(x^1)^2 + (x^2)^2}\right)\right)\sin\left(\arg(x^1 + ix^2)\right) \\ \log\left(\sqrt{(x^1)^2 + (x^2)^2}\right) \end{pmatrix}, \\
\rho_1(x^1, x^2) &= \cosh\left(x^1\right), \\
\rho_2(x^1, x^2) &= \frac{\cosh\left(\frac{1}{2}\log\left((x^1)^2 + (x^2)^2\right)\right)}{\sqrt{(x^1)^2 + (x^2)^2}}\,.
\end{aligned}
$$

r_1 is the typical parameterisation of a catenoid, while we consider the more complicated parameterisation r_2 to illustrate how holes in the fundamental domain can be mapped into vertical level curves on the catenoid. These parameterisations are illustrated in the right part of figure 4.1.

The conductivity tensor field γ is composed of three functions ξ, ζ, and $(\det\gamma)^{\frac{1}{2}}$:

$$
\gamma = (\det\gamma)^{\frac{1}{2}} \begin{pmatrix} \xi & \zeta \\ \zeta & \frac{1+\zeta^2}{\xi} \end{pmatrix}\,. \tag{4.48}
$$

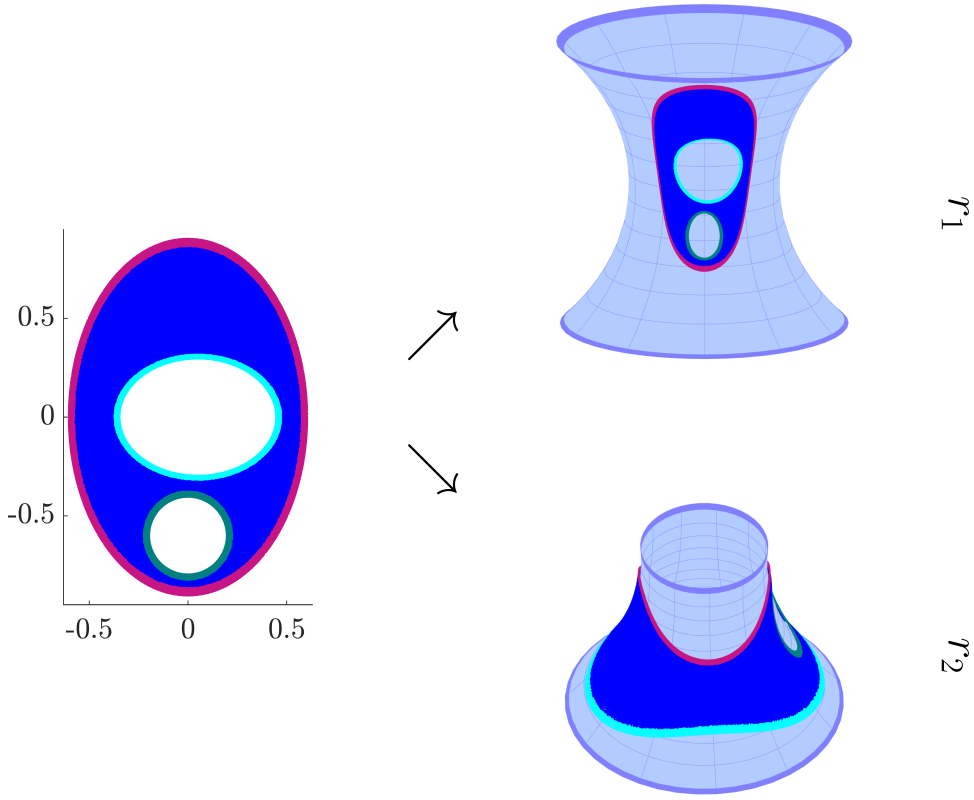

Figure 4.1: Illustration of the two different parameterisations r_1 and r_2 respectively.

The three functions ξ, ζ, and $(\det \gamma)^{\frac{1}{2}}$ are chosen to show a number of features to be reconstructed. These are illustrated in the fundamental domain N in the first row of figure 4.2. In accordance with [6] we use only three boundary conditions to generate the power densities. These are simple polynomials in x^1 and x^2 given by $(f_1, f_2, f_4) = (-x^2 - 0.1(x^2)^2, x^1 - x^2, 0.2x^1x^2 + x^2 - 0.1(x^1)^2)$ (the third boundary condition is $f_3 = f_2$). The reconstructions are shown on the catenoid in the second and third row of Figure 4.2.

4.3.1.3 Conclusion

We have presented a new geometric setting for the reconstruction of anisotropic conductivities from power densities. Our main result generalises the reconstruction method for the 2-dimensional Euclidean setting to 2-dimensional compact Riemannian manifolds with genus 0. The result is presented in a way that opens for further research questions in the setting of Riemannian manifolds with higher genus and possi-

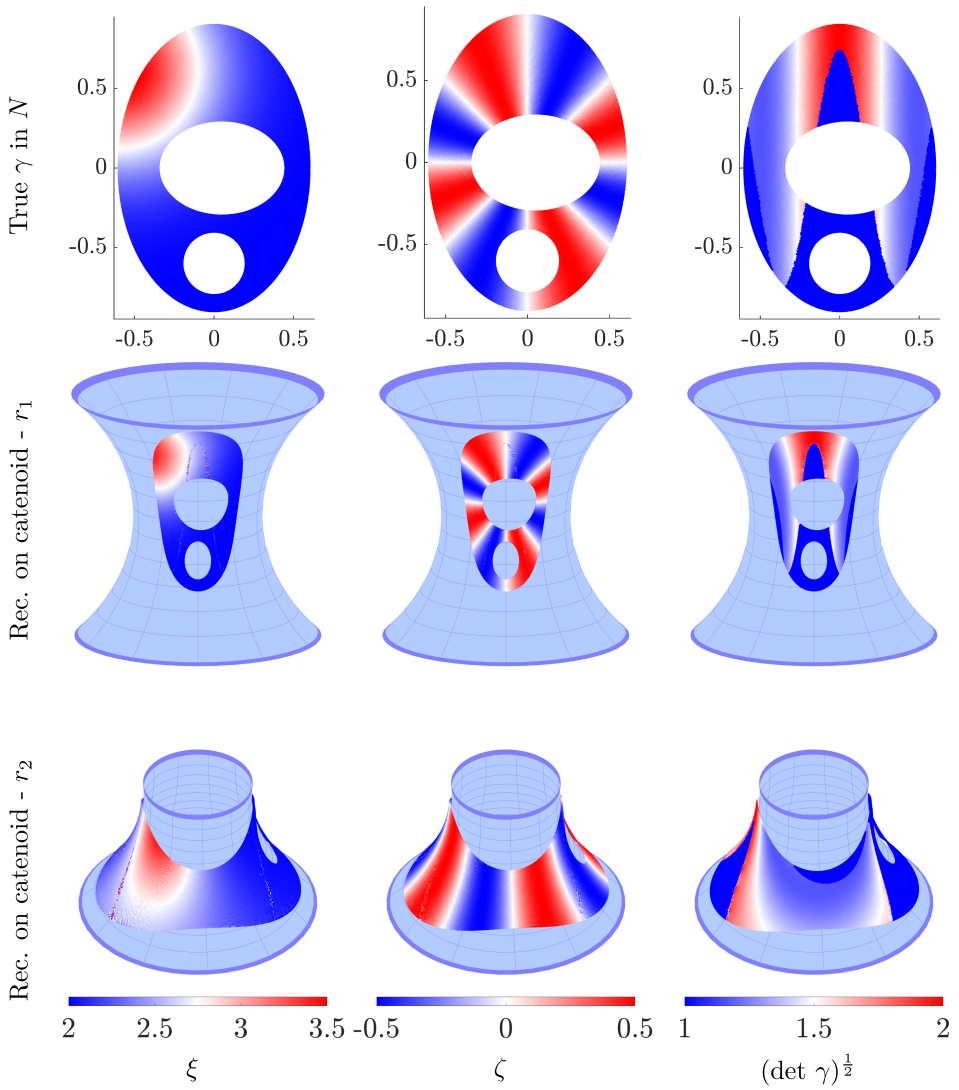

Figure 4.2: The true scalar functions ξ, ζ and $(\det \gamma)^{\frac{1}{2}}$ determining the conductivity in the plane (first row) and their reconstructions on a catenoid corresponding to the parameterisations r_1 and r_2 respectively (second and third row).

bly in higher dimensions. The approach applies to other similar inverse problems with internal data, in particular the reconstruction problem for anisotropic conductivities from *current densities*, c.f. [2, 3].

4.4 Future work

4.4.1 Current densities

4.4.1.1 Short summary of the reconstruction procedure of an anisotropic conductivity from current densities in the Euclidean plane

This is based on [2, 3].
One considers solutions u_i to the conductivity equation

$$\begin{cases} -\operatorname{div}(\gamma \nabla u_i) = 0 & \text{in } \Omega, \\ u_i = f_i & \text{on } \partial\Omega. \end{cases} \tag{4.49}$$

Here $\Omega \subset \mathbb{R}^2$ is an bounded domain with $C^{2,\alpha}$ boundary. $\gamma \in H^{5+\varepsilon}(\Omega)$ is a real 2×2 symmetric matrix that satisfies the uniform ellipticity condition

$$\lambda |\xi|^2 \leq \gamma \xi \cdot \xi \leq \Lambda |\xi|^2 \quad \text{for every } \xi = (\xi^1, \xi^2) \in \mathbb{R}^2,$$

for some $\lambda, \Lambda > 0$. The reconstruction procedure is characterised by reconstructing the anisotropic conductivity γ from internal current densities on the form

$$C_i = \gamma \nabla u_i, \quad 1 \leq i, j \leq 4.$$

Reconstruction of the anisotropy $\tilde{\gamma}$ This requires four measurements $C_i = \gamma \nabla u_i$ for which the following matrices M_1 and M_2 are linearly independent throughout Ω, where

$$M_k = \frac{1}{2} \left(Z_k C^T J + (Z_k C^T J)^T \right),$$

with

$$Z_1 = [\nabla \mu_1 \, \nabla \mu_2], \quad Z_2 = [\nabla \lambda_1 \, \nabla \lambda_2], \quad C = [C_1 \, C_2], \quad J = \begin{bmatrix} 0 & -1 \\ 1 & 0 \end{bmatrix}.$$

Furthermore, μ_1, μ_2, λ_1, and λ_2 are defined as:

$$(\mu_1, \mu_2) = \left(\frac{\det(\nabla u_3, \nabla u_2)}{\det(\nabla u_1, \nabla u_2)}, \frac{\det(\nabla u_1, \nabla u_3)}{\det(\nabla u_1, \nabla u_2)} \right),$$
$$(\lambda_1, \lambda_2) = \left(\frac{\det(\nabla u_4, \nabla u_2)}{\det(\nabla u_1, \nabla u_2)}, \frac{\det(\nabla u_1, \nabla u_4)}{\det(\nabla u_1, \nabla u_2)} \right).$$

The reconstruction formula is derived by applying the curl-operator $(J\nabla)\cdot$ to the following system of equations:

$$\nabla u_3 = \mu_1 \nabla u_1 + \mu_2 \nabla u_2, \tag{4.50a}$$
$$\nabla u_4 = \lambda_1 \nabla u_1 + \lambda_2 \nabla u_2. \tag{4.50b}$$

Using the fact that ∇u_i is curl-free and the formula $\nabla(f\,V) = \nabla f \cdot V + f\mathrm{div}(V)$, one can derive that $\tilde{\gamma}$ must be orthogonal to M_1 and M_2 (in the sense $\mathrm{tr}(\tilde{\gamma}M_1) = \mathrm{tr}(\tilde{\gamma}M_2) = 0$). Therefore, $\tilde{\gamma}$ must be parallel to the following matrix B, which is orthogonal to both M_1 and M_2:

$$B = \begin{bmatrix} 2M_{1,22}M_{2,12} - 2M_{1,12}M_{2,22} & M_{1,11}M_{2,22} - M_{1,22}M_{2,11} \\ M_{1,11}M_{2,22} - M_{1,22}M_{2,11} & 2M_{1,12}M_{2,11} - 2M_{1,11}M_{2,12} \end{bmatrix}.$$

This yields the following explicit reconstruction formula for $\tilde{\gamma}$:

$$\tilde{\gamma} = \mathrm{sign}(B_{11})(\det B)^{-\frac{1}{2}} B, \tag{4.51}$$

In order to be able to write the solutions ∇u_3 and ∇u_4 as linear combinations in the basis $(\nabla u_1, \nabla u_2)$, as in the system (4.50), it is required that u_1 and u_2 satisfy:

$$\inf_{x\in\Omega} |\det(\nabla u_1, \nabla u_2)| \geq c_1 > 0. \tag{4.52}$$

Reconstruction of $(\det\gamma)^{\frac{1}{2}}$ This requires the pair of measurements (C_1, C_2) and that condition (4.52) is satisfied. Similarly to the previous step it is derived from the fact that ∇u_i is curl-free and using the formula $\nabla(f\,V) = \nabla f \cdot V + f\mathrm{div}(V)$. Rewriting the equations $(J\nabla)\cdot\left((\det\gamma)^{-\frac{1}{2}}\tilde{\gamma}^{-1}\nabla u_i\right) = 0$ yields:

$$\nabla \log\left((\det\gamma)^{\frac{1}{2}}\right)\cdot(J\tilde{\gamma}^{-1}C_i) = (J\nabla)\cdot(\tilde{\gamma}^{-1}C_i),$$

for $i = 1, 2$. Combining these equations gives the reconstruction formula which involves integration of a gradient equation:

$$\nabla \log\left((\det\gamma)^{\frac{1}{2}}\right) = J\tilde{\gamma}(C^{-1})^T \begin{pmatrix} (J\nabla)\cdot(\tilde{\gamma}^{-1}C_1) \\ (J\nabla)\cdot(\tilde{\gamma}^{-1}C_2) \end{pmatrix}. \tag{4.53}$$

This is very similar to the reconstruction formula of an isotropic conductivity from power densities (see [1, Prop. 10.2]).

4.4.1.2 Thoughts on this approach on Riemannian manifolds

In following we discuss whether it is possible to generalise the reconstruction procedure in the Euclidean plane to a Riemannian manifold (M, g). We consider current density data $C_i^M = \gamma\,\mathrm{grad}_M(u_i)$ for $1 \leq i \leq 4$. The reconstruction procedure in the

Euclidean plane relies on the two important equations (4.51) and (4.53). These are both derived based on the fact that the gradients ∇u_i are curl-free. This is equivalent to the gradients satisfying $\operatorname{div}(J\nabla u_i) = 0$. It was shown in section 4.2 that the property $\operatorname{div}_M(J^M \operatorname{grad}_M(u_i)) = 0$ holds on (M, g) with the operator J^M defined as

$$J^M = \frac{1}{\sqrt{\det G}} \begin{bmatrix} -G_{12} & -G_{22} \\ G_{11} & G_{12} \end{bmatrix}.$$

This indicates that constructive reconstruction formulas on (M, g) are feasible, when one applies the operator $\operatorname{div}_M\left(J^M \cdot\right)$ to the system of equations:

$$\operatorname{grad}_M(u_3) = \mu_1 \operatorname{grad}_M(u_1) + \mu_2 \operatorname{grad}_M(u_2) \tag{4.54}$$

$$\operatorname{grad}_M(u_4) = \lambda_1 \operatorname{grad}_M(u_1) + \lambda_2 \operatorname{grad}_M(u_2). \tag{4.55}$$

Furthermore, we note that the derivations of formula (4.51) are simpler than for the formula to reconstruct $\tilde{A}$ from power densities. This gives the impression that one can generalise equation (4.51) for all types of Riemannian manifolds (not only manifolds with conformal or diagonal metric). In this case M_k and B will depend on the metric matrix function G. The same generalisation holds for formula (4.53), which is solely derived based on the fact that the gradients are curl-free.

The approach in paper C seems feasible as well, as the solutions satisfy the same PDE and the equations are similar. Here one can follow the reconstruction procedure in algorithm 5 with an appropriate transformation of the current density data on a conformal manifold: $C_i^E = \rho^2 C_i^N$.

4.4.2 Higher genus: A torus with disks removed

It would be of interest, whether the reconstruction approach described in section 4.3 for manifolds with genus zero could be generalised to manifolds with higher genus. As a first step we consider the example of a torus with a disk removed as illustrated in figure 4.3.

For the reconstruction procedure from power densities in the Euclidean plane it is discussed in section 3.1.2, whether there exist boundary functions so that the conditions for the reconstruction procedure were satisfied. Here it was shown in [6] that a construction with CGO solutions guarantees that there exists a set of four boundary conditions such that the Jacobian condition in (3.2) and the gradient condition in (3.3) are satisfied. By the equivalence in the PDEs between a conformal manifold and the Euclidean plane, this also applies to Riemannian manifolds with genus zero. In order to generalise this type of result one needs to work with periodic functions as illustrated for the torus in figure 4.3. To guarantee existence of boundary functions such that the corresponding solutions in periodic Sobolev spaces satisfy the Jacobian condition (4.4) and the gradient condition (4.5) we think of using the Runge approximation property. It is known that the unique continuation principle holds for our operator in periodic Sobolev spaces (see e.g. [11, p. 155]). To show

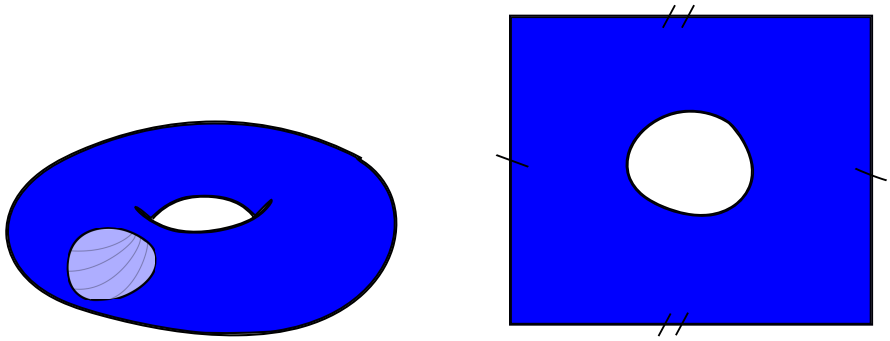

Torus with a disk removed. Parameter domain.

Figure 4.3: A higher genus example: A torus with a disk removed.

that the Runge approximation property holds, we think of using a similar approach as in section 3.2.2.1 for paper B. By compactness we might be able to show that there exists a finite number of boundary conditions so that the Jacobian condition (4.4) holds. It then requires some extra work to extend this result for the gradient condition (4.5), as the coordinate functions x_j and their gradients do not satisfy this condition.

4.4.2.1 Numerical investigations of the Jacobian on a torus

We investigated numerically for the simple case of $\gamma = \mathbb{I}_2$, whether it is possible to find a pair of boundary conditions (f_1, f_2) so that the corresponding Jacobian $\det(\nabla u_1, \nabla u_2)$ is non-vanishing on a torus with one or two disks removed. Figure 4.4 illustrates the solutions and the corresponding Jacobian for the coordinate functions as boundary functions: $f_1 = x_1$ and $f_2 = x_2$. For this choice of boundary conditions we always observed regions in which the Jacobian vanished. To illustrate how the size and number of disks removed influenced in which regions the Jacobian vanishes, we consider the case of a torus with one medium-sized disk removed, one big disk removed, and two disks removed. We see that in the case of one disk removed the small (and problematic) values of the Jacobian appear on a band towards the corners of the parameter domain, which are the regions most difficult to control from the disk removed in the middle. This problem cannot be solved by controlling the domain from two disks removed, but the location and size of the two disks removed influence the shape and location of the band of small values of the Jacobian. Figure 4.5 illustrates the solutions and Jacobian on a torus with a medium-sized disk removed for more oscillating boundary functions $f_1 = \cos(4\arg(x_1 + ix_2))$ and $f_2 = \sin(4\arg(x_1 + ix_2))$. The band of small values of the Jacobian is further towards the corners than in the case of the less oscillating boundary functions. As the regions of a vanishing Jacobian for these two cases in figure 4.4(a) and figure 4.5 do not overlap one could therefore combine these two pairs of boundary functions to obtain a non-vanishing Jacobian

over the whole domain. However, even for the simple case of $\gamma = \mathbb{I}_2$ we were not able to find a single pair of boundary conditions that yielded a non-vanishing Jacobian over the whole domain. Therefore, the approach of covering the domains with a finite number of balls as indicated for the theoretical result above seems also to be the approach to obtain numerical results.

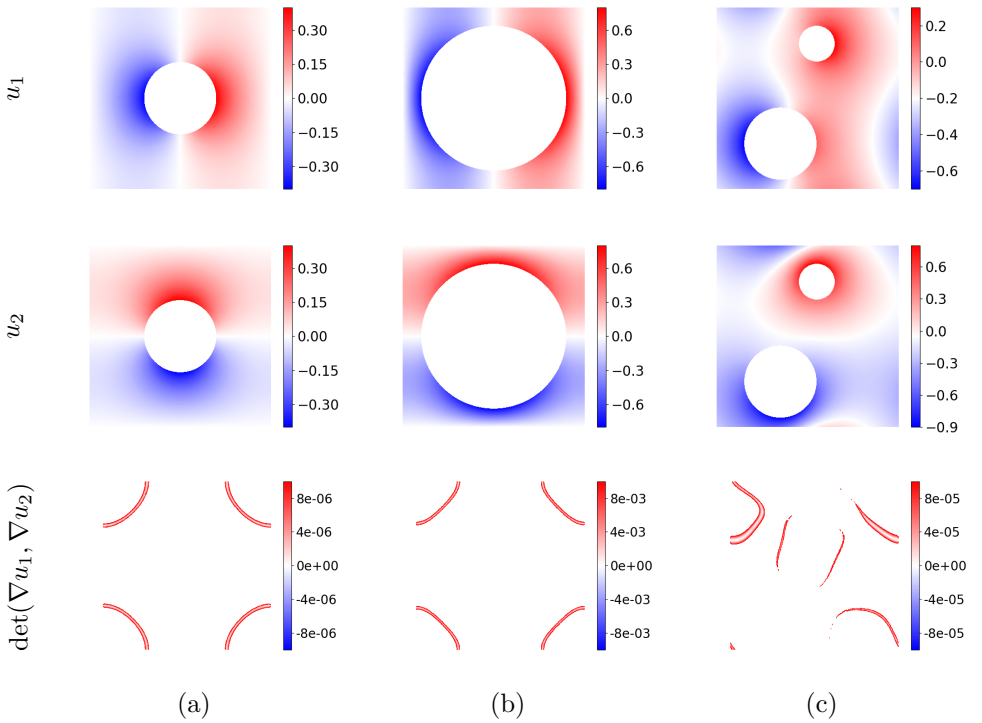

(a) (b) (c)

Figure 4.4: The solutions u_1, and u_2, and the Jacobian $\det(\nabla u_1, \nabla u_2)$ in the parameter domain of a torus with one or two disks removed. The boundary conditions $f_1 = x_1$ and $f_2 = x_2$ are used. For the Jacobian only the smallest values are illustrated in order to highlight in which region the Jacobian vanishes.

4.4.3 Thoughts on the reconstruction of the anisotropy $\tilde{\gamma}$ when the magnitude $(\det \gamma)$ is known

In some practical settings the magnitude of the conductivity, $(\det \gamma)$, is known, while the anisotropy, $\tilde{\gamma}$, is unknown. In this case, it is of interest whether one can reconstruct $\tilde{\gamma}$ from data corresponding to less than four measurements.

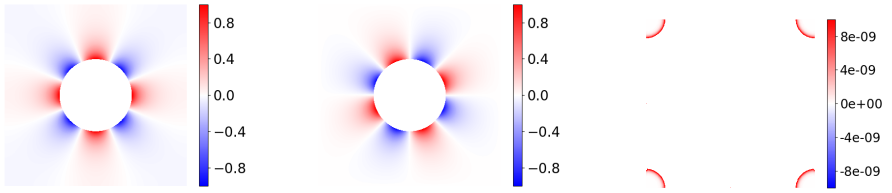

Figure 4.5: The solutions u_1, and u_2, and the Jacobian $\det(\nabla u_1, \nabla u_2)$ in the parameter domain of a torus with one disk removed. The boundary conditions $f_1 = \cos(4\arg(x_1 + ix_2))$ and $f_2 = \sin(4\arg(x_1 + ix_2))$ are used. For the Jacobian only the smallest values are illustrated in order to highlight that the Jacobian vanishes in the outermost corners of the parameter domain.

4.4.3.1 Current densities

We investigate, whether it is possible to reconstruct $\tilde{\gamma}$ with known $(\det \gamma)$ from two current density measurements $C_i = \gamma \nabla u_i$ in the Euclidean plane and if this result translates to a Riemannian manifold (M, g). As $(\det \gamma)$ is known one could try to use the formula (4.53) to reconstruct $\tilde{\gamma}$. As $\det \tilde{\gamma} = 1$ we parameterise it with functions $\lambda(x_1, x_2)$ and $\mu(x_1, x_2)$:

$$\tilde{\gamma}(\lambda, \mu) = \begin{bmatrix} \lambda(x_1, x_2) & \mu(x_1, x_2) \\ \mu(x_1, x_2) & \frac{1+\mu(x_1,x_2)^2}{\lambda(x_1,x_2)} \end{bmatrix}.$$

We insert this expression in (4.53). This yields the following non-linear system of first-order PDEs depending on $\lambda(x_1, x_2)$ and $\mu(x_1, x_2)$:

$$\begin{aligned} &-\left(\mu^2+1\right)\lambda\,\partial_1\lambda - (\mu^3+\mu)\,\partial_2\lambda + \lambda^2\mu\,\partial_1\mu \\ &-(\mu^2+1)\lambda\,\partial_2\mu + c_1\lambda^3\mu + c_2\lambda^2\mu^2 + (c_3 - L_1)\lambda^2 \\ &\qquad + c_4(\mu^3+\mu)\lambda + c_5(\mu^4 + 2\mu^2 + 1) = 0, \qquad (4.56a) \\ &\lambda\mu\,\partial_1\lambda + (1+\mu^2)\,\partial_2\lambda - \lambda^2\,\partial_1\mu - \lambda\mu\,\partial_2\mu - c_1\lambda^3 \\ &\qquad - c_2\lambda^2\mu - c_4\lambda\mu^2 + (c_6 - L_2)\lambda - c_5(\mu^3+\mu) = 0, \qquad (4.56b) \end{aligned}$$

with $\begin{bmatrix} L_1 \\ L_2 \end{bmatrix} = \nabla \log\left((\det\gamma)^{\frac{1}{2}}\right)$. The expressions c_i depend on entries of the matrix $C = [C_1\, C_2]$ and derivatives of these entries:

$$
\begin{aligned}
c_1 &= -\frac{C_{22}\partial_1 C_{21}}{\det C} + \frac{C_{21}\partial_1 C_{22}}{\det C},\\
c_2 &= \frac{C_{12}\partial_1 C_{21}}{\det C} - \frac{C_{22}\left(\partial_2 C_{21} - \partial_1 C_{11}\right)}{\det C} - \frac{C_{11}\partial_1 C_{22}}{\det C} + \frac{C_{21}\left(\partial_2 C_{22} - \partial_1 C_{12}\right)}{\det C},\\
c_3 &= \frac{C_{12}\partial_1 C_{21}}{\det C} - \frac{C_{11}\partial_1 C_{22}}{\det C},\\
c_4 &= \frac{C_{12}\left(\partial_2 C_{21} - \partial_1 C_{11}\right)}{\det C} + \frac{C_{22}\partial_2 C_{11}}{\det C} - \frac{C_{11}\left(\partial_2 C_{22} - \partial_1 C_{12}\right)}{\det C} - \frac{C_{21}\partial_2 C_{12}}{\det C},\\
c_5 &= -\frac{C_{12}\partial_2 C_{11}}{\det C} + \frac{C_{11}\partial_2 C_{12}}{\det C},\\
c_6 &= -\frac{C_{22}\partial_2 C_{11}}{\det C} + \frac{C_{21}\partial_2 C_{12}}{\det C}.
\end{aligned}
$$

In future work one has to investigate, whether this system has a unique pair of solutions. If this is the case, we think it would be possible to solve it numerically in FEniCS. If this approach succeeds, we believe that this result can be generalised to the manifold from our analysis in section 4.4.1.2.

4.4.3.2 Power densities

In contrast to current densities, it is be more complicated to reconstruct $\tilde{\gamma}$ from power density data $H_{ij} = \gamma\,\nabla u_i \cdot \nabla u_j$, corresponding to two measurements $1 \le i, j \le 2$ in the Euclidean plane. In this case one cannot rely on the formula below corresponding to equation (3.6):

$$
\nabla \log(\det A) = \frac{1}{2}\nabla \log\big(\det H^E\big) + \sum_{j,\ell=1}^{2} \left(\nabla \left(H^E\right)^{j\ell} \cdot \widetilde{A} S_\ell^E\right) \widetilde{A}^{-1} S_j^E,
$$

which is similar to the formula (4.53) for current densities. For the reconstruction approach from power densities there is an extra step involved, splitting the vector fields $S_i = A\nabla u_i$ from the power densities H_{ij} by reconstructing the angle function θ. In the formula above knowledge of θ is crucial in order to know the vector fields S_i. Therefore, one cannot use this formula to reconstruct $\tilde{A}$ without knowledge of θ. However, it is also not possible to reconstruct θ from the formula below corresponding to equation (3.7) as it depends on $\tilde{A}$:

$$
\widetilde{A}^2 \nabla\theta + [\widetilde{A}_2, \widetilde{A}_1] = \widetilde{A}^2 V_{12}^{E,a} - \frac{1}{2} J^E N^E.
$$

Thus, we think that one needs a different approach in order to reduce the amount of measurements to reconstruct $\tilde{\gamma}$. If this succeeds in the Euclidean plane there is a high chance from the analysis in section 4.2 and 4.3 that the result can be generalised to Riemannian manifolds.

Bibliography

[1] Giovanni Alberti and Yves Capdeboscq. *Lectures on elliptic methods for hybrid inverse problems*. Societe Mathematique De France, 2018. ISBN: 978-2-85629-872-5.

[2] Guillaume Bal, Chenxi Guo, and François Monard. "Imaging of anisotropic conductivities from current densities in two dimensions." In: *SIAM J. Imaging Sci.* 7.4 (2014), pages 2538–2557. DOI: 10.1137/140961754.

[3] Guillaume Bal, Chenxi Guo, and François Monard. "Inverse anisotropic conductivity from internal current densities." In: *Inverse Problems* 30.2 (2014), pages 025001, 21. ISSN: 0266-5611. DOI: 10.1088/0266-5611/30/2/025001.

[4] Xianfeng Gu and Shing-Tung Yau. "Computing conformal structures of surfaces." In: *Commun. Inf. Syst.* 2.2 (2002), pages 121–145. ISSN: 1526-7555. DOI: 10.4310/CIS.2002.v2.n2.a2.

[5] Xianfeng Gu et al. "Genus zero surface conformal mapping and its application to brain surface mapping." eng. In: *IEEE Transactions on Medical Imaging* 23.8 (2004), pages 949–958. ISSN: 1558254x, 02780062, 10112499. DOI: 10.1109/TMI.2004.831226.

[6] François Monard and Guillaume Bal. "Inverse anisotropic diffusion from power density measurements in two dimensions." eng. In: *Inverse Problems* 28.8 (2012), page 084001. ISSN: 13616420, 02665611. DOI: 10.1088/0266-5611/28/8/084001.

[7] Barrett O'Neill. *Semi-Riemannian geometry : with applications to relativity*. eng. Academic Press, 1983.

[8] Mikko Salo. "The Calderón problem on Riemannian manifolds." In: *Inverse problems and applications: inside out. II*. Volume 60. Math. Sci. Res. Inst. Publ. Cambridge Univ. Press, Cambridge, 2013, pages 167–247.

[9] Sandro Salsa. *Partial Differential Equations in Action*. Springer, 2016.

[10] R. Schoen and S.-T. Yau. *Lectures on harmonic maps*. Volume 2. International Press, 1997.

[11] Michael E. Taylor. "Pseudodifferential Operators." eng. In: *Partial Differential Equations II* (1996), pages 1–73. DOI: 10.1007/978-1-4757-4187-2_1.

[12] Michael Eugene Taylor. *Partial differential equations / Michael E. Taylor ; 1: Basic theory*. eng. Springer, 2011, xxii, 654 Seiten (unknown). ISBN: 1441970541, 144197055x, 9781441970541, 9781441970558, 144197055X.

CHAPTER 5

Concluding remarks

This chapter summarises the work covered in this thesis. In the preceding chapters different settings were considered for reconstruction of an electrical conductivity from power densities. A lot of work has gone into understanding this reconstruction problem on a 2D Riemannian manifold and generalising an existing reconstruction procedure from the Euclidean plane to the manifold, which is partly covered in paper C. Another large part of work went into implementing the reconstruction procedure for anisotropic conductivities in the Euclidean plane. This implementation was used for the spin-off projects on two limited view settings in the Euclidean plane as well. Supplemented with theoretical results this resulted in paper A and B.

The reconstruction problem on a 2D Riemannian manifold was a difficult task as the start of the project. There was no literature available on this topic and we were wondering whether we were asking the right questions for this setting and considering the right approach. It took some time to fully understand the reconstruction procedure in the Euclidean plane and how the assumptions and quantities would translate to the manifold. We realised relatively quickly that one of the main equations for the reconstruction procedure in the plane can be translated to the manifold almost one to one. However, the other main equation relies on the fact that a rotation matrix has a simple parameterisation in the Euclidean plane. This parameterisation is more complicated on the manifold, destroying the simple properties of the equation in the plane. Therefore, we were only able to generalise the second equation to the manifold when the Riemannian metric is conformal or diagonal. We did not find a way to generalise the equation for a general Riemannian manifold, but it is possible that there exists a different approach that will work.

During the process of generalising the reconstruction procedure from the plane to the manifold we realised that the conductivity equations between a conformal manifold and the plane are preserved. To our knowledge this result exists in the literature for isotropic, but not for anisotropic conductivities. This observation implies that one can solve the reconstruction procedure for general Riemannian manifolds: By the Poincaré-Koebe uniformisation theorem every compact Riemann surface has a conformal representation and constructive uniformisation approaches exist in the literature.

After the uniformisation one can simply use the Euclidean reconstruction procedure to recover the conductivity. This result is documented in paper C.

Simultaneous to addressing the reconstruction problem on the manifold, we started implementing the existing reconstruction procedure in the plane. In contrast to the original authors, we decided to implement the procedure in PYTHON using FENICS where it is easier to consider non-simply connected domains. The reconstruction procedure is split into two steps: Recovering the normalised anisotropy of the conductivity represented by two functions and afterwards recovering the magnitude of the conductivity represented by a third function. The second step corresponds to reconstructing an isotropic conductivity, and it was relatively straightforward to get this part to work in the implementation. The first part of recovering the anisotropy was a challenge in the implementation. It took us some time to realise that it required a mesh with a very high resolution and second order basis functions along each mesh interval to obtain reasonable results. The PYTHON code is now public available on GITLAB.

The results on a 2D Riemannian manifold open for possible future work. The result in paper C solely applies for manifolds with genus zero. Therefore, possible future work is to generalise these results to higher genus. One of the main assumptions for the reconstruction procedure is, that a pair of boundary functions is chosen so that the corresponding solutions to the conductivity equation have a non-vanishing Jacobian. For the genus zero case there is a result that guarantees existence of such boundary conditions. In order to generalise this result to higher genus, one needs to prove this result for periodic domains with a boundary. We think that this is possible by using the Runge approximation property.

Another possible topic for future work is generalising the work for power densities on Riemannian manifolds to current densities. For the Euclidean plane there exists an explicit reconstruction procedure, which is simpler than for power densities as one do not have to extract the current densities from the power density measurements. As this reconstruction procedure does not seem to rely on properties that simplify in the Euclidean plane, but not on the manifold, we are positive that the constructive procedure can be generalised to general 2D Riemannian manifolds. Alternatively, we think it is possible to consider the approach in paper C to reconstruct the conductivity from current densities by using a conformal representation of the manifold and solving the problem using the Euclidean reconstruction procedure.

Motivated by practical applications, another interesting question is, whether one can reconstruct the normalised anisotropy from less than four measurements when

the magnitude of the conductivity is known. This applies to reconstruction from both current and power densities and would be an interesting question in the Euclidean plane as well as on a 2D Riemannian manifold. There is a chance that it is possible to reconstruct the normalised anisotropy from two current density measurements. However, this would require solving a non-linear system of first order PDEs. Whether the system is solvable would require further investigations. If this is possible, we think that a similar approach will work on the manifold. A similar approach does not work for reconstruction from power densities, as there, compared to recovery from current densities, is an extra step of extracting the current densities from the power density measurements.

After we did the implementation of recovering anisotropic conductivities from power densities, we tested the implementation on a limited view setting that a previous PhD student, Bjørn Jensen, has worked on. In this limited view setting two- or three-dimensional domains in Euclidean are considered, where a part of the boundary can be controlled by a Dirichlet condition, while on the remaining boundary there is a no-flux condition. This resulted in paper B, where we prove an existence result of a finite number of boundary functions so that the corresponding Jacobian is non-vanishing locally. We supplemented this with numerical examples for a two-dimensional domain and a fixed pair of boundary conditions.

On the external stay the work on the limited view setting gave the idea for another possible research project. Here we studied a limited view setting for two-dimensional domains in the Euclidean plane, where a part of the boundary can be controlled by a Dirichlet condition, while on the remaining boundary there is a zero Dirichlet condition. For this setting we were interested in finding an explicit pair of boundary functions so that the corresponding Jacobian is non-vanishing over the whole domain. We adapted existing results from the full view setting to limited view and proposed sufficient conditions on the boundary functions so that the previous statement is true. This is related to the number of increasing and decreasing part of the functions along the boundary. In this setting it seemed natural to consider boundary functions that are discontinuous along the boundary. We were able to generalise the result to these types of functions by proving a weak maximum principle for weighted Sobolev spaces. This was supplemented by numerical examples by using the previous implementation. However, this required some extra work to make the procedure work in weighted Sobolev spaces, as the general framework in FEniCS only supports solving PDEs in classical Sobolev spaces. This work is documented in paper A.

In practical applications one is usually interested in Neumann rather than Dirichlet boundary conditions. Therefore, for possible future work it would be interesting whether the results in paper A can be generalised to a limited view setting with pure

Neumann instead of pure Dirichlet conditions. In the full view setting with Neumann conditions it is known that a non-vanishing Jacobian is related to the number of positive and negative parts of the function at the boundary. We think that the same sufficient conditions on the boundary functions as in paper A will work in this setting, as the zero Dirichlet condition in paper A on the non-controllable part of the boundary implies, that the number of increasing and decreasing parts is equivalent to the number of positive and negative parts of the function at the boundary. We think that this result will also hold for discontinuous boundary functions without the additional work on weighted Sobolev spaces, as in the Neumann case the existing result allows for discontinuous boundary functions.

APPENDIX A

Paper A: Jacobian of solutions to the conductivity equation in limited view

Mikko Salo, Hjørdis Schlüter. Jacobian of solutions to the conductivity equation in limited view.
Submitted to a journal. Preprint available on arXiv: `http://arxiv.org/abs/2207.03849`.

JACOBIAN OF SOLUTIONS TO THE CONDUCTIVITY EQUATION IN LIMITED VIEW

MIKKO SALO AND HJØRDIS SCHLÜTER

Abstract. The aim of hybrid inverse problems such as Acousto-Electric Tomography or Current Density Imaging is the reconstruction of the electrical conductivity in a domain that can only be accessed from its exterior. In the inversion procedure, the solutions to the conductivity equation play a central role. In particular, it is important that the Jacobian of the solutions is non-vanishing. In the present paper we address a two-dimensional limited view setting, where only a part of the boundary of the domain can be controlled by a non-zero Dirichlet condition, while on the remaining boundary there is a zero Dirichlet condition. For this setting, we propose sufficient conditions on the boundary functions so that the Jacobian of the corresponding solutions is non-vanishing. In that regard we allow for discontinuous boundary functions, which requires the use of solutions in weighted Sobolev spaces. We implement the procedure of reconstructing a conductivity from power density data numerically and investigate how this limited view setting affects the Jacobian and the quality of the reconstructions.

acousto-electric tomography, current density imaging, hybrid inverse problems, coupled physics imaging, non-vanishing Jacobian, conductivity equation

1. Introduction

In certain imaging applications it is important to know whether solutions u_1 and u_2 to the conductivity equation

$$\begin{cases} -\operatorname{div}(\sigma \nabla u_i) = 0 & \text{in } \Omega, \\ u_i = g_i & \text{on } \partial\Omega, \end{cases}$$

satisfy the following non-vanishing Jacobian condition:

$$\det[\nabla u_1(x)\, \nabla u_2(x)] \neq 0, \quad \text{for } x \in \Omega. \tag{1}$$

Here $\Omega \subset \mathbb{R}^2$ is a bounded Lipschitz domain and $\sigma \in L^\infty(\Omega, \mathbb{R}^{2\times 2})$ is an anisotropic conductivity. This question arises in Acousto-Electric Tomography that aims at reconstructing the unknown interior conductivity σ from internal data composed of power density measurements [ZW04; Amm+08]. Similar questions appear in other imaging methods including Current Density Imaging [WS12; Bal13; Li+21] and Magnetic Resonance Electric Impedance Tomography [SKW05; SW11] that aim at reconstructing the conductivity from current density measurements. These questions

Mikko Salo, 0000-0002-3681-6779

Department of Mathematics and Statistics, University of Jyväskylä, 40014 Jyväskylä, Finland
Hjørdis Schlüter, 0000-0001-6659-3863

Department of Applied Mathematics and Computer Science, Technical University of Denmark, 2800 Kgs. Lyngby, Denmark

E-mail addresses: mikko.j.salo@jyu.fi, hjsc@dtu.dk.

are relevant in any dimension $n \geq 2$, but in this article, we will restrict our attention only on the two-dimensional case.

The reconstruction procedure in Acousto-Electric Tomography is characterized by two steps: First reconstructing interior power density data $H_{ij} = \sigma \nabla u_i \cdot \nabla u_j$ from combined information from boundary measurements and perturbations by acoustic waves, and secondly reconstructing σ from the power density matrix $\mathbf{H} \in \mathbb{R}^{2\times 2}$. The non-vanishing Jacobian condition (1) is essential for the second step in the reconstruction procedure, as it requires inverting the matrix $\mathbf{H}$.

The question whether one can find conditions on the boundary functions g_1 and g_2 so that the non-vanishing Jacobian condition (1) is satisfied dates back to Radó in the 1920s. For the constant coefficient case $\sigma = \mathbf{I}_2$ an answer to this question is formulated in the Radó-Kneser-Choquet theorem [Rad26; Kne26; Cho45]. This result was generalized to non-constant coefficients in [Ale86; Ale87; AM94; AN01; BMN01; AN15]. For instance, [BMN01] require that $g = (g_1, g_2)$ is a C^1 diffeomorphism and maps $\partial\Omega$ onto the boundary of a convex domain for the condition (1) to hold. A discussion of results of this type is given in [AC18] (see also [Alb22] for recent work on random boundary data).

In this paper, we address the same question in a limited view setting that is characterized by a non-empty closed part of the boundary, $\Gamma \subset \partial\Omega$, which we can control, while on the rest of the boundary the potentials u_1 and u_2 are vanishing:

$$\begin{cases} -\mathrm{div}(\sigma \nabla u_i) = 0 & \text{in } \Omega, \\ u_i = f_i & \text{on } \Gamma \\ u_i = 0 & \text{on } \partial\Omega \backslash \Gamma. \end{cases} \tag{2}$$

The Radó-Kneser-Choquet type results mentioned above cannot be applied directly in limited view, as $g = (u_1, u_2)|_{\partial\Omega}$ is not injective. However, we show that the arguments for proving such results can be adapted to the limited view setting, and we formulate sufficient conditions under which the corresponding Jacobian is non-vanishing. We also allow the boundary functions to be discontinuous (e.g. piecewise smooth), which seems natural in this setting and requires the use of weighted Sobolev spaces. We illustrate by numerical simulations how these conditions can be used to reconstruct an isotropic conductivity from power density data. For the numerical simulations an analytic reconstruction approach is used [MB12b].

2. Main results

We will consider the conductivity equation $-\mathrm{div}(\sigma \nabla u) = 0$ in Ω, where the conductivity matrix σ is symmetric and satisfies for some $\lambda, \Lambda > 0$ the ellipticity condition

$$\lambda |\xi|^2 \leq \sigma^{jk} \xi_j \xi_k \leq \Lambda |\xi|^2 \text{ for a.e. } x \in \Omega \text{ and all } \xi \in \mathbb{R}^n. \tag{3}$$

The first result states that the presence of an interior critical point for a nonconstant solution u forces oscillations in its boundary data. The result is known for $H^{1/2}$ boundary data, see [AC18, Proposition 6.7], but we give an extension to the case where the boundary data can be slightly worse that $H^{1/2}$ (e.g. piecewise smooth). Boundary data in H^s with $s \leq 1/2$ may be discontinuous, and for such functions, we can use a quasicontinuous representative to talk about their pointwise values [AH96, Chapter 6]. The notation $H^1(\Omega, d^{1-2s})$ for weighted spaces is explained in Section 3.

Proposition 2.1. *Let $\Omega \subset \mathbb{R}^2$ be a simply connected bounded Lipschitz domain and let $\sigma \in C^{0,\alpha}(\overline{\Omega})$ satisfy (3). There is $\varepsilon > 0$ with the following property: if $f \in H^s(\partial\Omega)$ where $|s - 1/2| < \varepsilon$ and if $u \in H^1(\Omega, d^{1-2s})$ is a nonconstant solution of*

$$\begin{cases} -\mathrm{div}(\sigma \nabla u) = 0 & \text{in } \Omega, \\ u = f & \text{on } \partial\Omega, \end{cases}$$

and if $\nabla u(x_0) = 0$ for some $x_0 \in \Omega$, then there are $x_1, x_2, x_3, x_4 \in \partial\Omega$ that are in increasing order along $\partial\Omega$ such that

$$u(x_1) > u(x_0), \quad u(x_2) < u(x_0), \quad u(x_3) > u(x_0), \quad u(x_4) < u(x_0).$$

Proof. We follow the argument in [AC18, Proposition 6.7]. By [Sch90, Theorem 2.3.3] the interior regularity of u is $C^{1,\alpha}_{loc}(\Omega)$. As x_0 is a critical point of u it follows from [AC18, Proposition 6.6] that in a neighborhood U of x_0 the level set $\{x \in U : u(x) = u(x_0)\}$ is made of $m+1$ arcs intersecting with equal angles at x_0 for some $m \geq 1$. We note that by [AC18, Proposition 6.5 (i)] the set $\{x \in U : u(x) > u(x_0)\}$ is made of $m+1$ connected components that we denote by U_l^+:

$$\{x \in U : u(x) > u(x_0)\} = \bigcup_{l=1}^{m+1} U_l^+.$$

Furthermore, by the same proposition it follows that these connected components alternate with the corresponding connected components U_l^- of the set $\{x \in U : u(x) < u(x_0)\}$. We now consider the corresponding sets over the whole domain Ω. The components of $\{u(x) > u(x_0)\}$ are denoted by Ω_j^+ and

$$\{x \in \Omega : u(x) > u(x_0)\} = \bigcup_{j \in J} \Omega_j^+.$$

Similarly, the components of $\{u(x) < u(x_0)\}$ are denoted by Ω_j^- and

$$\{x \in \Omega : u(x) < u(x_0)\} = \bigcup_{k \in K} \Omega_k^-.$$

Now pick indices $j_1, j_2 \in J$ such that $U_1^+ \subset \Omega_{j_1}^+$ and $U_2^+ \subset \Omega_{j_2}^+$. It follows from theorem 3.6 that the weak maximum principle holds for $H^1(\Omega, d^{1-2s})$ solutions, so that if $u(x) > u(x_0)$ holds in the interior of the domains $\Omega_{j_1}^+$ and $\Omega_{j_2}^+$, then one must have $u(x_1) > u(x_0)$ and $u(x_3) > u(x_0)$ for some $x_1 \in \partial\Omega_{j_1}^+$ and $x_3 \in \partial\Omega_{j_2}^+$. Since $u(x) = u(x_0)$ for $x \in \partial\Omega_{j_i}^+ \cap \Omega$, we must have $x_1 \in \partial\Omega \cap \overline{\Omega}_{j_1}^+$ and $x_3 \in \partial\Omega \cap \overline{\Omega}_{j_2}^+$. By construction there exist indices $l_1, l_2 \in [1, .., m+1]$ so that $U_{l_1}^-$ is located between U_1^+ and U_2^+ and $U_{l_2}^-$ is located to the other side of U_2^+. We now pick indices $k_1, k_2 \in K$ such that $U_{l_1}^- \subset \Omega_{k_1}^-$ and $U_{l_2}^- \subset \Omega_{k_2}^-$. By the weak maximum principle (theorem 3.6) there then exist points $x_2 \in \partial\Omega \cap \overline{\Omega}_{k_1}^-$ and $x_4 \in \partial\Omega \cap \overline{\Omega}_{k_2}^-$ such that $u(x_2) < u(x_0)$ and $u(x_4) < u(x_0)$ yielding the desired statement. ∎

Let $\gamma : [0, \ell] \to \mathbb{R}^2$ be a C^1 curve (we do not require that $\gamma(0) = \gamma(\ell)$). We say that γ is regular if $\dot{\gamma}(t) \neq 0$ for all $t \in [0, \ell]$. For a regular curve, we may write a polar coordinate representation for the tangent vector $\dot{\gamma}(t)$ as

$$\dot{\gamma}(t) = r(t) e^{i\phi(t)}$$

where $r(t) = |\dot\gamma(t)|$ and $\phi(t)$ are continuous functions in $[0,\ell]$. The function

$$\arg(\dot\gamma(t)) := \phi(t)$$

is well defined modulo a constant in $2\pi\mathbb{Z}$. We define

$$\mathrm{Ind}(\dot\gamma) := \frac{\arg(\dot\gamma(\ell)) - \arg(\dot\gamma(0))}{2\pi}$$

If γ is closed, i.e. $\gamma(0) = \gamma(\ell)$, then $\mathrm{Ind}(\dot\gamma)$ is the winding number of the curve $\dot\gamma(t)$ (also called the rotation index of $\gamma(t)$), which is an integer. If γ is not closed but $\arg(\dot\gamma(t))$ is monotone (i.e. nondecreasing or nonincreasing), we may still interpret $\mathrm{Ind}(\dot\gamma)$ as the winding number of $\dot\gamma(t)$, and this is then a real number.

We now give sufficient conditions on a pair of boundary data vanishing outside an arc Γ such that the corresponding solutions u_1, u_2 satisfy $\det[\nabla u_1(x)\, \nabla u_2(x)] \neq 0$ everywhere in Ω. Condition (a) below is related to the case where $u_i|_{\partial\Omega}$ are continuous and condition (b) allows discontinuous boundary data.

Theorem 2.2. *Let $\Omega \subset \mathbb{R}^2$ be a bounded simply connected domain with C^1 boundary curve $\eta : [0, 2\pi] \to \partial\Omega$, and let $\sigma \in C^{0,\alpha}(\overline{\Omega}; \mathbb{R}^{2\times 2})$ satisfy (3). Let $\Gamma = \eta([0,\ell])$ be a closed arc in $\partial\Omega$. Let $f_1, f_2 \in C^1(\Gamma)$ be linearly independent, and assume that u_i is the unique solution of*

$$\begin{cases} -\mathrm{div}(\sigma\nabla u_i) = 0 & \text{in } \Omega, \\ u_i = f_i & \text{on } \Gamma \\ u_i = 0 & \text{on } \partial\Omega\backslash\Gamma. \end{cases} \tag{4}$$

Assume that the curve $\gamma : [0,\ell] \to \mathbb{R}^2$, $\gamma(t) = (f_1(\eta(t)), f_2(\eta(t)))$ is regular, $\arg(\dot\gamma(t))$ is monotone, and that one of the following holds:

(a) *$u_i|_{\partial\Omega}$ are continuous, and $|\mathrm{Ind}(\dot\gamma)| \leq 1$; or*

(b) *$u_i|_{\partial\Omega}$ are continuous at $\eta(0)$, and $|\mathrm{Ind}(\dot\gamma)| \leq 1/2$.*

Then $\det[\nabla u_1(x)\, \nabla u_2(x)] \neq 0$ for all $x \in \Omega$.

Proof. Assume that (a) or (b) holds, but one has $\det[\nabla u_1(x_0)\, \nabla u_2(x_0)] = 0$ for some $x_0 \in \Omega$. Then there is a vector $\vec\alpha = (\alpha_1, \alpha_2) \in \mathbb{R}^2 \setminus \{0\}$ such that the function

$$u = \alpha_1 u_1 + \alpha_2 u_2$$

satisfies $\nabla u(x_0) = 0$. Note that if u is a constant, then by the boundary condition one has $u \equiv 0$ and hence f_1 and f_2 would be linearly dependent. Thus, we may assume that u is nonconstant. Note that $u_i|_{\partial\Omega}$ are piecewise C^1 and hence they are also in $H^s(\partial\Omega)$ for any $s < 1/2$. This implies that $u_i \in H^1(\Omega, d^{1-2s})$ by Theorem 3.5. Then by Proposition 2.1 there exist distinct points $x_1, x_2, x_3, x_4 \in \partial\Omega$ that are in increasing order along $\partial\Omega$ such that

$$u(x_1) > u(x_0), \quad u(x_2) < u(x_0), \quad u(x_3) > u(x_0), \quad u(x_4) < u(x_0).$$

Consider the function $g : [0,\ell] \to \mathbb{R}$ given by

$$g(t) := u(\eta(t)) = \vec\alpha \cdot \gamma(t). \tag{5}$$

Extend g by zero to $[0, 2\pi)$. Writing $x_j = \eta(t_j)$ where $t_j \in [0, 2\pi)$, we have

$$g(t_1) > u(x_0), \quad g(t_2) < u(x_0), \quad g(t_3) > u(x_0), \quad g(t_4) < u(x_0). \tag{6}$$

We may assume that $t_1 < t_2 < t_3 < t_4$ (possibly after a cyclic permutation of the indices and after changing g to $-g$).

We now assume that (a) holds, and want to derive a contradiction with (6). The function g is C^1 on $[0, \ell]$ and its derivative satisfies

$$g'(t) = \vec{\alpha} \cdot \dot{\gamma}(t). \tag{7}$$

Since $\arg(\dot{\gamma}(t))$ is monotone and $|\mathrm{Ind}(\dot{\gamma}(t))| \leq 1$, it follows that $g'(t)$ either has at most two zeros in $[0, \ell]$, or has three zeros two of which are at $t = 0$ and $t = \ell$. Note that if the argument is not strictly monotone, we make the interpretation that some of these zeros of g' could be intervals. We also note that by (7) and monotonicity of $\arg(\dot{\gamma}(t))$, g' changes sign after each of these zeros. Now suppose that $u(x_0) \geq 0$. Using the assumption that $u|_{\partial\Omega}$ is continuous, we have $g(0) = 0$, and then (6) implies that g' is positive somewhere in $(0, t_1)$, negative somewhere in (t_1, t_2), positive somewhere in (t_2, t_3), and negative somewhere in (t_3, ℓ). On the other hand, if $u(x_0) < 0$, we use the fact that $g(\ell) = 0$ to obtain similarly that g' is negative somewhere in (t_1, t_2), positive somewhere in (t_2, t_3), negative somewhere in (t_3, t_4), and positive somewhere in (t_4, ℓ). In both cases g' has at least three zeros in $(0, \ell)$. Moreover, before the first such zero, after the last zero, and between each subsequent pair of these zeros there are points where g' is nonzero. This is a contradiction.

Assume that (b) holds. One has the formula (7) for $g'(t)$ on $[0, \ell]$. Since $\arg(\dot{\gamma}(t))$ is monotone and $|\mathrm{Ind}(\dot{\gamma}(t))| \leq 1/2$, $g'(t)$ either has at most one zero (that could be an interval) in $[0, \ell]$, or has two zeros (that could be intervals) which are at $t = 0$ and $t = \ell$. By the assumption that $u_i|_{\partial\Omega}$ is continuous at $t = 0$ it follows that $g(0) = 0$, while there may be a discontinuity at $t = \ell$. If one has $u(x_0) \geq 0$, it follows from (6) that g' is positive somewhere in $(0, t_1)$, negative somewhere in (t_1, t_2), and positive somewhere in (t_2, t_3). On the other hand if $u(x_0) < 0$, from (6) one sees that $t_4 \in (0, \ell]$ and hence g' is negative somewhere in (t_1, t_2), positive somewhere in (t_2, t_3), and negative somewhere in (t_3, t_4). In both cases g' has at least two zeros in $(0, \ell)$ and before, between, and after these zeros there are points where g' is nonzero. This is a contradiction. ∎

Remark 2.3. *In the setting of theorem 2.2, let* $\Gamma = \eta([0, \ell])$ *and* $\Gamma^d = \eta([0, \ell^d])$ *with* $\ell^d < \ell$. *Boundary functions* $f_1, f_2 \in C^1(\Gamma)$ *that satisfy the assumptions and condition (a) in theorem 2.2 can also be used to generate boundary functions* $f_1^d, f_2^d \in C^1(\Gamma^d)$ *whose zero extensions are discontinuous. Define* f_i^d *as*

$$f_i^d(\eta(t)) = f_i(\eta(t))\chi_{[0,\ell^d]}(t).$$

This yields solutions u_i^d *that satisfy* $\det[\nabla u_1^d(x)\, \nabla u_2^d(x)] \neq 0$. *This allows for boundary functions that are not captured in condition (b) in theorem 2.2, as in this case it is possible that* $1/2 < |\mathrm{Ind}(\dot{\gamma^d})|$, *where* $\gamma^d(t) = (f_1^d(\eta(t)), f_2^d(\eta(t)))$.

Proof. Assume that one has $\det[\nabla u_1^d(x_0)\, \nabla u_2^d(x_0)] = 0$ for some $x_0 \in \Omega$. Then there is a vector $\vec{\alpha} = (\alpha_1, \alpha_2) \in \mathbb{R}^2 \setminus \{0\}$ such that the function

$$u^d = \alpha_1 u_1^d + \alpha_2 u_2^d$$

satisfies $\nabla u^d(x_0) = 0$. As $u_i^d|_{\partial\Omega}$ is piecewise C^1 it follows by the analysis in the proof of theorem 2.2 that there exist distinct points $x_1, x_2, x_3, x_4 \in \partial\Omega$ that are in increasing order along $\partial\Omega$ such

that

$$u^d(x_1) > u^d(x_0), \quad u^d(x_2) < u^d(x_0), \quad u^d(x_3) > u^d(x_0), \quad u^d(x_4) < u^d(x_0).$$

We then consider the function $g^d : [0, \ell^d] \to \mathbb{R}$,

$$g^d(t) := u^d(\eta(t)) = (\vec{\alpha} \cdot \gamma(t))\chi_{[0,\ell^d]}(t)$$

where $\gamma(t) = (f_1(\eta(t)), f_2(\eta(t))$ for $t \in [0, \ell]$ as before. We extend g^d by zero to $[0, 2\pi)$. Writing $x_j = \eta(t_j)$ where $t_j \in [0, 2\pi)$, we have

$$g^d(t_1) > u^d(x_0), \quad g^d(t_2) < u^d(x_0), \quad g^d(t_3) > u^d(x_0), \quad g^d(t_4) < u^d(x_0). \tag{8}$$

Furthermore, we consider the function $g : [0, \ell] \to \mathbb{R}$ for the same vector $\vec{\alpha}$:

$$g(t) := \vec{\alpha} \cdot \gamma(t).$$

Since $\arg(\dot{\gamma}(t))$ is monotone and $|\mathrm{Ind}(\dot{\gamma})| \leq 1$, it follows that $g'(t)$ has at most two zeros in $(0, \ell)$, or three zeros two of which are at $t = 0$ and $t = \ell$. (Again these zeros could be intervals.) Since $u_j|_{\partial\Omega}$ are continuous, we have $f_j(\eta(0)) = f_j(\eta(\ell)) = 0$ and thus $g(0) = g(\ell) = 0$. Suppose that $g'(t)$ has exactly two zeros in $(0, \ell)$. Then since g' must change sign after each zero, there exist two intervals $(0, t_i)$ and (t_i, ℓ) so that either

$$g(t) \geq 0 \quad \text{for } t \in (0, t_i) \quad \text{and} \quad g(t) \leq 0 \quad \text{for } t \in (t_i, \ell),$$

or

$$g(t) \leq 0 \quad \text{for } t \in (0, t_i) \quad \text{and} \quad g(t) \geq 0 \quad \text{for } t \in (t_i, \ell).$$

On the other hand if $g'(t)$ has at most one zero, or three zeros two of which are at $t = 0$ and $t = \ell$, then either

$$g(t) \geq 0 \quad \text{for } t \in (0, \ell) \quad \text{or} \quad g(t) \leq 0 \quad \text{for } t \in (0, \ell).$$

The behavior of g translates to g^d, as g^d is the restriction of g to the interval $[0, \ell^d]$ with $\ell^d < \ell$. It follows that there are at most two intervals for which g^d is nonnegative and nonpositive respectively, and additionally $(g^d)'$ must change sign after each of its zeros. This is in contradiction with (8) as no matter if $u^d(x_0) \geq 0$ or $u^d(x_0) \leq 0$ it is not possible for g^d to have two points for which $g^d(t) \geq u(x_0)$ and two points for which $g^d(t) \leq u(x_0)$ in alternating order. ∎

Remark 2.4. *For boundary functions f_1 and f_2 that satisfy one of the conditions in theorem 2.2 it is determined by the order of the functions whether* $\det[\nabla u_1(x)\, \nabla u_2(x)]$ *is positive or negative for all $x \in \Omega$.*

3. Dirichlet problem in weighted spaces

Let $\Omega \subset \mathbb{R}^n$ be a bounded open set with Lipschitz boundary, and consider the operator

$$Lu = -\partial_j(\sigma^{jk}\partial_k u) + cu$$

where $\sigma^{jk}, c \in L^\infty(\Omega)$, $\sigma^{jk} = \sigma^{kj}$, and (σ^{jk}) is uniformly elliptic in the sense that for some $\lambda, \Lambda > 0$,

$$\lambda |\xi|^2 \leq \sigma^{jk}\xi_j\xi_k \leq \Lambda |\xi|^2 \text{ for a.e. } x \in \Omega \text{ and all } \xi \in \mathbb{R}^n. \tag{9}$$

We wish to consider the Dirichlet problem

$$Lu = 0 \text{ in } \Omega, \quad u = f \text{ on } \partial\Omega$$

in suitable weighted Sobolev spaces. For general references on weighted Sobolev spaces see [Tri78, Chapter 3] and [Kuf80]. The following theory in the L^2 setting is mostly in [Kuf80], but for completeness we also discuss the L^p theory following [Kim08] but with slightly different notation.

Definition 3.1. *Let $\Omega \subset \mathbb{R}^n$ be a bounded open set with Lipschitz boundary. Let $1 < p < \infty$ and $\alpha \in \mathbb{R}$, and let $d(x) = \operatorname{dist}(x, \partial\Omega)$. Consider the norms*

$$\|u\|_{L^p(\Omega,d^\alpha)} = \|ud^{\alpha/p}\|_{L^p(\Omega)},$$
$$\|u\|_{W^{1,p}(\Omega,d^\alpha)} = \|u\|_{L^p(\Omega,d^\alpha)} + \|\nabla u\|_{L^p(\Omega,d^\alpha)}.$$

Let $W^{1,p}(\Omega, d^\alpha)$ be the space of all $u \in L^p_{\mathrm{loc}}(\Omega)$ with $\|u\|_{W^{1,p}(\Omega,d^\alpha)} < \infty$. We also define $W^{1,p}_0(\Omega, d^\alpha)$ as the closure of $C^\infty_c(\Omega)$ in $W^{1,p}(\Omega, d^\alpha)$.

The spaces $W^{1,p}(\Omega, d^\alpha)$ and $W^{1,p}_0(\Omega, d^\alpha)$ are Banach spaces, and they are equal when $\alpha \le -1$ or $\alpha > p - 1$ (see [Kuf80, Proposition 9.10]). For $\alpha > -1$ the set $C^\infty(\overline{\Omega})$ is dense in $W^{1,p}(\Omega, d^\alpha)$ (see [Kuf80, Remark 7.2]). The trace space of $W^{1,p}(\Omega, d^\alpha)$ can then be identified with a Sobolev space on $\partial\Omega$ as follows.

For $1 < p < \infty$ and $0 < s < 1$, let $W^{s,p}(\partial\Omega)$ be the standard Sobolev space on $\partial\Omega$ defined via a partition of unity, C^1 boundary flattening transformations, and corresponding spaces on $\mathbb{R}^{n-1}$. Part (a) of the following trace theorem is given in [Kim08, Theorem 2.13] (see [Tri78, Section 3.6.1] for the case of C^∞ domains), and part (b) follows from [Kim08, Lemma 2.14, Remark 2.15 and Proposition 2.3] and Lemma 3.3 below.

Theorem 3.2. *Let $\Omega \subset \mathbb{R}^n$ be a bounded Lipschitz domain, let $1 < p < \infty$, and let $-1 < \alpha < p-1$.*

(a) *The trace operator $T : C^\infty(\overline{\Omega}) \to C(\partial\Omega)$, $Tu = u|_{\partial\Omega}$ extends as a bounded surjective operator*

$$T : W^{1,p}(\Omega, d^\alpha) \to W^{1-\frac{1+\alpha}{p},p}(\partial\Omega).$$

Moreover, T has a bounded right inverse $E : W^{1-\frac{1+\alpha}{p},p}(\partial\Omega) \to W^{1,p}(\Omega, d^\alpha)$.

(b) *The space $W^{1,p}_0(\Omega, d^\alpha)$ satisfies*

$$W^{1,p}_0(\Omega, d^\alpha) = \{u \in W^{1,p}(\Omega, d^\alpha) \,:\, Tu = 0\}$$
$$= \{u \in L^p(\Omega, d^{\alpha-p}) \,:\, \nabla u \in L^p(\Omega, d^\alpha)\}.$$

The three norms $\|\cdot\|_{W^{1,p}(\Omega,d^\alpha)}$, $\|\cdot\|_{L^p(\Omega,d^{\alpha-p})} + \|\nabla\cdot\|_{L^p(\Omega,d^\alpha)}$, and $\|\nabla\cdot\|_{L^p(\Omega,d^\alpha)}$ are equivalent norms on $W^{1,p}_0(\Omega, d^\alpha)$.

The following Hardy inequality is given in [Kuf80, Section 9.1]. However, for later purposes we need to make sure that the constant has a controlled dependence on α and hence we repeat the proof.

Lemma 3.3. *Let $\Omega \subset \mathbb{R}^n$ be a bounded Lipschitz domain, $1 < p < \infty$, and $\alpha \in \mathbb{R}$, $\alpha \neq p - 1$. There are $C, C_1 > 0$ only depending on Ω, n, p such that*

$$\|d^{(\alpha/p)-1}u\|_{L^p(\Omega)} \le CC_1^{\alpha/p}\left(1 + \frac{1}{|\alpha - p + 1|}\right)\|d^{\alpha/p}\nabla u\|_{L^p(\Omega)}$$

for any $u \in W^{1,p}_0(\Omega, d^\alpha)$.

Proof. We begin with the case of $\mathbb{R}^n_+ = \{x_n > 0\}$. Let $u \in C_c^\infty(\mathbb{R}^n_+)$. We integrate by parts over $\mathbb{R}^n_+$ and use the Hölder inequality to obtain

$$\begin{aligned}\int x_n^{\alpha-p} u^p \, dx &= \int \partial_n \left(\frac{x_n^{\alpha-p+1}}{\alpha-p+1} \right) u^p \, dx = -\frac{p}{\alpha-p+1} \int x_n^{\alpha-p+1-\alpha/p} u^{p-1} x_n^{\alpha/p} \partial_n u \, dx \\ &\leq \frac{p}{|\alpha-p+1|} \|x_n^{(\alpha/p)-1} u\|_{L^p}^{p-1} \|x_n^{\alpha/p} \partial_n u\|_{L^p}.\end{aligned}$$

This implies that for any $u \in C_c^\infty(\mathbb{R}^n_+)$, one has

$$\|x_n^{(\alpha/p)-1} u\|_{L^p} \leq \frac{p}{|\alpha-p+1|} \|x_n^{\alpha/p} \partial_n u\|_{L^p}.$$

Similarly, if $U = \{(x', x_n) \in \mathbb{R}^n \, : \, |x'| < r, \; x_n > h(x')\}$ where $r > 0$ and $h : \{|x'| \leq r\} \to \mathbb{R}$ is a Lipschitz function, and if $u \in C^\infty(\overline{U})$ vanishes near $\{x_n = h(x')\}$ and $\{x_n = \infty\}$, the same argument gives that

$$\|(x_n - h(x'))^{(\alpha/p)-1} u\|_{L^p(U)} \leq \frac{p}{|\alpha-p+1|} \|(x_n - h(x'))^{\alpha/p} \partial_n u\|_{L^p(U)}. \tag{10}$$

Now if Ω is a bounded Lipschitz domain, then $\partial\Omega$ can be covered by finitely many balls $B_1, \ldots, B_N$ such that for each j, after a rigid motion one has $B_j \cap \Omega = \{x_n > h_j(x')\} \cap \Omega$ where h_j is a Lipschitz function, and $d(x)$ in $B_j \cap \Omega$ is comparable to $x_n - h_j(x')$ (see [Kuf80, Corollary 4.8]). There is also an open set B_0 with $\overline{B}_0 \subset \Omega$ so that $\overline{\Omega}$ is covered by $B_0, \ldots, B_N$. Moreover, B_j and h_j only depend on Ω and not on p and α.

Let $u \in C_c^\infty(\Omega)$. We can now apply (10) in $B_j \cap \Omega$ for $j = 1, \ldots, N$ to obtain that

$$\|d^{(\alpha/p)-1} u\|_{L^p(B_j \cap \Omega)} \leq C \frac{C_1^{\alpha/p}}{|\alpha-p+1|} \|d^{\alpha/p} \nabla u\|_{L^p(\Omega)}.$$

In B_0, where $d(x)$ is comparable to 1, we can apply a Poincaré inequality as in [Kuf80, Section 9.1] and use the above estimates on $B_j \cap \Omega$ to get

$$\begin{aligned}\|d^{(\alpha/p)-1} u\|_{L^p(B_0)} &\leq C C_1^{\frac{\alpha}{p}} \|u\|_{L^p(B_0)} \leq C C_1^{\alpha/p} (\|\nabla u\|_{L^p(B_0)} + \|u\|_{L^p(B_0 \cap (B_1 \cup \ldots \cup B_N))}) \\ &\leq C C_1^{\alpha/p} \left(1 + \frac{1}{|\alpha-p+1|} \right) \|d^{\alpha/p} \nabla u\|_{L^p(\Omega)}.\end{aligned}$$

The result follows by adding these inequalities and using that $C_c^\infty(\Omega)$ is dense in $W_0^{1,p}(\Omega, d^\alpha)$. ∎

The next result, which follows from [Kim08, Theorem 3.7], states the solvability of the Dirichlet problem in weighted Sobolev spaces when the Dirichlet data is in $W^{s,p}(\partial\Omega)$.

Theorem 3.4. *Let $\Omega \subset \mathbb{R}^n$ be a bounded C^1 domain, let $1 < p < \infty$, and let $0 < s < 1$. Assume that σ^{jk} and c are Lipschitz continuous in $\overline{\Omega}$ with (σ^{jk}) satisfying (9), and assume that $c \geq 0$. Given any $f \in W^{s,p}(\partial\Omega)$, there is a unique solution $u \in W^{1,p}(\Omega, d^{p(1-s)-1})$ of the problem*

$$Lu = 0 \text{ in } \Omega, \quad u|_{\partial\Omega} = f.$$

One has the estimate

$$\|u\|_{W^{1,p}(\Omega, d^{p(1-s)-1})} \leq C \|f\|_{W^{s,p}(\partial\Omega)}$$

with C independent of f.

For $p = 2$ we obtain a similar result in weighted L^2 spaces $H^1(\Omega, d^\alpha) := W^{1,2}(\Omega, d^\alpha)$ under weaker conditions, but assuming that s is close to $1/2$.

Theorem 3.5. *Let $\Omega \subset \mathbb{R}^n$ be a bounded Lipschitz domain. Assume that $\sigma^{jk}, c \in L^\infty(\Omega)$ with (σ^{jk}) satisfying (9) and $c \geq 0$ a.e. in Ω. There is $\varepsilon > 0$ such that whenever $|s - 1/2| < \varepsilon$, then for any $f \in H^s(\partial\Omega)$ there is a unique solution $u \in H^1(\Omega, d^{1-2s})$ of the problem*

$$Lu = 0 \text{ in } \Omega, \quad u|_{\partial\Omega} = f.$$

One has the estimate

$$\|u\|_{H^1(\Omega, d^{1-2s})} \leq C\|f\|_{H^s(\partial\Omega)}$$

with C independent of f.

Proof. Note that $|s - 1/2| < \varepsilon$ implies $|1 - 2s| < 2\varepsilon$. If ε is chosen small enough, the result follows by combining [Kuf80, Theorem 14.4] and the trace theorem (Theorem 3.2) above. ∎

The next result gives a weak maximum principle for solutions in $H^1(\Omega, d^\alpha)$ when $|\alpha|$ is sufficiently small. This smallness condition is analogous to the condition that s is close to $1/2$ in Theorem 3.5.

Theorem 3.6. *Let $\Omega \subset \mathbb{R}^n$ be a bounded Lipschitz domain. Let $\sigma^{jk}, c \in L^\infty(\Omega)$ be such that (9) holds and $c \geq 0$ a.e. in Ω. There is $\varepsilon > 0$ such that if $|\alpha| \leq \varepsilon$ and $u \in H^1(\Omega, d^\alpha)$ solves*

$$-\partial_k(\sigma^{jk}\partial_j u) + cu = 0 \text{ in } \Omega$$

in the sense of distributions, and if $Tu \leq C$ a.e. on $\partial\Omega$, then $u \leq C$ in Ω. Similarly, if $Tu \geq C$ a.e. on $\partial\Omega$, then $u \geq C$ in Ω.

The proof uses the following simple result where we write $u_\pm = \max\{\pm u, 0\}$.

Lemma 3.7. *Let $\Omega \subset \mathbb{R}^n$ be a bounded open set and $\alpha \in \mathbb{R}$. If $u \in H^1(\Omega, d^\alpha)$, then $u_\pm \in H^1(\Omega, d^\alpha)$ and the weak derivatives satisfy*

$$\partial_j u_\pm = \begin{cases} \partial_j u & \text{in } \{\pm u > 0\}, \\ 0 & \text{elsewhere.} \end{cases}$$

If Ω has Lipschitz boundary and $-1 < \alpha < 1$, we also have $T(u_\pm) = (Tu)_\pm$.

Proof. If $u \in H^1(\Omega, d^\alpha)$, then it is standard that $u_\pm \in H^1_{\text{loc}}(\Omega)$ and that $\partial_j u_\pm$ satisfies the formula above locally in Ω. It follows directly that $u_\pm \in H^1(\Omega, d^\alpha)$. The formula $T(u_\pm) = (Tu)_\pm$ holds for $u \in C^\infty(\overline{\Omega})$, and it continues to hold for $u \in H^1(\Omega, d^\alpha)$ by density. ∎

Proof of Theorem 3.6. We will prove that if $Tu \leq 0$ a.e. on $\partial\Omega$, then $u \leq 0$ a.e. in Ω (the other statements follow easily from this). This will be done by testing the equation against $d^\alpha v$ where $v = u_+$. Let $u \in H^1(\Omega, d^\alpha)$ and $v \in C_c^\infty(\Omega)$, and define the bilinear form

$$B(u, v) = (\sigma^{jk}\partial_j u, \partial_k(d^\alpha v)) + (cu, d^\alpha v)$$

where the inner products are in $L^2(\Omega)$. Using the Leibniz rule gives

$$B(u, v) = (\sigma^{jk} d^{\alpha/2}\partial_j u, d^{\alpha/2}\partial_k v) + (\sigma^{jk} d^{\alpha/2}\partial_j u, \alpha(\partial_k d)d^{\alpha/2-1}v) + (cd^{\alpha/2}u, d^{\alpha/2}v). \tag{11}$$

Now $|\nabla d| \leq 1$. Using Theorem 3.2 (b), the identity (11) continues to hold for all $u \in H^1(\Omega, d^\alpha)$ and $v \in H^1_0(\Omega, d^\alpha)$ by density.

Finally, let u be a solution with $Tu \leq 0$ a.e. on $\partial\Omega$. Then $B(u,v) = 0$ for all $v \in H_0^1(\Omega, d^\alpha)$, and $T(u_+) = 0$ by Lemma 3.7. Thus we may choose $v = u_+$, which implies that

$$0 = B(u, u_+) = B(u_+, u_+) - B(u_-, u_+).$$

By Lemma 3.7 any product $\partial^\beta u_+ \partial^\gamma u_-$ vanishes a.e. in Ω for $|\beta|, |\gamma| \leq 1$. This implies that $B(u_-, u_+) = 0$, which yields $B(u_+, u_+) = 0$. We now use (11) with $u = v = u_+$, the assumption (9) for σ^{jk}, and the assumption that $c \geq 0$ to obtain that

$$\lambda \|d^{\alpha/2} \nabla u_+\|^2 \leq \Lambda\, |\alpha|\, \|d^{\alpha/2} \nabla u_+\|\, \|d^{\alpha/2-1} u_+\|.$$

Using the Hardy inequality from Lemma 3.3, we obtain that

$$\|d^{\alpha/2} \nabla u_+\|^2 \leq \frac{\Lambda}{\lambda}\, |\alpha|\, C C_1^{\alpha/2} \left(1 + \frac{1}{|\alpha - 1|}\right) \|d^{\alpha/2} \nabla u_+\|^2.$$

If ε is small enough and $|\alpha| \leq \varepsilon$, then the constant on the right is $\leq 1/2$. It follows that $\nabla u_+ = 0$, which implies that $u_+ = 0$ using that $Tu_+ = 0$. ∎

4. Reconstruction procedure

This section lists the reconstruction procedure for an isotropic conductivity σ from a 2×2 power density matrix $\mathbf{H}$ based on [MB12b]. One can extend this procedure for anisotropic conductivities by adding another step following the approach of [MB12a]. For simplicity, we limit ourselves to the isotropic case. Throughout this section we assume that the boundary functions f^1 and f^2 were chosen in accordance with theorem 2.2 so that the corresponding solutions u_1 and u_2 entering $\mathbf{H}$ satisfy the non-vanishing Jacobian constraint (1) and are ordered so that $\det[\nabla u_1\, \nabla u_2] > 0$.

The procedure is characterized by two steps. In the first step we reconstruct the angle θ that enables us to determine the functionals $\mathbf{S}_i = \sqrt{\sigma} \nabla u_i$ from the entries of $H_{ij} = \sigma \nabla u_i \cdot \nabla u_j$. In the second step, we reconstruct σ from the functionals $\mathbf{S}_i$.

4.1. Reconstruction of θ.

We consider the power density matrix $\mathbf{H}$ and the matrix $\mathbf{S}$ composed of the functionals $\mathbf{S}_1$ and $\mathbf{S}_2$: $\mathbf{S} = [\mathbf{S}_1\, \mathbf{S}_2]$. By definition, $\mathbf{H}$ is symmetric and by the Jacobian constraint and the lower bound on σ it follows that $\mathbf{H}$ is positive definite: For any $x = (x_1, x_2) \neq 0, x^T \mathbf{H} x = \sigma\, |x_1 \nabla u_1 + x_2 \nabla u_2|^2 > 0$ (since ∇u_1 and ∇u_2 are nonzero and linearly independent by the Jacobian constraint).

In order to split the functionals $\mathbf{S}_i$ from the entries of the power density data H_{ij}, $\mathbf{S}$ is orthonormalized into a $SO(2)$-valued matrix $\mathbf{R}$: $\mathbf{R} = \mathbf{S}\mathbf{T}^T$. By definition, $\mathbf{R}$ is orthogonal and has determinant one and the transfer matrix $\mathbf{T}$ is determined by the data. The question is, which matrices $\mathbf{T}$ satisfy the equality $\mathbf{R} = \mathbf{S}\mathbf{T}^T$ under the conditions on $\mathbf{R}$. This question has no unique answer, so several choices of $\mathbf{T}$ are possible, for instance $\mathbf{T} = \mathbf{H}^{-\frac{1}{2}}$ or obtaining $\mathbf{T}$ by Gram-Schmidt orthonormalization. As $\mathbf{R}$ is a rotation matrix, it is parameterized by the angle function θ as follows:

$$\mathbf{R}(\theta) = \begin{bmatrix} \cos\theta & -\sin\theta \\ \sin\theta & \cos\theta \end{bmatrix}.$$

From this definition, we see that once $\mathbf{T}$ and $\mathbf{S}$ are known, the function θ can be computed by

$$\theta = \arg(\mathbf{R}_1),$$

where $\mathbf{R}_1$ denotes the first column of $\mathbf{R}$. The orthonormalization technique and thus the choice of $\mathbf{T}$ influences the angle θ. Our choice of $\mathbf{T}$ and the corresponding interpretation of θ is discussed in subsection 4.3.

Defining $\mathbf{T} = (T_{ij})_{1\leq i,j\leq 2}$ and $\mathbf{T}^{-1} = (T^{ij})_{1\leq i,j\leq 2}$, and letting

$$\mathbf{V_{ij}} = \nabla(T_{i1})T^{1j} + \nabla(T_{i2})T^{2j},$$

then θ is determined by the following equation [MB12b, Eq. (65)]:

$$\nabla\theta = \mathbf{F}, \tag{12}$$

with

$$\mathbf{F} = \frac{1}{2}(\mathbf{V_{12}} - \mathbf{V_{21}} - \mathcal{J}\nabla\log D),$$

$\mathcal{J} = \begin{bmatrix} 0 & -1 \\ 1 & 0 \end{bmatrix}$, and $D = (H_{11}H_{22} - H_{12}^2)^{\frac{1}{2}}$. Once θ is known at at least one point on the boundary one can integrate $\mathbf{F}$ along curves originating from that point to obtain θ throughout the whole domain. Alternatively, when assuming that θ is known along the whole boundary one can apply the divergence operator to (12) and solve the following Poisson equation with Dirichlet boundary condition:

$$\begin{cases} \Delta\theta = \nabla\cdot\mathbf{F} & \text{in } \Omega, \\ \theta = \theta_{\text{true}} & \text{on } \partial\Omega. \end{cases} \tag{13}$$

In our implementation, we use the second option and discuss in subsection 4.3 knowledge of θ along the boundary.

4.2. **Reconstruction of σ.** Reconstruction of σ is based on [MB12b, Eq. (68)]

$$\nabla\log\sigma = \mathbf{G}, \tag{14}$$

with

$$\mathbf{G} = \cos(2\tilde{\theta})\mathbf{K} + \sin(2\tilde{\theta})\mathbf{K},$$
$$\mathbf{K} = \mathcal{U}(\mathbf{V_{11}} - \mathbf{V_{22}}) + \mathcal{J}\mathcal{U}(\mathbf{V_{12}} - \mathbf{V_{21}}) \quad \text{and} \quad \mathcal{U} = \begin{bmatrix} 1 & 0 \\ 0 & -1 \end{bmatrix}.$$

Similarly as for θ one need to solve a gradient equation to obtain σ and has the possibility of either integrating along curves or solving a Poisson equation, assuming knowledge of σ in one point or along the whole boundary respectively. We assume knowledge of σ along the whole boundary and solve the following Poisson equation with Dirichlet condition:

$$\begin{cases} \Delta\log(\sigma) = \nabla\cdot\mathbf{G} & \text{in } \Omega, \\ \log(\sigma) = \log(\sigma_{\text{true}}) & \text{on } \partial\Omega. \end{cases} \tag{15}$$

4.3. **Choice of the transfer matrix T and knowledge of θ.** For our implementation, we use Gram-Schmidt orthonormalization to obtain the transfer matrix $\mathbf{T}$:

$$\mathbf{T} = \begin{bmatrix} H_{11}^{-\frac{1}{2}} & 0 \\ -H_{12}H_{11}^{-\frac{1}{2}}D^{-1} & H_{11}^{\frac{1}{2}}D^{-1} \end{bmatrix}.$$

By the Jacobian constraint, it follows that $H_{11} > 0$ so that $\mathbf{T}$ is well-defined. As a direct consequence of using Gram-Schmidt orthonormalization the first column of $\mathbf{R}$ simplifies to:

$$\mathbf{R}_1 = T_{11}\mathbf{S}_1 + T_{12}\mathbf{S}_2 = \frac{\cancel{\sqrt{\sigma}}\nabla u_1}{\cancel{\sqrt{\sigma}}\,|\nabla u_1|}.$$

Therefore, the angle θ simply defines the angle between ∇u_1 and the x_1-axis. Hence,

$$\theta = \arg(\nabla u_1). \tag{16}$$

In addition, following this definition for $\mathbf{T}$ the vector fields $\mathbf{V_{ij}}$ can be written explicitly in terms of $\mathbf{H}$:

$$\begin{aligned} &\mathbf{V_{11}} = \nabla \log H_{11}^{-\frac{1}{2}}, && \mathbf{V_{12}} = 0, \\ &\mathbf{V_{21}} = -\frac{H_{11}}{D}\nabla\left(\frac{H_{12}}{H_{11}}\right), && \mathbf{V_{22}} = \nabla \log\left(\frac{H_{11}^{\frac{1}{2}}}{D}\right). \end{aligned} \tag{17}$$

Knowledge of θ at the boundary is essential for the reconstruction procedure. By this definition of $\mathbf{T}$, knowledge of θ is directly related to knowledge of the gradient ∇u_1 and the current $\sigma\nabla u_1$, as both vector fields have the same direction. We decompose $\sigma\nabla u_1$ into two parts with contribution from the unit outward normal ν and the tangent vector $\eta = \mathcal{J}\nu$:

$$\sigma\nabla u_1 = (\sigma\nabla u_1 \cdot \nu)\nu + (\sigma\nabla u_1 \cdot \eta)\eta.$$

As along the whole boundary u_1 and σ are known, the contribution from $\sigma\nabla u_1 \cdot t$ is known as well. Furthermore, along the part of the boundary $\partial\Omega\backslash\Gamma$ we have additional information as u_1 vanishes. Therefore, the only contribution is from the unit outward normal ν, so that on this part of the boundary $\sigma\nabla u_1$ has either the direction of ν, $-\nu$ or the zero vector. However, in order to have full information of θ along the boundary one needs knowledge about the Neumann data $\sigma\nabla u_1 \cdot \nu$.

5. Numerical Examples

The MATLAB and PYTHON code to generate the numerical examples can be found on GITLAB: GitLab code.

Our aim is to illustrate numerically how two boundary conditions can be selected so that the non-vanishing Jacobian condition (1) for corresponding solutions is satisfied in accordance with theorem 2.2. And we choose the order of the corresponding solutions so that $\det[\nabla u_1\, \nabla u_2] > 0$. Furthermore, we show numerically how this can be used to reconstruct the conductivity from power density data. For that purpose, we implemented the reconstruction procedure in section 4 in PYTHON and used FENICS [LMW12] to solve the PDEs. We use a fine mesh to generate our power density data and a coarser mesh to address the reconstruction problem. We use $N_{\text{data}} = 79281$ nodes in the high-resolution case, while for the coarser mesh we consider a resolution of $N_{\text{recon}} = 50845$ nodes. For both meshes, we use $\mathbb{P}_1$ elements. We consider the domain Ω to be the unit disk: $\Omega = B(\mathbf{0}, 1)$. Furthermore, we consider two test cases for an isotropic conductivity σ defined by:

$$\sigma_{\text{case }1}(x_1, x_2) = \begin{cases} 1 + e^{\left(2 - \frac{2}{1 - \frac{(x_1)^2 + (x_2)^2}{1 - 0.8^2}}\right)} & 0 \le (x_1)^2 + (x_2)^2 \le 0.8^2, \\ 1 & 0.8^2 \le (x_1)^2 + (x_2)^2 \le 1, \end{cases}$$

$$\sigma_{\text{case 2}}(x_1, x_2) = \begin{cases} 2 & \left(x_1 + \frac{1}{2}\right)^2 + (x_2)^2 \leq 0.3^2, \\ 2 & (x_1)^2 + \left(x_2 + \frac{1}{2}\right)^2 \leq 0.1^2, \\ 2 & \left(x_1 - \frac{1}{2}\right)^2 + \left(x_2 - \frac{1}{2}\right)^2 \leq 0.1^2, \\ 1 & \text{otherwise.} \end{cases}$$

for $(x_1, x_2) \in \Omega$. Figure 1 illustrates the conductivities. To investigate influence of the size of the boundary of control, Γ, we consider three different sizes that are outlined in figure 2.

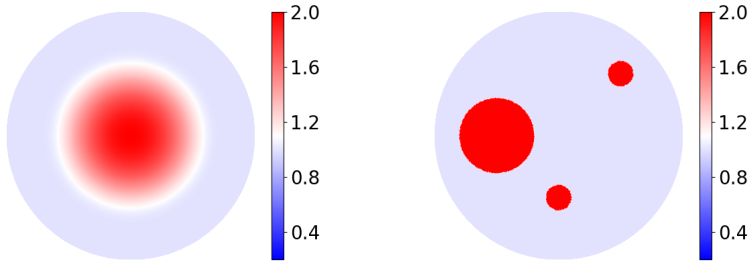

Case 1 Case 2

FIGURE 1. The conductivities σ used for the reconstruction procedure.

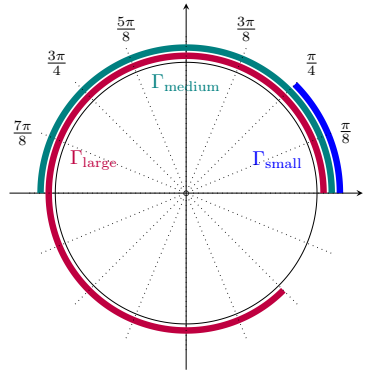

FIGURE 2. Different sizes of Γ used for the reconstruction procedure.

We demonstrate that the Jacobian constraint is satisfied for a choice of continuous and discontinuous boundary conditions in accordance with theorem 2.2. Note that as Ω is the unit disk the parameterization of the boundary satisfies $\eta(t) = t$. The following functions (f_1, f_2) yielding continuous boundary conditions satisfy condition (a) in theorem 2.2, as $\arg(\dot{\gamma})$ is strictly increasing and $|\text{ind}(\dot{\gamma})| = 1$:

$$(f_1^c(t), f_2^c(t)) = \begin{cases} (\cos(8t) - 1, \sin(8t)) & \text{for } \Gamma_{\text{small}} = \{t \in [0, \frac{\pi}{4}]\} \\ (\cos(2t) - 1, \sin(2t)) & \text{for } \Gamma_{\text{medium}} = \{t \in [0, \pi]\} \\ (\cos(\frac{8t}{7}) - 1, \sin(\frac{8t}{7})) & \text{for } \Gamma_{\text{large}} = \{t \in [0, \frac{7\pi}{4}]\}. \end{cases}$$

The corresponding functions $u_i^c|_{\partial\Omega}$ extended by zero along the whole boundary are illustrated in figure 3.

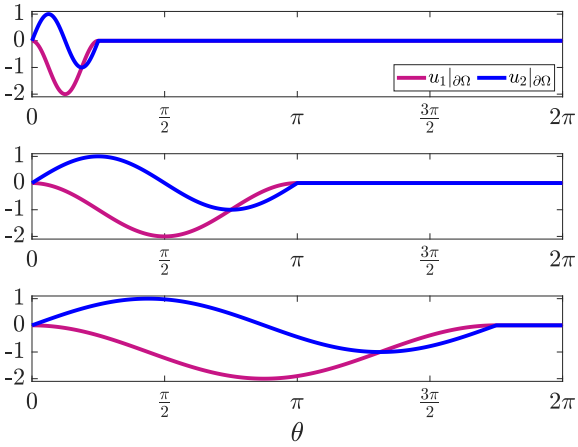

FIGURE 3. The continuous boundary functions $u_1^c|_{\partial\Omega}$ and $u_2^c|_{\partial\Omega}$ used for the reconstruction procedure for Γ_{small}, Γ_{medium} and Γ_{large} (top to bottom).

The following functions (f_1, f_2) yield discontinuous boundary conditions satisfying condition (b) in theorem 2.2, as $\arg(\dot{\gamma})$ is strictly increasing and $|\text{ind}(\dot{\gamma})| = 1/2$:

$$(f_1^d(t), f_2^d(t)) = \begin{cases} (\cos(4t) - 1, \sin(5t)) & \text{for } \Gamma_{\text{small}} = \{t \in [0, \frac{\pi}{4}]\} \\ (\cos(t) - 1, \sin(\frac{5t}{4})) & \text{for } \Gamma_{\text{medium}} = \{t \in [0, \pi]\} \\ (\cos(\frac{4t}{7}) - 1, \sin(\frac{5t}{7})) & \text{for } \Gamma_{\text{large}} = \{t \in [0, \frac{7\pi}{4}]\}. \end{cases}$$

The corresponding functions $u_i^d|_{\partial\Omega}$ extended by zero along the whole boundary are illustrated in figure 4.

We compute the corresponding solutions u_1 and u_2 and the three power densities H_{11}, H_{12} and H_{22}. It is not straightforward to compute the solutions numerically for discontinuous boundary conditions; therefore, the procedure is discussed in section 5.1. The solutions u_1 and u_2 are then illustrated in figure 6. From table 1 we see that the Jacobian condition is satisfied for all cases, as the determinant of $\mathbf{H}$ is positive. However, for a small boundary of control the values of the determinant are very small, so for Γ_{small} the minimum values are of order 10^{-14}. To investigate where the small values of $\det(\mathbf{H})$ concentrate, we illustrate the expression $\log(\det(\mathbf{H}))$ for continuous and discontinuous boundary conditions in figure 7. The expression $\log(\det(\mathbf{H}))$ will give us more nuances of the small values than the determinant itself. From the figure, it is evident that the small

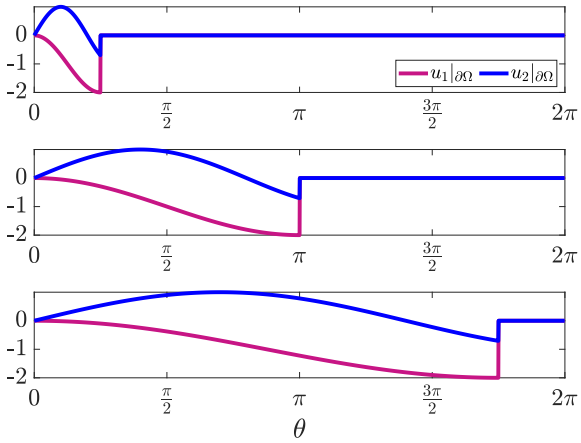

FIGURE 4. The discontinuous boundary functions $u_1^d|_{\partial\Omega}$ and $u_2^d|_{\partial\Omega}$ used for the reconstruction procedure for Γ_{small}, Γ_{medium} and Γ_{large} (top to bottom).

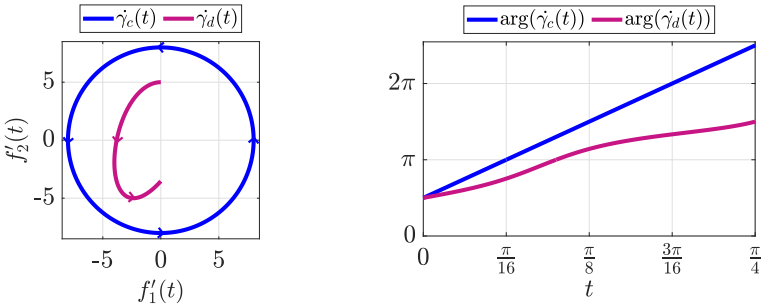

FIGURE 5. The curves $\dot{\gamma_c}(t) = (f_1^c(t), f_2^c(t))$ and $\dot{\gamma_d}(t) = (f_1^d(t), f_2^d(t))$ for continuous and discontinuous $u_i|_{\partial\Gamma}$ as in figure 3 and 4 respectively to give an idea about the winding numbers of $\dot{\gamma}$. The right figure shows their arguments in the case of Γ_{small} (for Γ_{medium} and Γ_{large} the behavior is identical).

values concentrate close to the boundary that we cannot control. Furthermore, the figure shows that for discontinuous boundary conditions there appear larger values of $\log(\det(\mathbf{H}))$ than for the continuous case, but these are mainly concentrated around the discontinuity. For the continuous boundary conditions, the maximal values are smaller, but they are more evenly distributed along the boundary of control. As the Jacobian condition is satisfied, we can use the reconstruction procedure outlined in section 4 to reconstruct the two conductivities $\sigma_{\text{case 1}}$ and $\sigma_{\text{case 2}}$. For the reconstruction procedure, we use knowledge of the true angle θ that can be computed by knowledge

of the true gradient ∇u_1.

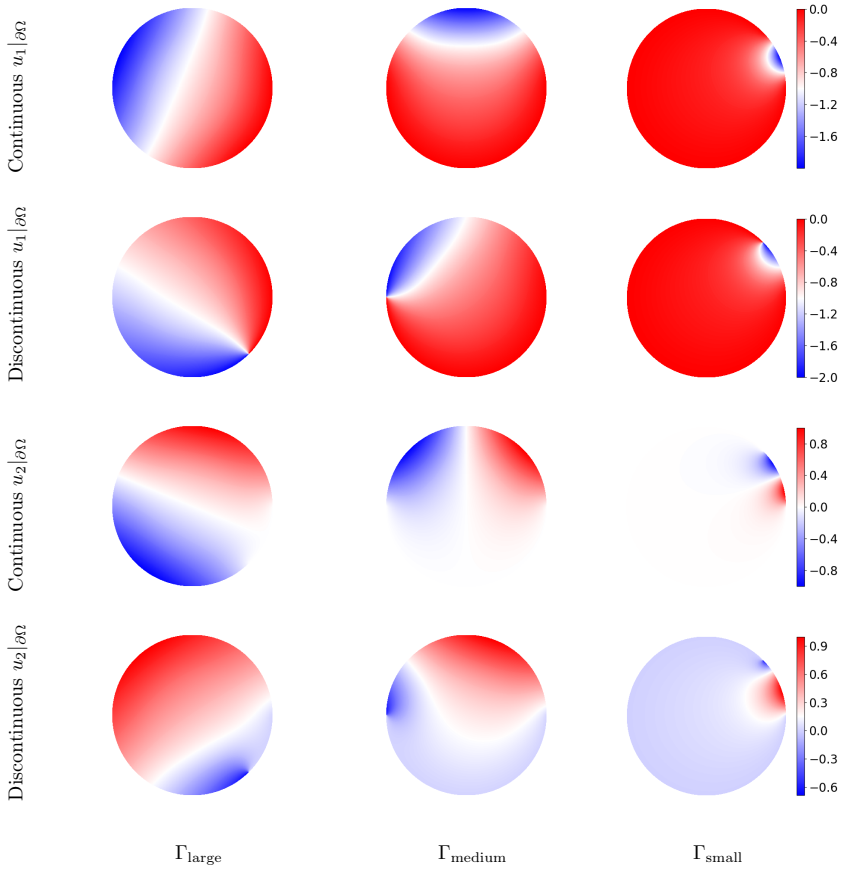

FIGURE 6. The solutions u_1 and u_2 induced by the discontinuous and continuous boundary conditions for σ as in case 1 and varying boundaries of control Γ_{large}, Γ_{medium} and Γ_{small}.

5.1. **Solving the conductivity equation numerically with discontinuous boundary functions $u_i^d|_{\partial\Omega}$.** It is a challenge numerically to use FENICS to compute the solutions with discontinuous boundary conditions as the solutions are only in $H^1(\Omega, d^{1-2s})$ and not in $H^1(\Omega)$. Using Lagrange basis functions one can define a H^1-function space, but this does not allow for discontinuities. To allow for discontinuities one has the possibility to define a function space using discontinuous Galerkin basis functions between the nodes, but in this way one loses interior regularity as well. Both possibilities are not optimal as in our case we only have a discontinuity

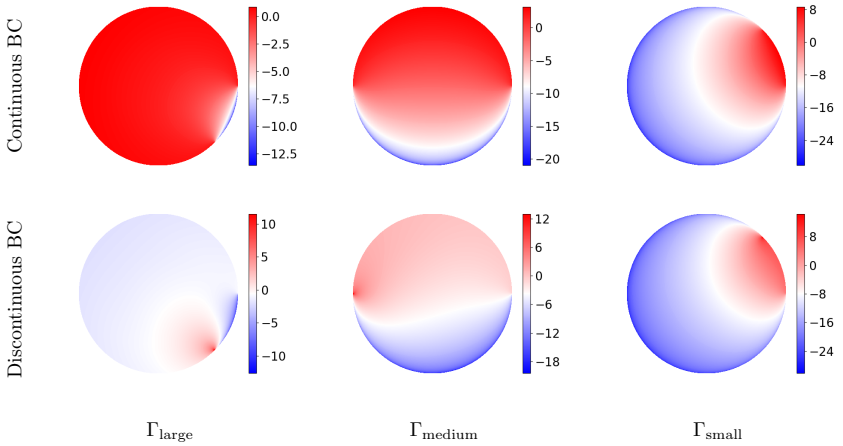

FIGURE 7. The expression $\log(\det(\mathbf{H}))$ for varying sizes of Γ, when using continuous and discontinuous boundary conditions. Large negative values (blue regions) correspond to values of $\det(\mathbf{H})$ close to zero.

at the boundary, while away from the boundary the function behaves like an H^1-function. For that purpose, we consider the functions $w_i = u_i - u_i^0$, were $u_i^0 \in H^1(\Omega, d^{1-2s})$ solves the Laplace equation with boundary conditions:

$$\begin{cases} \Delta u_i^0 = 0 & \text{in } \Omega, \\ u_i^0 = f_i & \text{on } \Gamma \\ u_i^0 = 0 & \text{on } \partial\Omega \backslash \Gamma. \end{cases} \tag{18}$$

Now w^i solves the following boundary value problem:

$$\begin{cases} -\operatorname{div}(\sigma \nabla w_i) = \operatorname{div}(\sigma \nabla u_i^0) & \text{in } \Omega, \\ w_i = 0 & \text{on } \partial\Omega. \end{cases} \tag{19}$$

As we consider conductivities σ that are one on and in a neighborhood of the boundary, the right hand side $\operatorname{div}(\sigma \nabla u_i^0)$ vanishes in a neighborhood where the discontinuity appears. Using these choices of σ thus ensure that the discontinuity is covered so that the right hand side satisfies $\operatorname{div}(\sigma \nabla u_i^0) \in H^{-1}(\Omega)$ implying that w_i is a solution in $H^1(\Omega)$. We solve the boundary value problem (18) semi-analytically for u_i^0 in MATLAB using the Fourier transform. This gives us the exact solution at each node apart from the Gibbs phenomenon happening at the discontinuity. Afterwards we solve the boundary value problem (19) for w_i in PYTHON using FENICS and compute the solution u_i as desired. In this way, we obtain the correct solution u_i at each node, but there still happens a smoothing between the nodes around the discontinuity, as we assign u_i to a H^1 function space using Lagrange basis functions.

5.2. **Reconstruction of θ.** We compute the true angle θ as the argument of ∇u_1 as highlighted in equation (16). Using the true angle as boundary condition for the boundary value problem (13)

we reconstruct θ by solving the problem numerically. This is repeated for the two conductivities as in figure 1, all different boundaries of control as in figure 2 and the continuous and discontinuous boundary conditions as in figure 3 and 4. The relative errors are shown in table 1 and table 2.

TABLE 1. Relative L^2 errors when using the continuous boundary conditions $(u_i^c|_{\partial\Omega})$ and the discontinuous boundary conditions $(u_i^d|_{\partial\Omega})$.

		Γ_{large}		Γ_{medium}		Γ_{small}	
		$u_i^c\|_{\partial\Omega}$	$u_i^d\|_{\partial\Omega}$	$u_i^c\|_{\partial\Omega}$	$u_i^d\|_{\partial\Omega}$	$u_i^c\|_{\partial\Omega}$	$u_i^d\|_{\partial\Omega}$
Min $\det(\mathbf{H})$	case 1	$1 \cdot 10^{-6}$	$3 \cdot 10^{-6}$	$8 \cdot 10^{-10}$	$1 \cdot 10^{-9}$	$8 \cdot 10^{-14}$	$8 \cdot 10^{-14}$
	case 2	$1 \cdot 10^{-6}$	$3 \cdot 10^{-6}$	$9 \cdot 10^{-10}$	$2 \cdot 10^{-9}$	$8 \cdot 10^{-14}$	$7 \cdot 10^{-14}$
Rel. L^2 error θ	case 1	1.62%	0.74%	1.19%	6.90%	-	-
	case 2	1.67%	0.75%	1.20%	7.11%	-	-
Rel. L^2 error σ	case 1	15.7%	15.6%	40.1%	39.9%	56.5%	56.3%
	case 2	15.0%	15.0%	40.0%	39.9%	56.9%	56.4%

TABLE 2. Relative L^2 errors of $(\cos(2\theta), \sin(2\theta))$ for Γ_{small}.

	Continuous BC	Discontinuous BC
case 1	(3.47%, 3.61%)	(5.34%, 5.44%)
case 2	(3.58%, 3.56%)	(5.40%, 5.38%)

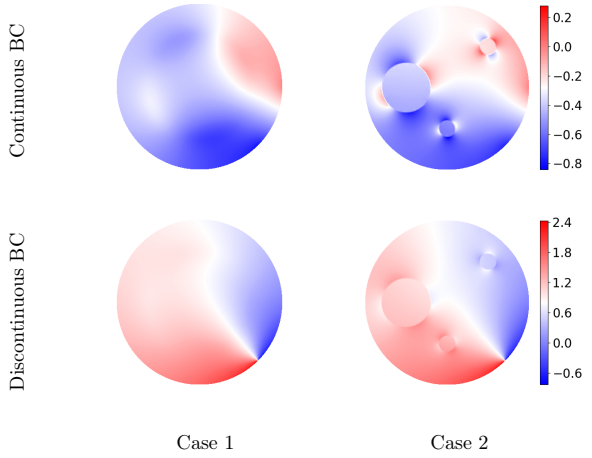

FIGURE 8. True θ for the different boundary conditions and different conductivities and having control over Γ_{large}.

Even though the errors range up to 7% the reconstructions with control over Γ_{large} or Γ_{medium} can barely be distinguished visually from the true θ. The only difference appears through minor artifacts along the part of the boundary that cannot be controlled. For that purpose in these cases, we only focus on the true expressions for θ. These are illustrated for Γ_{large} in figure 8 and

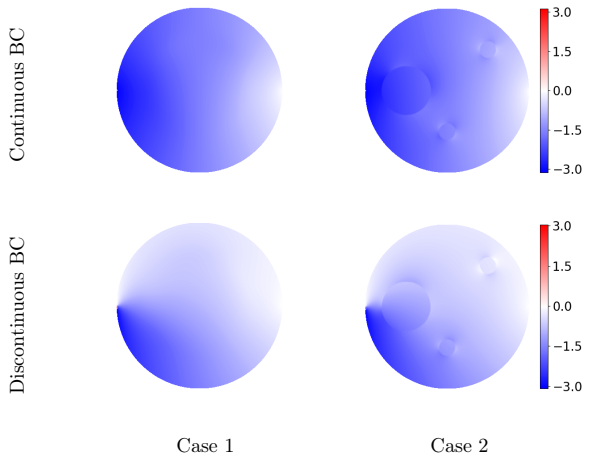

FIGURE 9. True θ for the different boundary conditions and different conductivities and having control over Γ_{medium}.

for Γ_{medium} in figure 9. From the figures we see that the discontinuities of u_i^d are reflected in θ as well, which follows directly from the definition of θ. Furthermore, θ differs for the two cases of σ: As the circular feature in $\sigma_{\text{case 1}}$ has a smooth edge its contours can barely be seen in the expression for θ. However, as there appear piecewise constant features in $\sigma_{\text{case 2}}$ the edges are clearly reflected in the expression for θ as well.

For some choices of the boundary conditions and Γ, the true angle θ changes values from $-\pi$ to π throughout Ω. This is here the case for both continuous and discontinuous boundary conditions and when Γ has the size of Γ_{small}. This behavior causes a curve of transitions. Along this curve the expression transitions through all values from $-\pi$ to π, instead of leaving a discontinuity, which would adhere to the periodic nature of the codmain. This is illustrated in the left part of figure 10 and a periodic color map is used to highlight the transition curve. A similar phenomenon was observed and addressed in [JKS22] and we use the same approach to address this issue. By the discussion in section 4.3 the direction of ∇u_1 corresponds to the direction of the unit normal ν, its opposite $-\nu$, or the zero vector along the boundary $\partial\Omega\backslash\Gamma_{\text{small}}$. If we investigate θ along the boundary in the right part of figure 10, we see that along $\partial\Omega\backslash\Gamma_{\text{small}}$ θ is a linear increasing function, as it corresponds to the angle between ν and the x_1-axis. The only deviations happen for $t \in [0, \frac{\pi}{4}]$, which is the boundary of control Γ_{small}. By this behavior of θ along $\partial\Omega\backslash\Gamma_{\text{small}}$ there happens a jump from π to $-\pi$ at $t = \pi$. An additional jump is induced by the boundary condition: For the continuous boundary condition there happens a jump at $t = \frac{\pi}{8}$ and for the discontinuous boundary condition there happens a jump at $t = \frac{\pi}{4}$. The smoothed discontinuities are a problem when using the true angle θ as a boundary condition in (13), therefore we define a modified version $\tilde{\theta}$ to be used as a boundary condition. As θ only appears as an input to the cosine and sine-functions in the reconstruction formula in (15), we can add and subtract multiples of 2π without changing the reconstruction. Therefore, we subtract 2π in the interval between the discontinuities to extend θ to

a more continuous function along the boundary. For continuous boundary conditions $\tilde{\theta}^c$ is defined as

$$\tilde{\theta}^c(t) = \begin{cases} \theta^c(t) - 2\pi & t \in \left[\frac{\pi}{8}, \pi\right], \\ \theta^c(t) & \text{otherwise.} \end{cases} \tag{20}$$

And for the discontinuous boundary condition:

$$\tilde{\theta}^d(t) = \begin{cases} \theta^d(t) - 2\pi & t \in \left[\frac{\pi}{4}, \pi\right], \\ \theta^d(t) & \text{otherwise.} \end{cases} \tag{21}$$

These functions are illustrated in the right part of figure 10 and used as a boundary condition when solving the boundary value problem (13).

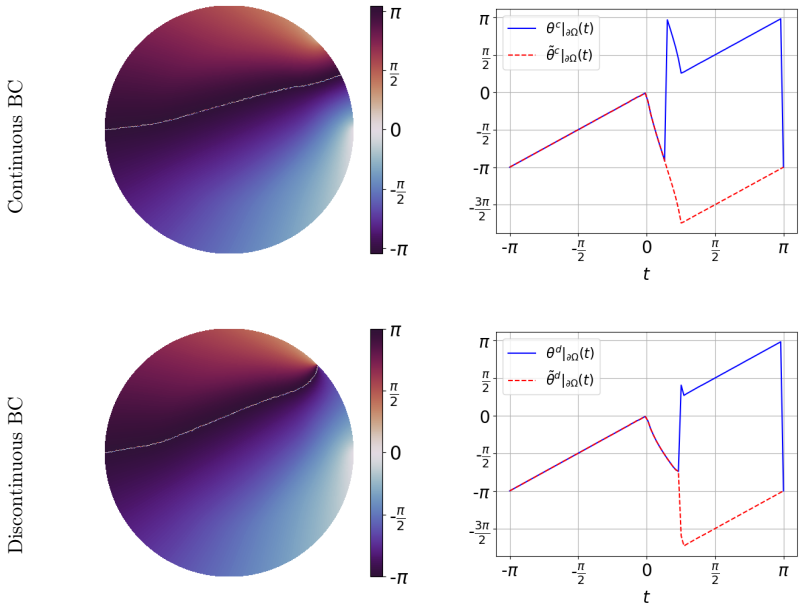

True θ

Comparing θ to a modified version $\tilde{\theta}$ along $\partial\Omega$

FIGURE 10. True expression for θ assigned to a smooth function space and using continuous and discontinuous boundary conditions. We consider the conductivity $\sigma_{\text{case 1}}$ and have control over Γ_{small}. The left part shows θ along the boundary together with modified versions $\tilde{\theta}$ defined in (20) and (21).

For these reconstructions θ it does no longer make sense to compare them to the true angles, so instead we compare the reconstructed $\cos(2\theta)$ to the true expression in figure 11, as this is the way

θ appears in the reconstruction formula for σ (15). The reconstruction errors are shown in table 2. From the figure, we see that there appear artifacts along the whole boundary $\partial\Omega\backslash\Gamma_{\text{small}}$. This is because this part of the boundary is difficult to control from the small boundary Γ_{small} so that the Jacobian constraint almost is violated close to this part of the boundary. This is seen from figure 7, as the values of $\det(\mathbf{H})$ are very small close to the boundary $\partial\Omega\backslash\Gamma_{\text{small}}$. And from table 1 we see the small values are of order 10^{-14}. These artifacts were not as visible for Γ_{large} and Γ_{medium}, as the smallest values of $\det(\mathbf{H})$ were larger than $3 \cdot 10^{-6}$ and $9 \cdot 10^{-10}$ respectively.

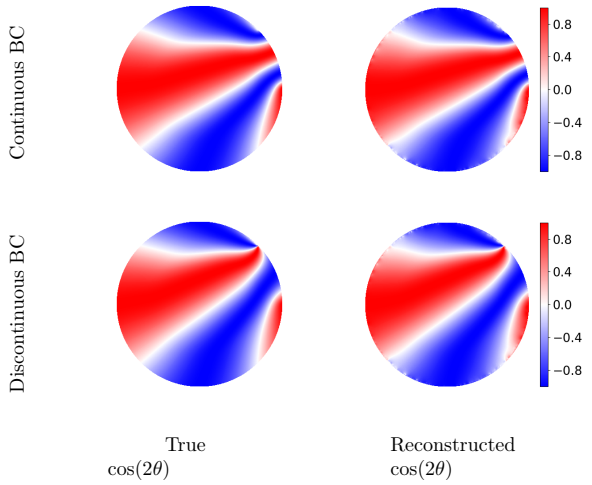

FIGURE 11. Reconstructions of $\cos(2\theta)$ compared to the true expression for the different boundary conditions. We consider the conductivity $\sigma_{\text{case 1}}$ and have control over Γ_{small}.

5.3. **Reconstruction of σ.** Using the reconstructions of θ we compute σ by solving the boundary value problem (15). The reconstructions of σ using the continuous boundary conditions are shown in figure 12. As seen from the relative errors in table 1 there is no significant difference in the quality of the reconstruction when using the continuous or discontinuous boundary conditions. It is therefore impossible to distinguish the reconstructions visually, so we only show the reconstructions using the continuous boundary conditions. From the figure we see that the quality of the reconstructions is highly affected by the size of the boundary of control Γ: The larger the boundary of control the better the reconstruction. For Γ_{large} the features in the reconstructions are still visible in almost the same intensity as for the true σ, only the shape of the circular feature in $\sigma_{\text{case 1}}$ is changed in the direction of $\partial\Omega\backslash\Gamma_{\text{large}}$. With decreasing size of Γ the intensity of the features is decreasing as well, so that for Γ_{small} the features have intensity close to 1 like the background of the true σ. Also in a large neighborhood of the boundary $\partial\Omega\backslash\Gamma$, the reconstruction has intensity close to 0, so that for Γ_{small} the reconstruction is dominated by intensity 0. When comparing performance for the two different conductivities σ we see that the reconstructions for

the piecewise constant conductivity $\sigma_{\text{case 2}}$ look almost better than for the smooth $\sigma_{\text{case 1}}$, as the piecewise constant edges of the three features in $\sigma_{\text{case 2}}$ are clearly visible in the reconstructions. This is due to the fact, that these edges are clearly visible in the data and in θ as can be seen from the right parts of figure 8 and figure 9. For $\sigma_{\text{case 1}}$ the shape of the feature is deformed a little bit towards $\partial\Omega\backslash\Gamma$, as the feature has a smooth edge. However, this difference in quality is not evident from the relative errors in table 1. Another take away from the reconstructions is that as $\sigma_{\text{case 2}}$ is composed of features that are closer and further away from the boundary of control as the feature in $\sigma_{\text{case 1}}$, we can see that there is a difference in the intensity of the three features. This is especially evident for Γ_{medium}, so that the feature closest to Γ_{medium} has intensity 1.8, which is almost the same intensity as the true $\sigma_{\text{case 2}}$. On the other hand, the feature furthest away from Γ_{medium} has intensity 1, which is the same as the background intensity of the true $\sigma_{\text{case 2}}$.

5.4. **Reconstruction of σ from noisy data.** We perturb the entries of the power density matrix $\mathbf{H}$ at each node with random noise:

$$\widetilde{H}_{ij} = H_{ij} + \frac{\alpha}{100} \frac{e_{ij}}{\|e_{ij}\|_{L^2}} H_{ij},$$

where α is the noise level and e_{ij} are entries in the matrix $\mathbf{E}$ that are normally distributed $e_{ij} \sim \mathcal{N}(0,1)$. We use `numpy.random.randn` to generate the elements e_{ij} and fix the seed `numpy.random.seed(50)`. After generating $\widetilde{\mathbf{H}}$, we make sure that it is symmetric by computing $\frac{1}{2}(\widetilde{\mathbf{H}} + \widetilde{\mathbf{H}}^T)$. Furthermore, for the reconstruction procedure it is essential that $\widetilde{\mathbf{H}}$ is positive definite so that we use a small positive lower bound L for the eigenvalues of $\widetilde{\mathbf{H}}$. This approach can be seen as a regularization method. We note that as ∇u_1 and ∇u_2 are parallel to the unit normal $\pm\nu$ on $\partial\Omega\backslash\Gamma$, the Jacobian constraint is violated on this part of the boundary. Therefore we would assume very small values of $\det(\widetilde{\mathbf{H}})$ close to this part of the boundary. However, in the approach of using a lower bound for the eigenvalues we might discard some of these values. Therefore, we choose the lower bound as small as possible in order to get a reasonable reconstruction that is not dominated by noise on these small values.

After these modifications on symmetry and positive definiteness, we use $\widetilde{\mathbf{H}}$ for reconstructing $\sigma_{\text{case 2}}$ for three different noise levels: $\alpha = 1\%$, $\alpha = 5\%$ and $\alpha = 10\%$. The results are shown in Figure 13, where we compare performance when using continuous and discontinuous boundary conditions. The lower bounds L used for reconstruction are documented in Table 3 and the relative errors of σ are shown in the same table. The reconstructions are all of similar quality when looking at the relative errors and how well the values at the red features matches with the true σ. However, for the discontinuous boundary condition the increasing noise level results in an artifact around the discontinuity. To account for this one needs to use significantly larger lower bounds for increasing noise level. In contrast, there is a gradual rise in the lower bound for increasing noise level when using continuous boundary conditions. The high lower bound in the case of discontinuous boundary conditions induces a light belt close to $\partial\Omega\backslash\Gamma$. This belt appears, as information in this region is discarded by the lower bound.

TABLE 3. Relative L^2 errors on $\sigma_{\text{case 2}}$ in presence of noise. To obtain a positive definite noisy matrix $\widetilde{\mathbf{H}}$, different lower bounds L for the eigenvalues of $\widetilde{\mathbf{H}}$ are used. The boundary of control is Γ_{medium}.

	Continous BC		Discontinuous BC	
	L	Relative error σ	L	Relative error σ
1% Noise	10^{-6}	40.7%	10^{-6}	38.9%
5% Noise	10^{-5}	41.4%	10^{-3}	41.7%
10% Noise	10^{-4}	40.6%	$2 \cdot 10^{-2}$	38.4%

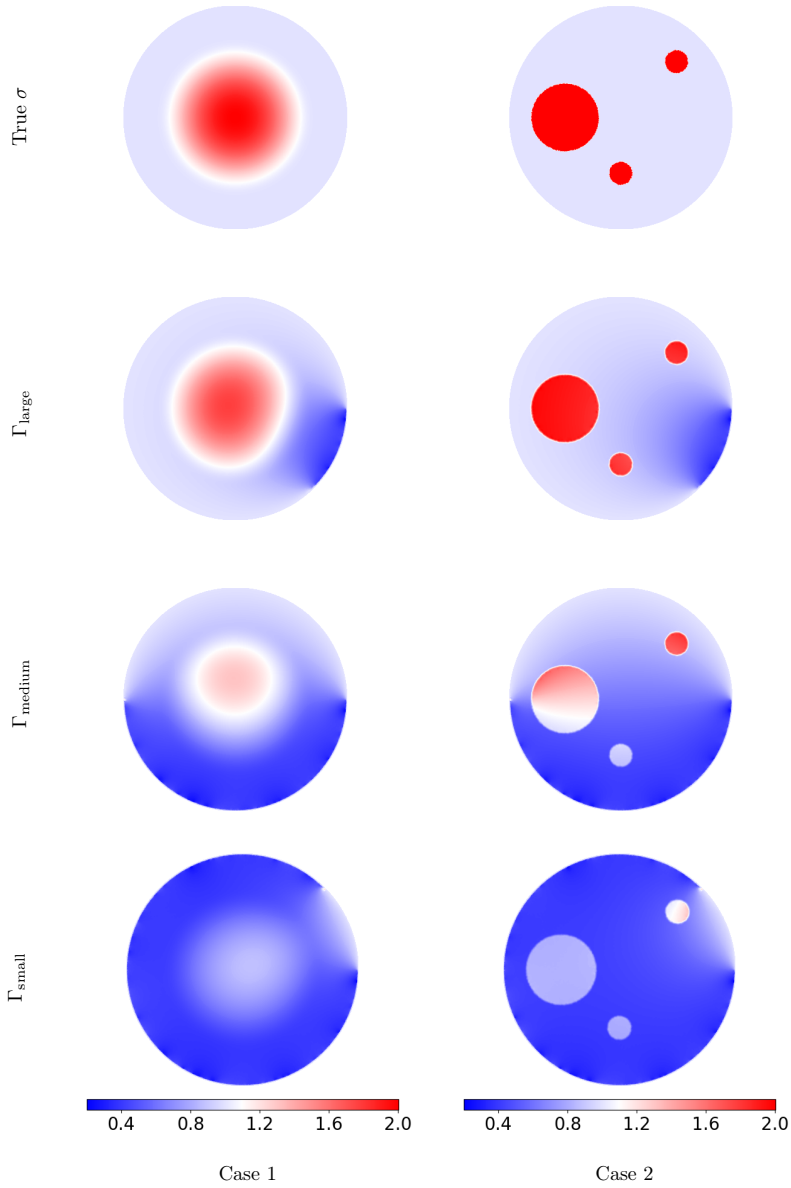

FIGURE 12. Reconstructions of σ as in test case 1 in the left column and as in test case 2 in the right column for varying sizes of Γ. The discontinuous boundary conditions are used.

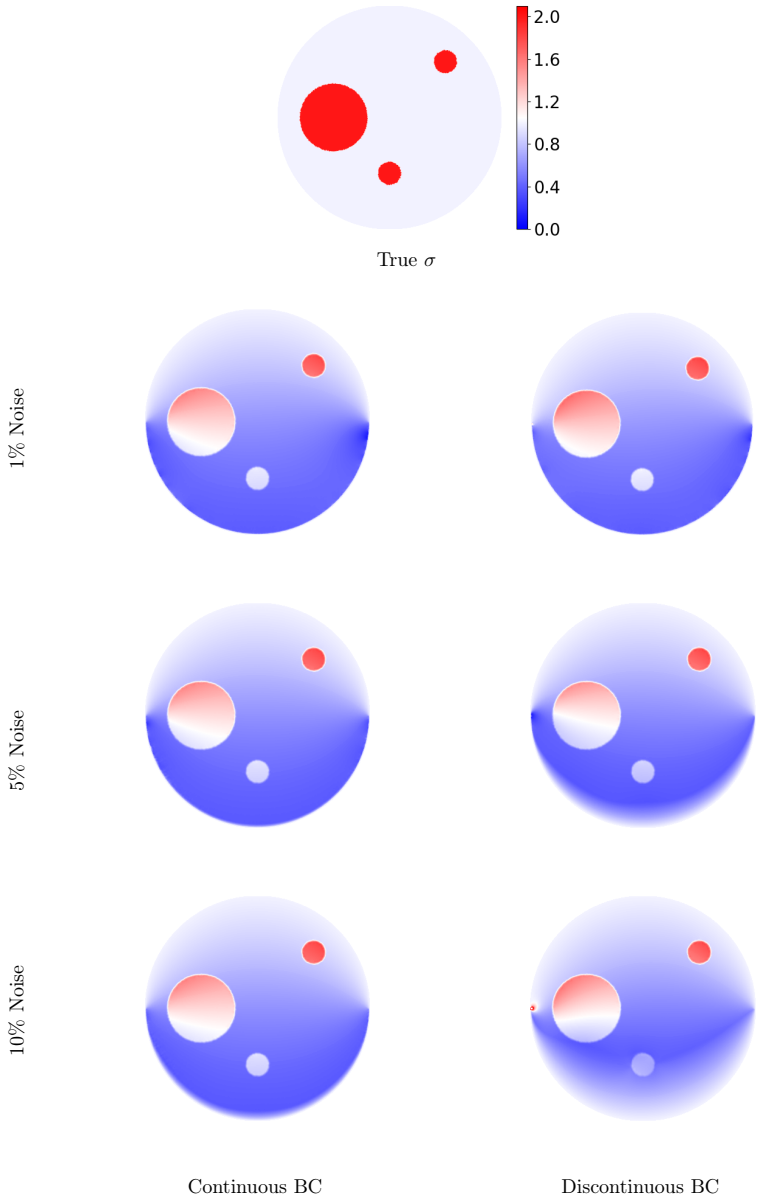

FIGURE 13. Reconstructions of $\sigma_{\text{case 2}}$ when $\mathbf{H}$ is perturbed with varying noise levels and with boundary of control Γ_{medium}. To obtain a positive definite noisy matrix $\widetilde{\mathbf{H}}$, different lower bounds L for the eigenvalues of $\widetilde{\mathbf{H}}$ are used.

6. Conclusions

In this work, we have derived sufficient conditions on two boundary functions so that the corresponding solutions to the conductivity equation satisfy a non-vanishing Jacobian constraint in limited view. This approach allows for boundary functions that have discontinuities. This is relevant for Acousto-Electric Tomography and Current Density Imaging both in limited view and in full view settings, as the conditions and thus the use of discontinuous boundary functions apply for both settings.

We illustrated how these conditions could be used for numerical examples of reconstructing the conductivity from power density data in limited view following the approach of [MB12b]. It was evident from the numerical examples how the non-vanishing Jacobian constraint was almost violated close to the boundary that could not be controlled. This follows from the zero Dirichlet condition on this part of the boundary: Here the two corresponding solutions have both the direction of the unit normal so that the non-vanishing Jacobian constraint cannot be satisfied on this part of the boundary. Nevertheless, without noise it was possible to obtain decent reconstructions of the conductivity especially for a large boundary of control. However, due to the very small values of the Jacobian it was impossible to add even small levels of noise while maintaining positive definiteness of the measurement matrix. To account for this, we used a small positive lower bound for the eigenvalues of the measurement matrix. This worked well in the numerical experiments even for high noise levels. However, in this approach especially values close to the part of the boundary that cannot be controlled are affected by the lower bound. When the lower bound is high this might be in contradiction with the assumption that values should be small in this region. This is especially a problem when using discontinuous boundary conditions as the lower bound needs to be chosen large when the noise level is high.

We mention that the proposed conditions in order to obtain solutions satisfying the non-vanishing Jacobian constraint are not optimal. Especially for the case of discontinuous boundary functions there is a possibility that 2.2 (b) can be relaxed, as we are aware of functions that are more general than allowed here as indicated in Remark 2.3.

Acknowledgements

The authors would like to express their sincere gratitude to Nuutti Hyvönen for suggesting how to solve the boundary value problem (4) numerically with discontinuous boundary conditions, and for providing the Matlab code to solve the boundary value problem (18) semi-analytically as discussed in section 5.1. M.S. was partly supported by the Academy of Finland (Centre of Excellence in Inverse Modelling and Imaging, grant 284715) and by the European Research Council under Horizon 2020 (ERC CoG 770924).

References

[AC18] Giovanni Alberti and Yves Capdeboscq. *Lectures on elliptic methods for hybrid inverse problems*. Societe Mathematique De France, 2018.

[AH96] David R. Adams and Lars Inge Hedberg. *Function spaces and potential theory*. Volume 314. Grundlehren der mathematischen Wissenschaften [Fundamental Principles of Mathematical Sciences]. Springer-Verlag, Berlin, 1996, pages xii+366. ISBN: 3-540-57060-8. DOI: 10.1007/978-3-662-03282-4. URL: https://doi.org/10.1007/978-3-662-03282-4.

[Alb22] Giovanni S. Alberti. *Non-zero constraints in elliptic PDE with random boundary values and applications to hybrid inverse problems*. 2022. DOI: 10.48550/ARXIV.2205.00994. URL: https://arxiv.org/abs/2205.00994.

[Ale86] Giovanni Alessandrini. "An identification problem for an elliptic equation in two variables". In: *Ann. Mat. Pura Appl. (4)* 145 (1986), pages 265–295. ISSN: 0003-4622. DOI: 10.1007/BF01790543. URL: https://doi-org.proxy.findit.cvt.dk/10.1007/BF01790543.

[Ale87] Giovanni Alessandrini. "Critical points of solutions of elliptic equations in two variables". In: *Ann. Scuola Norm. Sup. Pisa Cl. Sci. (4)* 14.2 (1987), 229–256 (1988). ISSN: 0391-173X. URL: http://www.numdam.org/item?id=ASNSP_1987_4_14_2_229_0.

[AM94] G. Alessandrini and R. Magnanini. "Elliptic equations in divergence form, geometric critical points of solutions, and Stekloff eigenfunctions". In: *SIAM J. Math. Anal.* 25.5 (1994), pages 1259–1268. ISSN: 0036-1410. DOI: 10.1137/S0036141093249080. URL: https://doi-org.proxy.findit.cvt.dk/10.1137/S0036141093249080.

[Amm+08] H. Ammari et al. "Electrical impedance tomography by elastic deformation". In: *SIAM J. Appl. Math.* 68.6 (2008), pages 1557–1573. ISSN: 0036-1399. DOI: 10.1137/070686408.

[AN01] Giovanni Alessandrini and Vincenzo Nesi. "Univalent σ-harmonic mappings". In: *Arch. Ration. Mech. Anal.* 158.2 (2001), pages 155–171. ISSN: 0003-9527. DOI: 10.1007/PL00004242. URL: https://doi-org.proxy.findit.cvt.dk/10.1007/PL00004242.

[AN15] G. Alessandrini and V. Nesi. "Quantitative estimates on jacobians for hybrid inverse problems". eng. In: *Bulletin of the South Ural State University, Series: Mathematical Modelling, Programming and Computer Software* 8.3 (2015), pages 25–41. ISSN: 23080256, 20710216. DOI: 10.14529/mmp150302.

[Bal13] Guillaume Bal. "Hybrid inverse problems and internal functionals". In: *Inverse problems and applications: inside out. II*. Volume 60. Math. Sci. Res. Inst. Publ. Cambridge Univ. Press, Cambridge, 2013, pages 325–368.

[BMN01] Patricia Bauman, Antonella Marini, and Vincenzo Nesi. "Univalent solutions of an elliptic system of partial differential equations arising in homogenization". In: *Indiana Univ. Math. J.* 50.2 (2001), pages 747–757. ISSN: 0022-2518. DOI: 10.1512/iumj.2001.50.1832. URL: https://doi-org.proxy.findit.cvt.dk/10.1512/iumj.2001.50.1832.

[Cho45] Gustave Choquet. "Sur un type de transformation analytique généralisant la représentation conforme et définie au moyen de fonctions harmoniques". In: *Bull. Sci. Math.* 69 (1945), pages 156–165.

[JKS22] Bjørn Jensen, Kim Knudsen, and Hjørdis Schlüter. *Conductivity reconstruction from power density data in limited view*. 2022. DOI: 10.48550/ARXIV.2202.12370. URL: https://arxiv.org/abs/2202.12370.

[Kim08] Doyoon Kim. "Elliptic equations with nonzero boundary conditions in weighted Sobolev spaces". In: *J. Math. Anal. Appl.* 337.2 (2008), pages 1465–1479. ISSN: 0022-247X. DOI: 10.1016/j.jmaa.2007.04.048.

[Kne26] Hellmuth Kneser. "Lösung der Aufgabe 41". In: *Jahresbericht der Deutschen Mathematiker-Vereinigung* 35 (1926), pages 123–124.

[Kuf80] Alois Kufner. *Weighted Sobolev spaces*. Volume 31. Teubner-Texte zur Mathematik [Teubner Texts in Mathematics]. With German, French and Russian summaries. BSB B. G. Teubner Verlagsgesellschaft, Leipzig, 1980, page 151.

[Li+21] Wei Li et al. "An acousto-electric inverse source problem". In: *SIAM J. Imaging Sci.* 14.4 (2021), pages 1601–1616. DOI: 10.1137/21M1406568. URL: https://doi.org/10.1137/21M1406568.

[LMW12] Anders Logg, Kent-Andre Mardal, and Garth Wells. *Automated solution of differential equations by the finite element method: The FEniCS book*. Volume 84. Springer Science & Business Media, 2012.

[MB12a] François Monard and Guillaume Bal. "Inverse anisotropic diffusion from power density measurements in two dimensions". In: *Inverse Problems* 28 (July 2012).

[MB12b] François Monard and Guillaume Bal. "Inverse diffusion problems with redundant internal information". In: *Inverse Problems and Imaging* 6.2 (2012), pages 289–313.

[Rad26] Tibor Radó. "Aufgabe 41". In: *Jahresbericht der Deutschen Mathematiker-Vereinigung* 35 (1926), page 49.

[Sch90] Friedmar Schulz. *Regularity Theory for Quasilinear Elliptic Systems and Monge—Ampère Equations in Two Dimensions*. Springer Berlin Heidelberg, 1990.

[SKW05] Jin Keun Seo, Ohin Kwon, and Eung Je Woo. "Magnetic resonance electrical impedance tomography (MREIT): conductivity and current density imaging". In: *Journal of Physics: Conference Series* 12 (January 2005), pages 140–155. DOI: 10.1088/1742-6596/12/1/014. URL: https://doi.org/10.1088/1742-6596/12/1/014.

[SW11] Jin Keun Seo and Eung Je Woo. "Magnetic resonance electrical impedance tomography (MREIT)". In: *SIAM Rev.* 53.1 (2011), pages 40–68. ISSN: 0036-1445. DOI: 10.1137/080742932. URL: https://doi-org.proxy.findit.cvt.dk/10.1137/080742932.

[Tri78] H. Triebel. *Interpolation theory, function spaces, differential operators*. VEB Deutscher Verlag der Wissenschaften, Berlin, 1978, page 528.

[WS12] Thomas Widlak and Otmar Scherzer. "Hybrid tomography for conductivity imaging". In: *Inverse Problems* 28.8 (2012), pages 084008, 28. ISSN: 0266-5611. DOI: 10.1088/0266-5611/28/8/084008. URL: https://doi.org/10.1088/0266-5611/28/8/084008.

[ZW04] Hao Zhang and Lihong V. Wang. "Acousto-electric tomography". In: *Photons Plus Ultrasound: Imaging and Sensing*. Volume 5320. SPIE, 2004, pages 145–149. DOI: 10.1117/12.532610.

APPENDIX B

Paper B: Conductivity reconstruction from power density data in limited view

Bjørn Jensen, Kim Knudsen, Hjørdis Schlüter. Conductivity reconstruction from power density data in limited view.
Submitted to a journal. Preprint available on arXiv: `https://arxiv.org/abs/2202.12370`.

CONDUCTIVITY RECONSTRUCTION FROM POWER DENSITY DATA IN LIMITED VIEW

BJØRN JENSEN, KIM KNUDSEN, AND HJØRDIS SCHLÜTER

Abstract. In Acousto-Electric tomography, the objective is to extract information about the interior electrical conductivity in a physical body from knowledge of the interior power density data generated from prescribed boundary conditions for the governing elliptic partial differential equation. In this note, we consider the problem when the controlled boundary conditions are applied only on a small subset of the full boundary. We demonstrate using the unique continuation principle that the Runge approximation property is valid also for this special case of limited view data. As a consequence, we guarantee the existence of finitely many boundary conditions such that the corresponding solutions locally satisfy a non-vanishing gradient condition. This condition is essential for conductivity reconstruction from power density data. In addition, we adapt an existing reconstruction method intended for the full data situation to our setting. We implement the method numerically and investigate the opportunities and shortcomings when reconstructing from two fixed boundary conditions.

Keywords: acousto-electric tomography, electrical impedance tomography, hybrid data tomography, coupled physics imaging, inverse problems, medical imaging

MSC2000: 35R30; 65N21

1. Introduction

Acousto-electric tomography (AET) [5, 19] is an imaging modality for obtaining information about the interior electrical conductivity in a physical body. By combining electrostatic boundary measurements during an acoustic excitation of the body, we first recover the so-called interior power density data and from there reconstruct the conductivity. In principle, the modality yields high resolution and high contrast images, but the practical feasibility is yet to be demonstrated [13].

The reconstruction problem in AET is fairly well understood in situations where the full boundary is available for the electrostatic measurements. In this manuscript we consider the more challenging problem in the limited view setting where we only have access to measurements on a possibly small part of the boundary. Our main result shows that reconstruction is feasible also in this setting, and in this way we generalize results pioneered in [6].

Bjørn Jensen, 0000-0002-4743-2631

Department of Mathematics and Statistics, University of Helsinki, 00560 Helsinki, Finland

Kim Knudsen, 0000-0002-4875-3074

Department of Applied Mathematics and Computer Science, Technical University of Denmark, 2800 Kgs. Lyngby, Denmark

Hjørdis Schlüter, 0000-0001-6659-3863

Department of Applied Mathematics and Computer Science, Technical University of Denmark, 2800 Kgs. Lyngby, Denmark

E-mail addresses: bjorn.jensen@helsinki.fi, kiknu@dtu.dk, hjsc@dtu.dk.

We now define the involved quantities and the model linking them. The limited boundary control is modelled by a prescribed voltage on part of the domain boundary with a no-flux condition applied elsewhere. To this end we consider a connected open set $\Omega \subset \mathbb{R}^d$, $d = 2, 3$ with Lipschitz boundary $\partial\Omega$ and let $\Gamma \subset \partial\Omega$ be nonempty and open. We assume the conductivity denoted by σ satisfies $\sigma \in L^\infty_+(\Omega)$, i.e. there exists $\lambda \in (0, 1)$ such that $\lambda \leq \sigma \leq \lambda^{-1}$ a.e. in Ω. If $d = 3$ we assume further that σ is Lipschitz on Ω. The model is described by the partial differential equation

$$Lu = -\nabla \cdot \sigma \nabla u = 0 \quad \text{in } \Omega, \tag{1.1a}$$

$$u = f \quad \text{on } \Gamma, \tag{1.1b}$$

$$L_\nu u = \sigma \partial_\nu u = 0 \quad \text{on } \partial\Omega \backslash \Gamma, \tag{1.1c}$$

where u is the electrical potential, ∇u the electrical field and $f \in H^{\frac{1}{2}}(\Gamma) := \{v|_\Gamma : v \in H^1(\Omega)\}$ the prescribed voltage under our control. ν denotes the outward unit normal to $\partial\Omega$. From standard elliptic theory we know that (1.1) has a unique solution $u \in H^1(\Omega)$ for each choice of boundary potential f.

In AET the data is given in terms of the mixed power density matrix $H \in \mathbb{R}^{d\times d}$ with elements

$$H_{ij} = \sigma \nabla u_i \cdot \nabla u_j. \tag{1.2}$$

The function u_i denotes the solution to (1.1) for a boundary condition f_i, $i = 1, \ldots, d$. The inverse problem of AET is to uniquely and constructively recover the unknown conductivity σ from H.

If we successfully pick f_i so that the electrical fields ∇u_i are linearly independent, then H satisfies the Jacobian constraint

$$\det \begin{bmatrix} \nabla u_1 & \cdots & \nabla u_d \end{bmatrix} \geq \delta > 0 \tag{1.3}$$

for some $\delta > 0$. This condition is crucial for the reconstruction problem in AET.

There is a rich mathematical literature on AET for the full boundary case ($\Gamma = \partial\Omega$). For the two-dimensional problem, the Jacobian constraint is essentially guaranteed by the Radó–Kneser–Choquet theorem using the two coordinate functions as boundary conditions. A reconstruction method is found in [6]. The anisotropic problem is considered in [15] with boundary conditions given in terms of complex geometrical optics (CGO) solutions generically depending on σ. In three dimensions, it is impossible to find three boundary conditions that can work for any conductivity [2], but again a CGO construction can be used to provide four solutions [6]. A different approach using the Runge approximation property can be used for both the isotropic and anisotropic problem in any dimension [7] yielding a finite number of boundary conditions. Further work to establish smaller upper bounds on the number of boundary conditions can be found in [4]. We refer to [3] for a complete overview.

Our main result states that even in the limited view setting there are a finite number of boundary conditions such that locally the solutions satisfy (1.3). The method relies on the Runge approximation property that will be established for the mixed problem (1.1). This approach is equivalent to the construction of so-called localized potentials [9]). We will in addition review the reconstruction method, emphasize the importance of (1.3), and investigate the possibilities and shortcomings in the limited view setting.

In Section 2, we recall the Runge approximation property and prove that the given PDE (1.1) satisfies the property. Section 3 gives the solutions satisfying the Jacobian constraint. In Section 4 we review for completeness the reconstruction formula for σ in terms of H in the case $d = 2$ following [6]. We end the story in Section 5 with a description of the numerical implementation and numerous computational experiments that shows the possibilities and limitations of limited view AET.

2. The Runge approximation property

In this section, we recall the Runge approximation property and ascertain that the property holds for our PDE in question (1.1). To prove that this property holds we make use of the unique continuation property, which is satisfied for the operators L and L_ν as defined in (1.1) [3, Lemma 7.5]. Given an open non-empty subset $\Sigma \subseteq \partial\Omega$ the unique continuation property states that if $u \in H^1(\Omega)$ is a solution to $Lu = 0$ in Ω, which further satisfies $u|_\Sigma = 0$ and $L_\nu u|_\Sigma = 0$, then u vanishes in all of Ω; i.e. $u = 0$ everywhere in Ω.

We state the definition of the Runge approximation property.

Definition 2.1 (Runge approximation property)**.** We say that L satisfies the *Runge approximation property* if for any simply connected Lipschitz domain $\Omega' \Subset \Omega$ and any $u \in H^1(\Omega')$ such that $Lu = 0$ in Ω' there exists a sequence $u_n \in H^1(\Omega)$ such that (a) $Lu_n = 0$ in Ω, and (b) $u_n|_{\Omega'} \to u$ in $L^2(\Omega')$.

It follows from the satisfaction of the unique continuation property that our PDE satisfies the Runge approximation property as well. The following lemma is a modified version of a similar result in [3, Thm. 7.7] and the proof follows the same general lines as well:

Theorem 2.2. *Let $\Omega \subset \mathbb{R}^d$ be a Lipschitz bounded domain and L as defined in* (1.1)*. Then L satisfies the Runge approximation property with the sequences (u_n) satisfying the boundary restriction $L_\nu u_n = 0$ on $\partial\Omega\backslash\Gamma$ for all $n \in \mathbb{N}$.*

Proof. Assume without loss of generality that Ω is connected. Take $\Omega' \Subset \Omega$ as in Definition 2.1 and $u \in H^1(\Omega')$ such that

$$Lu = 0 \quad \text{in } \Omega'.$$

Set $F := \{v|_{\Omega'} : v \in H^1(\Omega), Lv = 0 \text{ in } \Omega, L_\nu v = 0 \text{ on } \partial\Omega\backslash\Gamma\}$. Suppose by contradiction that the Runge approximation property does not hold that we managed to pick a u for which there is no sequence in F converging to u in L^2-norm. By the Hahn-Banach theorem there exists a functional $g \in L^2(\Omega')^*$ such that $g(u) \neq 0$ and $g(v) = 0$ for $v \in F$. In other words, there exists $g \in L^2(\Omega')$ such that $(g, u)_{L^2(\Omega')} \neq 0$ and $(g, v)_{L^2(\Omega')} = 0$ for all $v \in F$.

Consider now the extension by zero of g to Ω, which by an abuse of notation is still denoted by g. Let $V := \{\phi|_\Gamma : \phi \in H^{\frac{1}{2}}(\partial\Omega)\}$ and fix $\phi \in V$. Let $w, v \in H^1(\Omega)$ be the unique solutions to

$$\begin{aligned} Lw &= g \quad \text{in } \Omega, & \qquad Lv &= 0 \quad \text{in } \Omega, \\ w &= 0 \quad \text{on } \Gamma, & \text{and} \qquad v &= \phi \quad \text{on } \Gamma, \\ L_\nu w &= 0 \quad \text{on } \partial\Omega\backslash\Gamma, & L_\nu v &= 0 \quad \text{on } \partial\Omega\backslash\Gamma. \end{aligned}$$

By definition of g there holds $(g, v)_{L^2(\Omega)} = 0$. Thus, integration by parts shows

$$0 = -(v, g)_{L^2(\Omega)} = (Lv, w)_{L^2(\Omega)} - (v, Lw)_{L^2(\Omega)} = \int_\Gamma (L_\nu w)\phi \, \mathrm{d}\sigma.$$

Since the above holds for all $\phi \in H^{\frac{1}{2}}(\Gamma)$ we obtain $L_\nu w = 0$ on Γ. Observe now that w is solution to $Lw = 0$ in $\Omega\backslash\Omega'$ such that $w = 0$ and $L_\nu w = 0$ on Γ. In view of the unique continuation property we have $w = 0$ in $\Omega\backslash\Omega'$, therefore $w = 0$ and $L_\nu w = 0$ on $\partial\Omega'$. As a result, by integrating by parts we obtain

$$\begin{aligned}\int_{\Omega'} gu \,\mathrm{d}x &= \int_{\Omega'} (Lw)u \,\mathrm{d}x \\ &= \int_{\Omega'} \underbrace{(Lu)}_{=0} w \,\mathrm{d}x + \int_{\partial\Omega'} \underbrace{(L_\nu w)}_{=0} u \,\mathrm{d}s + \int_{\partial\Omega'} (L_\nu u) \underbrace{w}_{=0} \,\mathrm{d}s \\ &= 0,\end{aligned}$$

where the last identity follows from the definition of u. This contradicts the assumptions on g, since $(g, u)_{L^2(\Omega')} \neq 0$. □

By the application of Schauder estimates, Sobolev embedding and standard elliptic theory, assuming Lipschitz regularity for the coefficient yields the following result.

Lemma 2.3. *Assume σ is Lipschitz and let $\Omega' \Subset \Omega$, $x_0 \in \overline{\Omega'}$ and $s \in (0, \operatorname{dist}(\Omega', \partial\Omega))$. Let $u_0 \in C^{1,\alpha}(\Omega)$, $\alpha \in (0, 1)$ satisfy*

$$-\Delta u_0 = 0, \quad \text{in } B(x_0, s).$$

Then for any $\delta > 0$ there is an $r \in (0, s)$ and $u_{x_0,\delta} \in H^1(\Omega)$ satisfying $Lu_{x_0,\delta} = 0$ in Ω and $L_\nu u_{x_0,\delta} = 0$ on $\partial\Omega\backslash\Gamma$ such that

$$\|u_{x_0,\delta} - u_0\|_{C^1(\overline{B(x_0,r)})} \leq \delta.$$

The proof can be found in Appendix A. As any linear map u_0 satisfies the conditions of the lemma, the corollary is immediate.

Corollary 2.4. *Let σ, Ω' and x_0 be as in Lemma 2.3. For any $\delta > 0$ and $\mathbf{v} \in \mathbb{R}^d$ there is $r \in (0, 1)$ with $B(x_0, r) \subset \Omega'$ and $u_{x_0,\delta} \in H^1(\Omega)$ satisfying $Lu_{x_0,\delta} = 0$ in Ω and $L_\nu u_{x_0,\delta} = 0$ on $\partial\Omega\backslash\Gamma$ such that*

$$\|\nabla u_{x_0,\delta} - \mathbf{v}\|_{C^0(B(x_0,r))} \leq \delta.$$

3. Satisfying the Jacobian constraint

We summarize in this section how the above guarantees solutions that satisfies the Jacobian constraint. The treatment follows along the lines of [3, Sec. 7.3]:

First note that the canonical basis vectors $\mathbf{e}_j$ satisfies $\det\left[\mathbf{e}_1 \dots \mathbf{e}_d\right] = 1$, i.e. the Jacobian constraint. Next, fix a sufficiently small $\delta > 0$. Corollary 2.4 provides the existence of solutions to (1.1) (including suitable boundary conditions) that can approximate $v = \mathbf{e}_j$ locally in small balls. This is illustrated in Figure 1 if considered from the same relative origin then $\nabla\tilde{u}_j$ is contained in a cone C_j. Consequently, the solutions satisfy locally the Jacobian constraint. Finally, the union of such small balls is an open cover of Ω' and can, due to compactness of $\overline{\Omega'}$, be exhausted to a finite open cover with $M \in \mathbb{N}$ balls. As each ball requires a set of d boundary conditions to satisfy, we ultimately end up with Md boundary conditions.

The theorem is as follows:

Theorem 3.1. *Assume σ is Lipschitz continuous in $\overline{\Omega}$, and consider any compactly embedded domain $\Omega' \Subset \Omega$. Then there exists a finite set of boundary conditions $\{\phi_j\}_{j=1}^{Md}$ with corresponding*

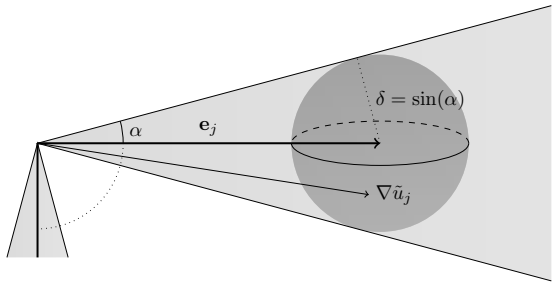

FIGURE 1. Illustration of the cone C_j and the ball of approximating vectors at most $\delta = \sin(\alpha)$ away from $\mathbf{e}_j$.

solutions $\{u_j\}_{j=1}^{Md}$ *to* (1.1) *with* $f = \phi_j$*, such that at any point* $x_0 \in \Omega'$ *there is an open neighborhood* V_{x_0} *of* x_0 *and a subset* $\{u_{n_1}, \ldots, u_{n_d}\}$ *satisfying*

$$\det \begin{bmatrix} \nabla u_{n_1}(x) & \cdots & \nabla u_{n_d}(x) \end{bmatrix} \geq \frac{1}{2}, \quad \textit{for all } x \in V_{x_0}$$

Proof. Let $\delta > 0$ be arbitrary. For each $x_0 \in \Omega'$, and $v = \mathbf{e}_j$, Corollary 2.4 gives an $r_j > 0$ and an approximating solution $\tilde{u}_j \in H^1(\Omega)$ satisfying $L\tilde{u}_j = 0$ in Ω and $L_\nu \tilde{u}_j = 0$ on $\partial\Omega \backslash \Gamma$ such that $\|\nabla \tilde{u}_j - \mathbf{e}_j\|_{C^0(B(x_0,r_j))} < \delta$ in $B(x_0, r_0)$ with $r_0 = \min(r_1, r_2, \ldots, r_d)$. By continuity of the determinant, by fixing δ sufficiently small we can guarantee

$$\left| \det \left[\nabla \tilde{u}_1 \ldots \nabla \tilde{u}_d \right] - \det \left[\mathbf{e}_1 \ldots \mathbf{e}_d \right] \right| < \frac{1}{2},$$

and by the reverse triangle inequality

$$\left| \det \left[\nabla \tilde{u}_1 \ldots \nabla \tilde{u}_d \right] \right| > \frac{1}{2}.$$

Since $\Omega' \Subset \Omega$, there is a finite subcover $\{B(x_m, r_m)\}_{m=1}^{M}$ of Ω' that yields the Md boundary conditions. □

4. Reconstruction formula

In this section we review without proofs the main formulas used for the reconstruction procedure based on [16] in order to prepare for the numerical experiments in section 5. We consider the case $d = 2$; for $d = 3$ we refer to [6]. Throughout this section we consider a power density matrix $\mathbf{H} = (H_{ij})_{1 \leq i,j \leq 2}$ for which the corresponding solutions u_1 and u_2 are assumed to satisfy the Jacobian constraint (1.3).

The derivation goes in 2 steps. The aim in the first step is to obtain $\mathbf{J}_i = \sqrt{\sigma} \nabla u_i$, $i = 1, 2$, from H_{ij}. $\mathbf{J}_i$ is the current density up to a factor of $\sqrt{\sigma}$; i.e. the current density is precisely $\sqrt{\sigma}\mathbf{J}_i$. In a slight abuse of the name, we call the first step the "current density step". The second step is the recovery of an equation for σ from $\mathbf{J}_i$. We call this the "conductivity step".

4.1. Current density step.

To this end consider the matrices $\mathbf{J} = \begin{bmatrix} \mathbf{J}_1 & \mathbf{J}_2 \end{bmatrix}$ and $\mathbf{H} = (H_{ij})_{1 \leq i,j \leq 2}$; the latter obviously symmetric. Under the assumed positive lower bound on σ and the Jacobian

constraint (1.3) it is easy to see that for any $\mathbf{x} = (x_1, x_2) \neq 0$, $\mathbf{x}^T\mathbf{H}\mathbf{x} = \sigma|\mathbf{q}_1 + \mathbf{q}_2|^2 > 0$, where $\mathbf{q}_i = x_i \nabla u_i \neq 0$ and $\mathbf{q}_1 \neq -\mathbf{q}_2$. Hence $\mathbf{H}$ is positive definite.

The matrix $\mathbf{J}$ is then orthonormalized into a $SO(2)$-valued matrix $\mathbf{R}$ via a transformation of the form $\mathbf{R} = \mathbf{J}\mathbf{T}^T$. By definition $\mathbf{R}$ is orthogonal and $\det \mathbf{R} = 1$. As $\mathbf{R}$ is a rotation matrix, it is parameterized by

$$\mathbf{R}(\theta) = \begin{bmatrix} \cos\theta & -\sin\theta \\ \sin\theta & \cos\theta \end{bmatrix},$$

dependent only on a single parameter θ. This definition implies that when the exact matrices $\mathbf{T}$ and $\mathbf{J}$ are known the function θ can be computed by

$$\theta = \text{argument}(R_{11} + iR_{21}). \tag{4.1}$$

Defining $\mathbf{T} = (T_{ij})_{1\leq i,j\leq 2}$ and $\mathbf{T}^{-1} = (T^{ij})_{1\leq i,j\leq 2}$, and letting

$$\mathbf{V_{ij}} = \nabla(T_{i1})T^{1j} + \nabla(T_{i2})T^{2j},$$

then θ is determined by the following equation [16, Eq. (65)]:

$$\nabla\theta = \mathbf{F}, \tag{4.2}$$

with

$$\mathbf{F} = \frac{1}{2}\left(\mathbf{V_{12}} - \mathbf{V_{21}} - \mathcal{J}\nabla \log D\right),$$

$\mathcal{J} = \begin{bmatrix} 0 & -1 \\ 1 & 0 \end{bmatrix}$, and $D = (H_{11}H_{22} - H_{12}^2)^{\frac{1}{2}}$. Applying the divergence operator to (4.2) yields the Poisson equation

$$\begin{cases} \Delta\theta = \nabla \cdot \mathbf{F} \text{ in } \Omega, \\ \theta \text{ given on } \partial\Omega. \end{cases} \tag{4.3}$$

We discuss in section 4.3 below that we can assume θ to be known on the whole boundary $\partial\Omega$.

4.2. **Conductivity step.** Reconstruction of σ is based on [16, eq. (68)]

$$\nabla \log\sigma = \mathbf{G} \tag{4.4}$$

with

$$\mathbf{G} = \cos(2\theta)\mathbf{K} + \sin(2\theta)\mathcal{J}\mathbf{K}$$

$$\mathbf{K} = \mathcal{U}(\mathbf{V_{11}} - \mathbf{V_{22}}) + \mathcal{J}\mathcal{U}(\mathbf{V_{12}} + \mathbf{V_{21}}) \quad \text{and} \quad \mathcal{U} = \begin{bmatrix} 1 & 0 \\ 0 & -1 \end{bmatrix}.$$

We assume that σ is known on the whole boundary $\partial\Omega$ and then reconstruct σ by solving the Poisson equation

$$\begin{cases} \Delta(\log(\sigma)) = \nabla \cdot \mathbf{G} \text{ in } \Omega, \\ \log(\sigma) \text{ given on } \partial\Omega. \end{cases} \tag{4.5}$$

4.3. **Choice of T and knowledge of θ.** The decomposition $\mathbf{R} = \mathbf{J}\mathbf{T}^T$ is not unique as any transfer matrix $\mathbf{T}_1$ that satisfies this equation for some rotation matrix $\mathbf{R}_1$ gives rise to another rotated transfer matrix $\mathbf{T}_2 = \overline{\mathbf{R}}^T\mathbf{T}_1$ that satisfies the same equation for the corresponding rotation matrix $\mathbf{R}_2 = \mathbf{R}_1\overline{\mathbf{R}}$. This holds true for any rotation matrix $\overline{\mathbf{R}}$. In theory, the choice of $\mathbf{T}$

will not influence the reconstruction procedure, as every choice of $\mathbf{T}$ with corresponding θ will work to extract the functionals $\mathbf{J}_i = \sqrt{\sigma}\nabla u_i$ from the entries of $H_{ij} = \sigma\nabla u_i \cdot \nabla u_j$. However, numerically a simple choice of $\mathbf{T}$ can be an advantage. For this reason, we choose Gram-Schmidt orthonormalization to obtain the following $\mathbf{T}$, as in this case the functionals $\mathbf{V_{ij}}$ have the simplified form as in (4.7):

$$\mathbf{T} = \begin{bmatrix} H_{11}^{-\frac{1}{2}} & 0 \\ -H_{12}H_{11}^{-\frac{1}{2}}D^{-1} & H_{11}^{\frac{1}{2}}D^{-1} \end{bmatrix}. \tag{4.6}$$

By the Jacobian constraint (1.3), $H_{11} > 0$ and thus $\mathbf{T}$ is well-defined. For this choice of $\mathbf{T}$ the function θ is given by the angle between ∇u_1 and the x_1-axis, as in this case the first column of $\mathbf{R}$ simplifies to

$$\mathbf{R_1} = T_{11}\mathbf{J_1} + T_{12}\mathbf{J_2} = \frac{\nabla u_1}{|\nabla u_1|}.$$

Using (4.1) we then calculate

$$\theta = \text{argument}(\partial_1 u_1 + i\partial_2 u_1).$$

In addition, the vector fields $\mathbf{V_{ij}}$ can be written explicitly in terms of $\mathbf{H}$:

$$\begin{aligned} &\mathbf{V_{11}} = \nabla \log H_{11}^{-\frac{1}{2}}, && \mathbf{V_{12}} = 0, \\ &\mathbf{V_{21}} = -\frac{H_{11}}{D}\nabla\left(\frac{H_{12}}{H_{11}}\right), && \mathbf{V_{22}} = \nabla \log\left(\frac{H_{11}^{\frac{1}{2}}}{D}\right). \end{aligned} \tag{4.7}$$

An outline of the reconstruction procedure using this choice for $\mathbf{T}$ is shown in Algorithm 1.

Knowledge of θ at the boundary is essential in the reconstruction procedure. The gradient equation (4.2) can be solved in two different ways for θ: Either by knowledge of θ at a single point and integrating along curves originating from that point, or by solving the Poisson problem (4.3), where knowledge of θ is required on the whole boundary. As we suggest the second option, the question is whether knowledge of θ at the boundary is a valid assumption. Information about θ is related to the gradient ∇u_1 and hence the current $\sigma\nabla u_1$, as both vector fields have the same direction. The functional $\sigma\nabla u_1$ can be decomposed into two parts with contribution from the unit outward normal ν and its direct orthogonal $\eta = \mathcal{J}\nu$:

$$\sigma\nabla u_1 = (\sigma\nabla u_1 \cdot \nu)\nu + (\sigma\nabla u_1 \cdot \eta)\eta.$$

Along the part of the boundary $\partial\Omega\backslash\Gamma$ the Neumann data is known, so that knowledge of $(\sigma\nabla u_1 \cdot \eta)\eta$ is required to determine $\sigma\nabla u_1$ along this part of the boundary. Along Γ the Dirichlet data and thus the directional derivative $(\nabla u_1 \cdot \eta)$ is known, so that knowledge of σ and $\sigma\nabla u_1 \cdot \nu$ is required to determine $\sigma\nabla u_1$ along Γ. This requires the following information on the different parts of the boundary:

- Knowledge of σ and the potential u_1 yield information about θ on $\partial\Omega\backslash\Gamma$
- Knowledge of σ and $\sigma\nabla u_1 \cdot \nu$ yield information about θ on Γ

However, along $\partial\Omega\backslash\Gamma$ the vanishing Neumann data gives us the additional information that $\sigma\nabla u_1$ is solely determined by the direct orthogonal η. Hence, on $\partial\Omega\backslash\Gamma$ the direction of $\sigma\nabla u_1$ is either η or $-\eta$. The sign of η is influenced by the choice of the boundary function f_1. By theorem B.1 (the weak maximum principle) the maximum and minimum of u_1 is attained at points $x_{\max}$ and

$x_{\min}$ on the Dirichlet boundary Γ. At these points ∇u_1 will then point outwards and inwards of the domain respectively, as the gradient points in the direction of highest increase. The maxima and minima of f_1 will therefore influence the direction of the current and this information can be used to determine sign of η and thus θ on $\partial\Omega\backslash\Gamma$.

Algorithm 1 Reconstruction procedure

Generating data: Choose a set of boundary conditions (f_1, f_2) so that the corresponding solutions satisfy the Jacobian constraint (1.3). Use the solutions to generate the power density matrix $\mathbf{H}$.

(1) Use the measurement matrix $\mathbf{H}$ to define $\mathbf{T}$ and the vector fields $\mathbf{V_{ij}}$ as in (4.6) and (4.7) respectively
(2) Reconstruct θ by solving the boundary value problem (4.3)
(3) Reconstruct σ by solving the boundary value problem (4.5)

5. Numerical Examples

The Matlab and Python code to generate the numerical examples can be found on GitLab: GitLab code.

To investigate the performance of the reconstruction algorithm in the limited view setting, we implement the algorithm in Python and used FEniCS [14] to solve the PDEs. Here we mainly focus on performance for two boundary conditions. We use a fine mesh to generate our power density data and a coarser mesh to address the reconstruction problem. Unless otherwise stated we used $N_{\text{data}} = 44880$ nodes in the high-resolution case, while for the smaller mesh we considered a resolution of $N_{\text{recon}} = 20100$ nodes. For both meshes, we use $\mathbb{P}_1$ elements. We consider the domain Ω to be the unit disk: $\Omega = B(\mathbf{0}, 1)$. Furthermore, we consider two test cases for the conductivity σ defined by:

$$\sigma_{\text{case 1}}(x^1, x^2) = 1 + e^{-5\left((x^1)^2+(x^2)^2\right)},$$

$$\sigma_{\text{case 2}}(x^1, x^2) = 1 + e^{-20\left(\left(x^1+\frac{1}{2}\right)^2+(x^2)^2\right)} + e^{-20\left((x^1)^2+\left(x^2+\frac{1}{2}\right)^2\right)} + e^{-50\left(\left(x^1-\frac{1}{2}\right)^2+\left(x^2-\frac{1}{2}\right)^2\right)},$$

for $(x^1, x^2) \in \Omega$. Figure 2 illustrates the conductivities.

To test the reconstruction procedure we follow the procedure as outlined in Section 4. To generate the power density data we simply consider the coordinate functions as boundary conditions:

$$(f_1, f_2) = (x^1, x^2), \quad (x^1, x^2) \in \Gamma.$$

We make this choice, as there is no theory developed on how to constructively choose the boundary functions in the case of mixed Dirichlet and Neumann conditions such that (1.3) is satisfied. However, for Dirichlet boundary conditions and when the domain is convex and 2-dimensional it is known that the coordinate functions $(f_1, f_2) = (x_1, x_2)$ yield solutions (u_1, u_2) so that these satisfy the Jacobian condition (see e.g. [**?**]). Motivated by this theory we limit ourselves to these boundary conditions.

We consider different sizes for the subset of the boundary, Γ, that we can control, and show these in Figure 3. For each choice of Γ we then solve the two PDEs using FEniCS and use the computed solutions u_1 and u_2 to generate the 3 power densities H_{11}, H_{12} and H_{22}. Furthermore, for comparison we compute the true angle θ from knowledge of the true gradient ∇u_1.

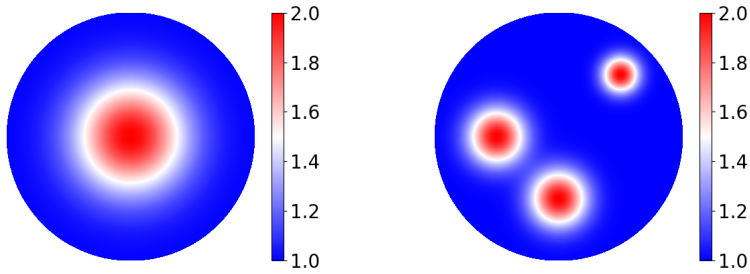

Case 1 Case 2

FIGURE 2. The conductivities σ used for the reconstruction procedure.

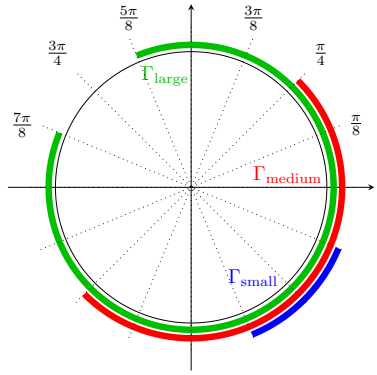

FIGURE 3. Different sizes of Γ used for the reconstruction procedure.

5.1. **Reconstruction of θ.** For the three different sizes of Γ, $\Gamma_{\text{large}}, \Gamma_{\text{medium}}$ and Γ_{small}, as seen in Figure 3, we reconstruct θ for σ defined as in test case 1. As θ is a function mapping from Ω to the unit circle S^1, which is a periodic space, we choose on $\partial\Omega$ a representation of θ which forms a continuous curve when unwrapping S^1 to an interval of $\mathbb{R}$. We denote this representation $\tilde{\theta}$ and it is constructed as follows.

$$\tilde{\theta} = \begin{cases} \theta + 2\pi & t \in \left[-\frac{\pi}{2}, -\frac{3\pi}{8}\right] \\ \theta & \text{otherwise.} \end{cases} \tag{5.1}$$

The representation is illustrated in Figure 4(a). This is done to avoid any discontinuous transitions, which could otherwise occur from θ taking values on alternating sides of the end points of the interval; this problem is illustrated in Figure 4(b). The special region in which we make the modification to obtain continuity is identified by considering the boundary conditions. As θ represents the angle between $-\eta$ and the x_1-axis a discontinuity, when viewing S^1 in $\mathbb{R}$ can be identified to occur at exactly the points $t = -\frac{\pi}{2}$ and $t - \frac{3\pi}{8}$.

Using the representation $\tilde{\theta}$ as a boundary condition, we reconstruct θ for the three different sizes of Γ. The reconstructions of θ are compared to the true expressions in Figure 5, while table 1 shows the relative L^2-error. For the smaller sizes of Γ there appear artifacts close to the boundary $\partial\Omega\backslash\Gamma$ otherwise there is no visual distinction between true expressions and reconstructions, which is reflected in the relative errors as well. Note that due to the above modifications we use $\sin(2\theta)$ instead of θ for comparison.

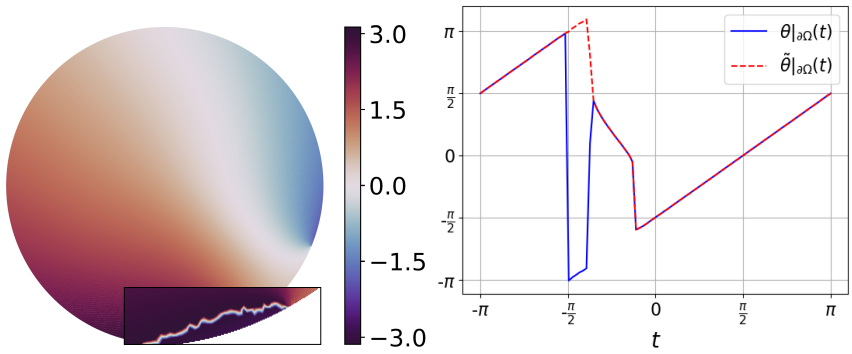

(a) True θ

(b) True θ and a modified version $\tilde{\theta}$ along the boundary $\partial\Omega$.

FIGURE 4. True expression for θ assigned to a smooth function space for σ as in test case 1 and having control over Γ_{small}. The right figure compares the same function to a modified version $\tilde{\theta}$ defined in (5.1) along the boundary.

TABLE 1. Relative L^2 errors for varying sizes of Γ.

		Γ_{large}	Γ_{medium}	Γ_{small}
Min $\det(\mathbf{H})$	case 1	$3.94 \cdot 10^{-6}$	$3.87 \cdot 10^{-10}$	$9.94 \cdot 10^{-18}$
	case 2	$2.94 \cdot 10^{-6}$	$3.57 \cdot 10^{-10}$	$1.07 \cdot 10^{-17}$
Rel. L^2 error	case 1	(0.79%,2.04%)	(1.40%,2.01%)	(2.24%,2.37%)
$(\cos(2\theta), \sin(2\theta))$	case 2	(0.77%,1.86%)	(1.41%,1.97%)	(2.25%,2.33%)
Rel. L^2 error σ	case 1	32.02%	104%	177%
	case 2	33.62%	108%	180%

5.2. **Reconstruction of σ.** We reconstruct σ for both test cases in Figure 2 and for the three different sizes of Γ. Here we use the reconstructed θ from the previous step. The results are shown in Figure 6; note that the intervals for the colorbars are different, as for smaller sizes of Γ there is more variation in the reconstructed σ. Furthermore, Table 1 shows the relative L^2-error in the reconstructions. Both visually and quantitatively, we see that the quality of the reconstructed σ decrease for decreasing size of Γ. Comparing the different test cases of σ, from the relative error we see that the quality of the reconstruction is slightly better for test case 1. The slight difference in quality may be explained by the fact that in test case 2 there are smaller features closer to the boundary. Overall, the decreasing quality for decreasing size of Γ may follow from the fact that the

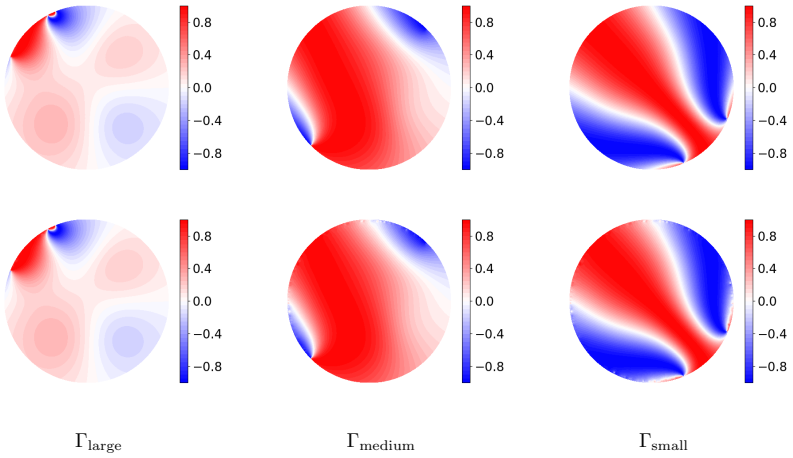

FIGURE 5. True expression for $\sin(2\theta)$ in the upper row and reconstructions in the lower row for varying sizes of Γ and σ being as in test case 1.

assumption of a non-vanishing determinant of H is almost violated for Γ_{small}. Figure 7 illustrates the expression $\log(\det(\mathbf{H}))$ for all sizes of Γ and their minimal values can be found in Table 1. We see from the Figure that with decreasing size of the boundary of control, the values of $\det(\mathbf{H})$ decrease close to $\partial\Omega\backslash\Gamma$. By assumption, the determinant should be non-vanishing everywhere in the domain, but for Γ_{small} the minimal value is $9.94 \cdot 10^{-18}$, and in comparison to values of the determinant elsewhere in the domain, this is effectively zero. As a consequence, the reconstruction in such regions of low determinants are not reliable, even though the algorithm does produce a result (see reconstructions in Figure 6 below.)

The size of Γ roughly reflects how large an amount of the domain can be controlled: While for Γ_{large} the reconstruction looks reasonable for most of the domain, for Γ_{medium} this is the case for about half of the domain and for Γ_{small} this does only apply for a small part of the domain. For the last two cases the part of the domain that is difficult to control is dominated by values of the reconstructed conductivity that are way higher than the true values and this is reflected in the high relative errors above 100%. What is common for all sizes of Γ is that there appear artifacts close to the part of the boundary that cannot be controlled, $\partial\Omega\backslash\Gamma$. For Γ_{medium} and Γ_{small} the artifacts occur at distinct points along the boundary. Further experiments showed that the locations of the artifacts seem not influenced by the choice of the boundary conditions. This indicates that the appearance of the artifacts is not caused by the PDE. However, we think that they are a mesh-dependent phenomenon. To understand what part in the reconstruction procedure induces the artifacts, we illustrate the fraction $\log\left(\frac{\sqrt{H_{11}}}{D}\right)$ in Figure 8. This fraction appears in the expression for $\mathbf{V_{22}}$ in (4.7) and then enters the right hand side of the reconstruction formula of σ in (4.4). We see from the figure that there appear small discontinuities at locations similar to the artifacts along the boundary $\partial\Omega\backslash\Gamma$. To obtain $\mathbf{V_{22}}$ one needs to compute the gradient of this function, which will cause the artifacts visible in the reconstruction. To support the theory

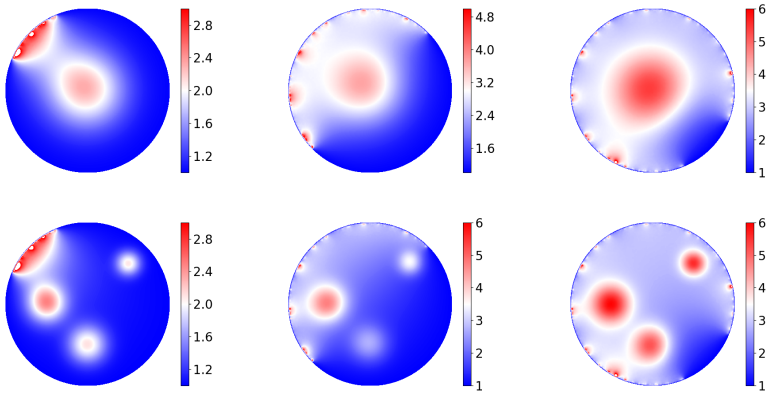

Γ_{large} Γ_{medium} Γ_{small}

FIGURE 6. Reconstructions of σ as in test case 1 for varying sizes of Γ in the upper row and for test case 2 in the lower row. Note that different color scales are used.

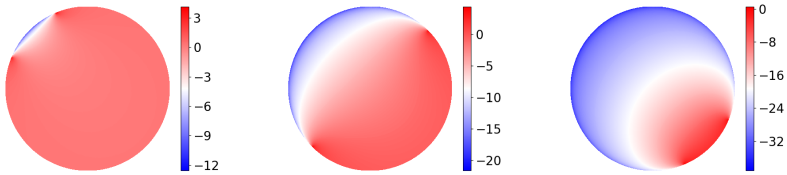

Γ_{large} Γ_{medium} Γ_{small}

FIGURE 7. The expression $\log(\det \mathbf{H})$ for varying sizes of Γ. Large negative values (blue regions) correspond to values of $\det \mathbf{H}$ close to zero.

that these are induced by the discretization of the domain, we compare the reconstruction of σ for finer meshes in Figure 9 and show the relative errors in Table 2. The mesh refinement does not make the artifacts disappear, but with increasing mesh size, the artifacts have less impact on the reconstruction, so that the relative errors decrease.

TABLE 2. Relative errors in the reconstructions for varying grid sizes N_{data} and N_{recon}, using test case 1 and controlling Γ_{medium}.

	number of nodes		
Grid size	N_{data}	N_{recon}	Relative L^2 error σ
N_{small}	44.880	20.100	103.7%
N_{medium}	79.281	44.880	86.38 %
N_{large}	124.265	79.281	78.85%

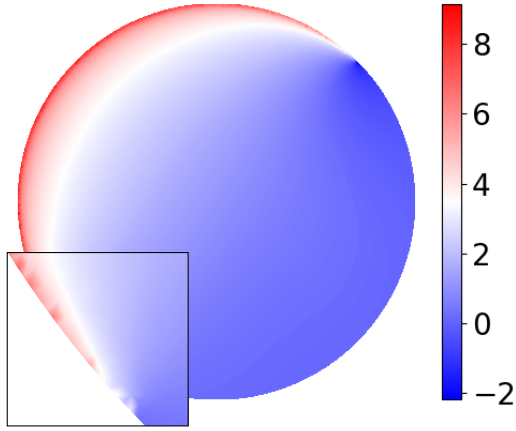

FIGURE 8. The fraction $\log\left(\frac{\sqrt{H_{11}}}{D}\right)$ in test case 1 when having control over Γ_{medium}. We zoom in on some of the discontinuities towards the boundary $\partial\Omega\backslash\Gamma$.

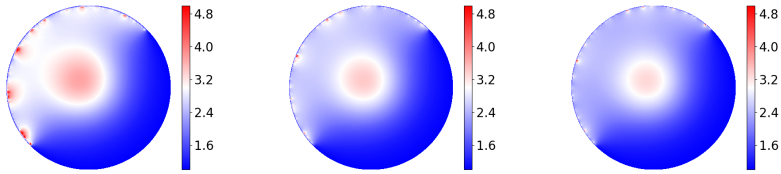

N_{small} N_{medium} N_{large}

FIGURE 9. Reconstructions of σ as in test case 1 for varying mesh sizes when having control over Γ_{medium}.

5.3. **Reconstruction of σ from noisy data.** We perturb the entries of the power density matrix $\mathbf{H}$ at each node with random noise:

$$\widetilde{H}_{ij} = H_{ij} + \frac{\alpha}{100}\frac{e_{ij}}{\|e_{ij}\|_{L^2}}H_{ij},$$

where α is the noise level and e_{ij} are entries in the matrix $\mathbf{E}$ that are normally distributed $e_{ij} \sim \mathcal{N}(0,1)$. We use `numpy.random.randn` to generate the elements e_{ij} and fix the seed `numpy.random.seed(50)`. The perturbation by random noise causes the Jacobian constraint to be violated close to the boundary $\partial\Omega\backslash\Gamma$. To enforce symmetry of $\widetilde{\mathbf{H}}$ we use $\frac{1}{2}(\widetilde{\mathbf{H}} + \widetilde{\mathbf{H}}^T)$ in the reconstruction procedure. Furthermore, to enforce positive definiteness of $\widetilde{\mathbf{H}}$ we use a small positive

lower bound for the eigenvalues of $\widetilde{\mathbf{H}}$. This procedure works like a regularization of the reconstruction, where the lower bound, L, is the regularization parameter. This behavior is illustrated for reconstructions of $\sigma_{\text{Case 2}}$ in figure 10 and three different lower bounds $L = 10^{-6}$, $L = 10^{-5}$ and $L = 10^{-4}$. Here $\mathbf{H}$ is perturbed with 5% noise and Γ_{medium} is used. When L is chosen too small relative to the noise level the reconstruction is dominated by the noise on the values of $\widetilde{\mathbf{H}}$ for which $\det(\widetilde{\mathbf{H}})$ is small. On the other hand, for a large value of L (like $L = 10^{-4}$ in this case) a lot of information close to $\partial\Omega\backslash\Gamma$ is discarded, where the values of $\det(\widetilde{\mathbf{H}})$ should be small, as the Jacobian constraint is violated at the boundary. Therefore, we choose the lower bound as small as possible, while still obtaining a reasonable reconstruction which is the case for $L = 10^{-5}$ in this case. Following this procedure, we reconstruct $\sigma_{\text{Case 2}}$ for three different noise levels $1\%, 5\%$ and 10% in Figure 11. Here the lower bounds $L = 10^{-6}$ (1% noise) and $L = 10^{-5}$ (5% and 10% noise) are used. Visually there appear more artifacts close to the boundary of control for increasing noise level. However, by choosing the suitable lower bound for each noise level the reconstructions are of similar quality. This makes it possible to add even higher levels of noise than 10%, but for increasing noise level one needs to use increasing lower bounds.

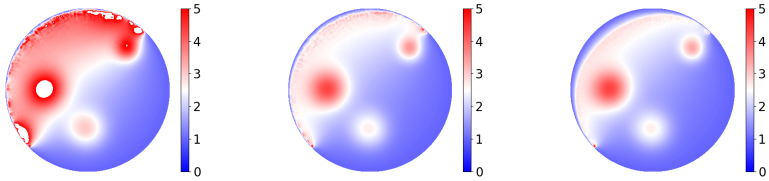

$L = 10^{-6}$ $L = 10^{-5}$ $L = 10^{-4}$

FIGURE 10. Reconstructions of σ as in test case 2 when corrupting the power density matrix with 5% noise and using the boundary of control Γ_{medium}. We use varying lower bounds L for the eigenvalues of $\widetilde{\mathbf{H}}$.

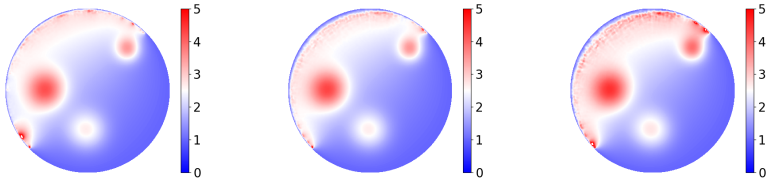

1% noise 5% noise 10% noise

FIGURE 11. Reconstructions of σ as in test case 2 when corrupting the power density matrix with varying noise levels and using the boundary of control Γ_{medium}. We use lower bounds L for the eigenvalues of $\widetilde{\mathbf{H}}$: $L = 10^{-6}$ (1% noise) and $L = 10^{-5}$ (5% and 10% noise).

6. Discussion and further work

In this work we have shown the existence of finitely many boundary conditions that make solutions to the governing elliptic PDE satisfy the Jacobian constraint. This is certainly relevant for AET, as it indicates that AET in the limited view setting is indeed feasible. Moreover, we consider a numerical reconstruction framework in this setting and address both possibilities and limitations for reconstruction based on three particular boundary conditions.

The results are based on the Runge approximation and hence they are not constructive. This immediately prompts the question of how to constructively find boundary conditions to satisfy the Jacobian constraint. An additional question concerns the reconstruction possibilities in the pragmatic choice of few boundary conditions. This is a question of deterioration of information with distance from the active part of the boundary as observed in [12] and [8]. We note additionally, that given the no-flux condition outside Γ, the electrical field on the boundary must be tangential; hence the Jacobian constraint can never be satisfied on this part of the boundary. The reconstruction problem thus gets hard in the proximity to the boundary.

The result here itself guarantees a limited number of required boundary conditions, however, it is not clear how large that number may be. It would be interesting to find an upper bound at least for certain geometries.

A final important question for further studies concerns the growth and behavior of the boundary conditions found via the Runge approximation. The Runge approximation has recently been studied quantitatively [17], and combining such results with our work could be an important step further.

Acknowledgements

BJ was supported by the Academy of Finland (grant no. 320022).

References

[1] Adams, R. A. and Fournier, J. J., *Sobolev spaces*, vol. 140, Elsevier, 2003.

[2] Alberti, G. S., Bal, G., and Di Cristo, M., *Critical points for elliptic equations with prescribed boundary conditions*, Archive for Rational Mechanics and Analysis 226 (2017), no. 1, 117–141 (eng).

[3] Alberti, G. S. and Capdeboscq, Y., *Lectures on elliptic methods for hybrid inverse problems*, vol. 25, Société Mathématique de France, 2018.

[4] Alberti, G. S. and Capdeboscq, Y., *Combining the Runge Approximation and the Whitney Embedding Theorem in Hybrid Imaging*, International Mathematics Research Notices 2022 (2020), no. 6, 4387–4406.

[5] Ammari, H., Bonnetier, E., Capdeboscq, Y., Tanter, M., and Fink, M., *Electrical impedance tomography by elastic deformation*, SIAM Journal on Applied Mathematics 68 (2008), no. 6, 1557–1573.

[6] Bal, G., Bonnetier, E., Monard, F., and Triki, F., *Inverse diffusion from knowledge of power densities*, Inverse Probl. Imaging 7 (2013), no. 2, 353–375.

[7] Bal, G., Guo, C., and Monard, F., *Imaging of anisotropic conductivities from current densities in two dimensions*, SIAM J. Imaging Sci. 7 (2014), no. 4, 2538–2557.

[8] Cristo, M. D. and Rondi, L., *Interior decay of solutions to elliptic equations with respect to frequencies at the boundary*, 2019.

[9] Gebauer, B., *Localized potentials in electrical impedance tomography*, Inverse Probl. Imaging 2 (2008), no. 2, 251–269.

[10] Giaquinta, M. and Martinazzi, L., *An introduction to the regularity theory for elliptic systems, harmonic maps and minimal graphs*, Springer Science & Business Media, 2013.

[11] Gilbarg, D. and Trudinger, N. S., *Elliptic partial differential equations of second order*, vol. 224, springer, 2015.

[12] Hubmer, S., Knudsen, K., Li, C., and Sherina, E., *Limited-angle Acousto-Electrical Tomography*, Inverse Problems in Science and Engineering (2018), 1–20.

[13] Jensen, B., Kirkeby, A., and Knudsen, K., *Feasibility of acousto-electric tomography (submitted)*, 2019.

[14] Logg, A., Mardal, K.-A., and Wells, G., *Automated solution of differential equations by the finite element method: The fenics book*, vol. 84, Springer Science & Business Media, 2012.

[15] Monard, F. and Bal, G., *Inverse anisotropic diffusion from power density measurements in two dimensions*, Inverse Problems 28 (2012), no. 8, 084001.

[16] Monard, F. and Bal, G., *Inverse diffusion problems with redundant internal information*, Inverse Problems and Imaging 6 (2012), no. 2, 289–313.

[17] Rüland, A. and Salo, M., *Quantitative Runge approximation and inverse problems*, Int. Math. Res. Not. IMRN 2019 (2019), no. 20, 6216–6234.

[18] Salsa, S., *Partial differential equations in action: from modelling to theory*, vol. 99, Springer, 2016.

[19] Zhang, H. and Wang, L. V., *Acousto-electric tomography*, Progress in Biomedical Optics and Imaging - Proceedings of Spie 5 (2004), no. 9, 20, 145–149 (eng).

Appendix A. Proof of Lemma 2.3

Proof of Lemma 2.3. We sketch the principal steps of the proof. It is derived from [3, Section 7.3].

Step 1.) Observe first that for any $g \in C^{0,\alpha}(B(x_0,s))$ we have

$$\|g - g(x_0)\|_{C^{0,\frac{\alpha}{2}}(\overline{B(x_0,s)})} \leq C_1 s^{\frac{\alpha}{2}} |g|_{C^{0,\alpha}(B(x_0,s))}, \tag{A.1}$$

where C_1 is an independent constant. [3, Eq. (7.28)]

Step 2.) Let u_s be the solution to the PDE problem

$$\begin{aligned} Lu_s &= 0 \quad \text{in } B(x_0,s), \\ u_s &= u_0 \quad \text{on } \partial B(x_0,s). \end{aligned}$$

Consider now $v_s = u_s - u_0$ and observer that it is the unique solution of

$$\begin{aligned} Lv_s &= -\nabla\cdot(\sigma - \sigma(x_0))\nabla u_0 \quad \text{in } B(x_0,s), \\ v_s &= 0 \qquad\qquad\qquad\qquad\quad \text{on } \partial B(x_0,s). \end{aligned}$$

Then by [3, Lem. 7.14] we have the estimate

$$\|v_s\|_{C^{1,\frac{\alpha}{2}}(\overline{B(x_0,s)})} \leq C_2 \|(\sigma - \sigma(x_0))\nabla u_0\|_{C^{0,\frac{\alpha}{2}}(\overline{B(x_0,s)})}.$$

By [11, Eq. (4.7)] and (A.1)

$$\|(\sigma - \sigma(x_0))\nabla u_0\|_{C^{0,\frac{\alpha}{2}}(\overline{B(x_0,s)})} \leq \|\sigma - \sigma(x_0)\|_{C^{0,\frac{\alpha}{2}}(\overline{B(x_0,s)})} \|\nabla u_0\|_{C^{0,\frac{\alpha}{2}}(\overline{B(x_0,s)})} \leq C_3 s^{\frac{\alpha}{2}}$$

where $C_3 = C_1 \|\nabla u_0\|_{C^{0,\frac{\alpha}{2}}(\overline{B(x_0,s)})} |\sigma|_{C^{0,\alpha}(B(x_0,s))}$. Therefore

$$\|u_s - u_0\|_{C^{1,\frac{\alpha}{2}}(\overline{B(x_0,s)})} \leq C_4 s^{\frac{\alpha}{2}}$$

with $C_4 = C_2 C_3$, and there is $\tilde{s} \in (0,s)$ such that

$$\|u_{\tilde{s}} - u_0\|_{C^{1,\frac{\alpha}{2}}(\overline{B(x_0,\tilde{s})})} \leq \frac{\delta}{2}. \tag{A.4}$$

Step 3.) Observe that $u_{\tilde{s}} \in H^1(B(x_0,\tilde{s})) \cap C^{1,\frac{\alpha}{2}}(B(x_0,\tilde{s}))$ and $Lu_{\tilde{s}} = 0$ in $B(x_0,\tilde{s})$. By Theorem 2.2 there is a sequence $u_n \in H^1(\Omega)$ satisfying $Lu_n = 0$ in Ω and $L_\nu u_n = 0$ on $\partial\Omega\backslash\Gamma$ and $u_n|_{B(x_0,\tilde{s})} \to u_{\tilde{s}}$ in $L^2(B(x_0,\tilde{s}))$.

Put $w_n = u_n - u_{\tilde{s}}$ then $w_n \in H^1(B(x_0,\tilde{s}))$ and satisfy $Lw_n = 0$ in $B(x_0,\tilde{s})$. By [10, Thm. 5.19] we have

$$\|\nabla w_n\|_{C^{0,\frac{\alpha}{2}}(\overline{B(x_0,\frac{\tilde{s}}{3})})} \leq C_5 \|\nabla w_n\|_{L^2(B(x_0,\frac{\tilde{s}}{2})} \tag{A.5}$$

with $C_5 \equiv C_5(x_0,\tilde{s},\sigma)$, thus $w_n \in C^{1,\frac{\alpha}{2}}(\overline{B(x_0,\frac{\tilde{s}}{3})})$. By [18, Thm. 8.25] we have

$$\|w_n\|_{H^2(B(x_0,\frac{\tilde{s}}{k+1}))} \leq C_6 \|w_n\|_{L^2(B(x_0,\frac{\tilde{s}}{k}))}, \tag{A.6}$$

where $C_6 \equiv C_6(x_0,\tilde{s},k,\sigma)$, and by Sobolev embedding [1] we have

$$\|w_n\|_{C^0(B(x_0,\frac{\tilde{s}}{3}))} \leq C_7 \|w_n\|_{H^2(B(x_0,\frac{\tilde{s}}{3}))} \tag{A.7}$$

where $C_7 \equiv C_7(x_0,\tilde{s})$.

By combining the estimates (A.5)–(A.7) we obtain

$$\|w_n\|_{C^{1,\frac{\alpha}{2}}(B(x_0,\frac{\tilde{s}}{3}))} \leq C_8 \|w_n\|_{L^2(B(x_0,\tilde{s}))} \to 0 \quad \text{as } n \to \infty,$$

where $C_8 = C_8(x_0, \tilde{s}, \sigma)$. Thus we have the strengthened convergence $u_n \to u_{\tilde{s}}$ in $C^{1,\frac{\alpha}{2}}(B(x_0, \frac{\tilde{s}}{3}))$. Hence we can pick $\tilde{n}$ such that

$$\|u_{\tilde{n}} - u_{\tilde{s}}\|_{C^{1,\frac{\alpha}{2}}(B(x_0,\frac{\tilde{s}}{3}))} \leq \frac{\delta}{2}. \tag{A.8}$$

Step 4.) Choose $r \in (0, \frac{\tilde{s}}{3})$. Combining the estimates (A.4) and (A.8) we then have

$$\|u_{\tilde{n}} - u_0\|_{C^1(\overline{B(x_0,r)})} \leq \|u_{\tilde{n}} - u_{\tilde{s}}\|_{C^{1,\frac{\alpha}{2}}(\overline{B(x_0,r)})} + \|u_{\tilde{s}} - u_0\|_{C^{1,\frac{\alpha}{2}}(\overline{B(x_0,r)})} \leq \frac{\delta}{2} + \frac{\delta}{2} = \delta.$$

□

Appendix B. Weak Maximum Principle for a mixed Dirichlet-Neumann problem

Theorem B.1 (Weak Maximum Principle)**.** *Let $\Omega \subset \mathbb{R}^n$ be a bounded connected Lipschitz domain and $\sigma \in L^\infty_+(\Omega)$. Let $u \in H^1(\Omega) \cap C(\overline{\Omega})$ be a solution to* (1.1) *so that it satisfies the variational equation*

$$\int_\Omega \sigma \nabla u \cdot \nabla v \, \mathrm{d}x = 0, \tag{B.1}$$

for all test functions $v \in H^1_{0,\Gamma}(\Omega)$. Here $H^1_{0,\Gamma}(\Omega)$ consists of the set of functions in $H^1(\Omega)$ with zero trace on Γ. Then the following are true:

1. *If $u \geq 0$ on Γ then $u \geq 0$ in Ω.*
2. *$\inf_{y\in\Gamma} u(y) \leq u(x) \leq \sup_{y\in\Gamma} u(y)$ for all $x \in \Omega$.*

Proof. This proof is based on [18, proof of Thm. 8.20], but for the convenience of the reader it is simplified to only cover the setting where the elliptic operator is composed of a diffusion term. Define $u^- = \max\{-u, 0\}$ and $u^+ = \max\{u, 0\}$. Since $u \in H^1(\Omega)$ then $|u|$, u^- and u^+ are also in $H^1(\Omega)$ [18, Prop. 7.68].

(1) Since $u \geq 0$ on Γ, the negative part u^- has zero trace on Γ. Hence, $u^- \in H^1_{0,\Gamma}$. Thus for the choice of the test function $v = u^-$, the variational equation (B.1) is

$$\int_\Omega \sigma \nabla u \cdot \nabla u^- \, \mathrm{d}x = 0.$$

This simplifies to the following as $\nabla u^- = \nabla u \, \chi_{u<0}$ a.e. in Ω, so there is only a contribution for $u < 0$ and in this case $u = -u^-$:

$$-\int_\Omega \sigma \nabla u^- \cdot \nabla u^- \, \mathrm{d}x = 0.$$

As $\sigma \in L^\infty_+(\Omega)$ it follows directly from this equation that $\nabla u^- = 0$ in $L^2(\Omega)$, implying $u^- = C$, where C is a constant. As u^- has zero trace on Γ it follows that $C = 0$. This implies $u^- = 0$ a.e. and therefore $u = u^+$ a.e. on Ω.

(2) Let $m_1 = \inf_{y\in\Gamma} u(y)$. Then $u - m_1 \geq 0$ and $u - m_1 \in H^1(\Omega)$ satisfies the variational equation (B.1), as m_1 is just a constant. By step (1) it then follows that $u - m_1 = (u - m_1)^+$ a.e. on Ω, hence $u \geq \inf_{y\in\Gamma} u(y)$ a.e. on Ω. Defining $m_2 = \sup_{y\in\Gamma} u(y)$ and using the same approach for the function $m_2 - u$ yields $u \leq \sup_{y\in\Gamma} u(y)$ a.e. on Ω.

□

APPENDIX C

Paper C: Reconstructing anisotropic conductivities on two-dimensional Riemannian manifolds from power densities

Kim Knudsen, Steen Markvorsen, Hjørdis Schlüter. Reconstructing anisotropic conductivities on two-dimensional Riemannian manifolds from power densities.
Manuscript under development. We aim at including results on Riemannian manifolds with higher genus as discussed in section 4.4.2. Preprint available on arXiv: `https://arxiv.org/abs/2202.12056`.

Reconstructing anisotropic conductivities on two-dimensional Riemannian manifolds from power densities

Kim Knudsen[a], Steen Markvorsen[a], Hjørdis Schlüter[a,b]

[a] *DTU Compute, Richard Petersens Plads, Kgs. Lyngby, 2800, Technical University of Denmark*
[b] *Corresponding author, e-mail: hjsc@dtu.dk*

Abstract

We consider an electrically conductive compact two-dimensional Riemannian manifold with a smooth boundary. This setting defines a natural conductive Laplacian on the manifold and hence also voltage potentials, current fields and corresponding power densities arising from suitable boundary conditions. Motivated by Acousto-Electric Tomography we show that if the manifold has genus zero and the metric is known, then the conductivity can be recovered uniquely and constructively from knowledge of a few power densities. We illustrate the reconstruction procedure numerically by an example of a conductivity on a non-simply connected surface in three-space.

Keywords: Elliptic PDE, Inverse Problem, Riemannian manifold, Conductivity
PACS: 02.20.Jr, 02.30.Zz, 02.40.Ky
2000 MSC: 35J20, 58J05

1. Introduction and statement of the main result

Let (M, g) denote the mentioned compact Riemannian manifold with smooth boundary ∂M. An electric conductivity on M is modelled by a – generally anisotropic – $(1,1)$ tensor field γ, which is selfadjoint and uniformly elliptic with respect to g, i.e. for some $\kappa > 1$ and for all tangent vectors v and w:

$$g(\gamma(v), w) = g(v, \gamma(w)) \quad \text{and} \quad \kappa^{-1} \|v\|_g^2 \leq g(\gamma(v), v) \leq \kappa \|v\|_g^2. \tag{1}$$

On the boundary ∂M we prescribe an electrostatic potential f that generates an interior voltage potential u. In the absence of interior sinks and sources, $u \in H^1(M)$ is characterized as the unique solution to the boundary value problem

$$\begin{cases} \operatorname{div}_g \left(\gamma \operatorname{grad}_g (u) \right) = 0 \text{ in } M, \\ u = f \text{ on } \partial M. \end{cases} \tag{2}$$

Existence and uniqueness of solutions to such an elliptic PDE on a manifold is classical, see e.g. [1]. The interior current field is $\gamma \operatorname{grad}_g (u)$, i.e. γ is the tensor turning the electric field $\operatorname{grad}_g (u)$ into the current field.

By considering m different boundary functions $f = f_i,\ 1 \leq i \leq m$, the corresponding solutions to equation (2) are denoted by u_i. They define the so-called power density $(m \times m)$-matrix H with elements:

$$H_{ij} = H_{ji} = g(\gamma \operatorname{grad}_g (u_i), \operatorname{grad}_g (u_j)) \quad \text{for} \quad 1 \leq i, j \leq m. \tag{3}$$

The inverse problem in Acousto-Electric Tomography [2, 3] is concerned with the above in a Euclidean setting and asks for the recovery of γ from knowledge of H. This problem was adressed for $n = 2$ in [4, 5, 6] and for dimensions $n \geq 3$ in [7, 8, 9]. It is highly related to the Calderón problem [10], see [11] for an account on this and related problems.

We conjecture the following: Suppose we know the manifold (M, g) and the power density matrix H associated with a number of sufficiently well-chosen boundary functions f_i. Then the conductivity tensor field γ is uniquely and constructively determined

As a first step towards this general conjecture, we prove it for all cases where the topology of the background manifold is simplest possible in a sense that we now explain:

Every 2-dimensional, compact, orientable Riemannian manifold is diffeomorphic to a handle-body, i.e. it consists of a number handles attached to a 2-sphere. This number is called the *genus* of the manifold. When M has k boundary components, its genus is related to the Euler characteristic $\chi(M)$ and k as follows: $p = 1 - (\chi + k)/2$, see [12].

With these preliminaries, we can now state our main result.

Theorem 1. *Let (M, g) denote a given compact 2-dimensional Riemannian manifold with genus $p = 0$, metric g and non-empty smooth boundary ∂M consisting of a finite number of boundary components. Suppose that γ is a conductivity tensor field on M, which is known only on the boundary ∂M. Then there exist $m = 4$ boundary functions f_i with induced corresponding power density matrix H, such that H determines γ uniquely and constructively on all of M.*

Our approach takes in particular advantage of the work in 2D by Monard and Bal [4]. In addition, the proof of Theorem 1 makes use of the Poincaré-Koebe uniformization theorem for compact Riemann surfaces (with boundary). Indeed, (M, g) admits a conformal isometric representation onto a *fundamental domain* in $\mathbb{R}^2$. When $p > 0$ the fundamental domain has extra boundary components that must be glued together to reconstruct the original manifold. We refer to [13, 14, 15] for a very general and constructive approach to this uniformization procedure.

For $p = 0$ the fundamental domain in $\mathbb{R}^2$ has no extra boundary components, so all boundaries are accessible for specifications of boundary functions, and (contrary to the cases $p > 0$) it is not needed for the PDE problem (2) to take periodicity across the extra boundary components into account.

Remark. *We note that the manifolds mentioned in Theorem 1 are very general in the sense that they do not need to be realizable as surfaces in $\mathbb{R}^3$ (with the induced metric).*

The main novelty of our work is the geometric setting and the application of the uniformization theorem allowing for the reduction to the known, Euclidean setting. The

outline is as follows: We prove Theorem 1 in Section 2. In Section 3 we review some details from the Euclidean reconstruction method and indicate how the key equations can be lifted to (M, g) using explicit reference to the conformal factor that is induced from the isometric conformal representation of (M, g) in $\mathbb{R}^2$. Finally, in Section 4, we present the result of a numerical implementation of the reconstruction procedure.

2. Proof of Theorem 1

With reference to the uniformization theorem, (M, g) is – via a conformal diffeomorphism – isometric to a compact domain N (with boundary) in the $\mathbb{R}^2$ equipped with the metric $g_N = \rho^2 \cdot g_E$. Here g_E denotes the Euclidean metric in $\mathbb{R}^2$ and ρ denotes the conformal factor induced from the uniformization – obtained e.g. from the constructive numerical approach of [13, 14, 15]. In this way (M, g) is isometric to (N, g_N). Since Theorem 1 is by definition only concerned with intrinsic metric properties of (M, g), we can therefore prove it purely in terms of (N, g_N) using standard coordinates x^1 and x^2 and the corresponding standard basis $\{\frac{\partial}{\partial x^1} = e_1\,,\ \frac{\partial}{\partial x^2} = e_2\}$ in $\mathbb{R}^2$. The metric g_N is then represented by the (2×2)-matrix function G with elements $G_{ij}(x^1, x^2) = \rho^2(x^1, x^2) \cdot \delta_{ij}$, and the conductivity tensor is represented by a (2×2)-matrix function with elements γ_i^j so that $\gamma(e_i)(x^1, x^2) = \sum_j \gamma_i^j(x^1, x^2) \cdot e_j$.

We will denote the first equation in (2) as the γ-Laplace equation for (M, g), and we will write it shorthand as $\Delta_g^\gamma(u) = 0$. In the isometric representation (N, g_N) of (M, g) we then have the following key observation:

Proposition 2. *Let $u(x^1, x^2)$ denote a smooth function on N. Then*

$$\Delta_{g_N}^\gamma(u)(x^1, x^2) = \frac{1}{\rho^2(x^1, x^2)} \cdot \Delta_{g_E}^\gamma(u)(x^1, x^2). \tag{4}$$

Proof. The g_N-gradient of the function u is expressed using the elements $G^{i,j}$ of the inverse matrix G^{-1} as follows:

$$\mathrm{grad}_{g_N}(u) = \sum_{ij} \frac{\partial u}{\partial x^i} \cdot G^{ij} \cdot e_j = \frac{1}{\rho^2} \cdot \sum_i \frac{\partial u}{\partial x^i} \cdot e_i = \frac{1}{\rho^2} \cdot \mathrm{grad}_{g_E}(u),$$

and the g_N-divergence of a vector field $V = \sum_i v^i \cdot e_i$ is in 2D:

$$\mathrm{div}_{g_N}(V) = \frac{1}{\sqrt{\det(G)}} \cdot \sum_i \frac{\partial}{\partial x^i} \left(v^i \cdot \sqrt{\det(G)} \right) = \frac{1}{\rho^2} \cdot \sum_i \frac{\partial}{\partial x^i} \left(v^i \cdot \rho^2 \right).$$

Insertion of $V = \gamma(\mathrm{grad}_{g_N}(u)) = \frac{1}{\rho^2} \cdot \gamma(\mathrm{grad}_{g_E}(u))$ now gives directly:

$$\mathrm{div}_{g_N}(\gamma(\mathrm{grad}_{g_N}(u))) = \frac{1}{\rho^2} \cdot \mathrm{div}_{g_E}(\gamma(\mathrm{grad}_{g_E}(u))),$$

and the proposition follows. □

Remark. *The identity* (4) *only holds in dimension* 2 *where we can use the fact that* $\sqrt{\det(G)} = \rho^2$ *– as is already well-known from the case of an isotropic conductivity* $\gamma_i^j(x^1, x^2) = q(x^1, x^2) \cdot \delta_i^j$ *for a positive function* q.

We prove Theorem 1 with (M, g) represented isometrically by (N, g_N) in $\mathbb{R}^2$. In view of proposition 2 we have that $\Delta^\gamma_{g_N}(u) = 0$ is equivalent to $\Delta^\gamma_{g_E}(u) = 0$ for all u, so that the the boundary value problem (2) then reads:

$$\begin{cases} \Delta^\gamma_{g_E}(u) = 0 \text{ in } N, \\ \qquad u = f \text{ on } \partial N. \end{cases} \tag{5}$$

The power density matrix H^N associated with m different boundary functions f_i on ∂N and corresponding solutions u_i to (5) on N is then

$$\begin{aligned} H^N_{ij} = H^N_{ji} &= g_N(\gamma \operatorname{grad}_N u_i, \operatorname{grad}_N u_j) \\ &= \frac{1}{\rho^2} \cdot g_E(\gamma \operatorname{grad}_E u_i, \operatorname{grad}_E u_j) \\ &= \frac{1}{\rho^2} \cdot H^E_{ij} \quad , \quad \text{for} \quad 1 \le i\,, j \le m. \end{aligned} \tag{6}$$

In other words, since ρ is known, if H^N_{ij} are known functions in N then H^E_{ij} are known as well. Theorem 1 now follows from the following specific version in the Euclidean plane (N, g_E) due to Monard and Bal [4, Theorem 2.2]:

Theorem 3. *Let* (N, g_E) *denote a given compact domain (with non-empty smooth boundary) in the Euclidean plane* $(\mathbb{R}^2, g_E)$. *Then for any conductivity tensor field* γ *on* N *which is known on the boundary of* N *there exists* $m = 4$ *boundary functions* f_i *with induced corresponding power density matrix* H^E, *such that* γ *is uniquely and constructively determined by* H^E *on all of* N.

3. The reconstruction procedure

For the convenience of the reader, we now survey key points and identities from the proof of Theorem 3 with a view to the expressions as they appear in (N, g_N). Next, we outline the reconstruction procedure.

3.1. The governing equations

Based on (the unknown) γ we introduce another smooth (1,1) tensor field A defined in each tangent space as $A^2(x) = \gamma(x)$ and based on A we define the vector fields $S_k = A \operatorname{grad}_N u_k$ for $1 \le k \le m$. Furthermore A is decomposed into two parts, so that

$$\tilde{A} = \det(A)^{\frac{1}{2}} A \quad \text{with} \quad \det(\tilde{A}) = 1.$$

For the reconstruction procedure $S = (S_1, S_2)$ is orthonormalized into an $SO(2)$-valued frame $R = (R_1, R_2)$, by finding T such that $R = ST^T$. The transfer matrix T gives rise to the four vector fields V_{ij} and thence V_{ij}^a:

$$V_{ij} = \sum_{k=1}^{2} \operatorname{grad}_N(T_{ik}) T^{kj}, \quad 1 \leq i, j \leq 2, \quad V_{ij}^a = \frac{1}{2}(V_{ij} - V_{ji}),$$

where T_{ik} and T^{kj} denote the entries in T and T^{-1} respectively. As R is a rotation matrix, it can be parameterized by a function θ as $R = \left(\begin{smallmatrix} \cos\theta & -\sin\theta \\ \sin\theta & \cos\theta \end{smallmatrix}\right)$. For the procedure to work, we need the following two conditions on the power density matrix H:

$$\min(\det(\operatorname{grad}_N u_1, \operatorname{grad}_N u_2), \det(\operatorname{grad}_N u_3, \operatorname{grad}_N u_4)) \geq c_0 > 0 \text{ for every } x \in N, \tag{7}$$

$$\operatorname{grad}_N \left(\log \left(\frac{\det(\operatorname{grad}_N u_1, \operatorname{grad}_N u_2)}{\det(\operatorname{grad}_N u_3, \operatorname{grad}_N u_4)} \right) \right) \neq 0 \text{ for every } x \in N. \tag{8}$$

The boundary functions f_i mentioned in theorem 3 are suitable for reconstruction of γ when the corresponding four solutions u_i satisfy the conditions above. Existence of such four boundary functions for any γ is guaranteed, c.f. [4, Lemma 2.1]. The reconstruction procedure is then based on two equations. Using that $\operatorname{div}_N(JA^{-1}S_k)$ vanishes on N for $k = 1, 2$, and with J defined as $J = \left(\begin{smallmatrix} 0 & -1 \\ 1 & 0 \end{smallmatrix}\right)$, we can derive the first equation (corresponding to [4, eq.(8)]):

$$\operatorname{grad}_N \log(\det A) = D + g(\operatorname{grad}_N H^{qp}, \tilde{A}\, S_p)\tilde{A}^{-1}\, S_q, \tag{9}$$

with $D = \frac{1}{2} \operatorname{grad}_N \log(\det H)$ and where H^{qp} denotes entries in H^{-1}. By writing the Lie bracket $[\tilde{A}R_2, \tilde{A}R_1]$ in two different ways we obtain the second equation (corresponding to [4, eq.(10)]):

$$\rho^2 \tilde{A}^2 \operatorname{grad}_N \theta + [\tilde{A}_2, \tilde{A}_1] = -\frac{1}{2} J \operatorname{grad}_N \rho^2 + \rho^2 \tilde{A}^2 V_{12}^a - \frac{1}{2}\rho^2 J D. \tag{10}$$

Here $[\tilde{A}_2, \tilde{A}_1]$ denotes the Lie bracket between columns of $\tilde{A}$. As already alluded to above, these equations can be directly expressed on (N, g_E) by substituting the following quantities:

$$H^N = \rho^{-2} H^E, \quad V_{12}^{N,a} = \rho^{-2} V_{12}^{E,a}, \quad D^N = \rho^{-2} D^E - \operatorname{grad}_E \rho^2.$$

3.2. Solving the inverse problem

Algorithm 1 Reconstruction procedure

Choose a set of boundary conditions (f_1, f_2, f_3, f_4) so that H^N satisfies (7) and (8).

1. Reconstruct $\tilde{A}$ by use of equation (10) and data from $m = 4$ boundary conditions
2. Reconstruct θ by use of equation (10) and data from $m = 2$ boundary conditions
3. Reconstruct $\det(\gamma)^{\frac{1}{2}}$ by use of equation (9) and data from $m = 2$ boundary conditions

Using the governing equations (9) and (10) we can derive the reconstruction procedure as presented in Algorithm 1. The first step corresponds to two pairs of boundary conditions giving rise to solutions and power density data that each satisfy equation (10). Subtracting them yields an algebraic equation to be solved for $\tilde{A}$. The condition (8) ensures that division by zero is avoided, while condition (7) ensures invertibility of each power density matrix corresponding to a pair of solutions. The second and third step correspond to solving gradient equations for θ and $\log(\det(\gamma)^{\frac{1}{2}})$ respectively (corresponding to [4, eq.(36) & (41)]). As the gradients of θ and $\det(\gamma)^{\frac{1}{2}}$ are known throughout N, we only need to know the values of these functions at a single point. Because then the functions can be reconstructed throughout N by integration of the gradients along curves originating from that point. Specifically, the knowledge of γ at the global minimum $x_m \in \partial N$ of f_1 at the boundary yields the value of θ at x_m. Indeed, by the choice of the transfer matrix

$$T = \begin{pmatrix} H_{11}^{-\frac{1}{2}} & 0 \\ -H_{12}H_{11}^{-\frac{1}{2}}(\det H)^{-\frac{1}{2}} & H_{11}^{\frac{1}{2}}(\det H)^{-\frac{1}{2}} \end{pmatrix},$$

we have that $R_1 = T_{11}S_1 + T_{12}S_2 = \frac{A\,\mathrm{grad}_N u_1}{|A\,\mathrm{grad}_N u_1|_N}$. Thus $\theta = \mathrm{argument}(R_{11} + iR_{21})$ is given by the angle between $A\,\mathrm{grad}_N u_1$ and the x_1-axis. By the maximum principle [16] u_1 achieves its minimum over N at x_m. Therefore, at this point the gradient points in the direction of highest increase of u_1 corresponding to $-\nu$, the inward normal vector ($\mathrm{grad}_N u_1$ cannot be zero as by the condition (7) $|\,\mathrm{grad}_N u_1|_N > 0$). Hence,

$$\frac{\mathrm{grad}_N u_1}{|\,\mathrm{grad}_N u_1|_N}(x_m) = -\nu(x_m) \quad \Rightarrow \quad A\,\mathrm{grad}_N u_1(x_m) = -|\,\mathrm{grad}_N u_1|_N A\,\nu(x_m),$$

so that θ is known at x_m, since it is solely determined by the direction of $A\,\mathrm{grad}_N u_1$.

4. A numerical example

The MATLAB and PYTHON code to generate the numerical example can be found on GITLAB: GitLab code. To illustrate the reconstruction procedure we consider a manifold $(N, g_N = \rho^2 \cdot g_E)$ represented by a catenoid. The fundamental domain N is seen in the upper images in Figure 1, and the catenoid is already 'uniformized' via the following analytic conformal representation r and corresponding conformal factor ρ:

$$r(x^1, x^2) = \begin{pmatrix} \cosh\left(\log\left(\sqrt{(x^1)^2 + (x^2)^2}\right)\right)\cos(\arg(x^1 + ix^2)) \\ \cosh\left(\log\left(\sqrt{(x^1)^2 + (x^2)^2}\right)\right)\sin(\arg(x^1 + ix^2)) \\ \log\left(\sqrt{(x^1)^2 + (x^2)^2}\right) \end{pmatrix},$$

$$\rho(x^1, x^2) = \frac{\cosh\left(\frac{1}{2}\log((x^1)^2 + (x^2)^2)\right)}{\sqrt{(x^1)^2 + (x^2)^2}}\,.$$

The conductivity tensor field γ is composed of three functions ξ, ζ and $(\det\gamma)^{\frac{1}{2}}$:

$$\gamma = (\det\gamma)^{\frac{1}{2}} \begin{pmatrix} \xi & \zeta \\ \zeta & \frac{1+\zeta^2}{\xi} \end{pmatrix}\,. \tag{11}$$

The three functions ξ, ζ and $(\det \gamma)^{\frac{1}{2}}$ are chosen to show a number of features to be reconstructed. These are illustrated in the fundamental domain N in the first row of figure 1. In accordance with [4] we use only three boundary conditions to generate the power densities. These are simple polynomials in x^1 and x^2 given by $(f_1, f_2, f_4) = (-x^2 - 0.1(x^2)^2, x^1 - x^2, 0.2x^1x^2 + x^2 - 0.1(x^1)^2)$ (the third boundary condition is $f_3 = f_2$.) The reconstructions are shown on the catenoid in the second row of Figure 1.

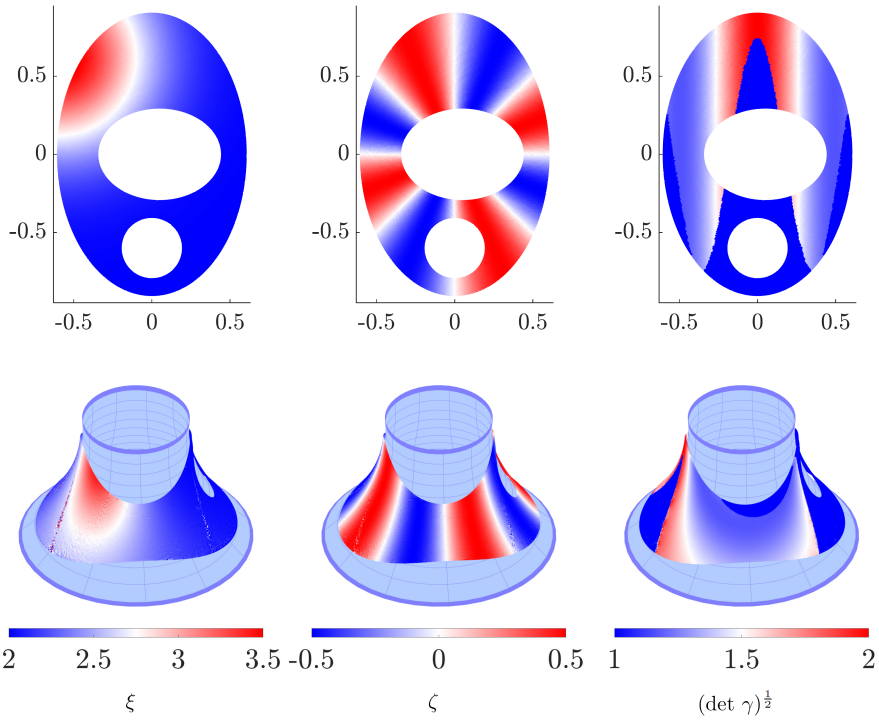

Figure 1: The true scalar functions ξ, ζ and $(\det \gamma)^{\frac{1}{2}}$ determining the conductivity in the plane (first row) and their reconstructions on a catenoid (second row).

5. Conclusion

We have presented a new geometric setting for the reconstruction of anisotropic conductivities from power densities. Our main result generalizes the reconstruction method for the 2-dimensional Euclidean setting to 2-dimensional compact Riemannian manifolds with genus 0. The result is presented in a way that opens for further research questions in the setting of Riemannian manifolds with higher genus and possibly in higher dimensions. The approach applies to other similar inverse problems with internal data, in particular the reconstruction problem for anisotropic conductivities from *current densities*, c.f. [17, 18].

Acknowledgements

This research did not receive any specific grant from funding agencies in the public, commercial, or not-for-profit sectors.

References

[1] M. Salo, The Calderón problem on Riemannian manifolds, in: Inverse problems and applications: inside out. II, Vol. 60 of Math. Sci. Res. Inst. Publ., Cambridge Univ. Press, Cambridge, 2013, pp. 167–247.

[2] H. Zhang, L. V. Wang, Acousto-electric tomography, in: Photons Plus Ultrasound: Imaging and Sensing, Vol. 5320, SPIE, 2004, pp. 145 – 149. doi:10.1117/12.532610.

[3] H. Ammari, E. Bonnetier, Y. Capdeboscq, M. Tanter, M. Fink, Electrical impedance tomography by elastic deformation, SIAM J. Appl. Math. 68 (6) (2008) 1557–1573. doi:10.1137/070686408.

[4] F. Monard, G. Bal, Inverse anisotropic diffusion from power density measurements in two dimensions, Inverse Problems 28 (8) (2012) 084001. doi:10.1088/0266-5611/28/8/084001.

[5] G. Bal, G. Uhlmann, Reconstruction of coefficients in scalar second-order elliptic equations from knowledge of their solutions, Comm. Pure Appl. Math. 66 (10) (2013) 1629–1652. doi:10.1002/cpa.21453.

[6] G. Bal, C. Guo, F. Monard, Linearized internal functionals for anisotropic conductivities, Inverse Probl. Imaging 8 (1) (2014) 1–22. doi:10.3934/ipi.2014.8.1.

[7] F. Monard, G. Bal, Inverse anisotropic conductivity from power densities in dimension $n \geq 3$, Comm. Partial Differential Equations 38 (7) (2013) 1183–1207. doi:10.1080/03605302.2013.787089.

[8] G. Bal, E. Bonnetier, F. Monard, F. Triki, Inverse diffusion from knowledge of power densities, Inverse Probl. Imaging 7 (2) (2013) 353–375. doi:10.3934/ipi.2013.7.353.

[9] F. Monard, D. Rim, Imaging of isotropic and anisotropic conductivities from power densities in three dimensions, Inverse Problems 34 (7) (2018) 075005. doi:10.1088/1361-6420/aabe5a.

[10] A.-P. Calderón, On an inverse boundary value problem, in: Seminar on Numerical Analysis and its Applications to Continuum Physics (Rio de Janeiro, 1980), Soc. Brasil. Mat., Rio de Janeiro, 1980, pp. 65–73.

[11] G. Uhlmann (Ed.), Inverse problems and applications: inside out. II, Vol. 60 of Mathematical Sciences Research Institute Publications, Cambridge University Press, Cambridge, 2013.

[12] M. W. Hirsch, Differential topology, Graduate Texts in Mathematics, No. 33, Springer-Verlag, New York-Heidelberg, 1976.

[13] X. Gu, S.-T. Yau, Computing conformal structures of surfaces, Commun. Inf. Syst. 2 (2) (2002) 121–145. doi:10.4310/CIS.2002.v2.n2.a2.

[14] X. Gu, Y. Wang, T. F. Chan, P. M. Thompson, S. T. Yau, Genus zero surface conformal mapping and its application to brain surface mapping, IEEE Transactions on Medical Imaging 23 (8) (2004) 949–958. doi:10.1109/TMI.2004.831226.

[15] R. Schoen, S.-T. Yau, Lectures on harmonic maps, Vol. 2, International Press, 1997.

[16] D. Gilbarg, N. S. Trudinger, Elliptic Partial Differential Equations of Second Order, Classics in Mathematics, U.S. Government Printing Office, 2001.

[17] G. Bal, C. Guo, F. Monard, Inverse anisotropic conductivity from internal current densities, Inverse Problems 30 (2) (2014) 025001, 21. doi:10.1088/0266-5611/30/2/025001.

[18] G. Bal, C. Guo, F. Monard, Imaging of anisotropic conductivities from current densities in two dimensions, SIAM J. Imaging Sci. 7 (4) (2014) 2538–2557. doi:10.1137/140961754.

{2.7182818284}ϑφερτυθιοπσδφγηξκλ